

co-sponsored by

The Electrochemical Society



The International Society of Electrochemistry



15th ABAF

BRNO 2014

Advanced Batteries, Accumulators
and Fuel Cells

INTERNATIONAL CONFERENCE

August 24th - August 28th 2014

Organised by:

Department of Electrical and Electronic Technology,
Faculty of Electrical Engineering and Communication,
Brno University of Technology

Organizing committee:

Jiří Vondrák
Marie Sedlaříková

Honourary Scientific Committee:

- Doron Aurbach, *Bar Ilan University, Israel*
- Ladislav Kaván, *Jaroslav Heyrovsky Institute of Physical Chemistry, Czech Republic*
- Tatjana Kulova, *Physical Chemistry and Electrochemistry of the RAS, Moscow*
- Chatenet Marian LEPMI, *St Martin d'Hères, Grenoble, France*
- Palani Balaya Faculty of Engineering, *Singapore*
- Vladislav Kharton, *CICECO, University of Aveira , Portugal*
- Renata Orinaková, *Department of Physical Chemistry, Faculty of Science, P.J. Šafárik University, Košice. Slovak Republic*
- Arnaldo Visintin, *INIFTA, University La Plata, Argentina*
- Petr Vanýsek, *Northern Illinois University, DeKalb, Illinois, USA*
- Jaroslav Cihlář, *FSI VUT Brno, Czech Republic*
- Silvia Real INIFTA, *University La Plata, Argentina*
- Gunter Fafilek, *TU Wien*
- Oumarou Savadogo, *Polytechnique Montréal, Montréal, Québec, CANADA*

Organisation Committee:

- Jiří Vondrák
- Marie Sedlaříková
- Vítězslav Novák
- Jiří Wagner
- Miroslav Zatloukal
- Tomáš Kazda
- Lucie Šimonová
- Jiří Libich
- Josef Máca

Program Committee:

- Jiří Vondrák
- Marie Sedlaříková
- Arnaldo Visintin
- Josef Máca
- Vítězslav Novák
- Petr Bača
- Tomáš Kazda
- Jiří Špínka
- Helena Polsterová
- Martin Frk
- Edita Hejátková
- Miroslav Zatloukal
- Jiří Šubarda
- Andrea Fedorková
- Jiří Libich
- Lucie Šimonová
- Zdenka Rozsivalová

Conference is sponsored by:



SIGMA-ALDRICH®



INVESTMENTS IN EDUCATION DEVELOPMENT



Centre for Research
and Utilization
of Renewable Energy

co-sponsored by

The Electrochemical Society

The International Society of Electrochemistry



We would like to express our thanks to the Brno University of Technology, Faculty of Electrical Engineering and Communication for support and help with organising 15th ABAF conference.

Partners:



Media partners:



Víme, co vám ve škole neřeknou



Contents

P. Vanýsek

ECS – The Electrochemical Society:

A Look at the Present with Our Vision for the Future.10

V. Novák, P. Vanýsek, and J. Cihlář

New Electrochemistry for New Materials at CEITEC.....14

Materials for lithium-ion batteries

B. Markovsky et al.

Li-Ion Batteries:

Recent Studies of Li and Mn-Rich $\text{Li}_x[\text{MnNiCo}]\text{O}_2$ Materials as Positive Electrodes16

A. M. Skundin

The Features of Charge-Discharge Curves of Electrodes Based on $\text{Li}_4\text{Ti}_5\text{O}_{12}$17

A. S. Fedorková, O. Čech, T. Kazda, R. Oriňáková, M. Sedlaříková

New Composite Cathodes For Li-Ion Batteries Based On Conversion Reaction20

O. Kaválek, J. Vondrák, P. Čudek

Intercalation of lithium into electrodeposited microstructured Pb layer23

P. R. Das, A. Gräfenstein, L. Komsiyyska, D. Ledwoch, O. Osters, G. Wittstock

Application Of Tosylate-doped poly(3,4-ethylenedioxy-thiophene) (PEDOT:p-TOS) and poly-o-methoxyaniline (POMA) as cathodic binders for Li-ion batteries27

R. M. Humana, M. G. Ortiz, J. E. Thomas, S. G. Real, A. Visintin

Preparation and Characterization of Graphite Anode for Lithium Ion Batteries28

T.L. Kulova

Transformations of Thin-Film Electrodes Based on Silicon Composites at Cycling30

E. M. Erickson, Ch. Ghanty, H. Sclar, O. Srur-Lavi, Y. Gofer, M. Weitman, B. Markovsky, D. Aurbach

Surface Chemistry of Lithium-ion Battery Electrodes in Several Electrolyte Systems34

A. Chekannikov, R. Kapaev, S. Novikova, T. Kulova, A. Skundin, A. Yaroslavtsev

Study of the electrochemical behaviour of lithium Iron phosphate doped by chromium and nickel35

H. Bültner, F. Peters, J. Schwenzel, G. Wittstock

In Situ Investigation on Spatiotemporal Changes of SEI Properties by SECM38

O. Savadogo and M. Talebi-Esfandarani

Fundamental aspects of noble metal doped LiFePO_4 cathode for Li-ion batteries applications39

R.D. Apostolova, V.P. Tsyachny, A. Markevich, O.S. Ksenzhek, E.M. Shembel, B. Markovsky, D. Aurbach

Diffusion of Li^+ in Thin Film Vanadium Oxides for Lithium Batteries41

<i>R.D. Apostolova, R.P. Peskov, E.M. Shembel</i> Compositions of Co-doped LiMn₂O₄ spinel with MCNT for Lithium Batteries	47
<i>T. Kazda, O. Čech, J. Vondrák, A. Fedorková Straková, A. Visintin, P. Čudek</i> Comparison of the properties of high voltage spinel cathode material depending on the method of synthesis	51
<i>T. Cetinkaya, M. Uysal, H. Akbulut</i> Highly Reversible Silicon/Carbon Nanofiber/Carbon Nanotube Nanocomposite Anodes for Lithium Ion Batteries	55
<i>N. I. Globa, V. A. Sirosh, V. D. Prisyazhnyi</i> Characteristics of FeS₂ in Electrolytes Based on DMC-LiAn Mixtures during galvanostatic cycling	56
<i>T. Kazda, J. Vondrák, M. Sedlaříková, P. Čudek</i> Influence of doping LiCoO₂ by potassium to electrochemical properties depending on time	57
<i>Jiyoung Kim, Junyoung Mun</i> Compatibility of room temperature ionic liquid electrolytes with hard carbon anode in lithium ion secondary batteries	61
<i>J. Libich, J. Vondrák, M. Sedlaříková, H. Matheislová, P. Bursíková, O. Suchý, R. Friedrichova</i> Simultaneous Thermal Analysis for Fire Safety of Lithium-ion Batteries	62
<i>J. Libich, J. Máca, M. Sedlaříková, J. Vondrák, A. Visintin</i> Compatibility of Aprotic Electrolytes with Negative Electrode Materials in Lithium-ion Batteries	66
<i>J. Maca, M. Sedlarikova, J. Vondrak and M. Frk</i> The phosphate flame retardant influence on aprotic electrolytes properties	70
<i>M. Frk, J. Maca, J. Libich</i> The permittivity study of aprotic solvents	73
<i>Junyoung Mun, Wonchang Choi, and Seung M. Oh</i> Surface modification of High Energy Density Positive Electrode for High-Performance Lithium-ion Batteries	76
<i>M. Uysal, T. Cetinkaya, A. Alp, H. Akbulut</i> Fabrication of Sn–Ni /MWCNT nanocomposite celectrodes for Li-ion batteries by pulse electrodeposition: Effects of Peak Current Density	77
<i>P. Vyroubal, J. Maxa, T. Kazda, J. Vondrák</i> Numerical Study of Lithium Ion Battery	78
<i>M. Sedlaříková, J. Máca, J. Vondrák, F. Křištofik</i> Decomposition of polar solvents for lithium batteries by high oxidation potential	82
<i>A. Kahoul</i> Effect of La Doping on Physical and Electrochemical Properties of Double Perovskite Sr₂FeMoO₆ Oxide	86

<i>P. Dvořák, M. Sedlaříková, J. Vondrák</i> Gel polymer electrolytes	88
<i>M. Musil, J. Vondrak</i> Transference number measurements on gel polymer electrolytes for Lithium-Ion batteries	92
New materials for fuel cells	
<i>S. Chauque, C. B. Robledo, E. P. M. Leiva, F. Y. Oliva and O. R. Cámara</i> Comparative Study of Different Alkali (Na, Li) Titanate Substrates as Active Materials for Anodes of Lithium Ion Batteries	95
<i>L. Dubau, M. Lopez-Haro, J. Durst, L. Guétaz, P. Bayle-Guillemaud, M. Chatenet, F. Maillard</i> Beyond Conventional Electrocatalysts: “Hollow” Nanoparticles for Improved and Sustainable Oxygen Reduction Reaction Activity	96
<i>Shen-Ming Chen, Rajkumar Devasenathipathy</i> Preparation of Graphene and Multiwalled Carbon Nanotube Composite Modified Electrode and their application in glucose/O₂ biofuel cell	97
<i>R. Oriňáková, M. Sabalová, L. Škantárová, A. Oriňák, A. Straková Fedorková</i> Nanostructured electrocatalytic materials for hydrogen evolution reaction	98
<i>M. Hashempour, S. Sharma, D. Gonzalez, G. Gupta, A. Vincenzo, M. Bestetti</i> Investigation on the Role of Individual Components of a CNT-RGO Hybrid Support in the ORR Activity of the PEMFC Catalyst	102
<i>A. Al-Musa, V. Kyriakou, N. Kaklidis, M. Al-Saleh, A. Al-Zahrani, G. E. Marnellos</i> Internal steam reforming of iso-octane on Co-based anodes in a solid oxide fuel cell	105
<i>J. Dundálek, J. Povedič, P. Mazúr, J. Vrána and J. Kosek</i> Development of Zinc-Air Fuel Cell	107
<i>Jin Yeong Kim, Sung Hoon Hong, Sang Hyun Ahn, Sung Gyu Pyo, Jong Hyun Jang, Soo-Kil Kim</i> Fabrication of Transition Metal Alloy Catalysts for Water Electrolysis using Electrodeposition	108
<i>Ji-Eun Lim, Uk Jae Lee, Sung Hoon Hong, Jin Yeong Kim, Sang Hyun Ahn, EunAe Cho, Hyoung-Juhn Kim, Jong Hyun Jang, Hyungbin Son, and Soo-Kil Kim</i> Electrodeposition-fabricated Alloy Catalysts for High Temperature Proton Exchange Membrane Fuel Cells	109
<i>V. Barbashov, E. Nesova</i> Pressure mechanism of conductivity in the ternary ZrO₂-systems	110
<i>B. Pierozynski</i> Hydrogen Evolution Reaction at Pd-Modified Nickel Foam Material	113
<i>M. Tkáč, K. Stehlik, M. Zychová</i> Hydrogen Technologies In The Project SUSEN At Research Center Rez	114

The other modern systems for batteries

P. Vanýsek, H. Tavassol, and K. L. Pilson

Electrochemistry in the electrochemical cells: There is more than just the working electrode118

T. Behofsits, M. Malys, G. Pani, G. Fafílek

Electrochemical properties of CeVO₄ and FeVO₄ at high temperatures122

J. Vrána, P. Mazúr, J. Pociďič, J. Dundálek, M. Bobák, and J. Kosek

Vanadium Redox Flow Battery – Electrolytes Preparation123

J. Vondrák, M. Sedlaříková and P. Špičák

Batteries Based on Sodium Intercalation124

H. Al-Fetlawi

Non-Isothermal Modeling and Simulation of a Soluble Lead-Acid Redox Flow Battery128

A. Gavrilović-Wohlmuther, A. Laskos, Ch. Zelger, B. Gollas, A. H. Whitehead

Zinc-Air Flow Batteries for Electrical Power Distribution Networks129

Application of batteries for electromobility and industry

P. Vorel, P. Prochazka, I. Pazdera, D. Cervinka

Rejuvenation of a NiFe accumulator from 1930's130

B. Polnik, B. Miedziński

Hydrogen explosion risk in mining locomotive unit136

Photovoltaic Systems

J. Maxa, P. Vyroubal, L. Šimonová

Thermal Analysis of Thermophotovoltaic Emitter140

L. Šimonová, J. Hylský, M. Frk, J. Šubarda

Heat transfer fluids for optimal year-round operation of solar thermal systems in Central Europe143

L. Šimonová, J. Kolář, P. Vyroubal

Analysis of the effect of heat on photovoltaic cells in thermophotovoltaic system145

S. Vaculík, P. Vyroubal, J. Maxa, J. Vaněk

Thermal Analysis Of The Photovoltaic Concentrator Cell.....147

J. Vanek, J. Zimakova, M. Sturm

Photovoltaic Modules Destruction Analysis150

Aqueous and special batteries

<i>D. Fryda, J. Zimáková, P. Bača</i> Preparation of Lead Electrodes For Measurement By Using AFM	154
<i>M. Kadlec, J. Zimáková, D. Fryda</i> Climatic Chamber Designed For Curring Positive Electrodes	157
<i>Jong Deok Park, Young Min Park , Haekyoung Kim</i> Hybrid membranes for vanadium redox flow battery	160
<i>J. Zimáková, D. Fryda, P. Bača</i> In Situ Observation of Morphology Changes on Lead Electrodes During Cyclic Voltammetry by Using AFM	162
<i>P. Křivík</i> Temperature changes in lead acid battery during pulse charging	165
<i>P. Vyroubal, P.Tošer, J.Maxa, P.Bača, S.Vaculík</i> Simulation of Current Distribution in Lead Acid Battery Grid Using FEM	170
<i>L. Chladil, P. Čudek, V. Novák</i> Pulse Deposition of Zinc in Alkaline Electrolytes for Ni-Zn Secondary Batteries	173
<i>L. Chladil, V. Novák</i> Improvement of Cyclability of Ni(OH)₂ in the Presence of Zincate Ions	177
 Miscelaneous	
<i>R. Fojtíková, P. Mazúr, J. Pociď, J. Maršálek and J. Kosek</i> Optimization of electro spraying for preparation of supercapacitive MnO₂-based electrode	181
<i>D. Dobrocký, O. Klanica, F. Onderka, J. Kadlec</i> The changes of surface texture parameters of the duplex systems: nitrated layer – coating at CoCrMo alloy	182
<i>M. Hashempour, A. Vincenzo, M. Bestetti, S. Sharma, D. Gonzalez</i> The Effect of Electrodeposited PANI on Corrosion Behavior of 316 Stainless Steel Coated by CVD Grown MWCNTs under PEMFC Bipolar Plate Working Condition	186
<i>F. Onderka, O. Klanica, D. Dobrocký</i> Electrochemical deposition of hydroxyapatite coatings on CoCrMo alloy	190
<i>L. Šimonová, J. Šubarda, J. Danovič</i> Protective coatings against thermal degradation of the metal thin film	195

ECS – The Electrochemical Society: A Look at the Present with Our Vision for the Future.

P. Vanýsek^{a,b}

^a Department of Biochemistry, Northern Illinois University, DeKalb, Illinois 60115, USA

^a CEITEC - Central European Institute of Technology BUT, Technická 3058/10, CZ-616 00 Brno,
Czech Republic

^b visiting from" Department of Chemistry and Biochemistry, Northern Illinois University, DeKalb,
Illinois 60115, USA

Electrochemical Society was founded in 1902 and its present mission is to promote materials science and electrochemistry. The Society often co-sponsors satellite meeting and meetings of other societies and organizations, including 2014 ABAF. This brief presentation will give a short introduction to the organization and activities of the Society. Additionally, the Society will publish a Transactions volume, o collection of presentations given at ABAF 2014. Brief information on logistics of the manuscript preparation and submission will be given.

ECS The Past and the Present

The mission of the Society is to advance theory and practice at the forefront of electrochemical and solid-state science and technology, and allied subjects. To encourage research, discussion, critical assessment, and dissemination of knowledge in these fields, the Society holds meetings, publishes scientific papers, fosters training and education of scientists and engineers, and cooperates with other organizations to promote science and technology in the public interest.

ECS is an international nonprofit, scientific society of more than 8,700 active members in over 75 countries engaged in solid-state and electrochemical science and technology. Some of the activities are as follows:

- International technical meetings in spring and fall
- International Satellite Conferences
- Top-ranked journals (presently four)
- Networking opportunities
- Student services: Chapter activities, fellowships, travel grants
- Award programs recognizing accomplishments and supporting research

Local activities of the membership are possible in several sections, which include Arizona, Brazil, Canada, Chicago, Chile, China, Cleveland, Detroit, Europe, Georgia, India, Israel,

Japan, Korea, Mexico, National Capital, New England, Pittsburgh, San Francisco, Taiwan, Texas and Twin Cities.

According to the more specific interests, the members can associate in one of thirteen topical divisions:

Batteries and Energy Storage

Chemical and Biological Sensors

- Corrosion Science and Technology
- Electrochemical/Electroless Deposition
- Electrochemical Engineering
- Fuel Cells, Electrolyzers, and Energy Conversion
- Organic and Bioelectrochemistry
- Physical and Analytical Electrochemistry
- Carbon Nanostructures and Devices
- Dielectric Science and Materials
- Electronic Materials and Processing
- Electronic and Photonic Devices, and Systems
- Luminescence and Display Materials, Devices, and Processing

With recognition of the importance of students for the future of the Society, ECS encourages formation of students groups, which are typically associated with a university. The list over the few years when this initiative started, grew significantly. Following are the groups on record as of July 2014.

Atlanta Student Chapter at Georgia Tech

Auburn University

Boston

Calgary

The California State University - Fullerton Division

Central Illinois

Colorado School of Mines

Drexel University

ECS Cleveland Section and Ernest B. Yeager Center for Electrochemical Sciences

Florida International University

Grand Valley State University

Indiana University

Kerala, India Student Chapter at CUSAT

Lahore, Pakistan

Montana State University
Montreal
New York Capital Region
Ohio University
Research Triangle
Rensselaer Polytechnic Institute
South Brazilian
SRM University
Technical University Brno
Tel Aviv University
The Ohio State University
Tyndall National Institute
University of British Columbia
University of California – Berkeley
University of California – Riverside
University of Central Florida
University of Cincinnati
University of Florida
University of Maryland
University of South Carolina
University of Tartu
University of Texas at Austin
University of Texas at Dallas
University of Virginia
Valley of the Sun – Central Arizona

Publications

Four peer-reviewed journals:

Journal of The Electrochemical Society

ECS Electrochemistry Letters

ECS Journal of Solid State Science and Technology

ECS Solid State Letters

Member magazine *Interface*

Monographs

Meeting Abstracts

ECS Transactions

How to publish in ECS Transactions

The submission is by "invitation only." The authors of presentations at the meeting will receive an automated e-mail, inviting them to submit the material. This invitation has a built-in password, hence only the author (the main author, or the presenting author) has access to this. Please, make an arrangement, if you want your co-author handle this.

The invitation comes usually about a week after the meeting and there is a window of about 2-3 weeks for the submission to be done. Please, download the template which is mentioned in the invitation and follow the formatting exactly. It will save time during editing.

After the submission window closes, the reviewers will have opportunity to check the papers and suggest corrections. If you are invited as a reviewer, please, be prompt. If you, as an author, receive a note to correct your manuscript, do it also promptly. The publication of the whole collection may be delayed by a single late author!

Once all is submitted, the volume editor (usually the meeting organizer) may write an introduction, help with arranging the order of the presentations, etc. Then, the ECS Staff will publish this material, on line. The text will be available to the members on-line via their membership benefits. Others will have to gain access via their institutional or individual subscriptions or ad-hoc payments.

Please, note that *Transactions* presently do not have impact factor. However, it is perfectly fine to publish an expanded material form Transactions in the Society Journal, which does have an impact factor.

Acknowledgments

This text was prepared based on material provided by the Electrochemical Society.

New Electrochemistry for New Materials at CEITEC

V. Novák^a, P. Vanýsek^{a,b}, and J. Cihlář^a,

^a CEITEC - Central European Institute of Technology BUT, Technická 3058/10, CZ-616 00 Brno, Czech Republic

^b visiting from: Department of Chemistry and Biochemistry, Northern Illinois University, DeKalb, Illinois 60115, USA

This presentation will give an overview of instrumental capabilities, manpower resources and general vision of electrochemical and materials projects to be carried out at CITED in the upcoming year.

CEITEC Research Overview

Central European Institute of Technology (CEITEC) was founded in June 2011 with funding from European Structural Funds and the Czech Ministry of Education, Youth and Sports. The institute is located in the city of Brno, Czech Republic. The objective of CEITEC is to create environment where high-level scientific discovery can be fostered as to be competitive on the world stage.

CEITEC is multidisciplinary institute with very broad interests, presently covering seven more specific areas:

- Advanced Nanotechnologies and Microtechnologies
- Advanced Materials
- Structural Biology
- Genomics and Proteomics of Plant Systems
- Molecular Medicine
- Brain and Mind Research
- Molecular Veterinary Medicine

CEITEC has a number of Core Facilities that offer access to cutting-edge and often expensive equipment to the research community. The goal is to provide a central hub of shared resources of instrumentation and well as technology development and services for both academic and industrial investigators.

The ability of external researchers to perform their experiments using the Core Facilities is via open access, funded by the Ministry of Education, Youth and Sports of the Czech Republic. Prospective users have to submit competitive proposals for the work. Once approved, the access is free to the users.

Following is a list of the facilities:

- Nanofabrication and Nanocharacterization
- Structural Analysis Laboratory
- Biomolecular Interactions and Crystallization
- X-ray Diffraction and Bio-SAXS Core Facility
- Nanobiotechnology Core Facility

- Josef Dadok National NMR Centre
- Cryo-electron Microscopy and Tomography
- Proteomics Core Facility
- Core Facility - Genomics
- Multimodal and Functional Imaging Laboratory

CEITEC and Electrochemistry

CEITEC facilities cater to the needs of electrochemists mostly in the areas of Advanced Materials and Nanofabrication and Nanocharacterization. The research in Advanced Materials covers their synthesis and analysis of their structure and properties. The research aim is to develop new materials with complex properties and to propose novel applications for these materials. The Advanced Materials research is further separated in focus on advanced ceramic materials, advanced polymeric materials and composites; and advanced metallic materials.

With the new facilities being build, new laboratory equipment was also purchased. Some of the new instrumentation for the Advanced Ceramic Materials is as follows: Measuring set of electrometers and femtoammeters, high voltage construction kit, precision capacitance automatic bridge, partial discharge measuring system, Set of climatic chambers, glove box, high temperature furnaces, thermoanalytical system with a mass spectrometer, catalytic reactor, photochemical reactor for study of photocatalytic activity of ceramic catalytic materials, Equipment for study of high temperature properties of ceramic membranes, Solid oxide fuel cells testing system, high pressure solvothermal reactor, ultrasonic spray pyrolysis reactor, chemical analysis of ceramic materials (ICP, sample decomposition), chemical vapor deposition system, screen printer, spray dryer and a glove box.

Acknowledgments

Some of the information compiled in this abstract was also loosely collected from the Internet.

References

1. P. Vyhnálková and J. Ondroušek, CEITEC Research Overview. Program Description Brochure. Brno 2013.

Li-Ion Batteries:
Recent Studies of Li and Mn-Rich $\text{Li}_x[\text{MnNiCo}]\text{O}_2$ Materials as Positive Electrodes

B. Markovsky et al.

Department of Chemistry, Bar-Ilan University, Ramat-Gan 52900, Israel

Abstract

This presentation at ABAF-2014 is dedicated to the study of Li and Mn rich $\text{Li}_x[\text{MnNiCo}]\text{O}_2$ cathode materials with an emphasis on the effect of AlF_3 coating on their electrochemical performance. The initial stoichiometry of these materials was $x\text{Li}_2\text{MnO}_3 \cdot (1-x)\text{LiMn}_y\text{Ni}_z\text{Co}_w\text{O}_2$ where x is in the range 0.4-0.5 and the $y:z:w$ ratio was as we reported in [1]. Their structure was considered on the basis of two-components model, namely monoclinic Li_2MnO_3 ($C2/m$) and rhombohedral LiMO_2 ($R-3m$) ($M=\text{Mn, Ni, Co}$) that are structurally compatible and closely integrated phases. Based on TEM studies we concluded that the coating had a crystalline tetragonal structure $t\text{-AlF}_3$ ($P4nmm$ symmetry) and AlF_3 nano-crystals were regularly distributed over the particles surface. Amorphous clusters of AlF_3 and/or other Al-containing species, like AlF_xO_y , $\text{Al}[\text{FOH}]$, etc. may also present, as it follows from solid-state NMR measurements. It was shown that electrodes comprising the AlF_3 -coated material exhibited higher reversible capacities of ~ 250 mAh/g at a $C/5$ rate, more stable cycling behavior, higher lithium storage capability at 60°C , and lower impedance measured during Li-deintercalation comparing to electrodes prepared from the uncoated material. An important finding is that $\text{Li}_x[\text{MnNiCo}]\text{O}_2 / \text{AlF}_3$ materials revealed much higher thermal stability both in the pristine (lithiated) and cycled (delithiated) states than their uncoated counterparts.

References

1. F. Amalraj et al. Journal of the Electrochemical Society, 160 (2) A324-A337 (2013).

The Features of Charge-Discharge Curves of Electrodes Based on $\text{Li}_4\text{Ti}_5\text{O}_{12}$

A. M. Skundin

Frumkin Institute of Physical Chemistry and Electrochemistry

Lithium titanate, $\text{Li}_4\text{Ti}_5\text{O}_{12}$, has attracted great interest as material of negative electrode of lithium-ion batteries. The salient feature of $\text{Li}_4\text{Ti}_5\text{O}_{12}$ -based electrodes consists in flatness of their charge/discharge curves. This phenomenon is explained by the fact that these electrodes present two-phase system $\text{Li}_4\text{Ti}_5\text{O}_{12}/\text{Li}_7\text{Ti}_5\text{O}_{12}$ in the course of charge/discharge. Indeed, mutual solubility of both phases is negligible; therefore, the charge (or discharge) results only in change of their ratio without appearing phases with variable composition. However, such flat curves reveal themselves only at low C-rates, and with the increase of rate, they gradually bends up (Fig.1).

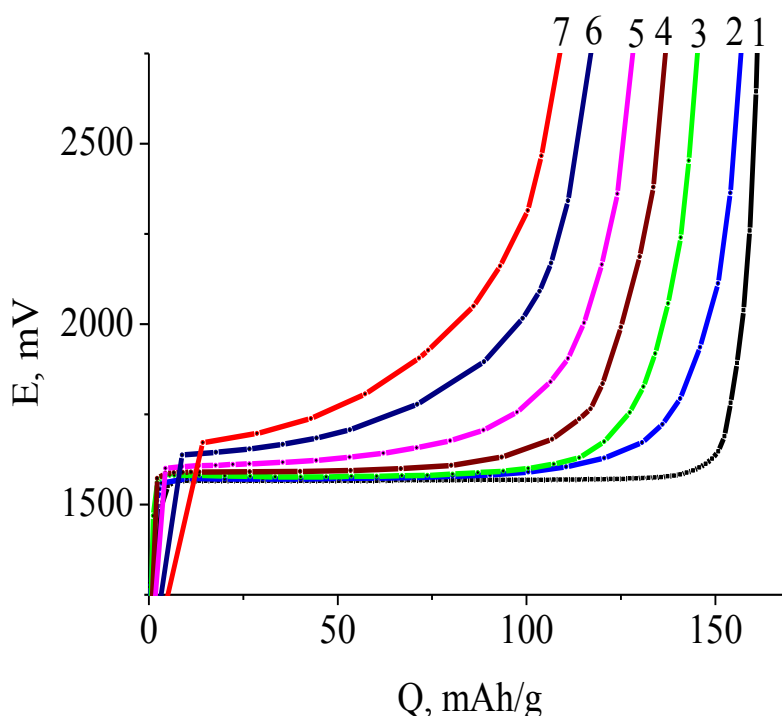


Figure 1. Discharge curves of $\text{Li}_7\text{Ti}_5\text{O}_{12}$ electrode with rates $C/8$ (1), $1.25C$ (2), $2.5C$ (3), $5C$ (4), $10C$ (5), $20C$ (6) and $40C$ (7)

The bending of charge/discharge curves with increasing C-rate is accompanied by decrease of the electrode capacity. Fig. 2 demonstrates rate dependence of discharge capacity Q for the same electrode depicted in logarithmic coordinates. One can see that this dependence is very weak at low rates, and obeys to well-known Peukert equation $Q = Q_0/I^\alpha$. Here I is discharge current, Q_0 and α are empirical constants. Unlike to other kinds of electrodes, the exponent α in this very case is rather low being close to 0.1.

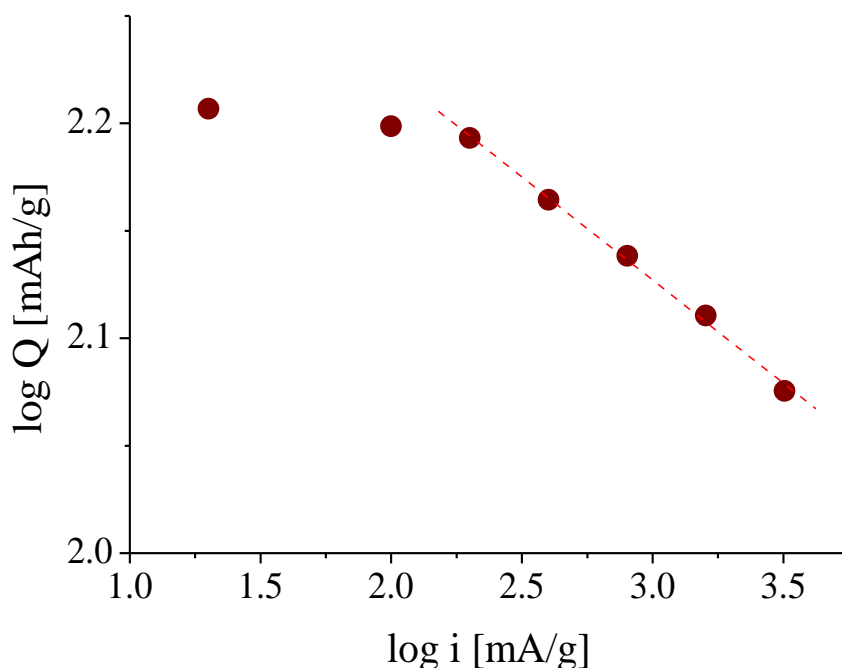


Figure 2. Discharge capacity vs. discharge current for $\text{Li}_7\text{Ti}_5\text{O}_{12}$ electrode

The exact mechanism of C-rate influence upon charge/discharge curves of titanate electrodes remains unknown up to now. In any case, there are several factors responsible for this effect. Every grain of titanate could be considered as some core-shell structure (Fig. 3). Completely charged grain consists of $\text{Li}_7\text{Ti}_5\text{O}_{12}$ having rather high electronic conductivity. During discharge the shell of $\text{Li}_4\text{Ti}_5\text{O}_{12}$ with extremely low conductivity is formed.

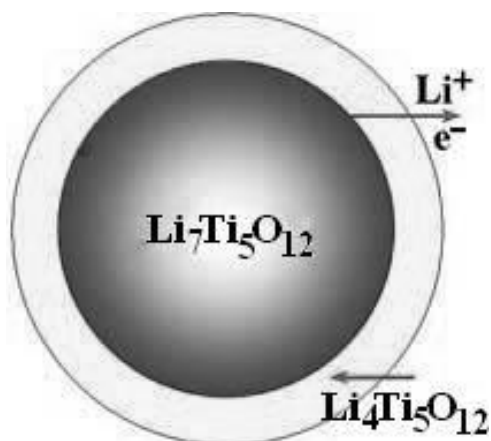
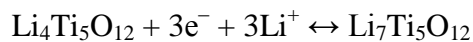


Figure 3. The model of core-shell structure of lithium titanate grain at discharge (upper arrow) and charge (lower arrow)

With due account for significant difference in conductivity of both phases one could suppose that in the course of discharge, total ohmic resistance would increase which would result in bending of discharge curves, especially at high C-rates. In this case during charge, when a shell of good conductor $\text{Li}_7\text{Ti}_5\text{O}_{12}$ is formed upon core of $\text{Li}_4\text{Ti}_5\text{O}_{12}$ the behavior of the system must be opposite.

However, this is far from being the case. Indeed, the curvature of charge curves increases in the course of charge, and this effect manifests itself the faster the higher C-rate.

It is worth mentioning that there are other components of total impedance besides ohmic resistance. The electrochemical reaction



has place at the interface between core and shell. The true area of this interface decreases with diminishing core diameter; therefore, the true current density sharply increases at the end of discharge or charge. It stands to logic that this very increase of true current density is the main reason of polarization increase.

Fig. 4 shows change of polarization resistance (in arbitrary units) in the course of discharge with different C-rates. Discharge degree q was calculated as relative volume of shell, polarization resistance was calculated as reciprocal area of the interface

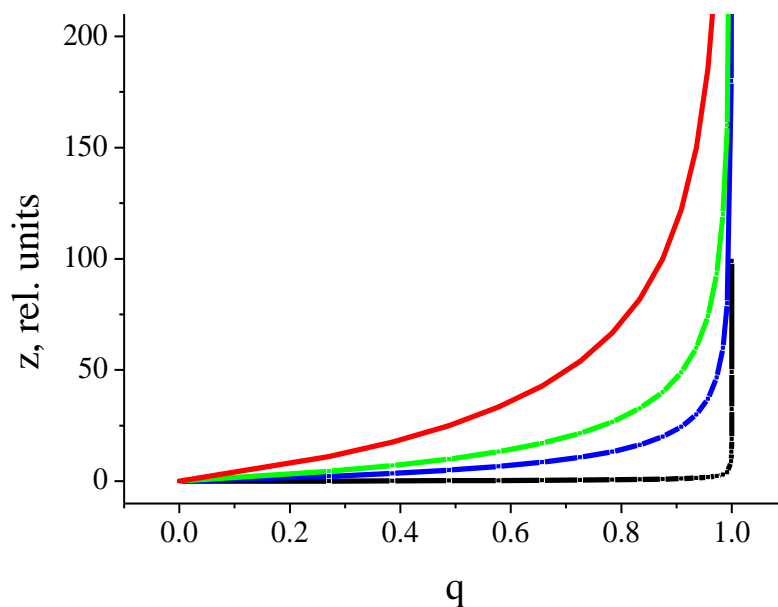


Figure 4. Polarization resistance vs. discharge degree for different C-rates (red>green>blue>black)

One can see certain similarity of curves in Figs. 1 and 4.

New Composite Cathodes For Li-Ion Batteries Based On Conversion Reaction

A. S. Fedorková^{1,2*}, O. Čech¹, T. Kazda¹, R. Oriňáková², M. Sedlaříková¹

¹ Department of Electrical and Electronic Technology, Faculty of Electrical Engineering and Communication, Brno University of Technology, Technická 10, 616 00 Brno, Czech Republic

² Institute of Chemistry, Faculty of Science, P.J. Šafárik University, Moyzesova 11, SK-041 54 Košice, Slovakia

* andrea.fedorkova@upjs.sk

Abstract

Lithium rechargeable secondary cells are currently being used as energy source in electronic devices, small portable devices and other electronics. Among the high-energy density storage systems, lithium-sulfur batteries, with energy density of 2600 Whkg⁻¹ (nearly 3~5 times than that of the traditional LIBs), holds the potential to serve as next generation of high energy battery. It possesses the advantages of low cost, environmentally benign and high safety characteristics. Sulfur-carbon (S-C) composites and sulfur-LiFePO₄ (S-LFP) composites were prepared with MWCNTs additive by evaporation and solid state reaction. It is found that the S-LFP cathode with MWCNTs shows improvement of not only discharge capacity but also cycling stability. It exhibits an initial discharge capacity of 1167 mAh/g sulfur, or 70% of theoretical capacity. The capacity of S-LFP-MWCNTs composite after 20 cycles was 80% of the initial value and remained stable.

INTRODUCTION

The lithium-sulfur battery is a “conversion” type battery, because the electrochemical reactions which take place during charging and discharging of the battery result in new chemical compounds [1-3] (Fig. 1). By contrast, lithium-ion batteries operate in accordance with the “insertion” principle. This means that lithium ions occupy spaces in the crystal structure of the cathode, without substantially changing the structure of the cathode material. The advantage of lithium-sulfur batteries is primarily their superior storage capacity (energy density - theoretical specific capacity is 1672 mAhg⁻¹), but they also excel in economic and environmental terms. Sulfur is a relatively inexpensive and abundant raw material, unlike expensive elements, such as cobalt, which are used in lithium-ion batteries. This is important because material costs make up a very large proportion of the total cost of a battery. From an environmental perspective, lithium-sulfur batteries also make it possible to avoid the use of heavy metals. However, various challenges are connected to the lithium sulfur cell chemistry, which need to be solved within systematic studies and by the development of new material concepts. In the present work, we report a simple method to synthesize S-C and S-LFP cathode material with MWCNTs as additional electronic conductor. SEM studies of morphological changes of the cathodes, thermogravimetry and charge–discharge performance of the S-C and S-LFP composites with MWCNTs were used to investigate and characterize the sulfur electrodes.

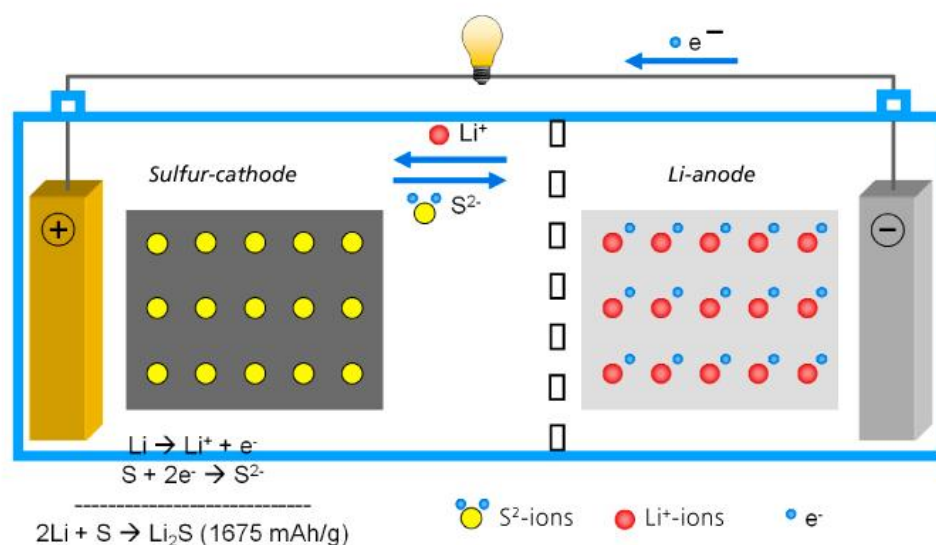


Figure 1. Conversion reaction in Li/S battery [4].

RESULTS AND DISCUSSION

Fig. 2 shows charge and discharge curves for the first two cycles. First charging for S-C sample (Fig. 2a) is very short because the phase of electrode material after cell assembly corresponds to the charged state of the cell. It can be noted that electrode formation in first two cycles occurs. In the discharge profile, two discharge plateaus (Plateau I and II) are observed. In the charge profile there are also two plateaus (Plateau III and IV) of the sulfur-carbon composite cathode. The discharge capacity of the second cycle is 1140 mAh/g-sulfur which is unmatched in comparison with conventional cathode active materials. For S-LFP composite cathode (Fig. 2b) we can observe two plateaus in charge and discharge profile. However, the initial charge/discharge capacities of the S-C composite are much higher than those of the S-LFP composite. This result indicates that the S-LFP composite has a relatively low potential polarization and good reversibility. The second discharge potential plateau of the S-C and S-LFP composite was much wider, contributing to the majority of the discharge capacity, and a high initial specific capacity of up to 1140 mAh/g-sulfur and 1167 mAh/g-sulfur respectively was obtained. These values correspond to 67% and 70% of the theoretical capacity of sulfur. This means at least 1.4 electrons per sulfur atom were involved in the electrochemical reactions of the S-LFP composite.

The morphologies of the S-based composite electrodes were investigated by SEM. Two different structures were observed for S-C composite. The surface of the Sulfur-Carbon sample is compact without cracks or holes but the structure is porous enough to enable Li^+ ion transport and electrolyte penetration. The porous and homogeneous basis of sample with MWCNTs is retained but addition of MWCNTs caused the formation of larger pores and holes. The MWCNTs are also clearly visible and provide the connections between S and C. In the case of S-LFP a coarser granularity is observed as compared with S-C. Yet, the corresponding S-LFP-MWCNTs composite presents a more homogeneous structure with oriented fibres of MWCNTs on the surface. Thus, the presence of MWCNTs in both samples was found to cause a significant change in porosity and homogeneity.

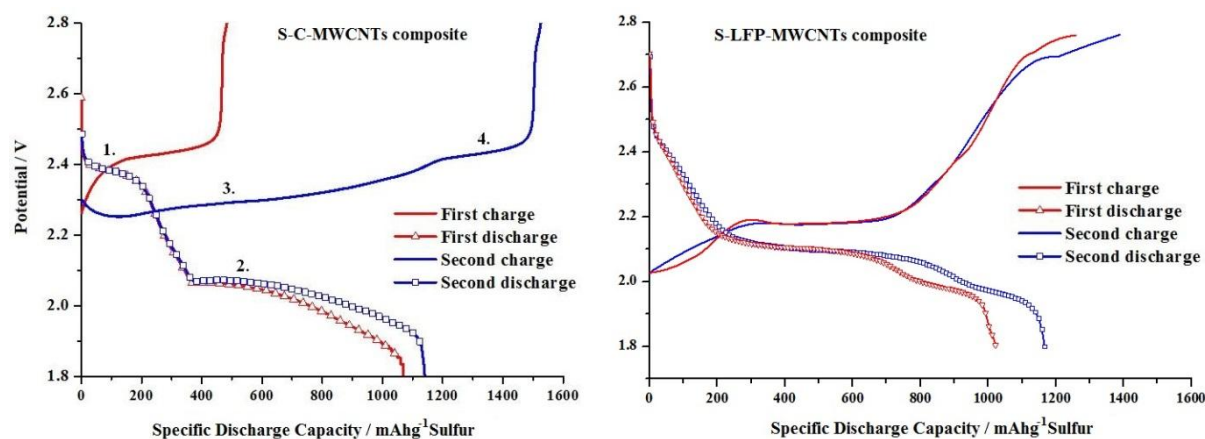


Figure 2. First two charge and discharge cycles of sulfur-carbon composite cathode (a) and sulfur-LFP cathode (b) at C-rate C/10.

CONCLUSIONS

Sulfur-carbon composite was synthesized by thermal heating of sulfur onto conductive carbon black (Super P). Sulfur-LFP composite was prepared by simple solid-state reaction in a ball mill. These simple methods have been shown here to produce very porous sulfur cathode composites. A high initial specific capacity of up to 1140 mAh/g-sulfur and 1167 mAh/g-sulfur respectively was obtained. These values correspond to 67% and 70% of the theoretical capacity of sulfur. This means at least 1.4 electrons per sulfur atom were involved in the electrochemical reactions of the S-LFP composite. The excellent electrochemical performance can be attributed to the homogeneous dispersion of MWCNTs in the composites, which not only accommodate the volume change during charge/discharge processes, and absorb the polysulfides byproducts but also provide stable electrical and ionic transfer channels.

ACKNOWLEDGEMENT

Authors gratefully acknowledge financial support from the Ministry of Education, Youth and Sports under projects No. LO1210 - "Energy for Sustainable Development (EN-PUR)" and CZ.1.07/2.3.00/30.0039 solved in the Centre for Research and Utilization of Renewable Energy and bilateral project No. 7AMB13AR008 between Czech Republic and Argentina.

REFERENCES

1. S. Thieme, J. Brückner, I. Bauer, M. Oschatz, L. Borchardt, H. Althues, S. Kaskel, *Journal of Materials Chemistry A*, 1 (32) (2013), 9225.
2. X. Ji, L.F. Nazar, *J. Mater. Chem.*, 20 (2010), 9821.
3. D. Aurbach, E. Pollak, R. Elazari, G. Salitra, *J. Electrochem. Soc.*, 156 (2009), A694.
4. <http://www.psi.ch/media/lithium-sulfur-battery>

Intercalation of lithium into electrodeposited microstructured Pb layer

O. Kaválek^a, J. Vondrák^a, P. Čudek^a

^a Department of Electrical and Electronic Technology, Brno University of Technology, Faculty of Electrical Engineering and Communication, Technická 10, 616 00 Brno, Czech Republic

Abstract

There were prepared lead electrode with electrochemical deposition. This electrode was used as cathode with LiCoO₂ as anode in electrochemical cell. This measure simulated lithium-ion cell for studying intercalation of lithium. Electrochemical intercalation of lead is important for the search of novel lithium batteries. It is known, that there elements of IVth group of periodic system of elements are among the candidates for that purpose. [1-4] In the case of elemental tin or silicium a great difficulty arises from extremely great volume change in the process of intercalation. A hypothesis has arisen that this can be bypassed by the use of nanostructured or microstructured metal as the host substance for the intercalation, the voids in them would absorb the volume changes without disintegration of the electrode material. The electrodeposition of elements from solutions of metal halides or metalloorganic compounds dissolved in aprotic polar solvents was expected to be the way how to obtain such materials. This contribution describes some experimental results from a section of our research in mentioned subject.

Experimental

The layers of microporous lead were deposited from a solution of PbCl₂ and LiCl in DMF. Electrochemical transient techniques available on the potentiostat Bio-Logic were used for measurement and evaluation of results.

An experimental all-metallic cell (El-Cell) was used to verify the function of the electrode in simulated condition of a lithium battery; the electrode LiCoO₂ and solution of LiClO₄ in PC served for the assembly of the cell.

Results

Deposition and morphology of the Pb layers

The layers of Pb were deposited on a copper foil in a simple cell which contained two lead counter electrodes, and which was fed from a laboratory voltage source. We used voltage 1,5 V to reach current of 35 mA onto a copper electrode of apparent area cca 2 cm². Short opposite polarisation with a reverse current cleaned the surface sufficiently. The morphology is shown in Fig. 1.

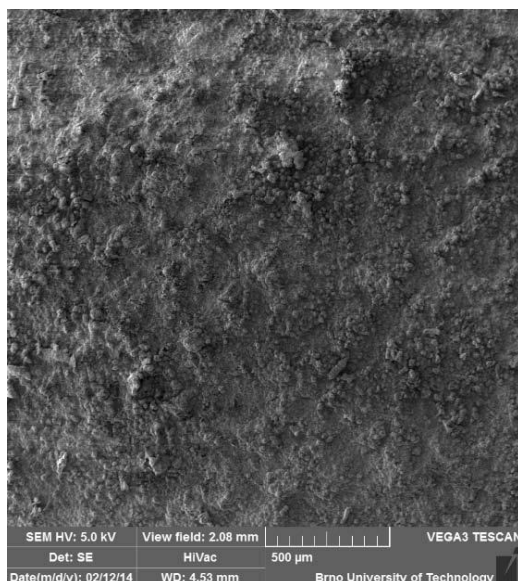


Figure 1. Morphology of electrodeposited Pb layer from SEM

Results in the model cell

Cyclic voltammetry. First 5 voltammetric cycles are plotted in Fig. 2. They were recorded on an electrode with apparent area 2.5 cm^2 at scan rate 0.5 mV/s . A double peak is clearly visible on both of them. The double peak at anodic branch was analysed and data are listed in Tab. 1. First, the charge of the peaks increased on subsequent cycles. Second, the ratio between number of atoms of lithium and lead is comparatively similar

and approaches the ratio 1 Li : 1 atoms of lithium.

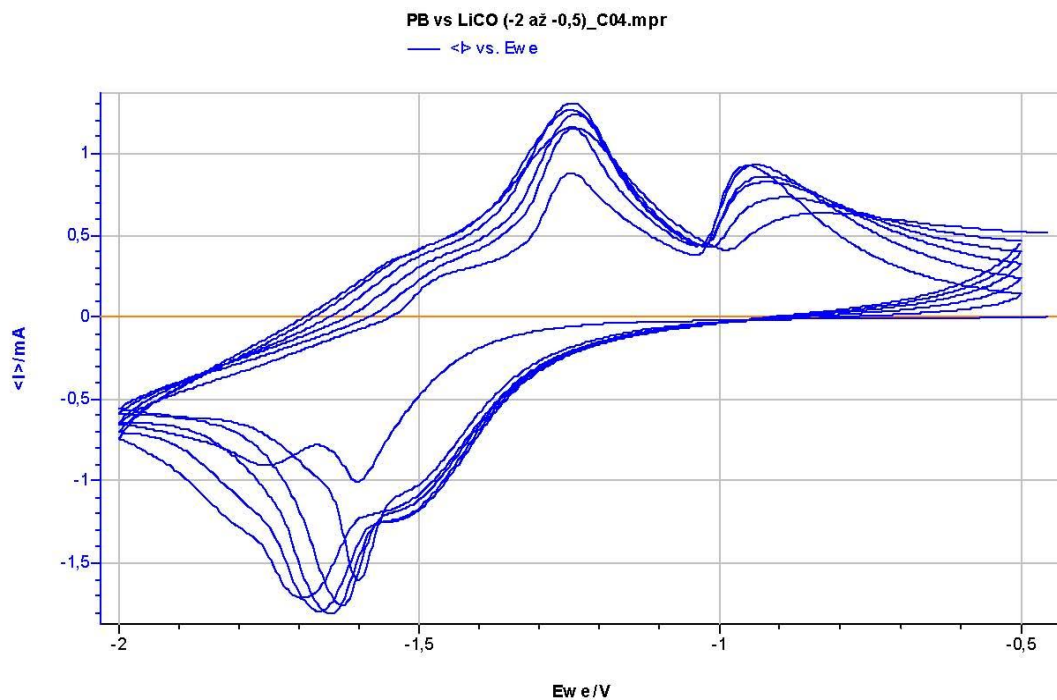


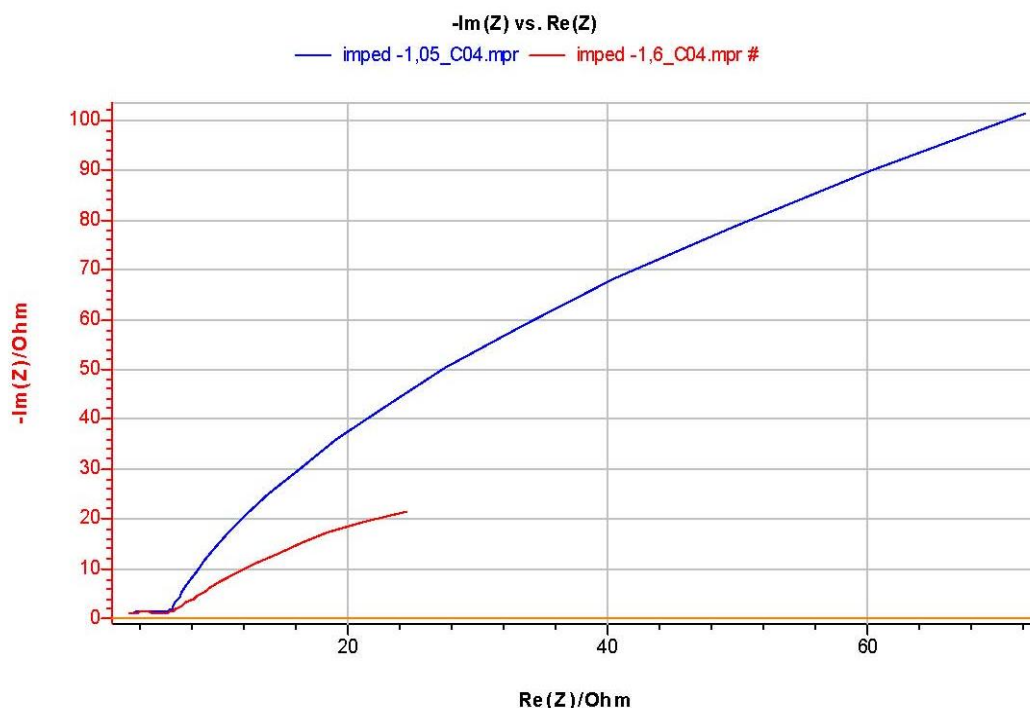
Figure 2. Voltammetry of a model lithium – ion cell

TABLE I. Quantity of lithium estimated from the charge of anodic peaks

Cycle no.	$I_{p,a}$	$Q_{p,a}$	n	Li/Pb (atoms)
1	0.482	964	9.99E-06	0.40
2	0.605	1210	1.26E-05	0.51
3	0.658	1320	1.37E-05	0.55
4	0.700	1400	1.45E-05	0.59
5	0.722	1440	1.50E-05	0.60

$I_{p,a}$ = peak current of anodic peak (mA), $Q_{p,a}$ = it is charge (mC), n = number of atoms (in mole) and Li/Pb is the ratio of named atoms absorbed by the layer

Impedance spectroscopy. The impedance spectrums at -1.05 and -1.6 V are shown in

**Figure 3.** Impedance spectroscopy of the experimental cell at -0,5 (blue) and -1,6 V (red)

We can see that the spectrum at -1.6 V (red curve) is close to a spectrum of an intercalation process on thin electrode layer, and the impedance at that potential is considerably lower.

A simple model containing elements R_1 parallel to Q_1 at high - frequency end and in series connected another chain R_2 and parallel the constant phase element Q_2 (with proper exponent a indicating the phase shift of the element CPE) for low frequencies was used for the description of the model. The high- frequency part corresponds to parasitic element of the cells apparently, while the other can be described as a CPE with phase shift almost 45° as it follows from the theory of porous electrodes. The parameters of the equivalent circuit as estimated by the software of the potentiostat are listed in Tab. 2. The latter component reflects the start of intercalation process quite clearly by its higher admittance.

TABLE II. Components of equivalent circuit of the cell at voltage -1.1 (blue) and -1.6 V (red)

Components	U=-1.05 V	U=-1.06 V
R1	314.900	88.740
Q1	0.001	0.006
a1	0.887	0.764
R2	6.738	7.250
Q2	0.001	0.001
a2	0.501	0.441

Units: Resistance in Ω , CPE in mS

Conclusions

From presented data we can deduce that the electrode material is able to incorporate lithium electrochemically in fairly high quantity, and that this process is reversible. Most likely, this process will not meet practical applications. However, it is interesting as this confirms the ability of similar structures to compensate volume changes caused by intercalation. Further, we can find an evidence for disadvantage of all microstructured or nanostructured materials. This problem arises from extremely thin layers of active materials. Therefore, the absolute capacity of 1 cm² of real working electrode is fairly low even if the parameters related to unit mass of the active materials seem to be interesting.

Investigation of electrodeposition of Si, Ge and Sn continues at the present.

Acknowledgments

This work was supported by the grant FEKT-S-14-2293 "Materials and technologies for electrotechnics II".

Authors gratefully acknowledges financial support from the Ministry of Education, Youth and Sports under projects No. LO1210 – „Energy for Sustainable Development (EN-PUR)“

References

1. Mohamedi, M., et al., Amorphous tin oxide films: preparation and characterization as an anode active material for lithium ion batteries.
2. Electrochimica Acta, 2001. **46**(8): p. 1161-1168.
3. Nasirpour, F., On the electrodeposition mechanism of Pb on copper substrate from a perchlorate solution studied by electrochemical quartz crystal microbalance. Ionics, 2011. **17**(4): p. 331-337.
4. Oh, J., et al., Electrochemical characteristics of Tin-based anode material for Liion secondary batteries. Journal of Ceramic Processing Research, 2008. **9**(1): p. 52-56.
5. Green, M., et al., Structured silicon anodes for lithium battery applications. Electrochemical and Solid State Letters, 2003. **6**(5): p. A75-A79.

Application Of Tosylate-doped poly(3,4-ethylenedioxy-thiophene) (PEDOT:*p*-TOS) and poly-*o*-methoxyaniline (POMA) as cathodic binders for Li-ion batteries

P. R. Das¹, A. Gräfenstein¹, L. Komsiyiska¹, D. Ledwoch¹, O. Osters¹, G. Wittstock²

¹ NEXT ENERGY • EWE Research Centre for Energy Technology at the University of Oldenburg, Carl-von Ossietzky-Str. 15, D-26129 Oldenburg, Germany

² Carl von Ossietzky Universität Oldenburg, Department of chemistry, D-26111 Oldenburg, Germany

Nowadays, conducting polymers (CP) find various technological applications due to their unique properties. For example polythiophene (PT), polypyrrole (PPy), polyaniline (PANI) and their derivatives are used in electrochromic displays, solar cells, sensors or as corrosion protection layers. There are several studies suggesting the use of CP as active electrode materials in Li-Ion batteries [1, 2]. Other studies report that coating the particles of active material by CP improves the overall battery performance [3-5]. An significant enhancement of the capacity of LiFePO₄ cathodes at high rates has been recently ascribed to the substitution of the inactive binder by PANI or PPy [6].

In the present contribution the application of two different CP in LiFePO₄ composite cathodes is demonstrated. Tosylate-doped poly(3,4-ethylenedioxy-thiophene) (PEDOT:*p*-TOS) and poly-*o*-methoxyaniline (POMA) were chemically synthesized and subsequently casted on plasma treated aluminum foil. The redox behavior of the obtained polymer films was studied in a common electrolyte for Li ion batteries using cyclic voltammetry. The PEDOT:*p*-TOS films showed stable capacitive behaviour, whereas in the case of POMA a redox reaction was observed in the potential range between 2.6 V and 4 V (vs. Li/Li⁺).

In addition, slurries containing 84% LiFePO₄, 10% carbon black, 6% binder material of corresponding CP were prepared and casted onto plasma treated aluminum current collector using the doctor blade technique. After drying and compressing process, LiFePO₄/POMA+PVDF and LiFePO₄/PEDOT:TOS+CMC composite layers with thicknesses of ca. 50 μm were obtained. The battery performance and the electrochemical behavior of the composite electrodes were studied in three electrode arrangement using Li-metal as reference and counter electrodes and compared to conventional CP-free LiFePO₄/PVDF cathodes. An increase in the voltage efficiency and the rate capability occurred in the case of the CP-containing cathodes. Furthermore LiFePO₄/POMA+PVDF cathodes showed 15% higher discharge capacity due to the redox reaction of POMA.

References

1. F. Goto, K. Abe, K. Ikabayashi, T. Yoshida, H. Morimoto, J. Power Sources 20 (1987) 243.
2. J. Manuel, Pr. Raghavan, Ch. Shin, M. Heo, J. Ahn, J. Noh, G. Cho, H. Ryu, H. Ahn, Mat. Res. B 45 (2010) 265.
3. A. Fedorková, A. Nacher-Alejos, P. Gómez-Romero, R. Oriňáková, D. Kaniansky, Electrochim. Acta 55 (2010) 943.
4. X. Liu, H. Li, De Li, M. Ishida, H. Zhou, J. Power Sources 243 (2013) 374.
5. Ch. Wu, X. Fang, X. Guo, Ya Mao, J. Ma, Ch. Zhao, Zh. Wang, L. Chen, J. Power Sources 231 (2013) 44.
6. Y. H. Huang and J. B. Goodenough., Chem. Mater. 20 (2008) 7237.

Preparation and Characterization of Graphite Anode for Lithium Ion Batteries

R. M. Humana^{a,b}, M. G. Ortiz^a, J. E. Thomas^a, S. G. Real^a, A. Visintin^a

^a Instituto de Investigaciones Fisicoquímicas Teóricas y Aplicadas (INIFTA), Facultad de Ciencias Exactas, UNLP, CCT La Plata-CONICET, CC 16, Suc. 4, (1900), La Plata, Argentina.

^b Facultad de Ciencias Exactas y Naturales, Universidad Nacional de Catamarca, Av. Belgrano N° 300 (4700), Catamarca, Argentina. E-mail: visintinarnaldo2@gmail.com

The lithium-ion batteries are energy storage systems of high performance and low cost for use in multiple portable devices. These require the use of increasingly smaller and lighter batteries with high energy and power density, fast charging and long service life. Moreover, these systems are promising for use in electric or hybrid vehicles. However, the successful use of the lithium in the field, requires improvements in relation to the properties of electrode materials, such as cost, energy density, cycle life, safety, and environmental compatibility. Currently, investigations are looking to improve the cell configuration by careful selection of the materials and components electrolytic¹. These batteries use carbon as anode material, usually synthetic graphite, because of its high coulombic efficiency and acceptable specific capacity for the formation of intercalation compounds (LiC₆)². Their low voltage increases the potential difference between the electrodes and therefore the energy density of the battery^{3,4}. In this paper, we present the methodology used to prepare and characterize the reversible and irreversible capacity and cyclic stability of graphite materials as anodes in lithium-ion batteries of commercial carbon (CR 1296) and Sungite carbon. We discuss the results obtained using electrochemical techniques for charging and discharging at different current densities, cyclic voltammetry and electrochemical impedance spectroscopy (EIS). Some of these results are presented in Figures 1 and 2.

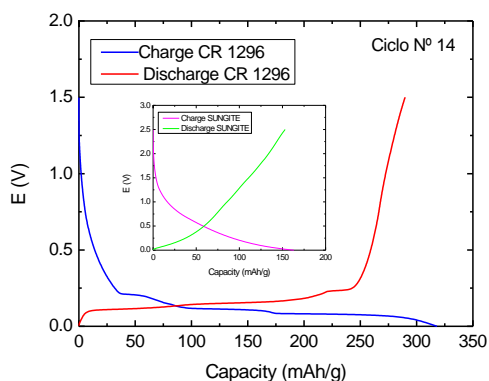


Figure 1. Charge - discharge curves

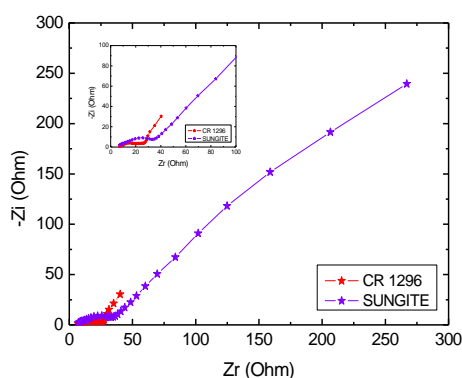


Figure 2. Nyquist's diagrams at 50% SOC.

Acknowledgements

This work was supported by the Agencia Nacional de Promoción Científica (ANPCyT), the Consejo Nacional de Investigaciones Científicas y Técnicas (CONICET) and the Universidad Nacional de La Plata. The authors thank the bilateral cooperation with the Faculty of Electrical Engineering and Communications, Brno University, Czech Republic.

References

1. J. Hassoun, D.-J. Lee, Y.-K. Sun, B. Scrosati, *Solid State Ionics* 202 (2011) 36 - 39.
2. P. Guo, H. Song, X. Chen, *Electrochemistry Communications* 11 (2009) 1320 - 1324.
3. B. Scrosati, *Electrochimica Acta* 45 (2000) 2461- 2466.
4. M. Wakihara, *Materials Science and Engineering* 33 (2001) 109 -134.

Transformations of Thin-Film Electrodes Based on Silicon Composites at Cycling

T.L. Kulova

Frumkin Institute of Physical Chemistry and Electrochemistry of the RAS, Moscow, Russia

tkulova@mail.ru

Introduction

Silicon is known to be very attractive material for negative electrodes of lithium-ion batteries due to its highest capability to insert lithium. At the same time it shows a huge volume change during lithiation. The volume expansion of crystal silicon electrode reaches by up to 400%. This phenomenon causes contraction of the lithiated silicon resulting in its destruction, namely cracking and pulverization. It is known also that certain successes were attained by using porous crystal silicon. In this case, depending on pore configuration the electrode stability at multiple insertion/extraction cycles could be enhanced. However, the development of thin-film electrodes based on amorphous silicon or silicon-composites remains the most promising way in creation of silicon electrodes. Up to now, reliable results on the cycling of the electrodes with 200-500 nm amorphous silicon films during 100-500 cycles were reported. Increase in film thickness (necessary for obtaining reasonable capacity per area unit) results in considerable degradation rate. The electrodes with silicon-oxygen-aluminum (Si-O-Al) composites demonstrate stable cycling at film thickness up to 2.5 μm , however increase of its thickness to 5 μm accompanies by fast degradation. The present work is aimed at studying of morphological and structural changing of such composite electrodes.

Experimental

The composite electrodes were synthesized with layer-by-layer magnetron sputtering of silicon and aluminum in oxygen environment onto titanium-foil supports. The thickness of the titanium-foil was about 10 μm . Thickness and morphology of initial composites and composites after 35 and 100 cycles were studied with high resolution scanning electron microscope (SEM) SUPRA 40. The electrochemical measurements were carried out in three-electrode cells with lithium auxiliary and reference electrodes. 1 M LiPF_6 in the mixture of ethylene carbonate, diethyl carbonate, and dimethyl carbonate (1:1:1) was used as an electrolyte. Before SEM investigation the cycled electrodes were washed with dry dimethoxyethane.

Results and Discussion

Figure 1 demonstrates cross section (split) of initial layered film with thickness *ca.* 2 μm (Fig. 1a). Dark strips correspond to amorphous silicon, whereas light strips correspond to areas enriched with aluminum. The higher magnification gives a possibility seeing columnar morphology of the composite film. Average atomic composition of the film was 80.9% Si, 11.8% O, and 7.3% Al.

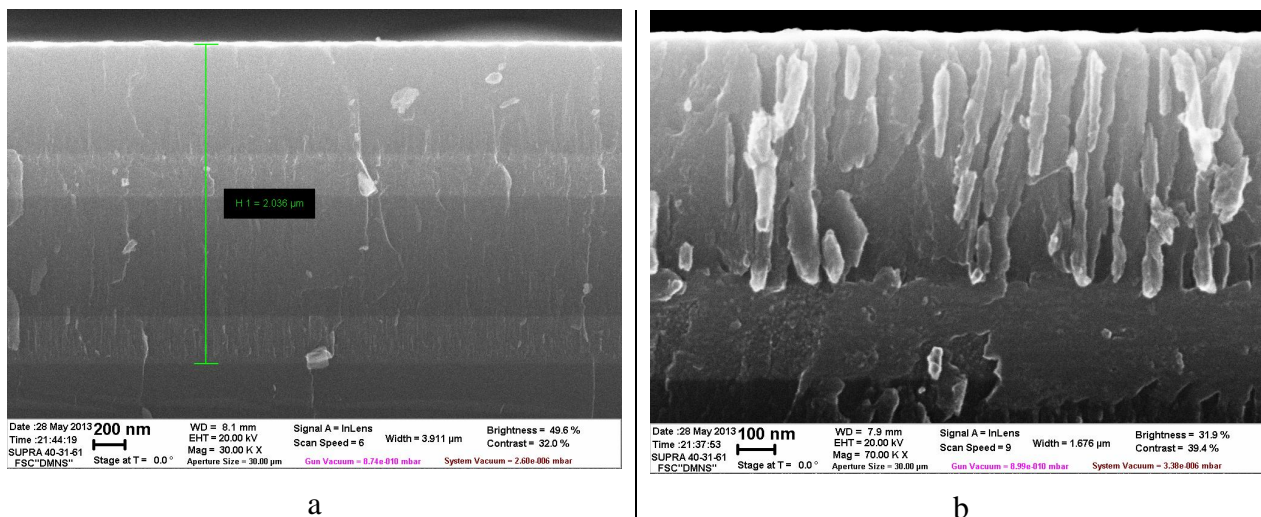


Figure 1. Cross-section of fresh-made composite electrode at lower (a) and higher (b) magnifications.

Fig. 2 shows results of galvanostatic cycling of the electrode with current density 0.1 mA/cm^2 (ca. 265 mA/g). One can see initial raise of discharge capacity during the first 10 cycles with rather stable cycling from tenth to thirty-fifth cycles and with following decline.

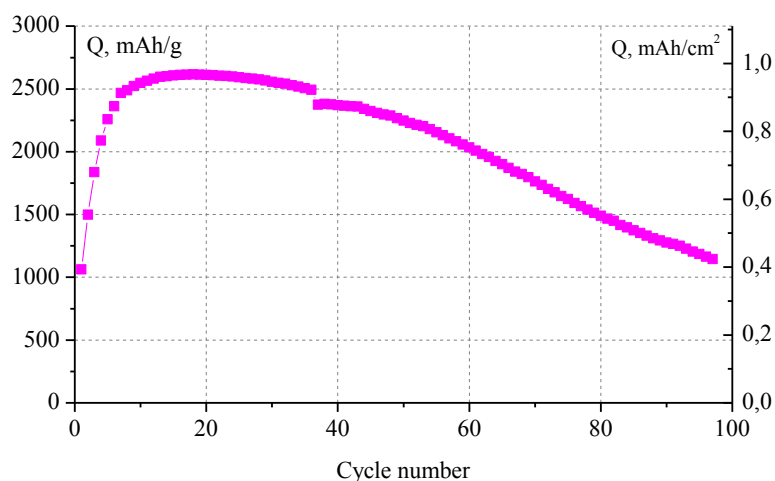


Figure 2. Cycling performance of the composite electrode.

Even after 38 cycles the appearance of the electrode has changed, and first of all, it became inhomogeneous. One can reveal at least two different areas at the electrode surface after such cycling, specifically, more light area, denoted as S1 and more dark area denoted as S2. Cross sections (splits) of these areas can be seen in Fig. 3.

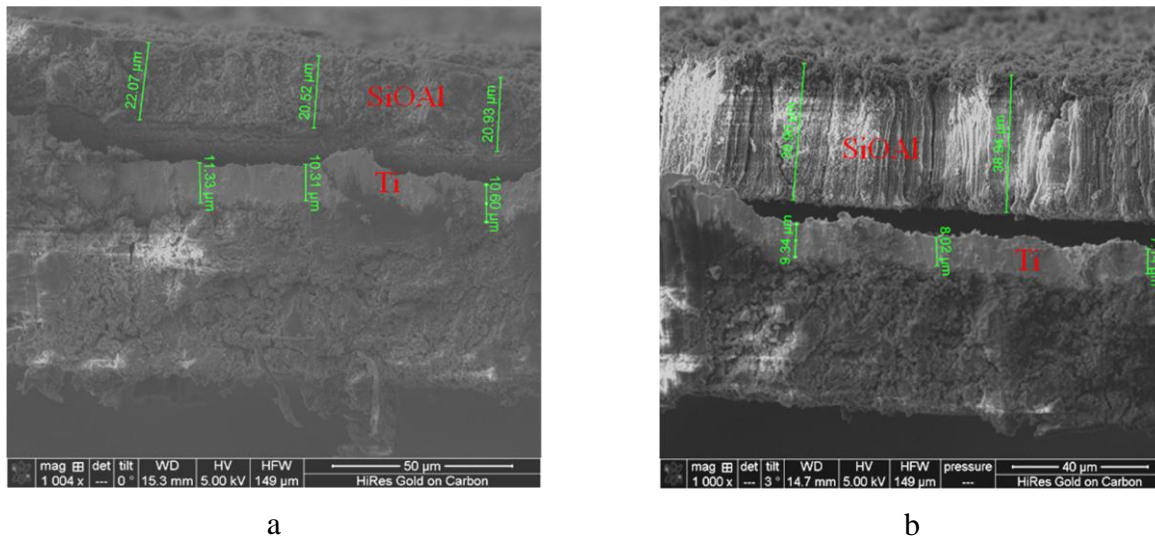


Figure 3. Cross section of area S1 (a) and area S2 (b) of the electrode after 38 cycles

The salient feature of Fig. 3 consists in considerable increase in film thickness in the result of cycling. The film thickness in the area S1 raised about ten-fold, and the film thickness in the area S2 raised about eighteen-fold (!). Similar effect, namely huge volume increase in the course of cycling was documented, e.g. in [1].

One can see also partial peeling-off the film (Fig. 3b), which is one of reasons of electrode degradation.

More prolonged cycling resulted in much more increase of film thickness. Fig. 4 shows cross section of two areas of the electrode after 100 cycles.

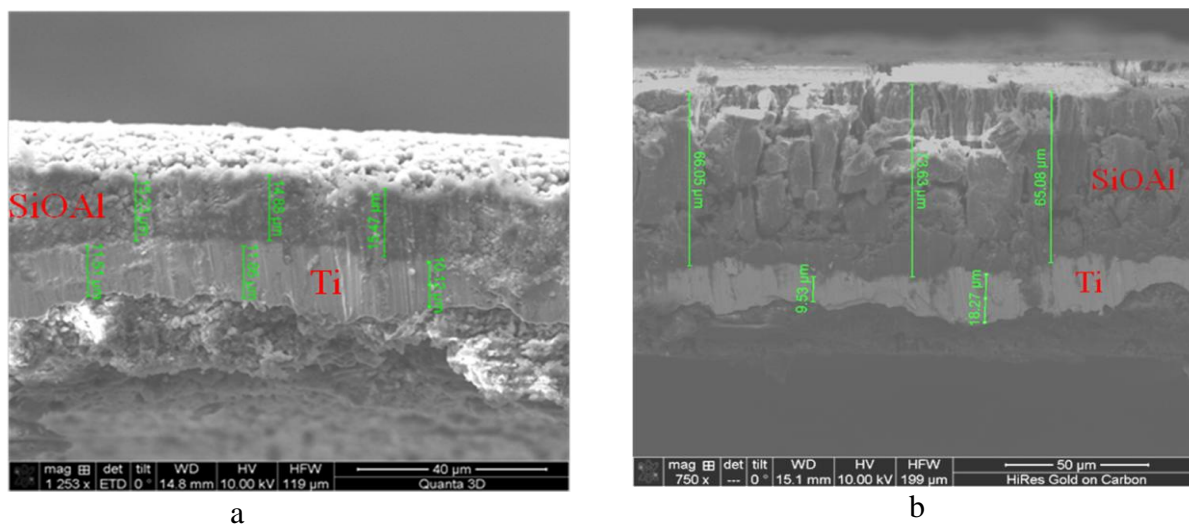


Figure 4. Cross section of two different areas of the electrode after 100 cycles

Fig. 4 demonstrates even high unevenness of the composite film. The film thickness in one area was as small as 15 μm, whereas thickness of other part of film was more than 65 μm. In this case some part of film was connected with solid electrolyte interphase. Average atomic composition of the film after 100 cycles was 18.19% Si, 34.45% O, 3.36% Al, 22.04% C, 13.11 F, 8.85% P.

Acknowledgement

This work was financially supported by Presidium of Russian Academy of Sciences, Program “Fundamental Researches to the benefit of development of Russian Federation Arctic zone”.

Reference

1. K. Nishikawa, H. Munakata, K. Kanamura. J. Power Sources. 2013. V. 243. P. 630-634.

Surface Chemistry of Lithium-ion Battery Electrodes in Several Electrolyte Systems

E. M. Erickson, Ch. Ghanty, H. Sclar, O. Srur-Lavi, Y. Gofer, M. Weitman, B. Markovsky,
D. Aurbach

Department of Chemistry, Bar-Ilan University, Ramat-Gan, Israel 52900

Abstract

Lithium ion battery (LIB) electrodes operate in severe regimes that cause partial decomposition of the electrolyte solutions, resulting in the formation of electrode surface films. On graphitic anodes, this film, the solid-electrolyte interphase (SEI), is extremely important because it protects the graphite from exfoliation during cycling. At cathodes, stable surface films can protect the electrolyte from further breakdown that increases cationic resistance through thicker film formation and lithium inventory loss. In recent years much attention has focused on the use of additives such as lithium bis(oxalato)borate (LiBOB) and vinylene carbonate (VC) to electrolyte solutions that can stabilize these SEI films at both electrodes.

The goal of our research is to characterize the films formed from these additives both with composite electrodes and through a fundamental potential dependent study on bare metal electrodes (Al and Cu), exploring the organic electrochemistry of LiBOB and VC additives. We will rely on AC impedance spectroscopy of positive and negative electrodes as well as surface characterization techniques such as XPS.

In this presentation we will demonstrate the impedance spectra of graphite anodes as well as Li[NiCoMn]O₂ cathodes in additive-free 3:7 EC:EMC/LiPF₆ solution and in those containing 0.25 wt % LiBOB and 2 wt % VC, through progressive cycling. It was established that the anode and cathode surface film impedance demonstrates a complex behavior upon cycling and second, that it is electrolyte dependent.

Impedance spectra fits will be utilized for modelling of film development throughout cycling. Conclusions from chronoamperometric measurement dependence on cycle number, additive and temperature will be used to explore the possible mechanisms of LiBOB and VC chemical and interfacial reactions.

Study of the electrochemical behaviour of lithium Iron phosphate doped by chromium and nickel

A. Chekannikov¹, R. Kapaev², S. Novikova², T. Kulova¹, A. Skundin¹, A. Yaroslavtsev²

¹⁾ A.N. Frumkin Institute of Physical chemistry and Electrochemistry Russian academy of sciences

²⁾ N.S. Kurnakov Institute of General and Inorganic Chemistry of the Russian Academy of Sciences
tkulova@mail.ru, andrey.chekannikov@gmail.com

Lithium iron phosphate is a prospective material for a lithium-ion battery positive electrode. The main disadvantage of LiFePO₄ is low electronic conductivity. Synthesis of LiFePO₄/carbon composites allows to increase electronic conductivity significantly. However, carbon in this composite material is not an active material. As a result, specific discharge capacity per weight of the total composite material will strongly depend on the percentage of carbon. Another way to increase the conductivity of lithium iron phosphate is doping of the material by the ions of transition metals. In this case, the doping ions can change their oxidation degree in the process of intercalation-extraction, i.e. participate in the electrochemical process and simultaneously enhance the electronic conductivity of lithium iron phosphate.

In this paper samples of pure and doped lithium iron phosphate of the following compositions were synthesized: LiFePO₄/C, Li_{0.99}Fe_{0.98}(CrNi)_{0.01}PO₄/C, Li_{0.975}Fe_{0.95}(CrNi)_{0.025}PO₄/C и Li_{0.95}Fe_{0.9}(CrNi)_{0.05}PO₄/C. All the samples were synthesized by the sol-gel method. Physicochemical properties of the samples were characterized by X-ray phase and thermogravimetric analysis and scanning electron microscopy. According to the received data all lithium iron phosphate samples crystallize in the orthorhombic modification of lithium iron phosphate with olivine structure. Average particle size of the obtained material varies between 50-100 nm. The carbon content was 4 wt%.

Electrodes for electrochemical studies were made by pasting the material (85% active material, 10% carbon black and 5% polyvinylidene fluoride dissolved in anhydrous N-methylpyrrolidone) on a substrate. Stainless steel mesh was used as a current collector. The electrochemical cell assembled in a sealed box with a dry argon atmosphere, contained a working electrode, a lithium counter electrode and the lithium reference electrode. The mass of LiFePO₄ on substrate was about 6–10 mg/cm². Electrochemical studies were performed in galvanostatic and potentiodynamic modes. The current density ranged from 20 to 1600 mA/g. Potential sweep rate was 0.1 mV / s. The solution of 1M LiPF₆ in a mixture of ethylene carbonate, diethyl carbonate, dimethyl carbonate (1:1:1) was used as electrolyte.

Figure 1 shows the change in discharge capacity of the investigated samples during cycling, as well as the charge-discharge curves for the second cycle. The discharge capacity of the undoped lithium iron phosphate on the first cycle at a current density of 20 mA/g was about 137 mA/g (theoretical capacity of LiFePO₄ is 170 mAh/g). It has been found that doping results in decreasing of the discharge capacity. Thus the discharge capacity of Li_{0.99}Fe_{0.98}(CrNi)_{0.01}PO₄/C, Li_{0.975}Fe_{0.95}(CrNi)_{0.025}PO₄/C and Li_{0.95}Fe_{0.9}(CrNi)_{0.05}PO₄/C samples reached 90, 109 and 123 mAh/g respectively.

Comparison of lithium iron phosphate charge-discharge curves with varying degrees of doping showed that doping increases the charge and discharge voltages. In addition doping reduces the difference between charge and discharge voltages (from 66 mV for LiFePO₄ / C to 53-54 mV for doped samples at a current density of 20 mA/g). Moreover, the shape of

$\text{Li}_{0.975}\text{Fe}_{0.95}(\text{CrNi})_{0.025}\text{PO}_4/\text{C}$ charge-discharge curve has changed (the second charge-discharge area has appeared).

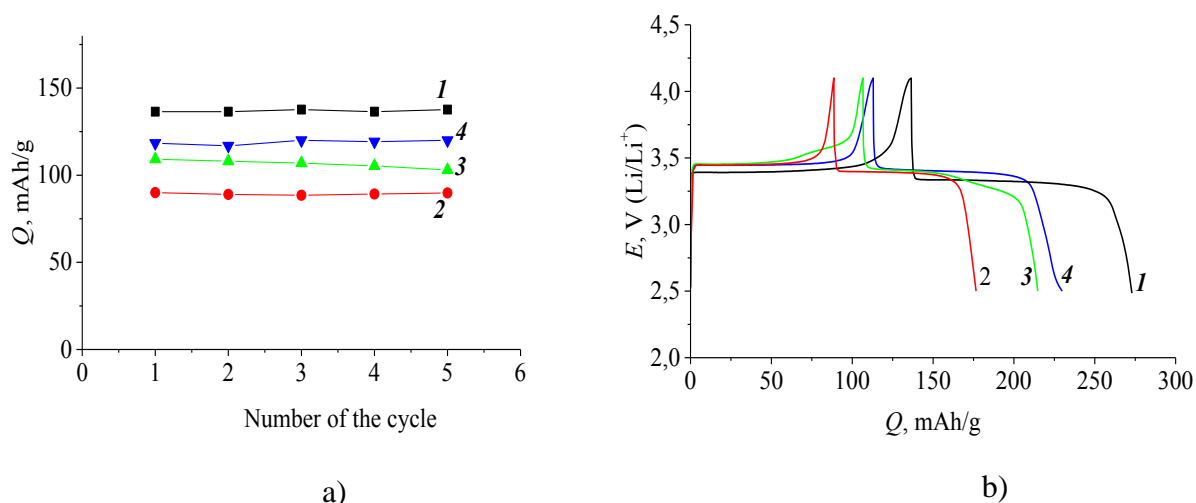


Figure 1. Changing of the discharge capacity during cycling (a) and charge-discharge curves (b) of lithium iron phosphate samples. Current density 20 mA/g. 1 – LiFePO_4/C , 2 – $\text{Li}_{0.99}\text{Fe}_{0.98}(\text{CrNi})_{0.01}\text{PO}_4/\text{C}$, 3 – $\text{Li}_{0.975}\text{Fe}_{0.95}(\text{CrNi})_{0.025}\text{PO}_4/\text{C}$, 4 – $\text{Li}_{0.95}\text{Fe}_{0.9}(\text{CrNi})_{0.05}\text{PO}_4/\text{C}$

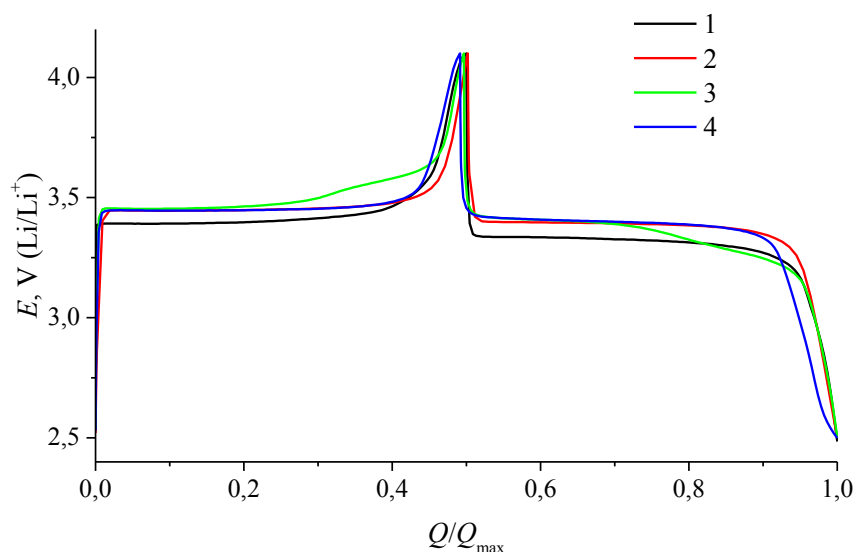


Figure 2. Charge-discharge curves of lithium iron phosphate samples 1 – LiFePO_4/C , 2 – $\text{Li}_{0.99}\text{Fe}_{0.98}(\text{CrNi})_{0.01}\text{PO}_4/\text{C}$, 3 – $\text{Li}_{0.975}\text{Fe}_{0.95}(\text{CrNi})_{0.025}\text{PO}_4/\text{C}$, 4 – $\text{Li}_{0.95}\text{Fe}_{0.9}(\text{CrNi})_{0.05}\text{PO}_4/\text{C}$.

Figure 3 shows the change in discharge capacity of lithium iron phosphate samples at different current densities, and the discharge capacity of the samples (Q) vs logarithm of the current density (i). This charts can be linearized with some approximation as $Q_n = Q_0 - k \lg i$, in the same time coefficient k for $\text{Li}_{0.99}\text{Fe}_{0.98}(\text{CrNi})_{0.01}\text{PO}_4/\text{C}$, $\text{Li}_{0.975}\text{Fe}_{0.95}(\text{CrNi})_{0.025}\text{PO}_4/\text{C}$ and $\text{Li}_{0.95}\text{Fe}_{0.9}(\text{CrNi})_{0.05}\text{PO}_4/\text{C}$ samples was 33, 39.5 and 41, respectively. For undoped samples coefficient k was 46.6, indicating stronger dependence of discharge capacity from current density for LiFePO_4/C compared with doped samples.

The dependence of discharge capacity from the current density i can be represented in logarithmic coordinates corresponding to the well-known Peukert's equation $Q = Q_0/i^\alpha$. For LiFePO_4/C and $\text{Li}_{0.975}\text{Fe}_{0.95}(\text{CrNi})_{0.025}\text{PO}_4/\text{C}$ this dependencies can be linearized in the entire range of investigated current densities. Besides, exponent α for LiFePO_4/C and $\text{Li}_{0.975}\text{Fe}_{0.95}(\text{CrNi})_{0.025}\text{PO}_4/\text{C}$ is 0.19 and 0.24 respectively. For $\text{Li}_{0.99}\text{Fe}_{0.98}(\text{CrNi})_{0.01}\text{PO}_4/\text{C}$ and $\text{Li}_{0.95}\text{Fe}_{0.9}(\text{CrNi})_{0.05}\text{PO}_4/\text{C}$ dependence $\lg Q$ from $\lg i$ splits in two sections with exponent α equal to 0.18 at small current densities and 0.51 at high current densities. The physical meaning of exponent α for two-phase electrode is a subject of a separate review.

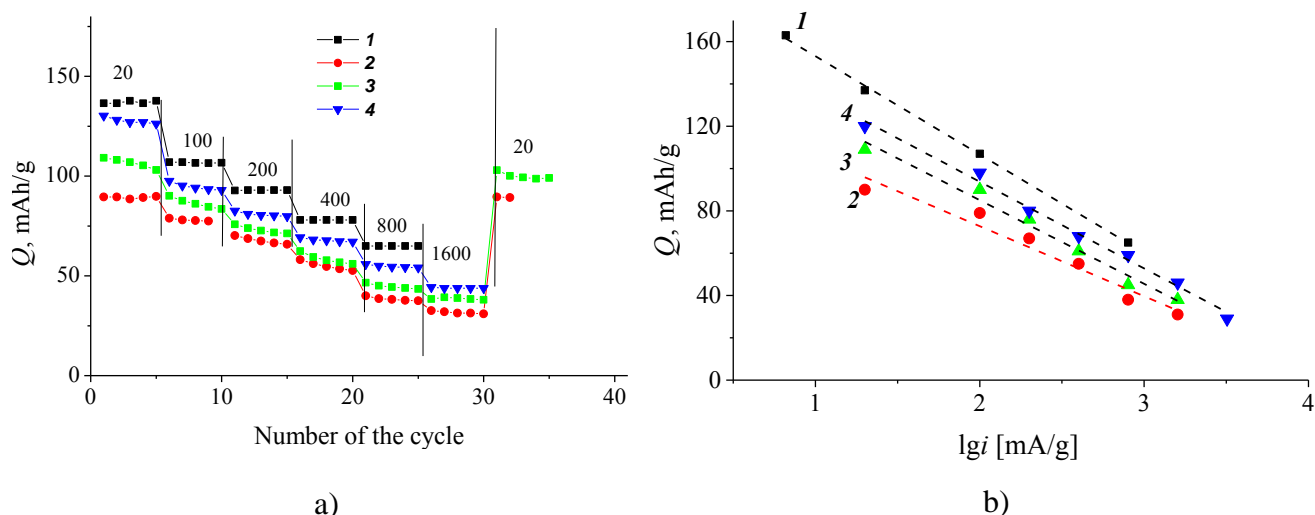


Figure 3. Changes in the discharge capacity during cycling (a) and the dependence of discharge capacity from current density in semi logarithmic coordinates (b) for samples of lithium iron phosphate. Current densities [mA / g] are shown on the figure. 1 – LiFePO_4/C , 2 – $\text{Li}_{0.99}\text{Fe}_{0.98}(\text{CrNi})_{0.01}\text{PO}_4/\text{C}$, 3 – $\text{Li}_{0.975}\text{Fe}_{0.95}(\text{CrNi})_{0.025}\text{PO}_4/\text{C}$, 4 – $\text{Li}_{0.95}\text{Fe}_{0.9}(\text{CrNi})_{0.05}\text{PO}_4/\text{C}$

Conclusion

Lithium iron phosphate samples doped simultaneously with chromium and nickel were synthesized by sol-gel method. Electrochemical studies showed that doping results in a decrease in discharge capacity of lithium iron phosphate compared with undoped sample. At the same time the dependence of discharge capacity versus current density for all of the doped samples is less pronounced. Despite the fact that insertion of a nickel-chromium dopant reduces the discharge capacity of LiFePO_4/C , quantitatively this effect decreases with increasing dopant content. This result contradicts the results obtained previously [1], and may show that the amount of a dopant and the size of particles of the doped samples have a comprehensive effect on the discharge capacity.

Acknowledgements

This study was financially supported by the Ministry of Education and Science of Russian Federation (Agreement no. 14.604.21.0126).

References

1. Novikova S., Yaroslavtsev S., Rusakov V., Kulova T., Skundin A., Yaroslavtsev A. // *Electrochimica Acta*. 2014. V. 122. P. 180 – 186.

In Situ Investigation on Spatiotemporal Changes of SEI Properties by SECM

H. Bülter¹, F. Peters², J. Schwenzel², G. Wittstock¹

¹Carl von Ossietzky University, Institute of Chemistry, 26111 Oldenburg, Germany

²Fraunhofer Institute for Manufacturing Technology and Advanced Materials IFAM, 26129 Oldenburg, Germany
heinz.buelter@uni-oldenburg.de

In our society Li-ion batteries are widely used, especially for small-scale devices. During the first charging process the solid-electrolyte-interface (SEI) between the electrode and electrolyte is formed by the decomposition of electrolyte components at the strongly reducing lithiated graphite. This layer is critical for the performance and safety of the Li-ion batteries.^[1] Characterization of the SEI is a difficult challenge, because of the variety of chemically similar components and enclosed electrolyte species. Furthermore, *ex situ* analysis of the SEI requires separation and isolation of the SEI, which may change the content and the structure of the SEI.^[2]

In our approach we use the feedback mode of scanning electrochemical microscopy (SECM) to investigate *in situ* the passivating properties of the SEI (Figure 1). Our results by SECM show *spatiotemporal* changes and demonstrate the dynamic behavior of SEI formation, damage and reformation. The results emphasize that *spatiotemporal* changes of the passivating SEI properties are highly localized. Further research using this methodology addresses specific consequences of solution additives on SEI formation/stability as well as the response of the SEI towards well defined mechanical stress within graphite electrodes. In addition, the volume changes of graphite composite anodes in standard battery electrolytes are characterized.

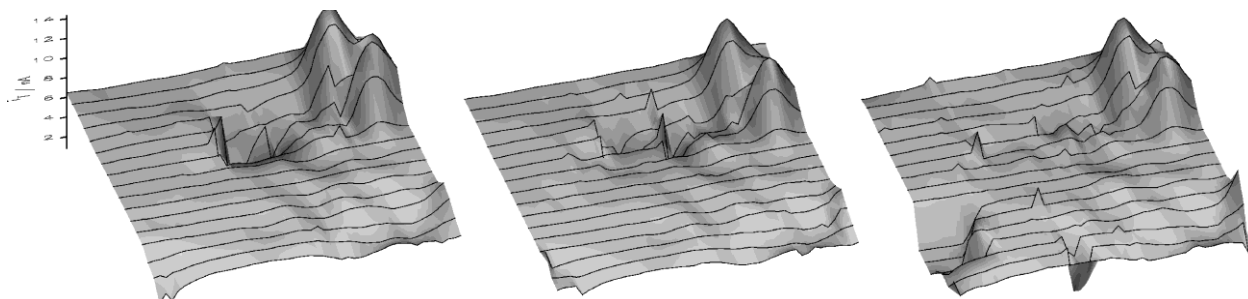


Figure 1. *In situ* observation of passivating SEI properties on a $240\ \mu\text{m} \times 240\ \mu\text{m}$ region of a graphite composite electrode over a time span of 4 hours.

References

1. S. Krueger, R. Kloepsch, J. Li, S. Nowak, S. Passerini, M. Winter, *J. Electrochem. Soc.* **2013**, *160*, A542.
2. P. Verma, P. Maire, P. Novák, *Electrochim. Acta* **2010**, *55*, 6332.

Fundamental aspects of noble metal doped LiFePO₄ cathode for Li-ion batteries applications.

O. Savadogo* and M. Talebi-Esfandarani

Laboratory of New Materials for Electrochemistry and Energy
Polytechnique Montréal
C.P. 6079, Succ. Centre Ville, Montréal, QC
Canada H3C 3A7

*Corresponding author: osavadogo@polymtl.ca , Phone: +1 514 3404725

Abstract

LiFePO₄/C and LiFe_{0.96}Pt_{0.04}PO₄/C nano composite cathode materials were synthesized using the sol-gel method in a nitrogen atmosphere. The XRD results indicate that substituting iron with platinum does not destroy the structure of LiFePO₄, but expands the lattice parameters and enlarges the cell volume. The electrochemical results show that platinum doping improves the electrochemical performance of LiFePO₄/C particles owing to the expansion of the lattice structure, which provides more space for Li ion diffusion. The, larger lattice structure parameters of the LiFe_{0.96}Pt_{0.04}PO₄/C material result in a high discharge capacity of 139 mAh g⁻¹ at rates of 10 C, as compared to 105 mAh g⁻¹ for undoped LiFePO₄/C

LiFePO₄ and LiFe_{0.96}Pt_{0.04}PO₄ composites were also synthesized using hydrothermal method.

The XPS results indicated that platinum doping does not change the chemical state of Fe (II). The SEM and BET results showed that platinum doping reduces the size of the particles. The electrochemical characterization of the electrodes using discharge capacity, cyclic voltammetry (CV) and electrochemical impedance spectroscopy (EIS) showed that the Li-ion cell based on LiFe_{0.96}Pt_{0.04}PO₄/C electrode exhibited better charge /discharge performance than those of LiFePO₄/C sample.

LiFePO₄/C, LiFe_{0.98}Pd_{0.02}PO₄/C, and LiFe_{0.96}Pd_{0.04}PO₄/C composite cathode materials were then synthesized using the sol-gel method. The results indicate that palladium doping facilitates the formation of impurities, like Li₃PO₄. Also, the lattice parameters of the LiFePO₄ structure decrease in size as the palladium content increases. The electrochemical results show that palladium doping decreases the electrochemical performance of LiFePO₄/C, owing to shrinking lattice parameters and the difficulty of achieving the diffusion of lithium ions into the structure during the intercalation/de-intercalation process. These results suggest that palladium doping by sol-gel method changes significantly the LiFePO₄ structure which may impact its performances as cathode for the lithium ion battery applications.

LiFePO₄ material was also synthesized using a hydrothermal method and different amounts of carbon from citric acid as the carbon source. LiFePO₄ coated with a small amount of carbon results in poor electrochemical performance, and too much carbon can prevent Li ion diffusion through the structure of the material and decrease its specific capacity. The thickness of the carbon coating must therefore be optimized. The LF/30C electrode shows the lowest value for R_{ct}, and the highest Li ion diffusion coefficient (1.62×10⁻¹³ cm²s⁻¹) rather than the other electrodes, due to the high electrical conductivity of the electrode and/or mobility of the Li ion. The LF/30C electrode exhibited the best specific discharge capacity of 167 mAh g⁻¹, which is close to the theoretical capacity of

LiFePO₄(170 mAh g⁻¹). The interpretations of these results need new approaches. The fundamental aspect related to the effect of the method of material preparation on these physical chemical and electrochemical performances will be discussed.

References

1. J. App. Electrochemistry (2014), in press
2. J. New Materials for Electrochemical Systems (2014), in press
3. Solid State Ionics (2014), in press

Diffusion of Li⁺ in Thin Film Vanadium Oxides for Lithium Batteries

R.D. Apostolova¹, V.P. Tsyachny¹, A. Markevich¹, O.S. Ksenzhek¹, E.M. Shembel¹,
B. Markovsky², D. Aurbach²

¹ Ukrainian State University of Chemical Technology, 5 Gagarin Ave.
Dnepropetrovsk

² Department of Chemistry, Bar-Ilan University, Ramat-Gan 52900
Israel

The electrochemical insertion of the Li⁺-ions during discharge in thin films of vanadium oxides V₂O_y is determined by their stoichiometry, thickness, structural and transport properties, the discharge rate and other factors. Among transport properties, the kinetic parameter – the effective diffusion coefficient of the lithium ions (DLi) plays an important role. We have established that the stoichiometry of the electrolytic deposits of vanadium oxides e-V₂O_y obtained from the oxovanadate solutions [1] depends upon the synthetic conditions and it varies from V₂O_y (y=4.3) to the orthorhombic V₂O₅ composition after the thermal treatment.

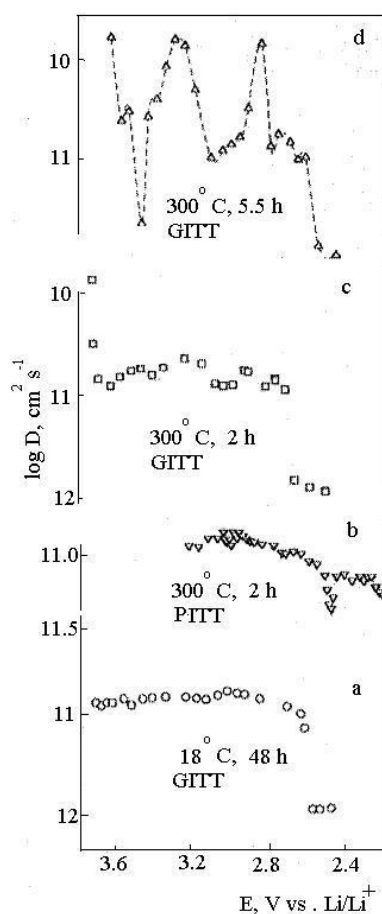


Figure 1.

GITT and PITT measurements of D_{Li}

We used a mathematical model of diffusion that does not include phase transitions in the electrode material in order to describe the Li discharge processes in V_2O_y thin films and demonstrated that increasing the V_2O_y film thickness up to 1.4 μ results in the discharge capacity of 3.2 C/cm² at the current density of 20 μ A/cm². It was found that the steady-state potential (both the theoretical value and that calculated from the experimental results) depends linearly upon the Li-intercalation level in the range of 0.3 – 0.7 x ($Li_xV_2O_5$).

For the vanadium oxides annealed at 350 – 450° C, the dependence of D_{Li} vs. electrode potential (E) is non-linear and demonstrates extreme values, which tend to increase with the increasing the annealing temperature. The minimal values of the diffusion coefficient correspond to the peak currents registered from the slow rate cyclic voltammograms of the V_2O_5 electrode that may relate to the phase transitions in the oxide.

Fig.1 demonstrates log D vs. E functional relationships obtained for vanadium oxide electrodes with a different thermal treatment. The value of D_{Li} remains almost constant (10^{-11} cm²/s) in a 3.7–2.4 V potential range in the case of a thermally nontreated electrode (fig.1 a).

There is a pronounced decrease of the D_{Li} values up to 10-12 cm²/s only at a discharge potential of 2.6 V. D_{Li} -evolution for crystalline V_2O_5 becomes complex and has extremes (Fig. 1 c, d). D_{Li} values obtained by GITT and PITT measurements correspond well with each other (Fig.1 b, c).

D_{Li} of the e- V_2O_y obtained upon Interruption current A mathematic diffusion model of Partly-Discharged $Li_xV_2O_5$ thin film electrodes upon Interruption current is put forward. The films were obtained by anodic deposition on stainless steel plates from 0.1 M vanadyl sulfate solutions at pH 1.65 [1] and were dried for 2.5 h at 120° C. Fig. 2 shows schematically the sequence in which the experimental curves were measured.

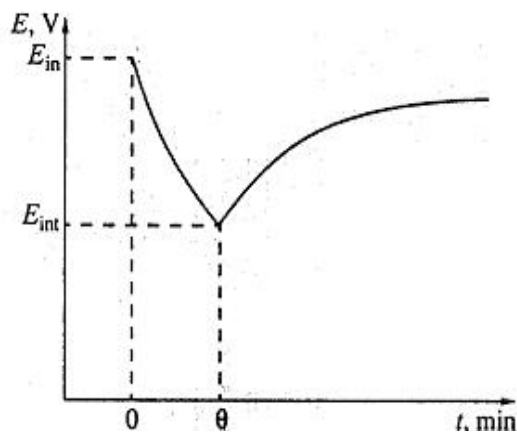


Figure 2. Scheme of the OCP measurements for Partly-Discharged $Li_xV_2O_5$ electrodes.

The electrode was discharged by applying a current (I) of 20 μ A/cm² from the potential E_{in} , which corresponds to an equilibrium state, to a final potential E_{int} . Then the current was switched off and the potential transient was measured for 6 h.

The potential growth rate upon interruption discharge current is proportional to the discharge current and inversely proportional to the film thickness (1):

$$\ln\left(\frac{dE_{t-\theta}}{dt}\right) = \ln \frac{IV_M (-dE_{eq}/d\delta)}{FL} - \frac{\pi^2 D}{L^2} (1-\theta) \quad (1)$$

VM – molar volume, δ – film thickness, F – Faraday constant, L – diffusion length, D – diffusion coefficient. According to (1), in the dE/dt vs. $(t - \theta)$ coordinates, we have a straight line, the slope of that allows the chemical diffusion coefficient of lithium ions to be calculated, and the intercept on the y-axis allows $dE_{eq}/d\delta$ to be assessed.

The mathematic model for the behavior of partly discharged electrodes upon interruption of the current was tested on 1.5 μm -thick V_2O_5 films. Fig. 3 shows the dependence of OCP for such a film on the Li intercalation degree x . In the range of x values from 0.3 to 0.74 the potential decreases linearly. Fig. 4 exemplifies the experimental transients of OCP for different current-interruption potentials.

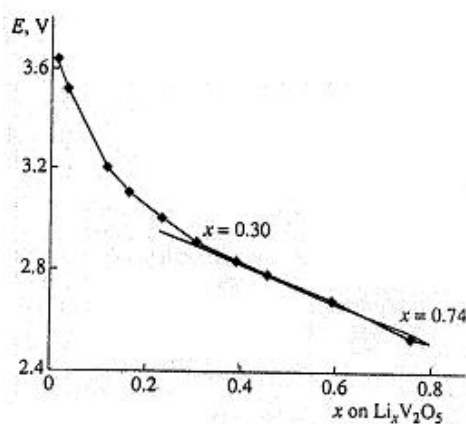


Figure 3. The dependence of OCP for V_2O_5 film on the Li intercalation degree x .

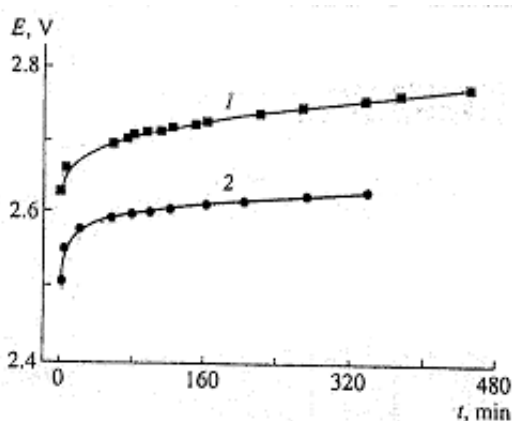


Figure 4. Variations in OCP for an $\text{Li}_x\text{V}_2\text{O}_5$ electrode at current-interruption potentials (1) 2.63 and (2) 2.50 V.

It is worth to note that the dependences of $\lg D_{\text{Li}} - E$ obtained for the Li-insertion in thin V_2O_5 films by PITT, GITT, and potential relaxation methods coincide well with one another and are in agreement with those measured for the sputtered V_2O_5 [2]. We have established that D_{Li} varies from 10-10 to 10-12 cm^2/s in the potential range of 3.7 – 2.0 V for vanadium oxide film annealed at 350–450° C.

The method of the network thermodynamics [3] was also used in this work to analyze diffusion coefficient of the Li⁺ in the intercalation processes corresponding to the following phase transition $\varepsilon \leftrightarrow \delta$ in V₂O₅ (2):



The method of the network thermodynamics is based on the mathematical model of diffusion of the Li⁺ in electrode material using the diffusion equation for one-dimensional system:

$$\frac{\partial c}{\partial t} = D \cdot \frac{\partial^2 c}{\partial x^2} \quad (3)$$

Equation (3), according to principles based on the network thermodynamics, may be transformed to the equation (4) [3]:

$$Z(t) = A1 \cdot \left\{ A0 \cdot t - 2 \cdot \sum_{k=1}^{\infty} \frac{1}{k^2} \exp[k^2 \cdot A0 \cdot t] \right\} + A2 \quad (4)$$

Where

$$A0 = \frac{\pi^2 \cdot D_{\text{Li}^+}}{\delta^2} \quad A1 = \frac{RT \cdot \delta}{(nF)^2 \cdot c \cdot D_{\text{Li}^+} \cdot \pi^2} \quad (5), (6)$$

$$A2 = R_f + A1 \cdot \frac{\pi^2}{3} \quad (7)$$

k – quantity of the exponents in the equation (4); t – relaxation time, s; δ – thickness of the electrochemical active layer, cm; D_{Li} – diffusion coefficient of the Li⁺ in the electrode structure, (cm²/s); R – gas constant, 8.31 J/mol•K; T – temperature, K; n - number of electrons in the electrochemical process (2); R_f – resistance of the electrode, $\Omega \cdot \text{cm}^2$. Equation (4) was used for approximation of the relaxation curves.

The description of research methods:

1. Method of current relaxation and transformation of this curve to relaxation of impedance during time.
2. Approximation of the relaxation curves according to the equation obtained on the basis of principles of the network thermodynamics. The goal of this approximation is determination of the variable factors (A0, A1 and A2) in the equation (4). Satisfactory approximation result can be obtained for k=3.
3. Calculation of the Li⁺ diffusion coefficient into V₂O₅ electrode according to the equation (5).

In the fig. 5 is shown relaxation of the current in time (curve a) and relaxation of the impedance of the electrode process (curve b). Last curve was obtained as a result of the next function:

$$Z(t) = \frac{\Delta E}{i(t)} \quad (8)$$

Where ΔE – step of the potential, V; i – current of relaxation, A/cm².

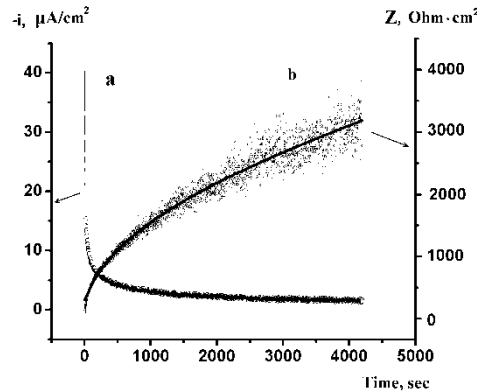


Figure 5. Change of a current (a) and impedance (b) in time. Amplitude of displacement of potential is 5 mV. Initial potential of V₂O₅-electrode is 3.20 V.

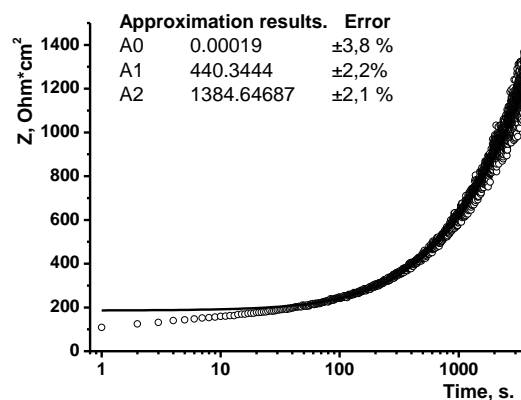


Figure 6. Change of impedance in time (curve b) transformed to the semi logarithmic coordinate. $k = 3$.

The example of the approximation result is shown on the fig. 6. Using these results for each potential of the V₂O₅ electrode (shown in fig.7), the diffusion coefficients of the Li⁺ in the electrode material structure was calculated and shown in the fig. 8.

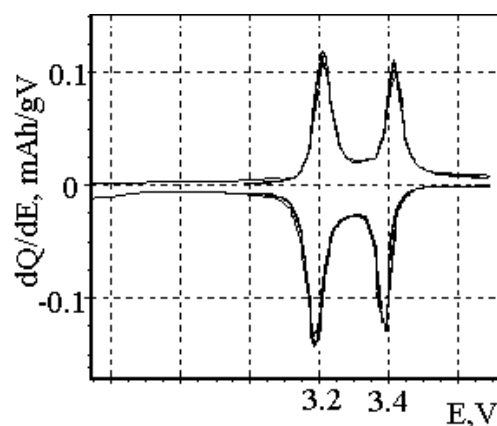


Figure 7. Dependence of the differential capacity of V₂O₅-electrode on the electrode potential.

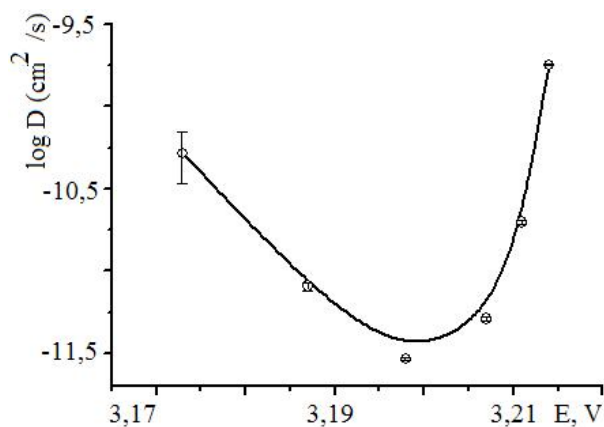


Figure 8. The Li⁺ diffusion coefficient at various potentials of V₂O₅-electrode.

References

1. E. Shembel, R. Apostolova, V. Nagirny, D. Aurbach, B. Markovsky, J. Power Sources 80–82 (1999) 480.
2. M.D. Levi, Z. Lu, D. Aurbach, Solid State Ionics 143 (2001) 309.
3. O.S. Ksenzhek, S.A. Petrova, "Electrochem. Soc. Inc." (1998) 132–139

Compositions of Co-doped LiMn₂O₄ spinel with MCNT for Lithium Batteries

R.D. Apostolova, R.P. Peskov, E.M. Shembel

Ukrainian State University of Chemical Technology, 5 Gagarin Ave.
Dnepropetrovsk

Much attention is paid to doping of LiMn₂O₄ spinel by different chemical elements for the improvement of discharge spinel characteristics in redox reactions with lithium [1]. Cobalt as one from these elements improves specific discharge characteristics and cycling ability of LiMn₂O₄ spinel in lithium recharged power sources at volume and superficial doping [2, 3]. According to Guohua et al. LiCo_{1/6}Mn_{11/6}O₄ showed good cycle performance with energy density of 370 Wh/kg at the 300th cycle [4].

Previously we reported the superiority of electrochemical characteristics of the mechanical mixtures of LiMn₂O₄ spinel with multiwall carbon nanotubes (MCNT) over those of spinel compositions with natural graphite in the prototypes of the Li-ion battery [5, 6]. Carbon conductive fillers, their nature and particle size plays the key role in the efficiency of the electrochemical transformation of spinel in Li-ion batteries. Electrodes based on the composition of the spinel and MCNT show a good cycling stability and efficiency at the discharge rate of 2C. The resistance of charge transport (R_{ct}) through the film/spinel composite surface is depends on the conductive filler. Value of R_{ct} decreases in spinel electrode in the presence of carbon filler (by the factor of thousand). Exchange current of spinel electrode increases under the influence of MCNT (from the order of 10^{-7} to 10^{-4} A·cm⁻²). The value of R_{ct} depends on the resistance in contacts between spinel particles and also between particles and current collectors. Contact resistance decreases under influence of MCNT with more efficiency than under influence of graphite because of small size of the particles with high surface area of the MCNT.

In the presented work we extended the investigation of spinel doping its by cobalt and using in the compositions with MCNT in the redox reactions with the Li ions with the goal of subsequent improvement of its discharge characteristics.

Experimental

The efficiency of repeated electrochemical transformation of Co-doped LiMn₂O₄ spinel in the compositions with MCNT in thin-film electrodes and thick spread (Co-doped LiMn₂O₄ spinel, MCNT, F-4/18N12X9T)-electrodes of lithium prototype accumulator have been analyzed. Co-doped LiMn₂O₄ spinel was obtained by annealing of stoichiometrical mixtures of LiMn₂O₄ spinel (Merck) with Co (NO₃)₂ · 6 H₂O (Co:Mn=2:98 %) during 2 hours at 650° C.

Thin film electrodes were made mechanically by embedding of Co-doped LiMn₂O₄ spinel powder with MCNT in ratio of 90:10% mas. into aluminum matrix with the size of (1.0×1.0×0.1) cm [5,6]. Mass of active spinel composition in the electrode is 0.23–0.28 mg·cm⁻². It does not contain the ballast component of traditional composite electrode – binder. MCNT synthesized by catalytic pyrolysis of ethylene was used as a conductive additive [5]. The outer diameter of nanotubes is about 10–30 nm, specific surface is 230 m²·g⁻¹. Composite thick spread electrodes (Co-doped LiMn₂O₄, MCNT, F-4/18N12X9T) of (1.0×1.0) cm have been produced by putting an active composition mass on a net, made of stainless still (18N12X9T). The active mass (15–25 mg·cm⁻²) consists of Co-doped LiMn₂O₄, carbon filler (MCNT) and F4 binder (polytetrafluorethylene)

mixture in the ratio of (80:10:10% mass.) in N-methyl-pyrrolidone with following heat treatment (250 °C, 5–7 h) in air atmosphere.

Electrochemical investigations were determined in coin batteries of 2325 size with Li auxiliary electrode and in the sealed 3-electrode cell with Li counter and Li/Li⁺ reference electrodes. Prototype battery and experimental cell were filled with electrolytes of the composition ethylencarbonate (EC, Merck), dimethylcarbonate (DMC, Merck), 1 M LiClO₄. Water content in electrolytes does not exceed 0.006% according to K. Fisher method. The assembly of prototypes and cells was carried out in a glove box in dried argon atmosphere.

The charge-discharge characteristics were plotted on a test bench with computer control and registration. The conductivity of spinel specimens has been determined by impedance spectroscopy method. Impedance spectra were obtained using analytical VoltaLab PGZ301 radiometer. Impedance spectra were acquired in frequency series of 100 kHz–0.01 Hz using ZView, ZPlot softwares (Scribner Associates).

Results and discussion

It was found that cobalt-doping increase the conductivity of LiMn₂O₄ spinel (table 1).

TABLE I. – Comparative conductivity of spinel specimens in extruded pellets

Compound	Conductivity, S·cm ⁻¹	
	291 K	323 K
LiMn ₂ O ₄	3.3·10 ⁻⁶	0.9·10 ⁻⁵
Co-doped LiMn ₂ O ₄	2·10 ⁻⁵	5·10 ⁻⁵

In the work possibility of cycling of Co-doped LiMn₂O₄ in the compositions with MCNT has been established depending on discharge current density, number of cycles and temperature for using in thin layer lithium recharged power sources (fig. 1).

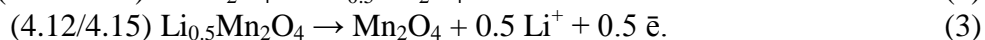
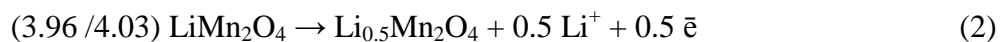
Discharge-charge curves of thin film Co-doped LiMn₂O₄ compositions with MCNT was evaluated at current density of 1C for 30, 50, 100,150, 200th cycles is shown in fig.1 a. Charging of Co-doped compositions was provided at 1C. The changes of discharge capacity (Q_d) depending on current density is shown in fig. 1, b. Discharge capacity at 40 C equals to 75% (90 mAh/g) of one obtained in the first cycle. The capacity of LiMn₂O₄ compositions with MCNT without cobalt reaches 80 mAh/g at 20 C.

Satisfactory cycling performance of Co-doped LiMn₂O₄ compositions with MCNT was obtained at low temperatures (fig.1, c). Q_d=104 mAh/g at 273 K, Q_d=93 mAh/g at 258 K when i_{dich}=1C.

In impedance investigations of Co-doped LiMn₂O₄ compositions with MCNT the resistance of charge transport (R_{ct}) through film/spinel composite surface have been established at temperature (297, 258 K) depending on discharge capacity, that changes at long run cycling. The values of exchange current i₀ were obtained using Butler-Volmer regularity (1) for maxima of electrochemical activity of Co-doped LiMn₂O₄ in the compositions with MCNT in redox reactions with lithium (2, 3):

$$R_{ct} = \frac{RT}{nFi_0} \cdot (1)$$

On cyclic voltammograms two redox-couples with current peaks close 4.00 V are observed: 3.96 /4.03 and 4.12/4.15 V. They are specific for LiMn_2O_4 spinel and correspond to the reactions (2, 3) representing two-stage processes of deintercalation/intercalation of Li ions from/in tetrahedral sites of spinel structure:



Maximal electrochemical activity was determined at potentials of $E_{\text{dch}2}=4.12$, $E_{\text{dch}1}=3.96$ V in intercalation processes and $E_{\text{ch}1}=4.03$ V, $E_{\text{ch}2}=4.15$ V in deintercalation processes. The values of i_0 at high discharge capacity ($Q_{\text{dch}}=117\text{--}120$ mAh/g in 7-50th cycles) and at its degradation ($Q_{\text{dch}}=85$ mAh/g in 250-270th cycles) are presented in the table 2.

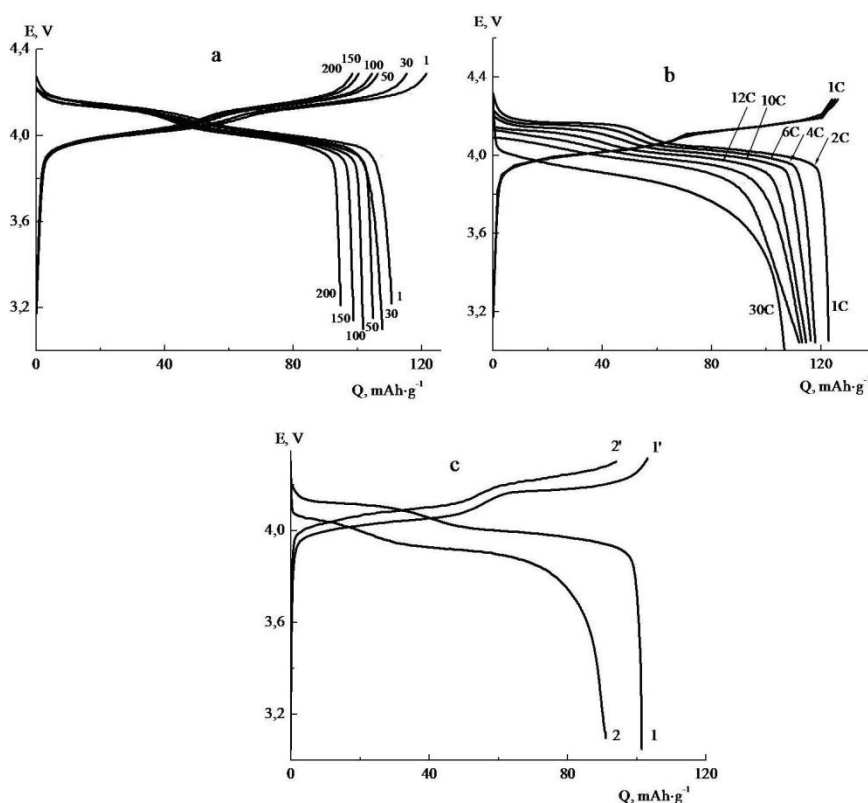


Figure 1. Discharge-charge curves of thin film Co-doped LiMn_2O_4 in the compositions with MCNT in lithium accumulator prototype depending on: a) cycle number; b) discharge rate (C); c) temperature. Temperature, K: a, b) room; c) curve 1 - 273; curve 2 - 258. $i_d = 1\text{C}$ for a, c).

TABLE II. The values of exchange current i_0 of Co-doped LiMn_2O_4 in the compositions with MCNT in redox reactions with lithium depending on the temperature and discharge capacity

E, V	i_0 at 297 K		i_0 at 258 K	
	$Q_1=117\text{--}120$, mAh/g	$Q_2=85\text{--}87$, mAh/g	$Q_1=93$, mAh/g	$Q_2=71$, mAh/g
$E_{\text{ch}1}=4.03$	$6.92 \cdot 10^{-4}$	$3.63 \cdot 10^{-4}$	$8.50 \cdot 10^{-5}$	$1.48 \cdot 10^{-5}$
$E_{\text{ch}2}=4.15$	$4.40 \cdot 10^{-4}$	$2.21 \cdot 10^{-4}$	$3.96 \cdot 10^{-5}$	$0.92 \cdot 10^{-5}$
$E_{\text{dch}2}=4.11$	$5.13 \cdot 10^{-4}$	$2.91 \cdot 10^{-4}$	$2.71 \cdot 10^{-5}$	-
$E_{\text{dch}1}=3.99$	$7.54 \cdot 10^{-4}$	$4.21 \cdot 10^{-4}$	$5.97 \cdot 10^{-5}$	$1.26 \cdot 10^{-5}$

Exchange current i_0 in average two times decreases at cycling when Q_d decreases from $Q_1=120$ mAh/g to $Q_2=85$ mAh/g at the room temperature. The value of i_0 changes at 258 K more considerably (in average 4-5 times) when Q_d decreases from $Q_1=93$ mAh/g in the 5-10 cycles to $Q_2=71$ mAh/g after long cycling.

Discharge capacity of thick volume electrodes on the base Co-doped LiMn_2O_4 spinel in the compositions with MCNT in redox reactions with lithium equals to 130-125 mAh/g at $i_{\text{dch}}=0.15$ C, and 125–120 mAh/g at 1C (fig. 2).

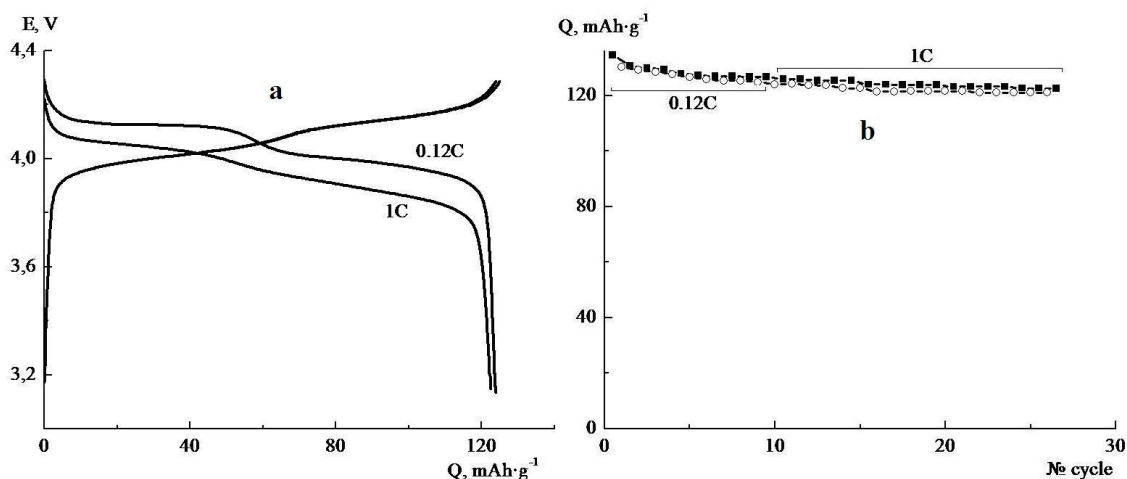


Figure 2. Discharge-charge characteristics of volume (Co-doped LiMn_2O_4 , MCNT)- electrodes in lithium accumulator; a) discharge-charge curves on dependence C; b) discharge capacity on dependence cycle number and C. Room temperature.

We continue the analysis of degradational processes in redox reactions of (Co-doped LiMn_2O_4 spinel, MCNT)-composition with representation of results in the future.

References

1. Liu Qiuling, Wang Shengping, Tan Haibo, Yang Zhigao, Zeng Jian // *Energies* 6 (2013) 1718.
2. W. Baochen, X. Yougyao, F. Li and Z. Dongjang // *J. Power Sources* 43–44 (1993) 539.
3. R. Bittihn, R. Herr, and D. Hoge // *J. Power Sources* 43–44 (1993) 223.
4. Li Guohua, H. Ikuta, T. Uchida, and M. Wakihara // *J. Electrochem. Soc.* 143 (1996) 178.
5. Peskov R., Apostolova R., Shembel E., Danilov M. // *Abstr. 14th Int. Conf. ABAF “Advanced batteries, Accumulators and Fuel Cells”*, Brno 2013: p. 48–51.
6. R. Apostolova, R. Peskov, E. Shembel // *Solid State Electrochem.* / DOI 10.1007/s 10008–013–2350–6. Publ. 19 January 2014.

Comparison of the properties of high voltage spinel cathode material depending on the method of synthesis

T. Kazda^a, O. Čech^a, J. Vondrák^a, A. Fedorková Straková^a, A. Visintin^b, P. Čudek^a

^a Department of Electrical and Electronic Technology, Faculty of Electrical Engineering and Communication, BUT, Technická 10, 616 00 Brno, Czech Republic

^b Instituto de Investigaciones Físicoquímicas Teóricas y Aplicadas (INIFTA), UNLP, CCT La Plata-CONICET, CC 16, Suc. 4, CP 1900, La Plata, Argentina

The most widely used cathode materials for lithium-ion accumulators nowadays are based on LiCoO_2 , LiFePO_4 or LiMnO_4 . These materials are supposed to be replaced by battery systems with new generation of cathode materials such as sulphur-based or high-voltage cathode materials in the future. This article is focused on the study of electrochemical properties of high voltage cathode material $\text{LiCr}_{0.1}\text{Ni}_{0.4}\text{Mn}_{1.5}\text{O}_4$ depending on the process of synthesis.

Samples were prepared via solid state reaction with the temperature as independent variable where electrochemical charge/discharge capacity retention was observed during cycling. The synthesized materials were also studied by SEM.

Introduction

The development of cathode materials with high energy density is important for applications requiring high performance such as electromobility [1]. One of the most promising materials is $\text{LiNi}_{0.5}\text{Mn}_{1.5}\text{O}_4$ due to its high operation voltage close to 4.7 V and high stability. This cathode material reports the high voltage properties with respect to several oxidation steps of manganese cation where Mn^{3+} oxidizes to Mn^{4+} at 4 V vs Li and subsequently Ni^{2+} is oxidized to Ni^{3+} at the voltage range of 4.7 – 4.8 V vs Li until reaches the Ni^{4+} [2]. Despite the indisputable benefits of raised operating voltage, the material is not yet commercially used due to its negative aspects related to low capacity retention. The main drawback of investigated material is the rapid fading of capacity during cycling especially at high temperatures. It was showed that this issue can be overcome by several approaches such as particle size reduction, partial cation substitution and surface modification. Nanoscaling in general increases the active surface area and thus rises the diffusion rate but does not affect the intrinsic conductivity of the crystal. On the other hand, doping may affect the crystalline structure and stability of $\text{LiNi}_{0.5}\text{Mn}_{1.5}\text{O}_4$, electronic conductivity and capacity retention are hereby increased which also leads to improved cyclability and better performance at high C-rates [3]. Cr is one of the elements which can be the cathode material successfully doped with. The binding energy of Cr-O is higher than the binding energy of Mn-O and Ni-O and also the formation of impurities such as $\text{Li}_x\text{Ni}_{1-x}\text{O}$ is reduced during synthesis which also leads to an increase of capacity. There is also another important effect of doping by chromium that a new electrochemical redox change is observed during cycling where Cr^{3+} changes its state to Cr^{4+} and the voltage of discharge plateau is shifted as high as ~ 4.9 V [4]. The last method of improving the properties of the material is surface modification of $\text{LiNi}_{0.5}\text{Mn}_{1.5}\text{O}_4$. Materials such as Al_2O_3 , ZnO and SiO_2 are used for coating. This process leads to the protection of the particles and

reduces the formation of the SEI layer. Cyclability and stability at high loads are therefore improved [5].

Experimental

The method of solid state reaction was utilised for the synthesis of $\text{LiCr}_{0.1}\text{Ni}_{0.4}\text{Mn}_{1.5}\text{O}_4$ samples. Sample A was prepared by two-step annealing process and the three-step annealing process was used for the preparation of sample B. Materials based on carbonates and oxides were used as starting precursors for the synthesis. Li_2CO_3 (Lithium(II) carbonate), MnCO_3 (Manganese carbonate), NiO (Nickel oxide) and Cr_2O_3 (Chromium(III) oxide) were used as obtained from Sigma-Aldrich. Materials were mixed in a stoichiometric ratio of 0.02 mol and milled together for 4h. The obtained mixture was split to two samples and processed separately by different procedure. Both samples A and B were first annealed at 600 °C for 10 hours followed by annealing at 900 °C for 15 hours. Sample B was then processed also in third step which was the annealing at 700 °C for another 15 hours. Entire processing was carried out in high temperature batch furnace at ambient atmosphere. Electrode slurry was prepared by mixing obtained samples with NMP (N-Methyl-2-pyrrolidone) (solvent), PVDF (Polyvinylidene fluoride) (binder) and conductive carbon support Super P in the ratio of 80% active material, 10% of Super P and 10% of PVDF. The electrode slurry was subsequently casted by doctor-blade on Al foil, dried and pressed by the pressure of 3200 kg/cm². A disc electrode with the diameter of 18 mm was cut out of the coated aluminium foil and investigated in El-Cell[®] ECC-STD electrochemical test cell. The cell assembly was carried out in an M-Braun argon filled glove box. Metallic lithium was used as the counter electrode and the LiPF_6 EC:DMC 1:2 w/w electrolyte was soaked in a glass fibre separator. Galvanostatic charge and discharge cycling was utilized as method for investigation of capacity retention with potential window from 3.0 V to 5.1 V versus Li/Li^+ . First two cycles were used for calculation of the cell capacity and the charge and discharge rate was then set to 0.5C. The scanning electron microscopy was also used for characterization of obtained $\text{LiNi}_{0.5}\text{Mn}_{1.5}\text{O}_4$ -A and $\text{LiNi}_{0.5}\text{Mn}_{1.5}\text{O}_4$ -B samples with the TESCAN VEGA3 XMU equipment.

The materials $\text{LiCr}_{0.1}\text{Ni}_{0.4}\text{Mn}_{1.5}\text{O}_4$ - A and $\text{LiCr}_{0.1}\text{Ni}_{0.4}\text{Mn}_{1.5}\text{O}_4$ - B were analysed using SEM microscopy. We can see structure of the synthesised materials on Fig. 1, the field of view for both samples is 41.5 μm . Both the samples exhibit good macro-crystalline structure. Particle size of the $\text{LiCr}_{0.1}\text{Ni}_{0.4}\text{Mn}_{1.5}\text{O}_4$ - A is slightly smaller than $\text{LiCr}_{0.1}\text{Ni}_{0.4}\text{Mn}_{1.5}\text{O}_4$ - B.

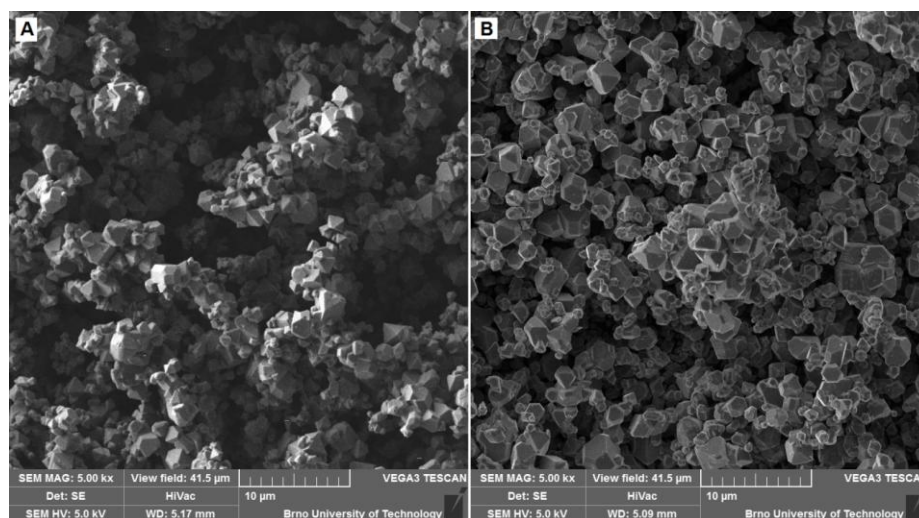


Figure 1. SEM analysis of the samples A) $\text{LiCr}_{0.1}\text{Ni}_{0.4}\text{Mn}_{1.5}\text{O}_4$ - A, B) $\text{LiCr}_{0.1}\text{Ni}_{0.4}\text{Mn}_{1.5}\text{O}_4$ - B; view field used - 41.5 μm

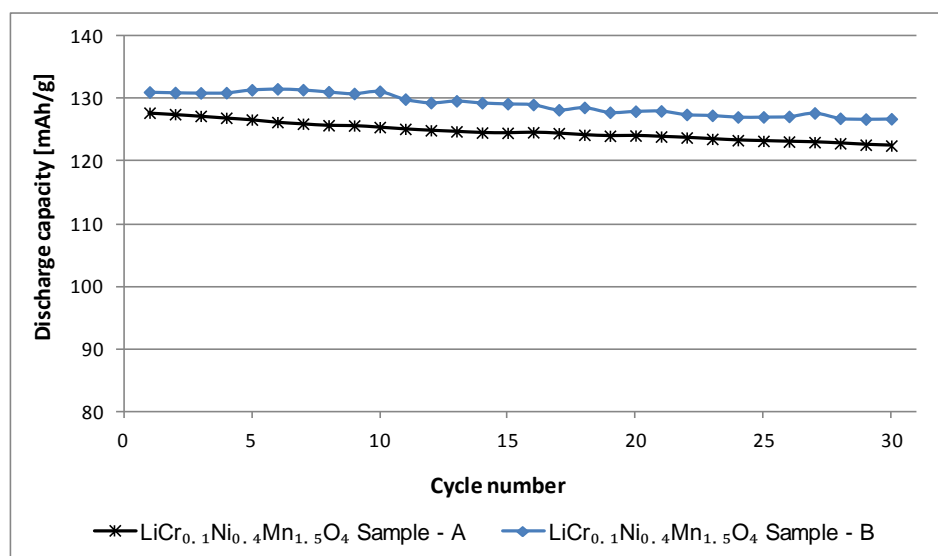


Figure 2. Comparison of capacity change during cycling of the materials $\text{LiCr}_{0.1}\text{Ni}_{0.4}\text{Mn}_{1.5}\text{O}_4$ - A and $\text{LiCr}_{0.1}\text{Ni}_{0.4}\text{Mn}_{1.5}\text{O}_4$ - B

The cycling performances of both samples are depicted in Fig. 2. Discharge capacity during cycling of sample $\text{LiCr}_{0.1}\text{Ni}_{0.4}\text{Mn}_{1.5}\text{O}_4$ - B is always higher than $\text{LiCr}_{0.1}\text{Ni}_{0.4}\text{Mn}_{1.5}\text{O}_4$ - A. Sample $\text{LiCr}_{0.1}\text{Ni}_{0.4}\text{Mn}_{1.5}\text{O}_4$ - B also shows better capacity retention than $\text{LiCr}_{0.1}\text{Ni}_{0.4}\text{Mn}_{1.5}\text{O}_4$ - A. Capacity fading of the sample $\text{LiCr}_{0.1}\text{Ni}_{0.4}\text{Mn}_{1.5}\text{O}_4$ - B is smaller than $\text{LiCr}_{0.1}\text{Ni}_{0.4}\text{Mn}_{1.5}\text{O}_4$ - A. Discharge curves of both samples have similar shapes as we can see in Fig. 3. $\text{LiCr}_{0.1}\text{Ni}_{0.4}\text{Mn}_{1.5}\text{O}_4$ - A shows in the first cycle slightly higher potential of the discharge plateau and longer discharge plateau at 4 V than $\text{LiCr}_{0.1}\text{Ni}_{0.4}\text{Mn}_{1.5}\text{O}_4$ - B.

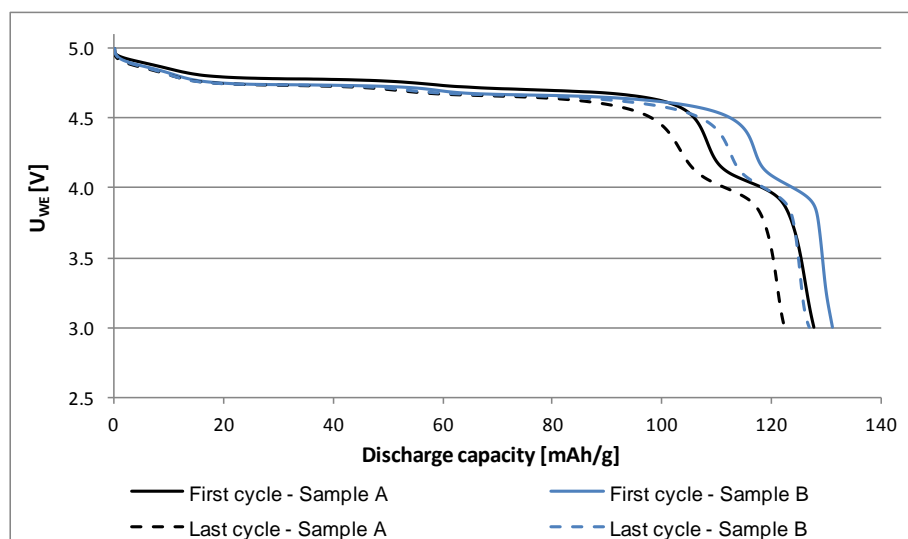


Figure 3. Comparison of the first discharge cycles of the materials $\text{LiCr}_{0.1}\text{Ni}_{0.4}\text{Mn}_{1.5}\text{O}_4$ - A and $\text{LiCr}_{0.1}\text{Ni}_{0.4}\text{Mn}_{1.5}\text{O}_4$ - B

Conclusion

The obtained results show that both methods of synthesis are useful for the synthesis of the cathode material $\text{LiCr}_{0.1}\text{Ni}_{0.4}\text{Mn}_{1.5}\text{O}_4$. Furthermore it is evident that using the three-step annealing

leads to better results in terms of capacity and capacity retention of the $\text{LiCr}_{0.1}\text{Ni}_{0.4}\text{Mn}_{1.5}\text{O}_4$ cathode material. Material prepared by this method lost 3.3% of its capacity after thirty cycles at 0.5 C compared with 4.1% loss for the sample prepared by the two-step annealing method. The sample prepared by the three-step annealing method also exhibit higher capacity during the whole cycling.

Acknowledgments

This work was financially supported by the FEI Company, the Centre for Research and Utilization of Renewable Energy under project No. LO1210 – „Energy for Sustainable Development (EN-PUR)“, FEKT-S-14-2293 project and mainly by the project 7AMB13AR008 – bilateral cooperation between the Czech Republic and Argentina.

References

1. T. Yoshida, K. Kitoh, T. Mori, H. Katsukawa, J.-I. Yamaki, *Electrochem. Solid-State Lett.* **9** (2006) A458.
2. Y. Fan, J. Wang, Z. Tang, W. Hea, J. Zhang, *Electrochim. Acta* **52** (2007) 3870–3875.
3. S. J. R. Prabakar, S. C. Han, S. P. Singh, D. K. Lee, K.-S. Sohn and M. Pyo, *Journal of Power Sources*, **209**, 57(2012).
4. X. Nie, B. Zhong, M. Chen, K. Yin, L. Li, H. Liu and X. Guo, *Electrochimica Acta*, **97**, 184 (2012).
5. Lithium Ion Batteries - New Developments. InTech, 2012-02-24. ISBN 978-953-51-0077-5.

Highly Reversible Silicon/Carbon Nanofiber/Carbon Nanotube Nanocomposite Anodes for Lithium Ion Batteries

T. Cetinkaya, M. Uysal, H. Akbulut

Sakarya University, Engineering Faculty, Department of Metallurgical & Materials Engineering, Esentepe Campus, 54187, Sakarya/TURKEY

Silicon has the highest theoretical specific capacity (4200 mAh g^{-1}) and is a promising anode material for next-generation Lithium ion batteries (LIBs). However, due to low intrinsic conductivity, poor cycling stability and huge volume change (400%) of the silicon during charging and discharging process, it cannot use as a commercial LIB anode material. Because, huge volume change causes structural failure of the silicon active mass particles during lithium insertion/extraction process, hence permanent capacity fading. Several strategies have been used to overcome this problem, such as decreasing particle-size, using carbon active matrixes (CNT, CNF or Graphene etc.) due to high electric conductivity, flexibility and good mechanical properties

In the study, Silicon/Carbon Nanofiber/Multi-Wall Carbon Nanotube (Si/CNF/MWCNT) nanocomposite anode materials were produced by mechanical milling and subsequently then heat treatment methods. For this aim, selected amount of Si nano powders, MWCNTs, and PAN (Polyacrylonitrile) dissolved in N-Methylpyrrolidone solution and then added in the 80 ml stainless steel bowl in Ar-filled glove box and mechanically milled for 1 h using planetary ball mill. After mechanical milling process, the mixture was dried at $150 \text{ }^\circ\text{C}$ in open air and subsequently then annealed at $800 \text{ }^\circ\text{C}$ with a heating rate $5 \text{ }^\circ\text{C min}^{-1}$ for 4 h to decompose of PAN to form PAN-based CNF in flowing argon medium by using a quartz tube furnace. After annealing process Si/CNF/CNT nanocomposite powders was produced. For preparation of the electrode, a slurry was prepared with nanocomposite powders and PVDF binder and then the slurry coated on the copper foil by doctor blade and dried in vacuum oven. In order to investigate effect of CNT on the electrochemical performance of the electrode, amount of CNT was altered in the nanocomposite. The physical characterization of the nanocomposite structures were carried out using scanning electron microscopy, X-ray diffraction patterns and Raman Spectroscopy. For electrochemical characterization of the nanocomposite electrodes, CR2016 test cells were assembled in Ar-filled glove box and prepared nanocomposite electrodes were used as working electrode, lithium foil is used as counter electrode, 1 M LiPF_6 dissolved in EC:DMC (1:1 in volume) used as electrolyte. The working and counter electrodes were separated with polypropylene separator. The cycling test of the electrodes were performed between 0.05 V and 1.5 V at a constant current. In order to investigate electrochemical reactions between electrodes and electrolyte, cyclic voltammetry test was carried out at a scan rate of 0.1 mV s^{-1} .

Keywords: Silicon, CNF, MWCNT, Nanocomposite Electrode, Electrochemical Performance

Characteristics of FeS₂ in Electrolytes Based on DMC-LiAn Mixtures during galvanostatic cycling

N. I. Globa, V. A. Sirosh, V. D. Prisyazhnyi

Inter-Agency Department of Electrochemical Energy Systems, Ukrainian NAS, Kyiv 03680,
Ukraine

gnl-n@mail.ru, gnl-n@ukr.net

The specific capacity of natural pyrite (FeS₂) was investigated by galvanostatic cycling method. Investigation was carried out in electrolytes consisting of dimethyl carbonate (DMC) and a lithium salt (LiBF₄, LiClO₄, LiN(CF₃SO₂)₂). It was shown that the specific capacity of FeS₂ and its stability during cycling depend on the concentration and nature anion lithium salt. The best characteristics of the FeS₂ during cycling are attained in DMC – LiClO₄ and DMC – LiN(CF₃SO₂)₂ electrolytes at salt concentration in the range of 0.1 – 0.2 mole fraction (m.f.).

Influence of doping LiCoO₂ by potassium to electrochemical properties depending on time

T. Kazda^a, J. Vondrák^a, M. Sedlaříková^a, P. Čudek^a

^a Department of Electrical and Electronic Technology, Faculty of Electrical Engineering and Communication, BUT, Technická 10, 616 00 Brno, Czech Republic

LiCoO₂ is one of the most commonly used cathode materials in lithium-ion accumulators. There are also some disadvantages given by its structure beside a number of advantages. One of them is its instability. This article focuses on improving its stability from the perspective of cyclability depending on the time elapsed from the synthesis. Solid state reaction method was chosen as the method of synthesis of this material and as the method of stabilizing the structure by doping by other element - in this case by potassium.

Introduction

Lithium metal oxide cathode materials for lithium ion accumulators have been extensively studied for several decades. The reason is their high voltage and high energy density. The company Sony has combined LiCoO₂ cathode with a carbon anode thus creating the first successful Li-ion accumulator which currently dominates the market [1]. The carbon anode which forms together with lithium the compound LiC₆ during the reaction makes the accumulator much safer than if we used separate lithium as there is much lower probability of the formation of dendrites [1, 2]. Practically usable capacity of LiCoO₂ cell is ~ 130 mAh/g, which is only a half of the total amount of lithium that can be deintercalated without the loss of capacity due to the structural changes in LiCoO₂ [1]. This is related with the high reactivity and very low stability of the electrode with low content of lithium. Potential of this material against lithium is ~ 3.9 V. LiCoO₂ is a commonly used material because its preparation is easy compared with the preparation of other oxides. Although LiCoO₂ dominates on the market with lithium ion accumulators the cobalt reserves are limited which makes its price high [1-3]. The price subsequently limits the field of application of LiCoO₂ to small cells for use in computers, mobile phones or cameras [4]. The disadvantage of this material is its low load capability. It should not be discharged and charged with currents higher than 1 C as it could lead to warming-up. The optimal charging current should be set to the maximum value of 0.8 C [5]. These disadvantages can be compensated by doping the material with other elements [6].

Experimental

Solid state synthesis method was chosen for the synthesis of materials LiCoO₂ and Li_{0.975}K_{0.025}CoO₂. Li₂CO₃ (lithium carbonate), CoCO₃ (cobalt carbonate) and KCO₃ (potassium carbonate) were used as basic materials for the production. These three materials were mixed in the amount equivalent of 0.02 mol. The materials were milled for thirty minutes using a ball mill and subsequently embedded in a ceramic dish, in which they were annealed for 30 h at 400 °C. The calcined material was pulverized again and then pressed by the pressure of 800 kg/cm², and the resulting pellet was again calcined at the temperature of 650 °C for 8 h. Grinding, pelleting and annealing were repeated in the next step of the process, this time at 950 °C for 8 h. The grinding

mill was each time thoroughly rinsed with distilled water followed by alcohol and dried. The resulting material was milled for thirty minutes in a ball mill and was subsequently turned into a mixture consisting of NMP (N-methyl-2-pyrrolidone), binder PVDF (Polyvinylidene fluoride) and Super P carbon. The weight ratio of the materials was LiCoO₂ 80%, Super P 10%, PVDF 10%. The resulting mixture was applied onto Al foil using a special rod to create 150 micron layers. This was later dried and pressed using the pressure of 3200 kg/cm². A disc was punched out of the coated aluminum foil with the diameter of 18 mm and it was inserted into the EI-Cell © ECC-STD electrochemical cell assembled in argon atmosphere inside a glove box. Pure lithium was used as the anode material and the electrolyte was DC:DMC 1:1 with 1M LiPF₆ impregnated in a glass fiber separator. Galvanic-static charge and discharge cycling was used for the measurements and the potential window was set from 2.5 to 4.2 V versus lithium. There were always two discharge and charge cycles carried out, during which charge and discharge current was calculated to be 0.5 C using the weight of the sample, provided the capacity of the material is 120 mAh/g. The actual capacity of the sample was deduced from these two cycles and the sample was then cycled twenty times with the current of 0.5 C. The resulting materials were also investigated after their creation using SEM microscopy. The SEM microscope TESCAN VEGA3 XMU was used for these analyses.

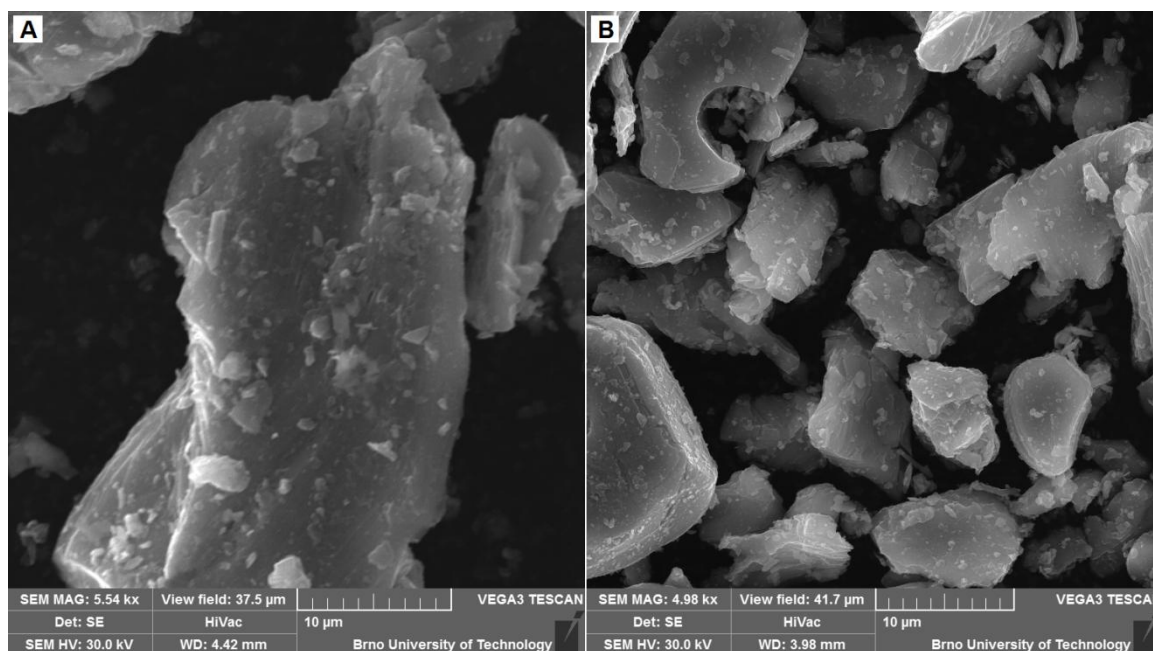


Figure 1. SEM analysis of the samples A) LiCoO₂ and B) Li_{0.975}K_{0.025}CoO₂

The materials LiCoO₂ and Li_{0.975}K_{0.025}CoO₂ were analysed using SEM microscopy. We can see the structures of synthesised materials in Fig. 1. It is possible to observe the layer structure of synthesised LiCoO₂ sample and for Li_{0.975}K_{0.025}CoO₂ too. The size of the particles of Li_{0.975}K_{0.025}CoO₂ is around 10 μm. The particles of LiCoO₂ are bigger.

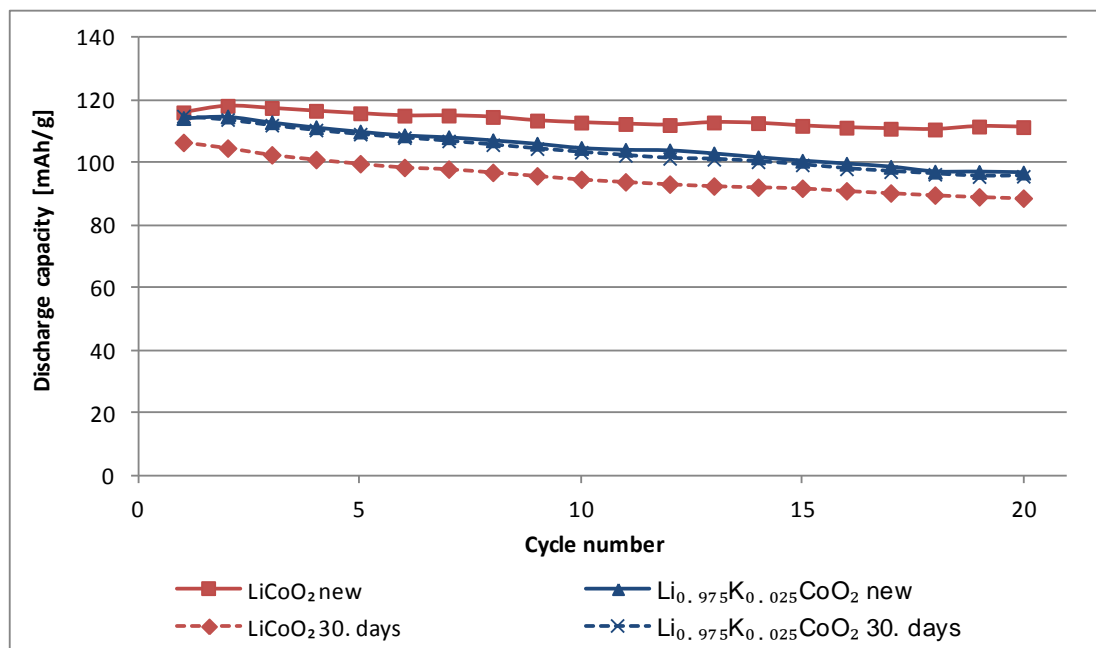


Figure 2. Comparison of capacity change during cycling of the materials LiCoO_2 and $\text{Li}_{0.975}\text{K}_{0.025}\text{CoO}_2$ with different time from synthesis

The cycling performances of LiCoO_2 and $\text{Li}_{0.975}\text{K}_{0.025}\text{CoO}_2$ samples are depicted in Fig. 2. Discharge capacity during cycling of the sample LiCoO_2 new is the highest of all the samples and its capacity is very stable. The sample $\text{Li}_{0.975}\text{K}_{0.025}\text{CoO}_2$ new showed lower capacity than LiCoO_2 new and it was stable since the sixteenth cycle. The $\text{Li}_{0.975}\text{K}_{0.025}\text{CoO}_2$ 30. days sample showed practically the same curve as $\text{Li}_{0.975}\text{K}_{0.025}\text{CoO}_2$ new. There is no change in material properties after thirty days. The sample LiCoO_2 30. days showed the worst stability and capacity during cycling.

Conclusion

It was found that this synthesis process is suitable for preparing of the materials LiCoO_2 and $\text{Li}_{0.975}\text{K}_{0.025}\text{CoO}_2$. The new material LiCoO_2 showed higher capacity and stability during cycling than $\text{Li}_{0.975}\text{K}_{0.025}\text{CoO}_2$. The material of LiCoO_2 showed after thirty days deterioration of stability and capacity. The material $\text{Li}_{0.975}\text{K}_{0.025}\text{CoO}_2$ exhibited the same characteristics after thirty days which implies that doping of the material LiCoO_2 by potassium leads to stabilization of the structure of the material and maintaining the electrochemical properties.

Acknowledgments

This work was financially supported by the FEI Company, the Centre for Research and Utilization of Renewable Energy under the project No. LO1210 – „Energy for Sustainable Development (EN-PUR)“, and FEKT-S-14-2293 project.

References

1. D. Linden and T. B. Reddy, *Handbook of Batteries*, McGraw-Hill (2002).
2. W. A. Van Schalkwijk and B. Scrosati, *Advances in Lithium-Ion Batteries*, Kluwer Academic/Plenum Publishers (2002).

3. T. Ohzuku and R. J. Brodd, *Journal of Power Sources*, **174**, 449 (2007).
4. E. I. Santiago, A. V. C. Andrade, C. O. Paiva-Santos and L. O. S. Bulhões, *Solid State Ion.*, **158**, 91 (2003).
5. M. S. Whittingham, *Chemical reviews*, **104**, 4271 (2004).
6. J. Bludská, J. Vondrák, P. Stopka and I. Jakubec, *Journal of Power Sources*, **39**, 313 (1992).

Compatibility of room temperature ionic liquid electrolytes with hard carbon anode in lithium ion secondary batteries

Jiyoung Kim*, Junyoung Mun*

¹Department of Energy and Chemical Engineering, Incheon National University, 119 Academy-ro, Songdo-dong, Yeonsu-gu, Incheon 406-772 (Republic of Korea)

E-mail: jkim@incheon.ac.kr, jymun@incheon.ac.kr

Tel. +82-32-835-8876

The safety problem is one of the critical issues to be solved for a widespread use of lithium ion battery (LIB). In this point, the room-temperature ionic liquids (RTILs) are considered as alternative electrolytes to the conventional organic electrolyte owing to their special physical characteristics of non-flammability and non-volatility. However, several limitations such as low conductivity, high freezing point and poor cathodic stability have been pointed out. Among these, it is the one of most critical issues for the application to lithium ion batteries that co-intercalation of RTIL-cation into graphene layers during lithiation sequence. In this presentation, hard carbon material is adopted as anode material because it has low reaction potential like graphite and contains a little graphene layers. Hard carbon composite electrode and lithium foil was assembled with synthesized RTIL electrolyte (EMIm-TFSI, PMPyr-TFSI, PMPip-TFSI) in which 1 M LiTFSI salt dissolved. The electrochemical behaviors of hard carbon material in RTIL electrolyte are analyzed to explicate the behavior of lithium ion redox cycle and the prevention of RTIL co-intercalation by electrochemical methods and Raman spectroscopy. The assembled hard carbon/1 M LiTFSI in RTIL/Li half cell exhibits good cycleability and high coulombic efficiency without any additional film forming agent. From the results of cyclic voltammetry and Raman spectroscopy, it was proved that RTILs did not co-intercalated to hard carbon materials. It is concluded that the RTIL co-intercalation is successfully avoided by using hard carbon anode and furthermore, it can be a prospective candidate of active material for novel LIB based on RTIL electrolyte.

Simultaneous Thermal Analysis for Fire Safety of Lithium-ion Batteries

J. Libich^c, J. Vondrák^a, M. Sedlařiová^a, H. Matheislová^b, P. Bursíková^b, O. Suchý^b, R. Friedrichova^b

^a Department of Electrical and Electronic Technology, Faculty of Electrical Engineering and Communication, Brno University of Technology, Brno, 616 00, Czech Republic

^b Technical Institute of Fire Protection, Ministry of the Interior of Czech Republic, Praha 4, 143 01, Czech Republic

^c Centre for Research and Utilization of Renewable Energy, Technická 10, Brno, 616 00, Czech Republic

Lithium-ion batteries are widely spread at consumer electronic devices, they appear as sufficient energy source for propulsion drive of electric vehicles. Their using in this high power application brings lot of advantages but marks the question of fire safety of Lithium-ion batteries. This short research presents testing of electrode materials using in Lithium-ion batteries by Simultaneous Thermal Analysis (STA). Within research were performed several tests of lithium-ion batteries in which batteries were overcharged, short circuited, charged with ten times of rated current. In the other part of testing the STA of our negative electrode material specimens was performed on STA i1500 device. The specimens of negative electrode material were represented by natural graphite in two forms, initial and lithiated. Lithiated graphite material can be considered as negative electrode material in charged state. Were used two analysis methods TG (Thermogravimetry) and DCS (Differential Scanning Calorimetry).

Introduction

The STA technique provides information about material composition and quantitative representation of its components (elements). The information are acquired through combustion or evaporation process which occurs during material heating. The Differential Scanning Calorimetry (DSC) is a technique for measuring energy necessary to establish a nearly zero temperature difference between a sample and an reference material. There are two types of DSC systems in common use, which fall under differential calorimetric methods:

- power-compensation DSC
- heat-flux DSC

DSC with power-compensation

DSC wit power-compensation is also called as „reverse“ DTA (differential thermal analysis). In comparison, DTA measures differences in temperature between a sample and a reference (when they are both put under the same heat), whereas essence of power-compensation DSC is keep both the reference and the sample at the same temperature. This type of DSC is characterized by two separate measuring boxes (furnaces) and by two heat sources. DSC measures electric power, that is needed to maintain constant temperature of both samples. The result of a DSC experiment is a curve

$dQ / dt = f(t)$, where Q is heat energy and this curve has peaks as well as the curve generated from DTA. Distinction from DTA lies in their opposite („reverse“) orientation relative to the x-axes. For endothermic process in DTA is value of the temperature difference negative, while to endothermic process in DSC corresponds positive value of heat energy. [1,2,3,4]

DCS with heat-flux

The second type is method of DSC with heat-flux. Measuring the difference in power is replaced by measuring the temperature difference between the sample and the reference, which are enclosed in the same furnace and are connected by the thermal bridge. With the knowledge of the thermal resistance between the furnace, the sample and the reference, can be the heat flow from the sample (or to the sample) considered proportional to the temperature difference. The temperature of the sample is measured by a thermocouple, which is in contact with this sample.

Termogravimetrie (TG)

It is one of the basic methods of thermal analysis and belongs to dynamic analytical methods. The basic principle is to measure the weight change of analyzed sample during its continuous heating or cooling. The weight changes are expressed in relation to temperature. [5,6]

$$m = f(T) \quad [1]$$

or in relation to time

$$m = f(t) \quad [2]$$

Weight changes of substances during their heating can be expressed by equation

$$m_{AB} (s) = m_A (s) + m_B (g) \quad [3.1]$$

Upon heating gaseous component is released, causing a decrease in weight of the test substance. We meet with these changes for example during thermal decomposition of calcium oxalate monohydrate.

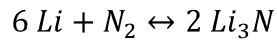
It may occur reversal phenomenon, where the substance reacts during heating with gas, and therefore increases its own weight. The equation of weight change can be written as:

$$m_A (s) + m_B (g) = m_{AB} (s) \quad [3.2]$$

An example could be oxidation of non-noble metals, where arises oxide or hydroxide of the respective (/corresponding) metal. [7,8,9]

Results and Discussion

We have tested charged and non-charged graphite material by STA method under inert atmosphere, the non-charged graphite characteristics are shown in Figure 2 below. The charged graphite material characteristics are depicted in Figure 1 below. In Figure 1 can be seen high peak that is located at temperature approx. 270° C. This peak represents the combustion of lithium, that was intercalated into graphite, with nitrogen. The reaction is expressed by equation (4) below.



[4]

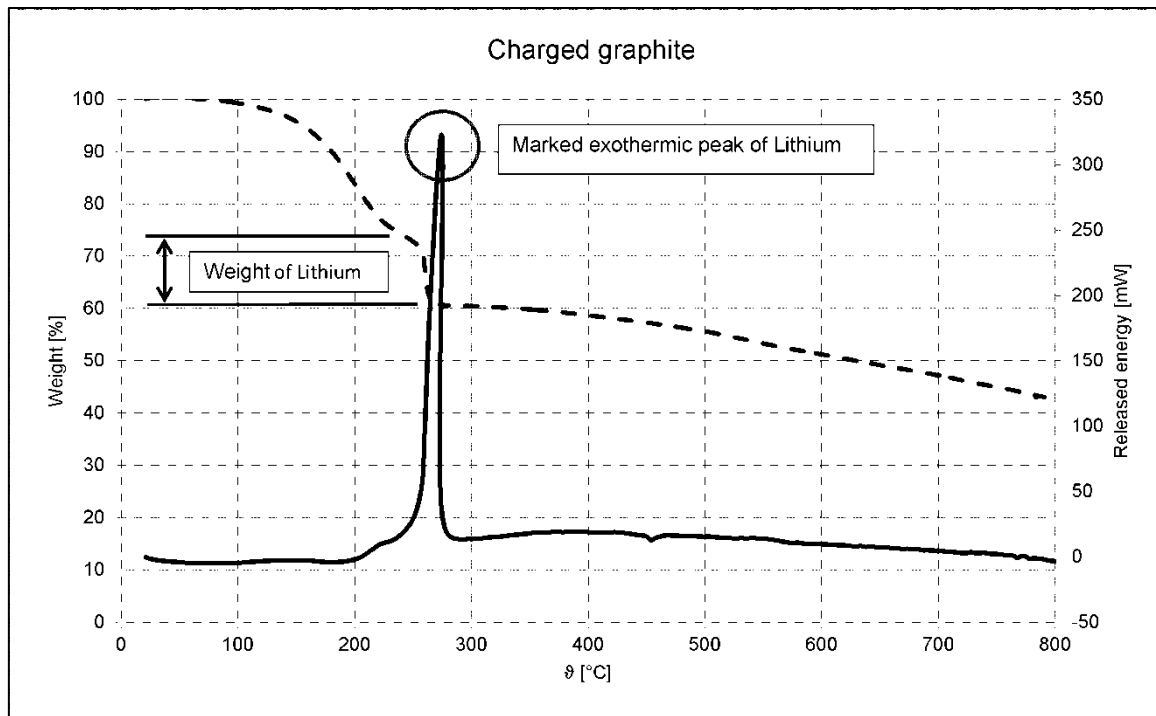


Figure 1. Exothermic peak of lithium combustion.

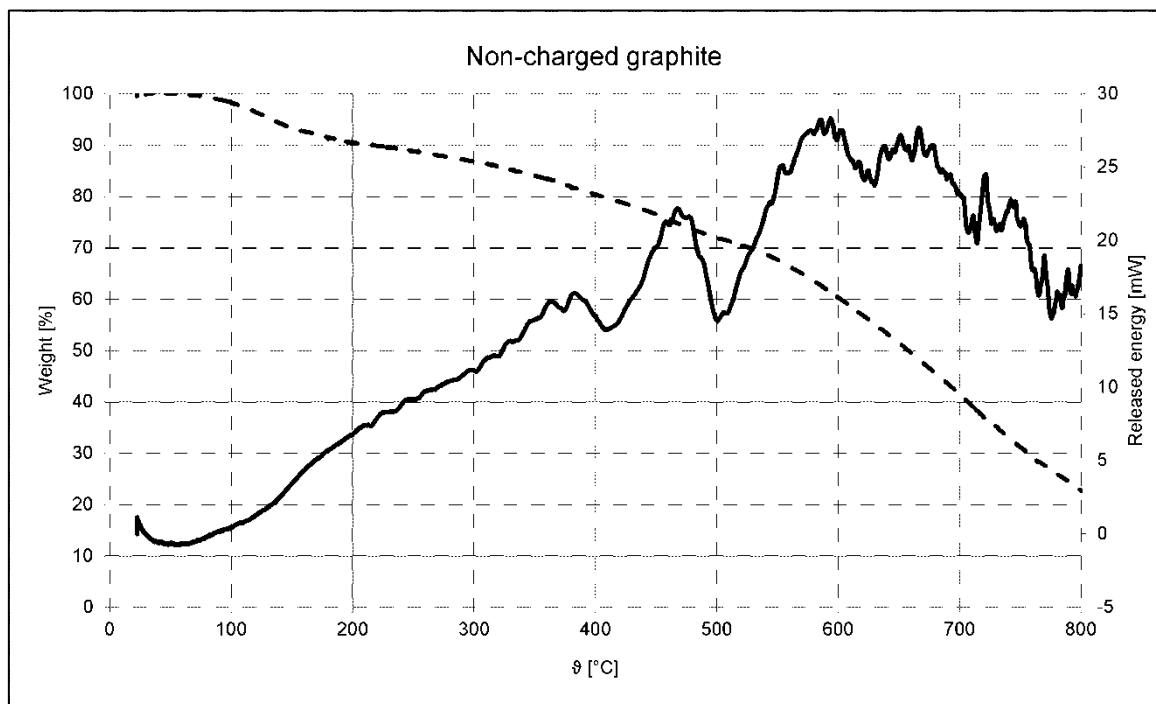


Figure 2. Initial graphite without lithium, discharged negative electrode.

Within experiments with negative electrode materials and lithium-ion batteries which were carried out in our research has been evaluated influence of heat onto material behavior. During high current drawn from battery is produced heat especially on negative electrode, this amount of heat can very easily reach temperature above 200° C. It can cause electrolyte decomposition at the first stage followed by oxidation of lithium to lithium nitride Li_3N . Generally, has to be considered electrolyte stability, as the most heat sensitive component of lithium-ion battery.

Acknowledgments

This work was financially supported by the Centre for Research and Utilization of Renewable Energy under project No. LO1210 – „Energy for Sustainable Development (EN-PUR)“.

References

1. J. Zhang, B. Wu, J. Huang, *J. of Power Sources*, 259(1), (2014).
2. W. Jiang, T. Tran, X. Song, K. Kinoshita, *J. of Power Sources*, 85(2), (2000).
3. B. Kang, K. Honda, T. Aki, T. Omasa, H. Ohtake, D. Warren and J. M. Woodall, *Thermochimica Acta*, 517(12), (2011).
4. J.H Suwardie, R Artiaga, *Thermochimica Acta*, 357-358(1), (2000).
5. G. Guigay, J. Eliasson, D. Gojkovic, L. G. Bengtsson, *B. Fire Technology*, 45, (2009).
6. N. A. Hoffman, E.R. Galea, *Fire Protection Engineering*, 3(4), (1991).
7. L. Zhao, I. Watanabe, T. Doi, S. Okada, J. Yamaki, *J. of Power Sources*, 161, (2006).
8. 97/01968 Anode based on prelithiated carbonaceous material for secondary lithium battery, *Fuel and Energy Abstracts*, 38(3), (1997).
9. J. Libich, J.Vondrák, M. Sedlářiková, O. Dvořák, H. Buřičová, Editors, PV 13, p.163-168, *Advanced Batteries Accumulators and Fuel Cells (ABAF 13th)*, Proceedings, Brno, CZ (2012).

Compatibility of Aprotic Electrolytes with Negative Electrode Materials in Lithium-ion Batteries

J. Libich, J. Máca, M. Sedlaříková, J. Vondrák, A. Visintin

Department of Electrical and Electronic Technology, The Faculty of Electrical Engineering and Communication, Brno University of Technology, Technická 3058/10 616 00, Brno, Czech Republic

This short research presents an introduction to the fire safety of Lithium-ion batteries. Nowadays, as the most weak part of aprotic battery is its aprotic electrolyte. The aprotic electrolyte (commonly the mixture of aprotic solvents) that is used in Lithium-ion batteries have got low flash point with poor thermal stability. This paper describes using sulfolane as an aprotic solvent in Lithium-ion battery. Measurements were focused on performance, cyclability and stability of aprotic electrolyte with relation of graphite material as a negative electrode. Like a possible substitution of graphite, the LTO material was used and tested. Lithium Titanate Oxide (LTO) seems to be promising negative electrode material for Lithium-ion batteries.

Introduction

Lithium-ion batteries are without doubts one of the most promising kind of electrochemical energy sources. Nowadays, the quick development of lithium-ion batteries (hereinafter LiBs) going to get new sorts of LiBs with better capacity characteristics, higher specific voltage, high cyclability, material stability and other parameters. Using of LiBs in electronic applications like small portable devices is well-known, with evolution of electric cars, getting interesting to using the LiBs for electric propulsion. With using of LiBs in electric vehicles, as in high power applications, is coming to the forefront the question of safety of LiBs. In LiB system is most problematic part, by the viewpoint of fire safety, aprotic electrolyte. Aprotic electrolytes use in LiBs, have poor thermal resistance, during thermal stressing occurs to electrolyte decomposition. Product of electrolyte decomposition can take gas or solid state and getting worse battery characteristics and may lead to evolution of hydrogen gas. The evolution of hydrogen and other gasses may cause dangerous mixture in case of contact with oxygen, especially in enclosure space. For high power applications is necessary to find out aprotic electrolyte that can be stable in wide range of temperatures at maintaining of good electric conductivity. Another request on aprotic electrolyte can be set as electrochemical compatibility with electrode material in the range of working electric potential window. The most widespread material for negative electrode into LiBs is graphite. Graphite is stable and good working active material, its operation is based on intercalation reaction of lithium atoms among grapheme sheets. Negative electrodes made from graphite have discharge potential

plateau around 0.25 V vs. Li/Li⁺ and theoretical capacity 372 mAh/g. In LiB's cell arises on negative electrode and electrolyte interface the Solid Electrolyte Interface (SEI) layer. The layer is being formed during first few charge-discharge cycles and is made by the decompositions products of electrolyte. Properties of SEI layer significantly influences LiB characteristics like self-discharge rate, current loading, lifespan and cyclability of LiB etc. This layer is necessary for proper operation of LiB. The composition, constitution and structure of SEI layer depends on the electrolytes which were used, thus on aprotic solvents used in.

Among the new materials for negative electrode, which have been discovered in recent times, belongs Lithium Titanate Oxide, Li₄Ti₅O₁₂ (LTO). LTO has in comparison with graphite different spinel structure, good reversibility and stability. The LTO material has the higher discharge potential plateau approx. 1.55 V vs. Li/Li⁺, theoretical capacity of LTO is 175 mAh/g. The high redox potential of LTO reduces electric power that can be supplied to load, this drawback can be solved by using high voltage positive materials for example LiNi_{0.5}Mn_{1.5}O₄. This high voltage materials give nominal voltage around 4.9 V vs. Li/Li⁺ in comparison with standard cathode materials which provide voltage around 3.7 V vs. Li/Li⁺. On the other hand, as an advantage of high working potential allows to using different kinds of electrolyte solvents without their decomposition at low electrode potential. The high working electrode potential also inhibits the growth of lithium dendrites, which may cause a short circuit of cell.

Results and Discussion

In experiments were used two kinds of negative electrode materials for LiB. Natural graphite, type COND CR5995 (manufacturer Graphite Týn. s.r.o.) and alternative material to conventional graphite the LTO. As an electrolyte was used sulfolane (C₄H₈O₂S) with LiPF₆ salt in 1 mol concentration. First measurement was performed as a set of graphite electrode (as negative electrode) and sulfolane electrolyte. The cell was connected in half-cell arrangement, where the counter electrode was made from metal lithium. Obtained characteristics are depicted in Figure 1 and Figure 2 below.

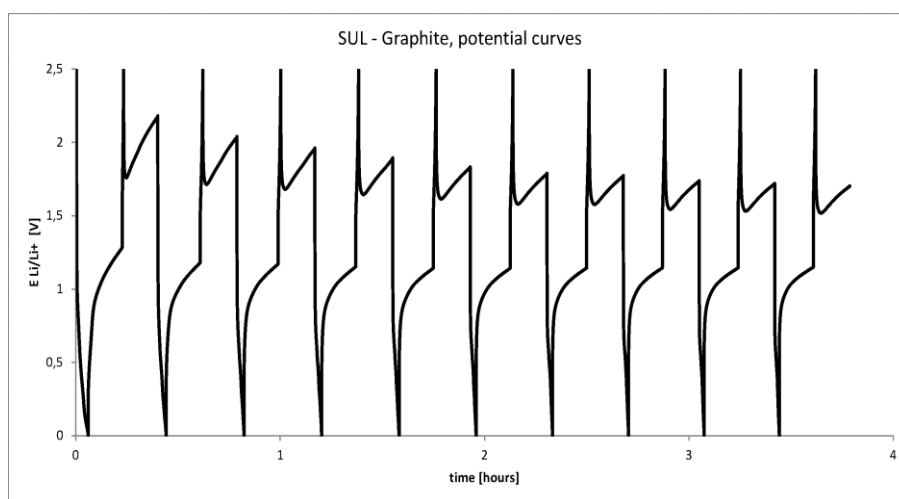


Figure 1. Charge-discharge characteristics of graphite.

As is shown in Figures, the graphite material is decomposed by sulfolane solvent, thus it is losing almost all its potential capacity. The maximum capacity in first cycle is 5 mAh/g. Based on these poor results, has been approached to testing of LTO material that has got spinel intercalation structure.

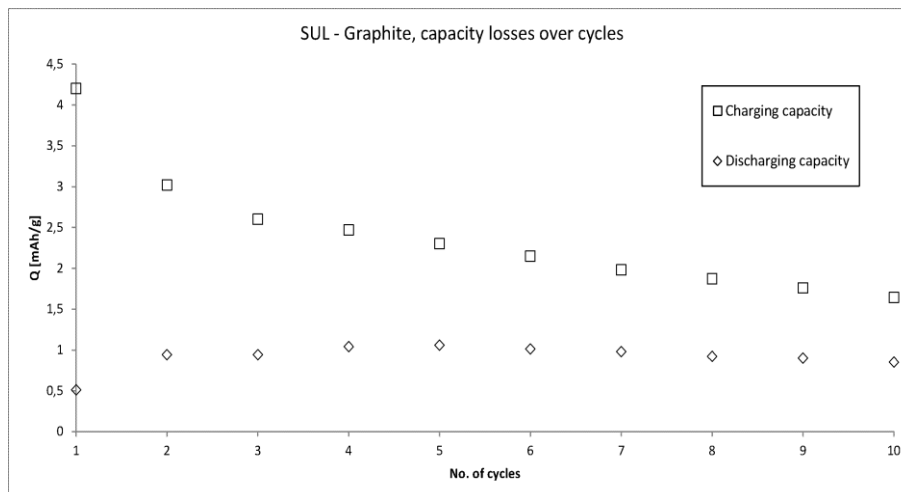


Figure 2. Capacity performance development through 10 cycles.

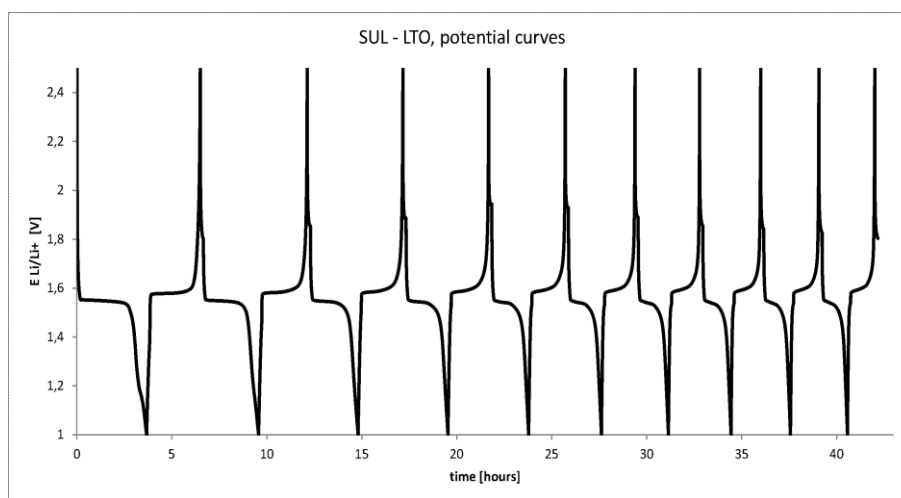


Figure 3. Charge-discharge characteristics of LTO.

As can be seen from Figure 3 above, there is no LTO material decomposition by sulfolane. The capacity performance reach its maximum in first charging cycle where it hit 119mAh/g. This results allow to keep on LTO testing and opening another space for further research of LTO material as one of the most promising material for negative electrode for LiB.

Acknowledgments

This work was supported by project the Centre for Research and Utilization of Renewable Energy under project No. LO1210 – „Energy for Sustainable Development (EN-PUR)“ and

specific research FEKT-S-14-2293 (Materials and technologies for electronics II). Bilateral project between Czech Republic and Argentina, Mobility 7AMB13AR008 Development of new lithium-ion batteries for storage of electric energy.

References

1. J. Ni, W. Liu, J. Liu, L. Gao, J. Chen, I, *Electrochemistry Communications*, 35, (2013).
2. Ch. Lin, B. Ding, Y. Xin, F. Cheng, M. O. Lai, L. Lu, H. Zhou, *Journal of Power Sources*, 248, (2014).
3. M. B. Dines, *Materials Research Bulletin*, 10 (4), (1975).
4. K. Ariyoshi, T. Ohzuku, In *Encyclopedia of Electrochemical Power Sources*, (2009).
5. N. Takami, H. Inagaki, Y. Tatebayashi, H. Saruwatari, K. Honda, S. Egusa, *Journal of Power Sources*, 244, (2013).
6. B.V. Ratnakumar, M.C. Smart, S. Surampudi, *Journal of Power Sources*, 97–98, (2001).
7. K. Sang-Pil, C.T. Adri, D. Van, B.S. Vivek, *Journal of Power Sources*, 196(20),(2011).
8. M. L. Lee, Y. H. Li, S. Ch. Liao, J. M. Chen, J. W. Yeh, H. C. Shih, *Electrochimica Acta*, 112, (2013).
9. M. Kitta, T. Matsuda, Y. Maeda, T. Akita, S. Tanaka, Y. Kido, M. Kohyama, *Surface Science*, 619, (2014).

The phosphate flame retardant influence on aprotic electrolytes properties

J. Maca¹, M. Sedlarikova², J. Vondrak² and M. Frk²

¹Centre for Research and Utilization of Renewable Energy, Technická 10, Brno, 616 00, Czech Republic

²Brno University of Technology, Technická 10, Brno, 616 00, Czech Republic

The fire safety and temperature stability is very important property of solvents used in electrolytes. This question is discussed in these days because of more and more use of lithium ion batteries in industry. The lithium ion batteries with aprotic electrolytes are used not only in small electronic devices but also in larger industrial use as well as in car industry. Due this reasons are the electrolytes with flame retardant tested. This article is focused on change of specific conductivity of electrolytes by adding different flame retardants into electrolytes. According to the results the most suitable flame retardant is selected and suggested to use in aprotic electrolytes.

1. Introduction

Lithium - ion batteries are composed from four main compounds positive electrode created from some kind of oxides with lithium, electrolytes compound from organic non aqua electrolytes with dissolved lithium salt, negative electrode consisting of special type of carbon and from packaging. The electrolytes should be compatible to all the another parts. It is impossible to use water based electrolytes due the use of lithium in batteries or for example used the dimethylsulfoxide as a solvents for electrolytes because of the etching of plastics materials used for packaging the batteries.

Another point of view is the temperature window and the fire safety of batteries. It is possible to use a protective circuit, which guard the voltage, current and temperature on cell or use a special material which is less flammable from the physical nature of its existence. To this are also fall the flame retardants additives. The positive properties, which go along with the flame retardant, are well known from other parts of electro technical industry such as the printed board circuits[1]. To main demands taken on flame retardants is large efficiency by small volume amount, zero or minimal influence on other parameters of based materials, less toxicity, easy recycling and low price.

1.1 Flame Retardants

Generally are the flame retarders called substances with slow down or disabled the phenomena which arising during the burning process (creating and spread of flame). The flame retardants are used for all state of matter solid, liquid and gas. The flame retardants act into burning in specific phase of this process e.g. by increasing the temperature, decomposition of substances or

by the actual combustion. In practice is combined several different types of flame retardants to multiplicity the desired influence[2,3].

The flame retardants used in production process can be divided be two possibilities of interacting with the base material. The flame retardants, from this view, can be divided into additive and reactive. Other possibility to divided the flame retardants is according to their chemical composition ant that on phosphor, bor of silicon base[3].

For selecting the right flame retardant it is necessary to keep in mind its influence on electrolytes. In this work it is investigated the influence of flame retardant on specific conductivity. It was selected the retardants by this parameters: relative permittivity ε , melting point ϑ_m and flashpoint ϑ_f . The parameters of selected flame retardants are listed in Table I. It was decided to choose the phosphor base retardants because they are one of the cheapest and most used flame retardant (TEP - triethyl phosphate, TPP - triphenyl phosphate, DMMP - dimethyl methylphosphonate).

TABLE I. Properties of selected flame retardant

Flame retardant	ε [-]	ϑ_m [°C]	ϑ_f [°C]
TEP	13	-56	107
TPP	3.5	48 - 50	220
DMMP	22.3	-50	69

2. Experimental

The two electrode conductivity sinking cell and electrochemical impedance spectroscopy (on potentiostate Biologic) was used for the specific conductivity determination. The measurement was performed in frequency range from 1 MHz to 100 Hz and sinus potential with amplitude 10mV. The measurements were carried out in ambient conditions in a sealed vessel to prevent the humidity contamination of the sample.

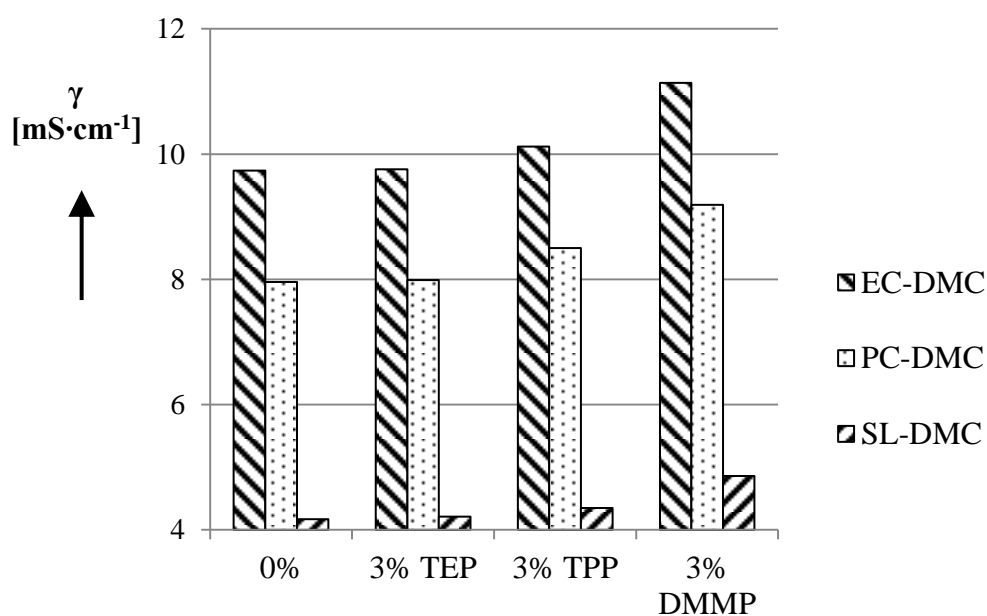


Figure 1. The influence of different flame retardants on solvents mixtures specific conductivity

3. Discussion

From the results and graphic interpretation on figure 1 is visible that all used flame retardant increased the specific conductivity of the base electrolyte. The most promised flame retardant seem to be DMMP which increased the specific conductivity mostly. The specific conductivity of standard used electrolytes EC – DMC (ethylene carbonate – dimethyl carbonate) was increased by 14.4% by using DMMP and even the electrolyte compound from SL – DMC (sulfolane – dimethyl carbonate) by 16.5% in case of use DMMP. Less polar additives increase the fluidity faster than lowering the permittivity. The increase of specific conductivity by adding a flame retardant is caused because of lowering the dynamic viscosity. In farther work will be necessary to determine the optimum among of flame retardant additive and its influence on electrode material.

Acknowledgement

This work was supported by the grant FEKT-S-14-2293 "Materiály a technologie pro elektrotechniku II" , LO1210 - Energy for Sustainable Development (EN-PUR) and project CZ.1.07/2.3.00/20.0103 "Support for human resources and transfer of knowledge in conditions of international cooperation of research teams".

4. References

1. C. C. Zhang, F. S. Zhang., Recovery of triphenyl phosphate from waste printed circuit boards by solvothermal process., *Chemical Engineering Journal* 240 (2014) 10–15 pp.
2. Janošová M. Aditiva užívaná pro snížení hořlavosti styrenových kopolymerů. Zlín: University of Tomáše Bati in Zlín, faculty of technology 2009, 72 pp.
3. Types of chemical flame retardants. [online] 15.7.2014
4. <http://www.epa.gov/dfe/pubs/flameret/altrep-v1/altrep-v1a-sec2.pdf>

The permittivity study of aprotic solvents

M. Frk¹, J. Maca², J. Libich²

¹Brno University of Technology, Technická 10, Brno, 616 00, Czech Republic

²Centre for Research and Utilization of Renewable Energy, Technická 10, Brno, 616 00, Czech Republic

Lithium ion batteries are commonly used around the world. In dependence on the batteries application it is possible to use them as stationary power sources, power mobile devices or as electro mobile propulsion. The batteries have to be safe in all conditions of use. That is the reason for do a research and innovation on materials which will increase the fire safety and lower the risk of burn or explosion. The main goal of this paper is to determine the influence of low flammable solvent dimethyl sulfone on permittivity with ethylene carbonate mixtures. The ethylene carbonate is the most used solvent for electrolytes in lithium ion batteries. In this work is the relative permittivity dependence in temperature window 30°C do 90°C determined.

Introduction

The benefits of lithium ion batteries are known for many years and thank to them the lithium ion batteries become absolutely common part of our day lives. Between their advantages belongs low self-discharge, high voltage for cell, high capacity and high capacity related to weight. On other hand a big disadvantage is high price caused by difficult production technology. By the manufacturing in is necessary to use protective argon atmosphere to prevent the air and air humidity reach the batteries. Manufacturing of the raw lithium into state suitable to use in batteries is also not the simplest. Lithium is also relative rare element in earth crust. Lithium usage also brings a limit to electrolytes and solvents which are compatible with it. Water as a most common solvent is not possible to work with lithium due the strong reaction with it and due the high cell voltage which is above the voltage of water decomposition[1]. These reasons bring the attention to polar aprotic organic solvents such as propylene carbonate, ethylene carbonate dimethyl carbonate etc[2,3]. These solvents can work in such conditions.

One of the main properties which the solvent have to possess is higher permittivity and that $\varepsilon > 30$ [4]. The reason is to be able to dissociate salts to ions. That why the permittivity of ethylene carbonate and dimethyl sulfone mixtures was research. The second solvent dimethyl sulfone was chosen as component which should increase the fire safety of electrolyte. The selected properties of used solvents are listed in Table I where ε is relative permittivity at 1 MHz frequency, v_m is the melting point of the solvent and v_f is the flash point temperature. The flash point is in this paper taken as main safety parameter due flammability.

TABLE I. Properties of used aprotic solvents[4,5]

	ethylene carbonate	dimethyl sulfone
ε [-]	89	48
v_m [°C]	36	110
v_f [°C]	152	143

Experimental

The relative permittivity was determined by comparing the capacitor capacity. In the first step the capacity of an air capacitor was measured and then the capacity of the same capacitor but with the solvent mixture used as dielectric. The difference between capacities was used for calculation of relative permittivity and that for frequency 1 MHz. The measurement was carried out in a temperature window above the melting point of each solvent. In our case for solvents ethylene carbonate (EC) and dimethyl sulfone (DMSO) in a temperature range from 40 °C to 90 °C.

The used salt was lithium perchlorate LiClO_4 (Sigma Aldrich company) in 1 mol/l concentration. The salt was dissolved in EC – DMSO mixture and in different samples the volume of DMSO was changed. The volume of DMSO was varied from 0 vol% to a level close to the saturation limit[6].

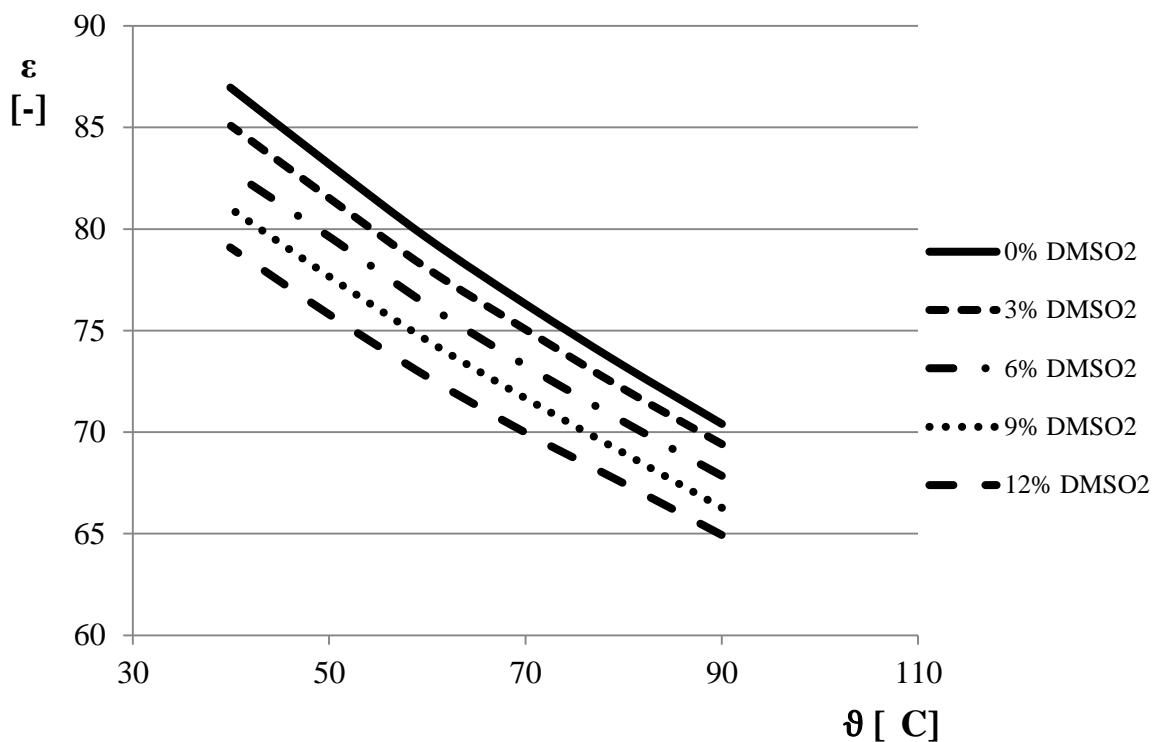


Figure 1. The temperature dependence of relative permittivity of EC – DMSO2

Discussion

The decrease of relative permittivity of each sample with temperature which is shown in Fig. 1 is caused by thermal moving of molecules. In higher temperatures the molecules do not change their directions to the electric field as easily as in low temperature due the higher thermal moving. This causes the decrease of the permittivity. The results clearly show that the DMSO₂ in EC – DMSO₂ system greatly reduced the permittivity. The decrease of permittivity is caused by increased volume share the lower permittivity solvent. On other hand the permittivity in whole temperature window does not get below the necessary limit $\epsilon > 30$.

Acknowledgement

This work was supported by the grant FEKT-S-14-2293 "Materiály a technologie pro elektrotechniku II", LO1210 - Energy for Sustainable Development (EN-PUR) and project CZ.1.07/2.3.00/20.0103 "Support for human resources and transfer of knowledge in conditions of international cooperation of research teams".

References

1. S. Sawada, T. Yamaki, T. Maeno, M. Asano, A. Suzuki, T. Terai, Y. Maekawa. Solid polymer electrolyte water electrolysis systems for hydrogen production based on our newly developed membranes, Part I: Analysis of voltagecurrent characteristics. Progress in Nuclear Energy 50 (2008) pp. 443-448
2. G. Eichinger, M. Fabian. Comparison of organic and inorganic gelation agents in ethylene carbonate based electrolytes for lithium-ion batteries. Journal of Power Sources 68 (1997). pp. 381-38
3. C.R. Yang, Y.Y. Wang, C.C. Wan., Composition analysis of the passive film on the carbon electrode of a lithium-ion battery with an EC-based electrolyte., Journal of Power Sources 72 (1998). pp. 66–70
4. Marcus Y. The properties of solvents. John Wiley & Sons Ltd Publishing, (1998) 399 p.
5. Maca, J.; Frk, M.; Rozsivalova, Z.; Sedlarikova, M. Properties Of Sulfolane Base Aprotic Electrolytes. Portugaliae, Electrochimica Acta, (2014), vol. 6, pp. 12-20. ISSN: 1647- 1571.
6. J. Maca, M. Frk, M. Sedlarikova,. Properties of Electrolytes for Li - ion Batteries with Higher Fire Safety. ICREPQ 13. Bilbao. (2013). pp. 261-264. ISBN: 978-84-695-6965- 8

Surface modification of High Energy Density Positive Electrode for High-Performance Lithium-ion Batteries

Junyoung Mun¹, Wonchang Choi², and Seung M. Oh³

¹Department of Energy and Chemical Engineering, Incheon National University, 119 Academy-ro, Songdo-dong, Yeonsu-gu, Incheon 406-772 (Republic of Korea)

²Center for Energy Convergence, KIST, Hwarangno 14gil 5
Seongbuk-gu 136-791 (Republic of Korea)

³World Class University (WCU) program of Chemical Convergence for Energy & Environment (C2E2), School of Chemical and Biological Engineering, Seoul National University (SNU), Seoul 151-744, Republic of Korea, E-mail: seungoh@snu.ac.kr

A coating of carbon nanotubes is formed on an oxide cathode material, for the first time by a simple and easily scalable physical method by applying shear stress onto the oxide material comprising multiwall carbon nanotubes. X-ray diffraction patterns and cross-sectional scanning electron micrographs reveal that a high level of carbon nanotube coating can be achieved without any chemical or physical breakdown of the oxide cathode structure. The microstructures of the prepared samples are investigated by Raman and X-ray photoelectron spectroscopies. Even when the electrode has small carbon content, it exhibits higher conductivity, rate capability, and specific discharge capacity compared to the pristine samples. This observation is attributed to the suppression of contact resistance, surface film resistance and occurrence of fast charge-transfer reactions, as confirmed by electrochemical impedance spectroscopy. Finally, a full cell comprising carbon nanotube-coated cathode is fabricated and shown to exhibit improved discharge capacity and stable cyclability.

Fabrication of Sn–Ni /MWCNT nanocomposite electrodes for Li-ion batteries by pulse electrodeposition: Effects of Peak Current Density

M. Uysal*, T. Cetinkaya, A. Alp, H. Akbulut

Sakarya University Engineering Faculty, Department of Metallurgical & Materials Engineering, Esentepe Campus, 54187, Sakarya, Turkey

* Corresponding Author:

Tel: +90 264 295 5795

Fax: +90 264 295 5601

e-mail: mehmetu@sakarya.edu.tr

To reduce irreversible capacity and improve cycle performance of tin electrodes, Sn–Ni/MWCNT nanocomposite electrodes were prepared at constant electrodeposition conditions (pulse on-time T_{on} at 5 ms and pulse off-time T_{off} at 5 ms) but with different the peak current densities were investigated. by pulse electrodeposition method using copper substrate as current collector. MWCNTs were aimed to co-deposit from the suspended MWCNT in the electrolyte to increase buffering effect and conductivity. The effects of peak current density on the surface morphology, microstructure, and electrochemical properties were investigated. Surface morphology of produced Sn-Ni/MWCNT composites were characterized by scanning electron microscopy (SEM). Energy dispersive spectroscopy (EDS) was conducted to understand the elemental surface composition of composites. X-ray diffraction (XRD) analysis was carried out to investigate structure of Sn-Ni/MWCNT composites. Raman spectroscopy was used to determine the existence of MWCNT in the Sn–Ni matrix. The electrochemical performances of Sn-Ni/MWCNT composite electrodes have been investigated by charge/discharge tests, cyclic voltammetric experiments. The discharge capacity cyclically tested cells by a battery tester at a constant current in the voltage range between 0.02 V – 1.5 V. The peak current density were shown to be a crucial factor to improve Sn-Ni/MWCNT composite anodes for cycleability and reversible capacity.

Keywords: Sn-Ni/MWCNT nanocomposite, pulsed electro co-deposition, energy storage, Li batteries.

Numerical Study of Lithium Ion Battery

P. Vyroubal, J. Maxa, T. Kazda, J. Vondrák

Department of Electrical and Electronic Technology, Faculty of Electrical Engineering and Communication, BUT, Technická 10, 616 00 Brno, ČR

Corresponding author: Petr Vyroubal (xvyrou02@stud.feec.vutbr.cz)

Phone: +420 541 146 154

Abstract

The lithium-ion battery is an ideal candidate for a wide variety of applications due to its high energy/power density and operating voltage. Lithium-ion batteries are used as a primary and a secondary power source. We focus on the use of secondary power sources. This article deals with the possibilities of numerical simulations of lithium ion batteries. The real battery datasheet will be compared with simulation results and with real measurements. For numerical study of the lithium-ion battery Comsol Multiphysics and MatLab Simulink will be used.

Comsol Multiphysics is tool for modeling and simulating engineering tasks. The problems we want to solve in real life are always based on multiphysics phenomena. Thus it's required to take into account interaction between two or more physics domains at one time. Comsol Multiphysics is defined for solving these complex problems [1].

In chemical modules you can find predefined physical interface for analysis of chemical reactions, transport of diluted species or species transport in porous media. Electrochemistry modules provide interface for design and simulation of battery or fuel cell life cycle. Comsol Multiphysics includes also option to model process of galvanization or corrosion [2].

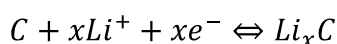
MatLab Simulink is a block diagram environment for multi-domain simulation and Model-Based Design. It supports system-level design, simulation, automatic code generation, and continuous test and verification of embedded systems [3].

Lithium-ion batteries are used as a primary and a secondary power source. This article focuses on the use of secondary sources of power. This type of batteries gains more and more importance due to their higher specific capacity, longer life and lower self-discharge compared with conventional batteries such as NiCd or NiMH. These properties are based on the use of lithium and intercalation materials from which the electrodes are formed. These substances are characterized by the ability to release and then incorporate lithium ions in their structure, thereby these batteries differ from the conventional ones, in which chemical conversion of anode and cathode material takes place. Another advantage is that these accumulators use only a small amount of electrolyte, which serves only as ion conductor, thus again goes to reducing the size of these batteries. The following equations describe the function of lithium-ion batteries. In these equations LiMO_2 metal oxide is used as a cathode material such LiCoO_2 or LiNiO_2 . C is typically used as the anode material [4].

Reaction at the positive electrode of Li-Ion cells:



Reaction at the negative electrode of Li-Ion cells:



Summary reaction:

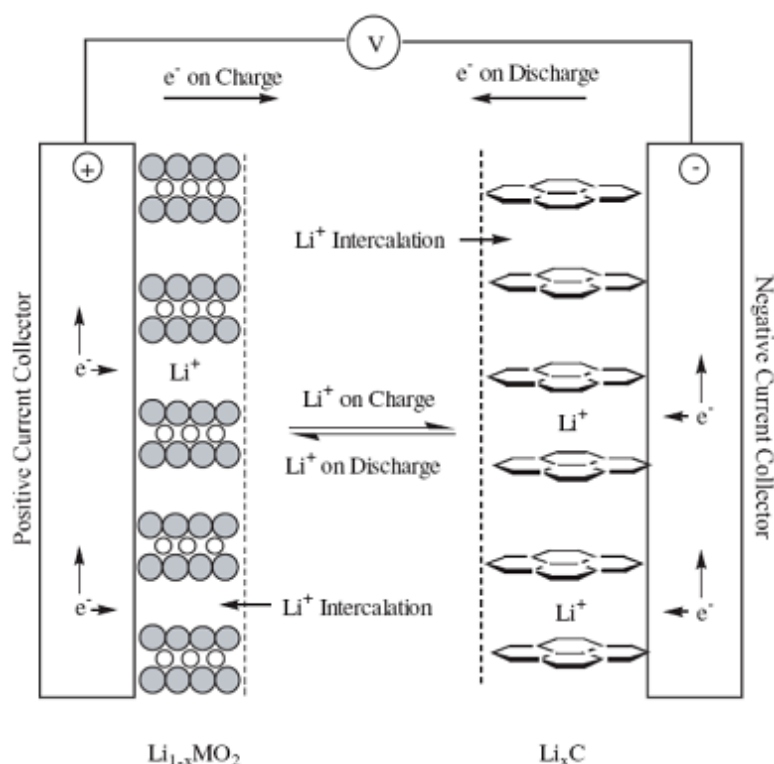
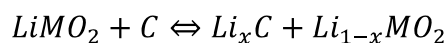


Figure 1. The principle of function of Li-ion accumulators [2].

Currently the most used material for positive electrode in lithium-ion cells is LiCoO_2 and its modification. This type of material was used in the first commercial lithium-ion batteries made by Sony in 1991. It is a material with a layered structure, which voltage against lithium in pure form is 3.88V and capacity $\sim 155\text{mAh/g}$. Its disadvantage is worse temperature and cycling stability. A modification by using Ni is very common. Material $\text{LiNi}_{1-x}\text{Co}_x\text{O}_2$ shows better stability and higher capacity than the default material, but it is slightly less thermally stable. The final properties depend on the content of Co. Specific capacity of the material is from 190mAh/g to 220mAh/g . Similarly voltage against lithium varies from 3.72 V to 3.78 V depending on the content of Co. LiFePO_4 was created as its possible replacement. The first notes about the material LiFePO_4 are dated from 1997. LiFePO_4 material is the latest of a group of materials for lithium-ion cells and is characterized by olivine structure, high stability and shelf life. It is composed of ecological and cheap materials and shows the voltage 3.3 V versus lithium and capacity of 170mAh/g . This material gradually begins to replace older types of cathode materials [5], [6].

The cylindrical cell continues to be one of the most widely used packaging styles for primary and secondary batteries. The advantages are ease of manufacture and good mechanical stability. The tubular cylinder has the ability to withstand internal pressures without deforming. Figure 2 shows a cross section of a cell [7].

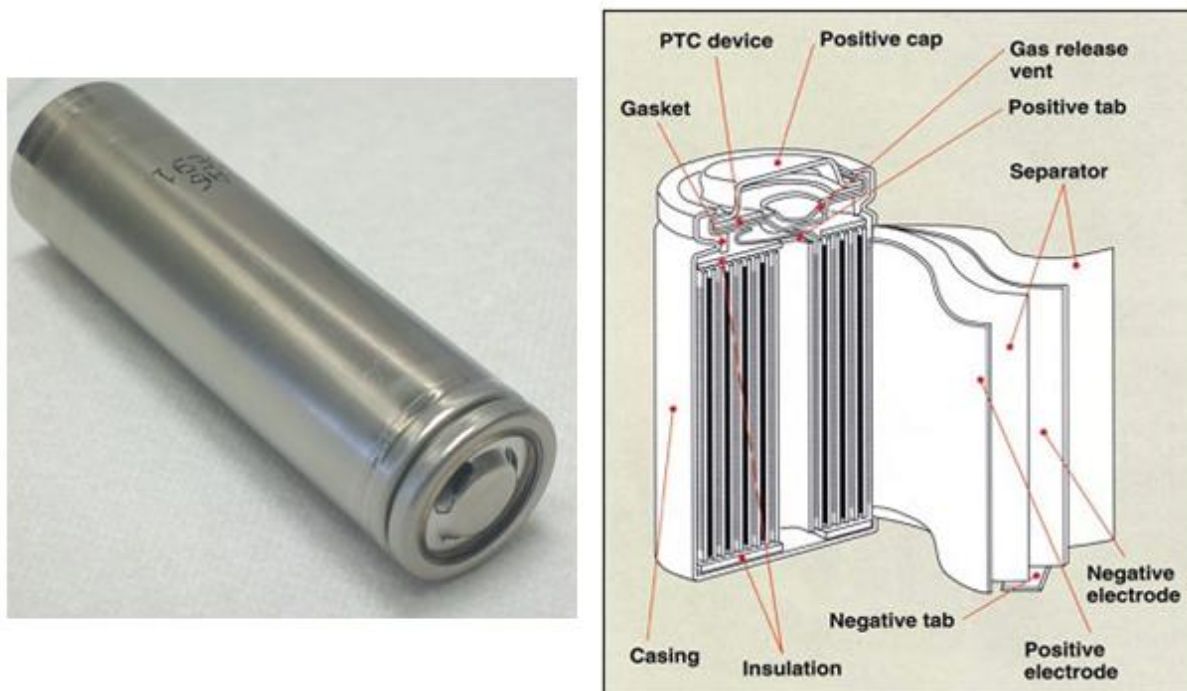


Figure 2. Cross section of a lithium-ion cylindrical cell [8].

A Samsung battery with capacity 3000mAh and a nominal voltage 3.7V was selected as the sample for real measurement.

The VMP3 potentiostat (Biologic) with attached VMP3B-20 booster was used for the measuring of discharge curves. The measurement procedure was set accordingly to the datasheet. Two discharging currents were selected - namely 0.2C and 0.5C. Charging was done using the CC-CV method. For the first measurement charging current was set to 0.2C (600mA) and the maximum charging potential was set to 4.2V. This was followed by CV charging until current dropped to 0.05C (150mA). Discharging was done by discharging current 0.2C (600mA), cut-off potential was set to 2.75V. Charging current for the second measurement was set to 0.5C (1500 mA) and the maximum charging potential was set to 4.2V. This was followed by CV charging until current dropped to 0.05C (150mA). After that discharging by discharging current 0.5C (1500 mA) was used. Cut-off potential was set to 2.75V.

Conclusion

For the modelling of chemical processes it is necessary to know their mathematical interpretation and how the simulation software proceeds during the solution. It is important to respect the geometry of the model and generated computational mesh. The quality of the computational mesh has the greatest influence on the actual computational time. The simulation will be more accurate if the computational mesh is finer and better quality.

Acknowledgment

Authors gratefully acknowledges financial support from the Centre for Research and Utilization of Renewable Energy under project No. LO1210 – „Energy for Sustainable Development (EN-PUR)“, by the specific graduate research of the Brno University of Technology No. FEKT-S-14-2293.

References

1. CAI, L., WHITE, R. E. Mathematical modeling of a lithium ion battery with thermal effects in COMSOL Inc. Multiphysics (MP) software. *Journal of Power Sources* [online]. 2011, vol. 196, issue 14, pp. 5985-5989 [cit. 2014-03-26]. DOI: 10.1016/j.jpowsour.2011.03.017.
Available from: <http://linkinghub.elsevier.com/retrieve/pii/S0378775311005994>
2. NYMAN, A., EKSTROM, H. Modeling the lithium ion battery. Comsol, Burlington USA. [online]. [cit. 2014-03-26]. Available from: <http://www.comsol.com/>.
3. TREMBLAY, O. Experimental Validation of a Battery Dynamic Model for EV Applications. *World Electric Vehicle Journal* 3 2009. Vol. 3, ISBN 2032-6653.
4. LINDEN, D., REDDY, T. B. Handbook of batteries. 3rd ed. New York, NY: McGraw-Hill, 2002, 1 v. (various pagings). ISBN 00-713-5978-8.
5. VYROUBAL, P., MAXA, J., VONDRÁK, J., KAZDA, T. Modeling and Numerical Simulation of Lithium Ion Battery. In *Advanced Batteries Accumulators and Fuel Cells - 13th*, Brno 2012.
6. VAN SCHALKWIJK, W. A., SCROSATI, B. *Advances in lithium-ion batteries*. New York, NY: Kluwer Academic/Plenum Publishers, 2002. ISBN 978-0-306-47508-5.
7. SPOTNITZ, R., FRANKLIN, J. Abuse behavior of high-power, lithium-ion cells. *Journal of Power Sources* [online]. 2003, vol. 113, issue 1, pp. 81-100 [cit. 2014-03-26]. DOI: 10.1016/S0378-7753(02)00488-3.
Available from: <http://linkinghub.elsevier.com/retrieve/pii/S0378775302004883>
8. COLCLASURE, A. M. Thermodynamically consistent modeling of elementary electrochemistry in lithium-ion batteries. *Electrochimica Acta* [online]. 2010, vol. 55, issue 28, pp. 8960-8973 [cit. 2014-04-01]. DOI: 10.1016/j.electacta.2010.08.018. Available from: <http://linkinghub.elsevier.com/retrieve/pii/S0013468610010789>

Decomposition of polar solvents for lithium batteries by high oxidation potential

M. Sedlaříková^{1*}, J. Máca¹, J. Vondrák¹, F. Křištofik²

¹Centre for Research and Utilization of Renewable Energy, Technická 3058/10, Brno, 616 00, Czech Republic

²Department of Electrical and Electronic Technology, Faculty of Electrical Engineering and Communications

Brno University of Technology

Correspondence author: sedlara@seznam.cz

If a secondary cell (accumulator) is charged to 100 %, a question arises on the nature of other electrode processes occurring as a result of continued attempts of charging. It is fairly simple in the case of aqueous batteries which produce just hydrogen and oxygen in such a situation. It is not so simple to understand in lithium secondary cells, in which the water to be decomposed is absent. Overcharging of anhydrous batteries must be investigated and prevented satisfactorily. The aim of this contribution is to gain at least fundamental knowledge of such a process in electrolytes suitable for lithium batteries.

1. Experimental

1.1 Experimental arrangement

Two cells were used for the decomposition of the electrolytes by high current.

Variant A was a simple glass vessel containing two hard carbon electrodes and filled by the tested electrolyte. The electrolyte was exposed to current of 10 – 200 mA for 30 minutes. Samples taken from the vessel were used for estimation of conductivity and flash point.

Variant B was a cell designed so that even small amounts of gases formed at the positive electrode were withdrawn by a micro syringe and analysed by gas chromatography. The vessel was designed so that the resistance of the electrolyte permitted rather high current (10 to 30 mA). It is depicted in Fig. 1.

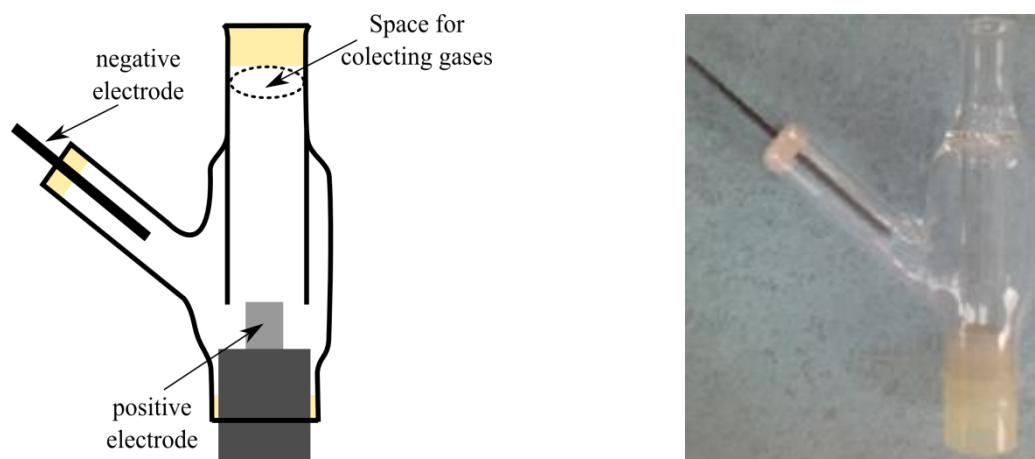


Figure 1. Cell for accumulating of gases generated at the electrode

1.2 Electrolytes

Solutions of LiClO_4 , NaClO_4 or LiPF_6 either in propylene carbonate (PC) or sulfolane (SL) were tested. Triethylphosphate (TEP) was added in several tests as its application can be used as a flame retardant.

2 Results

2.1 Conductivity change

Measured changes of conductivity are listed in Tab. 1. We see expected lower conductivities of solutions containing sulfolane. Another interesting point is higher conductivity of equivalent sodium salts. Finally, the treating by high current caused a marked lowering of conductivity in all cases.

Table I. Change of conductivity caused by exposition to high anodic current in variant A.

Sample	γ Fresh [mS/cm]	γ Exposed to current [mS/cm]
$\text{LiClO}_4 // \text{PC}$	7.58	7.39
$\text{LiClO}_4 // \text{SL}$	3.35	3.24
$\text{LiClO}_4 // \text{PC} + \text{TEP}$	8.78	8.29
$\text{LiClO}_4 // \text{SL} + \text{TEP}$	3.68	3.58
$\text{LiPF}_6 // \text{PC}$	9.00	4.98
$\text{LiPF}_6 // \text{SL}$	3.56	2.09
$\text{LiPF}_6 // \text{PC} + \text{TEP}$	9.58	9.14
$\text{LiPF}_6 // \text{SL} + \text{TEP}$	3.91	3.14
$\text{NaClO}_4 // \text{PC}$	9.28	8.66
$\text{LiClO}_4 // \text{PC} + \text{TEP}$	8.95	8.74

2.2 Flash point

The flash points are listed in Tab. 2. The changes of flash point are not so dramatic, and in several cases we can see the decrease of flash point by exposition to anodic current and a positive effect on TEP on increasing of the flash point value.

Table II. Changes of flash point (flash point in °C)

Sample	v Fresh [°C]	v Exposed to current [°C]
LiClO ₄ // PC	138.0	138.0
LiClO ₄ // SL	162.0	162.0
LiClO ₄ // PC + TEP	145.5	135.0
LiClO ₄ // SL + TEP	167.0	167.0
LiPF ₆ // PC	135.5	132.5
LiPF ₆ // SUL	164.5	157.0
LiPF ₆ // PC + TEP	150.0	145.0
LiPF ₆ // SL + TEP	173.0	167.0
NaClO ₄ // PC	138.0	124.0
NaClO ₄ // PC + TEP	144.5	144.5

2.3 Examples of gas chromatography

The GC was recorded on the device CHROM-5. Examples of results are shown in Fig. 2 for a PC containing electrolyte and for the samples obtained from electrolyte containing SL. Undoubtedly, the solutions prepared from PC + TEP exhibited just one simple peak, which is supposed to be just CO₂. Contrary to that, the chromatogram of a sample obtained from SL + TEP electrolyte is more complex and indicates the formation of components with fairly higher elution time.

It is almost impossible to indicate the nature of volatile components at present. We expect to repeat these experiments using some instrumentation enabled with mass spectrometric detection of gas composition. However, looking on the structures of both cyclic compounds one can suggest, that the strong oxidation causes some splitting the heteroatom with its oxygen atoms off the structure.

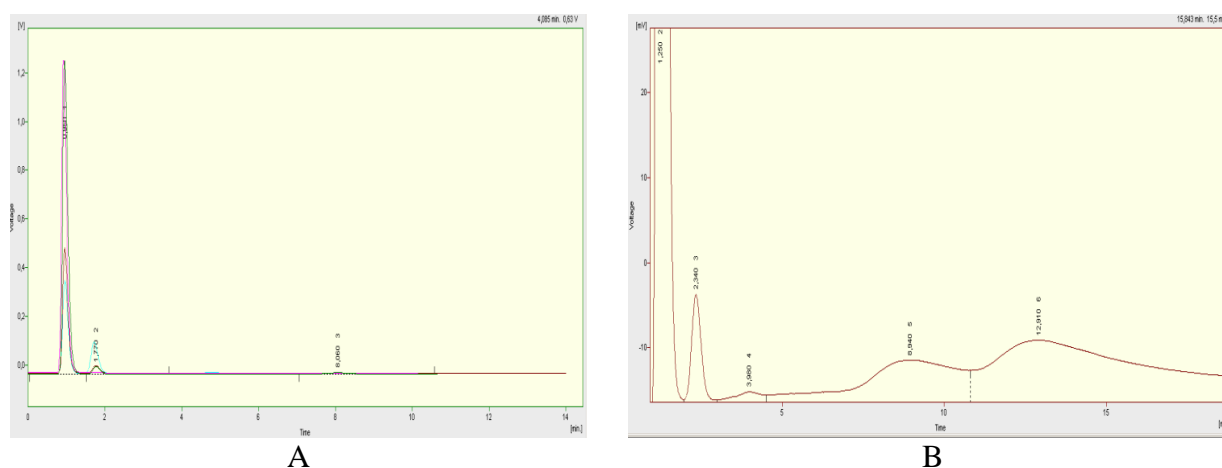


Figure 2. A) Analysis of gases formed from a solution based on PC + TEP, B) Analysis of gases formed from a solution based on SL + TEP

3 Discussion

In the case of all tested samples, the decrease of conductivity and flash point is observed. If we consider the molecules of both solvents, then cleaving of CO₂ seems quite probable from PC. In this case, the remnants are no more of cyclic nature, therefore much lower permittivity and higher volatility should be expected. Something analogical has to be expected to be formed from electrolytes containing SL. Of course, no more than speculations are possible under circumstances.

4 Acknowledgement

Authors gratefully acknowledge financial support from the grant FEKT-S-14-2293 "Materiály a technologie pro elektrotechniku II", LO1210 - Energy for Sustainable Development (EN-PUR)

Effect of La Doping on Physical and Electrochemical Properties of Double Perovskite $\text{Sr}_2\text{FeMoO}_6$ Oxide

A. Kahoul

Laboratoire d'Energétique et d'Electrochimie du Solide, Faculté de Technologie,
Université Sétif-1, 19000 Sétif, Algérie

Corresponding author: kahoulabdelkrim@yahoo.fr

KEYWORDS: Double perovskite, La doping, Oxygen electrode

ABSTRACT. Electrochemical reduction and evolution of oxygen are of considerable interest in many electrochemical devices such as metal-air batteries, fuel cells and water electrolyzers [1]. Perovskite oxides of the general formula ABO_3 are an important class of materials that have been extensively studied as electrocatalysts not only for the oxygen evolution but for its reduction as well, and can thus be used simultaneously as bifunctional electrode.

A subclass of perovskite known as “double perovskite” on which we are working is represented by the general formula $\text{A}_2\text{BB}'\text{O}_6$ (where A is an alkaline-earth atom such as Sr, and B and B' are transition-metal atoms like Fe [2] or Co [3], and Mo). It has been reported that the electron doping in $\text{Sr}_2\text{FeMoO}_6$, achieved via the substitution of a divalent alkaline earth Sr^{2+} by a trivalent La^{3+} ion, increases disorder in Fe/Mo sublattice of $\text{Sr}_{2-x}\text{La}_x\text{FeMoO}_6$, leading to a low electrical resistivity and to a semi-conducting character [2]. The crystal structure of $\text{Sr}_2\text{FeMoO}_6$ can be cubic or tetragonal with regular arrangement of corner-sharing FeO_6 and MoO_6 octahedra. This specific arrangement of alternating different cations can be of great interest in the electrochemical activity, since the properties of perovskites as electrocatalysts are generally determined by the nature, oxidation states and relative arrangement of B-site cations.

It is well known that the electrochemical activity in perovskite oxides are frequently related to electrical resistivity and electronic delocalisation. From this point of view, the semi-conducting double perovskite seems to be a good candidate to show interesting electrocatalytic properties for oxygen reduction and evolution reactions. With this purpose in mind, we present the results concerning La doping effects on the structural (Fig.1), grain morphology, and electrical properties of $\text{Sr}_{2-x}\text{La}_x\text{FeMoO}_6$ oxides. We investigate also the electrochemical behavior of such compounds prepared as oxygen electrode films in energy conversion device.

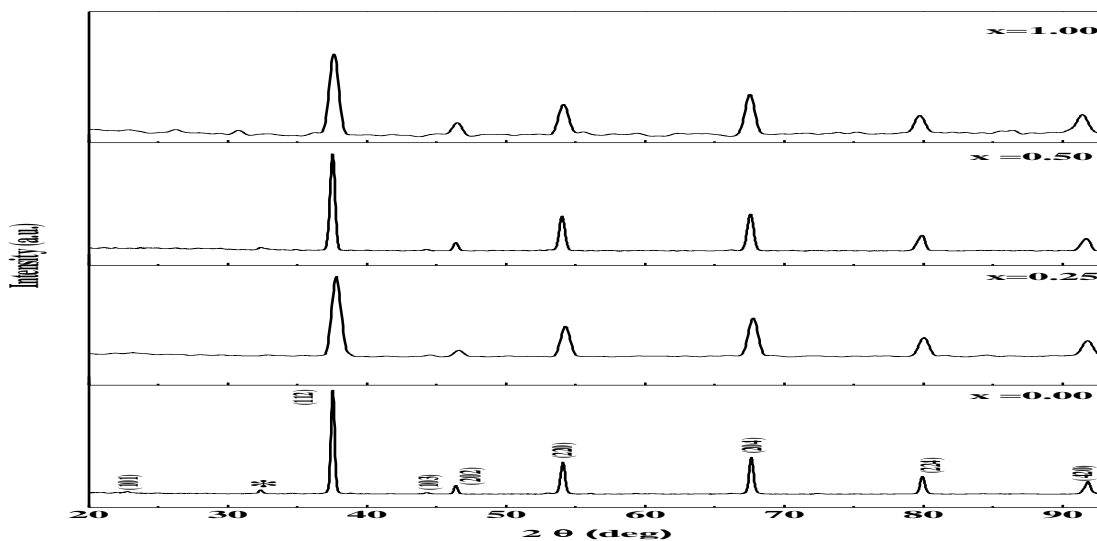


Figure 1. X-ray diffraction patterns for $Sr_{2-x}La_xFeMoO_6$ ($x=0, 0.25, 0.50$ and 1). The star indicates the reflexion of $SrMoO_4$ impurity phase.

References

1. A. Hammouche, A. Kahoul, D.U. Sauer, R.W. De Doncker, *J. Power Sources* **153** 239 (2006).
2. A. Kahoul, A. Azizi, S. Colis, A. S., D. Stoeffler, R. Moubah, G. Schmerber, C. Leuvrey, A. Dinia, *J. Appl. Phys.* **104** 123903 (2008).
3. A. Azizi, A. Kahoul, G. Schmerber, S. Colis, A. Dinia, *Int. J. Modern Phys.* **22** 3579 (2008).

Gel polymer electrolytes

P. Dvořák, M. Sedlaříková, J. Vondrák

Department of Electrical and Electronic Technology, Brno University of Technology,
Faculty of Electrical Engineering and Communication, Technická 3058/10 616 00 Brno, Czech
Republic.

Corresponding author: Petr Dvořák
E-mail address: dvorakp@feec.vutbr.cz

Gel polymer electrolytes containing immobilized different types of salts (LiPF₆, LiBF₄, TEABF₄) in aprotic solvents (PC, EC:DEC, EC DMC) were prepared by UV polymerization. Electrolytes were optimized to achieve suitable ionic conductivity (up to 7,5 mS/cm) and good mechanical stability. The electrochemical stability up to 4 V was determined on stainless steel electrode by voltammetrical measurements.

Introduction

Polymer electrolytes are an essential part of modern power sources. Their electrochemical and mechanical properties have been investigated since 1980. Liquid electrolytes as the medium for ion transport between electrodes of a device are being replaced by solid or gel (semi-solid) electrolytes. This is because electrochemical power sources based on liquid electrolytes are usually associated with problems of leakage, self-discharge, corrosion, bulky design etc. Application of the gel electrolytes includes lithium batteries, supercapacitors and electrochromic devices. [1-3]

In our recent paper we present results of investigation of MMA and EOEMA based electrolytes with three types of salts and solvents.

Experimental

Materials

All chemicals were purchased from Sigma-Aldrich. Monomers methyl methacrylate (MMA) and 2-ethoxyethyl were distilled under reduced pressure. Cross-linking agents ethylene glycol dimethacrylate (EDMA) and 1,6-hexandiol dimethacrylate (HexadiMA), polymerization initiator benzoine ethylether (BEE), ethylene carbonate (EC), propylene carbonate (PC) and dimethyl carbonate (DMC) were used as received. Lithium salts TEABF₄, LiBF₄ and LiPF₆ were dehydrated in Ar₂ atmosphere at 50°C for 24 hours. All chemicals were stored at 4°C in the glove box refrigerator.

Gel polymer electrolyte preparation

The initial mixture was prepared in the glove box under argon atmosphere and consisted liquid electrolyte (salt and solvent), monomer MMA or EOEMA (20 mol% of liquid electrolyte), cross-linking agent EDMA or HexadiMA (3,5 mol% of monomer), polymerization initiator BEE (1 mol% of monomer). In the case of gels with TEABF₄, was amount of cross-linking agent 9 mol% of monomer.

Gel electrolytes were prepared using direct radical polymerization initiated by UV 500 W light and took 40 minutes at room temperature. The procedure was carried out in mold formed from PTFE plate, packing distance PTFE frame and glass plate. Mold was closed using screw clamps.

Obtained samples of GPEs with area 4 cm x 4 cm and thickness corresponding with type of used PTFE seal (0,8 mm) were more or less elastic and transparent.

Equipment and measurements

Potentiostat VMP3 (Biologic) was used for electrochemical measurements. Samples of gel polymer electrolytes were investigated in stainless steel cells (El-Cell, type ECC-Std).

Conductivity measurements were performed by using impedance spectroscopy in the frequency range from 100 kHz to 0,1 Hz.

Electrochemical window (EW) of GPE was measured by linear sweep voltammetry (LSV) with scanate 0,5 mV/s in the potential range 0 to 3,5 V.

Results and discussion

All prepared electrolytes were elastic, transparent and homogenous membranes of a thickness 0,8 mm. All used chemicals are colorless; therefore the prepared membranes are highly transparent.

In the Table 1 are ionic conductivities of all prepared gel polymer electrolytes at the temperature 25 °C.

Table I. Ionic conductivity of gel electrolytes

		γ [mS/cm]				
		c [mol/l]	0,25	0,5	0,75	1
EOEMA+EDMA	LiBF ₄ in EC:DMC (1:1 wt.)	1,08	1,61	2,22	0,91	
	LiPF ₆ in PC	0,93	1,32	1,01	1,23	
	TEABF ₄ in EC:DEC (1:1 wt.)	1,19	1,55	3,00	-	
		γ [mS/cm]				
		c [mol/l]	0,25	0,5	0,75	1
EOEMA+HexadiMA	LiBF ₄ in EC:DMC (1:1 wt.)	2,04	2,68	2,07	1,63	
	LiPF ₆ in PC	0,90	1,39	1,22	1,38	
	TEABF ₄ in EC:DEC (1:1 wt.)	1,17	1,71	2,93	-	
		γ [mS/cm]				
		c [mol/l]	0,25	0,5	0,75	1
MMA+EDMA	LiBF ₄ in EC:DMC (1:1 wt.)	1,85	2,01	2,16	1,68	
	LiPF ₆ in PC	2,86	1,85	1,97	1,75	
	TEABF ₄ in EC:DEC (1:1 wt.)	3,43	4,84	4,27	-	
		γ [mS/cm]				
		c [mol/l]	0,25	0,5	0,75	1
MMA+HexadiMA	LiBF ₄ in EC:DMC (1:1 wt.)	1,75	1,83	2,55	2,06	
	LiPF ₆ in PC	3,15	2,25	1,85	1,57	
	TEABF ₄ in EC:DEC (1:1 wt.)	2,19	5,29	7,46	-	

Electrolytes 1 mol/l TEABF₄ in EC:DEC (wt.) weren't measured due to precipitation of the salt during preparation of gel.

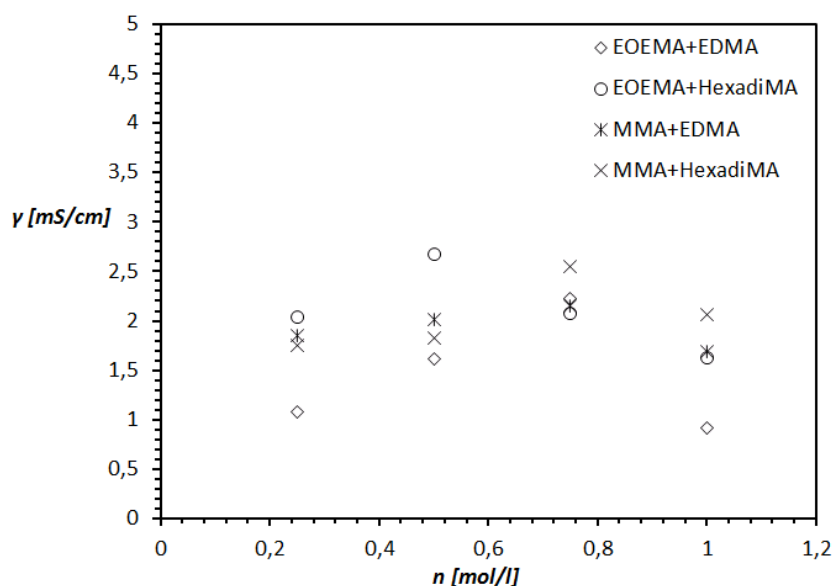


Figure 1. Dependence of ionic conductivity of gel polymer electrolytes on LiBF₄ concentration

For actual lithium ion battery and supercapacitor, the cell potential can reach up to 4 V. In the Table 2 are shown values of the voltage at the current $I = 5 \mu\text{A}$ and $10 \mu\text{A}$, which corresponds to current density $J = 2 \mu\text{A}/\text{cm}^2$ and $4 \mu\text{A}/\text{cm}^2$.

Table II. Electrochemical stability of gel polymer electrolytes

	MMA		EOEMA	
	I = 5 μA	I = 10 μA	I = 5 μA	I = 10 μA
	U [V]			
0,5 mol/l LiPF ₆ v PC	1,97	2,32	1,64	1,92
0,5 mol/l LiBF ₄ v EC:DMC (1:1 hm.)	1,55	2,01	0,28	0,88
0,5 mol/l TEABF ₄ v EC:DEC (1:1 hm.)	1,78	2,18	0,92	1,13
	U _{cell} [V]			
0,5 mol/l LiPF ₆ v PC	3,94	4,64	3,28	3,8
0,5 mol/l LiBF ₄ v EC:DMC (1:1 hm.)	3,1	4	0,56	1,76
0,5 mol/l TEABF ₄ v EC:DEC (1:1 hm.)	3,56	4,36	1,84	2,2

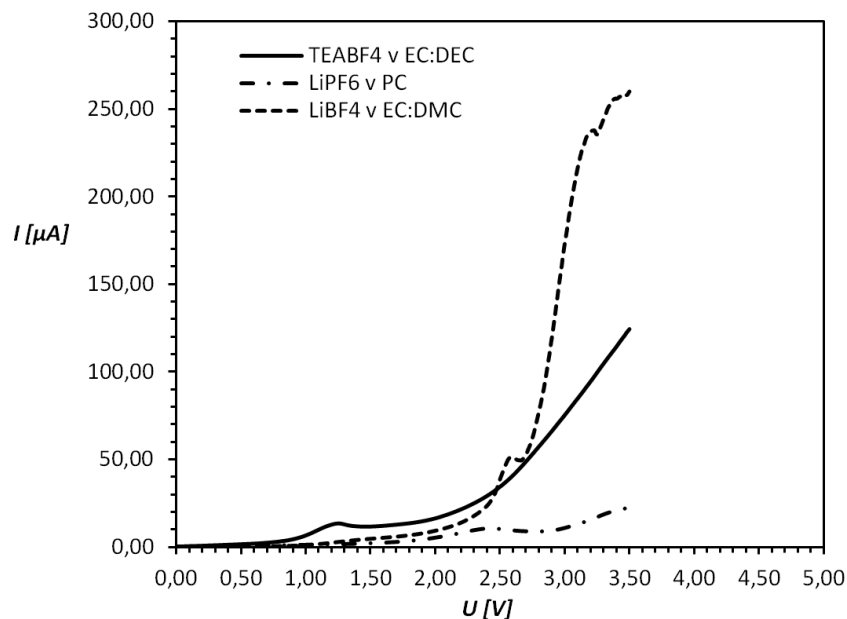


Figure 2. LSV of MMA based gel polymer electrolytes.

Conclusion

MMA or EOEMA based gel polymer electrolytes were successfully prepared by direct polymerization process and their electrochemical properties were investigated. The maximum ionic conductivity was found to reach 7,5 mS/cm (TEABF₄) and 2,7 mS/cm (LiPF₆) at 25 °C. The electrochemical window was stable up to 4 V with LiPF₆ and TEABF₄ salts.

Acknowledgements

This work was supported by the grants „Support for human resources and transfer of knowledge in conditions of international cooperation of research teams“ CZ.1.07/2.3.00/20.0103 and FEKT-S-14-2293.

References

1. Cesar Sequeira, Diogo Santos, *Polymer electrolytes: fundamentals and applications*. Cambridge: Woodhead Publishing, 2010. ISBN 18-456-9772-3.
2. Jeffrey W. Fergus, *Ceramic and polymeric solid electrolytes for lithium-ion batteries*, Journal of Power Sources, Volume 195, Issue 15, 1 August 2010, Pages 4554-4569, ISSN 0378-7753
3. S. K. Tripathi, Ashish Gupta, Manhu Kumari, *Studies on electrical conductivity and dielectric behaviour of PVdF–HFP–PMMA–NaI polymer blend electrolyte*, Bull. Mater. Sci., Volume 35, No. 6, November 2012, Pages 969–975

Transference number measurements on gel polymer electrolytes for Lithium-Ion batteries

M. Musil, J. Vondrak

Department of Electrotechnology, Brno University of Technology, Faculty of Electrical Engineering and Communication, Technická 3058/10 616 00 Brno, Czech Republic.

Corresponding author: Michal Musil
E-mail address: michal.musil@phd.feec.vutbr.cz

Gel polymer electrolytes for Lithium-Ion batteries based on MMA and LiPF₆ in EC:DMC (1:1 wt.) with different salt concentration were prepared by radical photo polymerization. These samples were measured on transference number using Bruce-Vincent method based on combination of *DC* polarization and *AC* Electrochemical Impedance Spectroscopy (EIS) techniques. This method gave values ranging from 0.24 at 0.05 mol l⁻¹ LiPF₆ to 0.69 at 1 mol l⁻¹ LiPF₆ salt concentration.

Introduction

Transference number is dimensionless parameter which gives information about the contribution of the particular charged species present in the bulk of electrolyte to the overall charge transport across the measured system. In case of a simple binary electrolyte with dissociated salt C⁺ A⁻, it can be described with following expression:

$$t_c = \frac{I_c}{I_c + I_A} \quad [1]$$

where t_c is cation transference number, I_c is current carried by cations and I_A is current carried by anions. Value of t_c lay exclusively in range from 0 to 1. In most real electrolyte systems based on organic solvents, the salt is not usually fully dissociated. Even if we try to use appropriate combination of solvents, it is due to a combination of insufficient permittivity of the solvent and high concentration of salt, which is required in Lithium-Ion batteries.

If the salt is not completely dissociated, some equilibria will exist in which associated species are formed. These species types are e. g. ion-pairs, triplets and larger clusters of ions. They all may be mobile within the electrolyte and can contribute to the charge transport. We suppose, that cations is the active electrode specie.

Both cations and anions are mobile in considered gel polymer electrolytes. When conductivity applying small *AC* potential over the electrolyte is measured, it takes into consideration the charge transport contribution from all the charged mobile ionic species mentioned above. When a *DC* current passes through the bulk of electrolyte, the charge is initially transported by both the mobile positive charged species and the mobile negative charged species. A concentration gradient will develop within the electrolyte gradually because electrodes are blocking towards the anions and the charge is transported through the electrolyte only by the mobile positive charged species. Uncharged mobile species may be also present in electrolyte. Uncharged ones will be transported by the concentration gradient and thus contribute to the charge transport.

Bruce-Vincent method

Several methods have been introduced to measure transference number. The DC polarization method (Bruce-Vincent) is very easy to use on gel polymer electrolytes. This method is based on measuring the current initially and after the steady state condition due to small potential applied over the cell. This method therefore provides a transference number based on both mobile charged species and mobile uncharged species, which may be higher, than transference numbers found using Hittorf method based on concentration change close to the non-blocking electrodes. Moreover, when the transference number is measured by both methods, the difference between the measured transference numbers will be an indication of the amount and mobility of uncharged ionic species.

$$T_+ = \frac{I_{ss} V - I_0 R_0}{I_0 V - I_{ss} R_{ss}} \quad [2]$$

U is applied DC potential difference, I_0 and I_{ss} are values of current obtained from DC polarization curves, represent the initial and steady state current flowing through the cell. R_0 and R_{ss} obtained from AC impedance spectra, represent the initial and steady state resistance. The applied DC potential difference was 10 mV. The frequency range of AC impedance was set from 100 kHz to 10 mHz.

Conclusion

PMMA-based gel polymer electrolytes were successfully prepared by direct polymerization processes and measured on transference number. This Bruce-Vincent method gave values ranging from 0.24 at 0.05 mol l⁻¹ LiPF₆ to 0.69 at 1 mol l⁻¹ LiPF₆ salt concentration in accordance to previous works.

Acknowledgements

Authors gratefully acknowledge financial support from the Centre for Research and Utilization of Renewable Energy under project No. LO1210 – „Energy for Sustainable Development (EN-PUR)“ and the grant FEKT-S-14-2293.

References

1. AROF, A.K., M.Z. KUFIAN, M.F. SYUKUR, M.F. AZIZ, A.E. ABDELRAHMAN and S.R. MAJID. 2012. Electrical double layer capacitor using poly(methyl methacrylate)–C4BO8Li gel polymer electrolyte and carbonaceous material from shells of mata kucing (*Dimocarpus longan*) fruit. *Electrochimica Acta*. Vol. 74, p. 39-45.
2. BRUCE, P. 1988. Conductivity and transference number measurements on polymer electrolytes. *Solid State Ionics*. 28-30, p. 918-922.
3. BRUCE, Peter G., Martin T. HARDGRAVE and Colin A. VINCENT. 1992. dc Polarization of polymer electrolytes. *Electrochimica Acta*. Vol. 37, issue 9, p. 1517-1520.
4. CRIVELLO, J.V.. 2012. Photopolymerization. *Polymer Science: A Comprehensive Reference*. New York: Elsevier, p. 919-955. ISBN 9780080878621.
5. EVANS, James, Colin A. VINCENT and Peter G. BRUCE. 1987. Electrochemical measurement of transference numbers in polymer electrolytes. *Polymer*. Vol. 28, issue 13, p. 815-2328.

6. GEORÉN, Peter and Göran LINDBERGH. 2001. Characterisation and modelling of the transport properties in lithium battery polymer electrolytes. *Electrochimica Acta*. Vol. 47, issue 4, p. 577-587.
7. GOLODNITSKY, D. 2009. Electrolytes: Single Lithium Ion Conducting Polymers. *Encyclopedia of electrochemical power sources - 5 vol. set*. Tel Aviv, Israel: Elsevier, p. 112-128. ISBN 9780444520937.
8. GUVENDIREN, M., B. PURCELL and J.A. BURDICK. 2012. Photopolymerizable Systems. *Polymer Science: A Comprehensive Reference*. Philadelphia: Elsevier, p. 413. ISBN 9780080878621.
9. HUTCHISON, J. and A. LEDWITH. 1973. Mechanisms and relative efficiencies in radical polymerization photoinitiated by benzoin, benzoin methyl ether and benzil. *Polymer*. Vol. 14, issue 9, p. 405-408.
10. MOAD, G. 2012. Radical Polymerization. *Polymer Science: A Comprehensive Reference*. Australia: Elsevier, p. 59. ISBN 9780080878621.
11. OLSEN, IbI., Rene KOKSBANG and Eivind SKOU. 1995. Transference number measurements on a hybrid polymer electrolyte. *Electrochimica Acta*. Vol. 40, issue 11, p. 1701-1706.

Comparative Study of Different Alkali (Na, Li) Titanate Substrates as Active Materials for Anodes of Lithium Ion Batteries

S. Chauque^a, C. B. Robledo^b, E. P. M. Leiva^b, F. Y. Oliva^a and O. R. Cámara^a

^a INFIQC - Department of Physical Chemistry, Universidad Nacional de Córdoba, Ciudad Universitaria CP5000, Córdoba, Argentina

^b INFIQC - Department of Mathematics and Physics, Universidad Nacional de Córdoba, Ciudad Universitaria CP5000, Córdoba, Argentina

The relationship between structure and lithium storage capacity of different titanate samples as anode materials for lithium ion batteries is discussed. $\text{Li}_4\text{Ti}_5\text{O}_{12}$, $\text{Na}_2\text{Ti}_3\text{O}_7$ and $\text{Na}_2\text{Ti}_6\text{O}_{13}$ were synthesized by solid-state reaction. The structure, surface and morphology of the samples were characterized by SEM, XRD and RAMAN spectroscopy, and the electrochemical performance was studied by galvanostatic charge-discharge cycling, cyclic voltammetry, electrochemical impedance spectroscopy and rate capability. The lithium titanate presented the highest capacity of the three electrodes, together with the most reversible potential plateau (at 1.6 V vs Li^+/Li^0) and the best response in rate capability at increasing discharge currents. Diffusion coefficients of Li^+ ions into the titanate matrices were obtained, showing the highest value for the lithium titanate compound. Between both sodium titanates, $\text{Na}_2\text{Ti}_6\text{O}_{13}$ presented the highest specific capacity and the best discharge retention.

Beyond Conventional Electrocatalysts: “Hollow” Nanoparticles for Improved and Sustainable Oxygen Reduction Reaction Activity

L. Dubau^{1,2}, M. Lopez-Haro^{1,2,3}, J. Durst⁴, L. Guétaz⁵, P. Bayle-Guillemaud³, M. Chatenet^{1,2}, F. Maillard^{1,2}

¹ Univ. Grenoble Alpes, LEPMI, F-38000 Grenoble, France

² CNRS, LEPMI, F-38000 Grenoble, France

³ CEA, INAC/UJF-Grenoble 1, UMR-E, SP2M, LEMMA, Minatec, 38054 Grenoble Cedex 9, France

⁴ Institute of Technical Electrochemistry, Technische Universität München, Lichtenbergstrasse 4, D-85748, Garching, Germany

⁵ CEA, LITEN, Département des Technologies de l'Hydrogène, Laboratoire des Composants PEM, 17 rue des Martyrs, 38054 Grenoble, France

laetitia.dubau@lepmi.grenoble-inp.fr

This paper describes the synthesis and the characterization of “hollow” Pt-rich/C nanocrystallites (Figure 1A) for the oxygen reduction reaction (ORR). Their specific activity reach a 3-fold (Figure 1B) and 5-fold enhancement over conventional “solid” Pt/C nanocrystallites of the same size in liquid electrolyte and during real proton-exchange membrane fuel cell (PEMFC) testing, respectively. More importantly, the “hollow” nanoparticles can sustain this level of performance during accelerated stress tests in both liquid and solid electrolyte. The average contraction of the Pt lattice by 1 % (Figure 1C) and the Pt coordination number ($N_{Pt} = 7.5$) point towards the presence of vacancies in the Pt-rich shell, which may account for their improved catalytic properties.

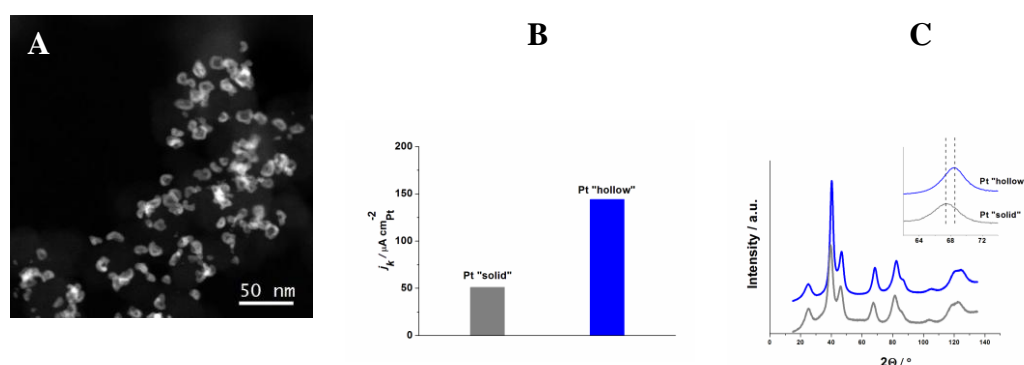


Figure 1. (A) Aberration-corrected high resolution high angle annular dark field scanning transmission electron microscopy of the “hollow” Pt-rich/C nanoparticles (B) ORR specific activity measured at 0.90 V vs. the reversible hydrogen electrode (RHE) in 0.1 M H₂SO₄ and (C) X-ray diffraction pattern of the “hollow” Pt-rich/C and of the reference “solid” Pt/C nanoparticles.

Preparation of Graphene and Multiwalled Carbon Nanotube Composite Modified Electrode and their application in glucose/O₂ biofuel cell

Shen-Ming Chen*, Rajkumar Devasenathipathy

Department of Chemical Engineering and Biotechnology, National Taipei University of Technology, No.1, Section 3, Chung-Hsiao East Road, Taipei 106, Taiwan (R.O.C).

Abstract

We have constructed a glucose/O₂ biofuel cell (BFC) with electrochemically reduced graphene oxide–multiwalled carbon nanotube (ERGO–MWCNT) modified glassy carbon electrode (GCE) as anode and graphene–Pt composite modified GCE as cathode. . The composition and structure of the resulting ERGO–MWCNT and graphene–Pt were confirmed by cyclic voltammetry (CV), scanning electron microscopy (SEM), ultraviolet- visible (UV-Vis) spectroscopy, energy dispersive X-ray spectroscopy (EDX) and X-ray diffraction (XRD) studies The electrochemical characterization results show that enzyme GOx was well immobilized onto the composite modified electrode. Moreover the composite modified film exhibits excellent catalytic ability towards the oxidation of glucose in the presence of redox mediator hydroquinone (HQ). Graphene–Pt composite has been prepared by simple sodium borohydride reduction method and characterized. The graphene–Pt composite modified GCE shows good electrocatalytic activity towards O₂ reduction. A membraneless glucose/O₂biofuel cell (BFC) has been developed by employing ERGO–MWCNT modified GCE as anode and graphene–Pt as cathode. The maximum power density of 46 $\mu\text{W cm}^{-2}$ was achieved for the constructed biofuel. The results showed that graphene based composites are potential candidates for the development of efficient biofuel cells.

Nanostructured electrocatalytic materials for hydrogen evolution reaction

R. Oriňáková^{1*}, M. Sabalová², L. Škantárová¹, A. Oriňák¹, A. Straková Fedorková^{1,3}

¹Department of Physical Chemistry, Institute of Chemistry, Faculty of Science, P.J. Šafárik University, Moyzesova 11, SK-041 54 Košice, Slovak Republic

²Department of Physical and Theoretical Chemistry, Faculty of Natural Sciences, Comenius University, Mlynská dolina, SK-84215 Bratislava 4, Slovak Republic

³Department of Electrical and Electronic Technology, Faculty of Electrical Engineering and Communication, Brno University of Technology, Technická 10, CZ-61600 Brno, Czech Republic

*Corresponding author. Tel.: +421 55 2342328; fax: +421 55 6222124.

E-mail address: Renata.Orinakova@upjs.sk

Introduction

Hydrogen, as the friendliest fuel to the environment is expected to play a major role in the development of sustainable energy. It came up to the stage because of the largest energy density, ease to produce, and its broad applications (1-4). The most desirable source of hydrogen is water. Electrocatalytic hydrogen evolution reaction (HER) is one of the most efficient methods for large-scale hydrogen production, where the pure hydrogen can be supplied by environmentally friendly energy sources, without evolution of the green-house gas (1, 5, 6). The main operating cost of the hydrogen evolution is the cost of electricity. Hence, the efficient and low-cost electrocatalysts are indispensable in this electrochemical process. The research and development efforts have been recently focused on the minimizing ohmic resistance, lowering overpotential through improving cell and electrode design and using electrode material with higher electrocatalytic activity (5).

HER has the potential to provide a sustainable energy supply for the future, but its commercial application is hampered by the use of precious platinum catalysts. Electrochemical production of hydrogen from water has been directed to the search for non-noble metal based and earth-abundant catalysts (7).

The current generated at an electrode is proportional to the active surface of catalyst on the electrode surface, so more active electrocatalysts can be formed from nanomaterials, because nanomaterials have a higher surface area to volume ratio. The applications of highly active nanomaterials in the field of catalysis for fuel cells reactions such as methanol oxidation and hydrogen and oxygen evolution reactions have attracted the attention of many scientific researchers and became one of the most important topics. The electrocatalytic activity and the stability of the nanomaterials during the course of a reaction are a concern for nearly all electrodes. Recently, shape-control of the nanoparticles has become an imperative task due to the fact that most of the reactions in fuel cells are sensitive to the surface structure of the catalysts.

Effective electrocatalysts are now routinely prepared by the modification of conducting polymers by electrodeposition and dispersion of catalyst particles on a preformed polymer (4, 8) or by incorporation of metal crystals or crystal aggregates in conducting polymer films during monomer polymerization (9, 10).

The scope of our work includes the use of the electrochemically deposited silver nanoparticles, as a novel cost-effective nanostructured catalysts with high activity towards the HER in acid media. The electrocatalytic activity of such catalysts can be enhanced by the use of conducting polymers as substrates.

Experimental

The electrochemical experiments were carried out in a conventional three-electrode cell using an Autolab PGSTAT 302N potentiostat, interfaced to a computer. The counter electrode was a large-area platinum electrode. The reference electrode was an Ag/AgCl/3 mol/l KCl electrode. The working electrode was a paraffin impregnated graphite electrode (PIGE) of surface area 1.13 cm². To obtain reproducible results, the surface of PIGE was before electrodeposition of an electrocatalytic layer carefully renewed, mechanically polished using sand paper and glossy paper, rinsed with distilled water and finally electrochemically cleaned in 0.1 mol/l H₂SO₄ by potentiodynamic cycling in potential range from -200 to -1200 mV (vs. Ag/AgCl/3 mol/l KCl) at 1mV/s. The platinum electrode was cleaned in nitric acid (1:1) and rinsed with distilled water before use.

Electrochemical formation of PPy layer on PIGE was carried out in 0.6 mol/l aqueous pyrrole solution with pH = 2.2 using cyclic voltammetry in 5 cycles within the potential limits from -1100 to +1100mV (vs. Ag/AgCl/3 mol/l KCl) at the potential scan rate 25 mV/s. 0.1M NaCl solution was chosen as the supporting electrolyte.

Electrodeposition of Ag nanoparticles onto PIGE or PPy surface was performed potentiodynamically between -350 and -1000mV (vs. Ag/AgCl/3 mol/l KCl) from the electrolyte solution containing 1 mmol/l AgNO₃ and 0.1 mol/l NaNO₃ at scan rate 12.5 mV/s in 10, 20 or 40 cycles. In order to reduce any nickel oxides spontaneously formed on the electrocatalytic layer, the prepared electrodes were polarized in 0.1 mol/l H₂SO₄ at -500 mV (vs. Ag/AgCl/3 mol/l KCl) for 5min.

The electrocatalytic activity of PPy/Ag layers in the hydrogen evolution reaction was studied between -1200 and +200 mV (vs. Ag/AgCl/3 mol/l KCl) in 0.1 mol/l H₂SO₄ solution at a scan rate 1mV/s at room temperature.

Chemicals used in research were purchased from Sigma-Aldrich or Merck Company, and were used without further purification. All measurements were made in an oxygen-free solution, which was achieved by continuous purging of the cell electrolyte with argon gas.

The surface morphology of prepared PPy/Ag electrodes were characterised by scanning electron microscopy in combination with energy dispersive X-ray microanalysis (SEM/EDX) (Tesla BS 340 with EDX LINK ISIS microanalyser operated at 20 kV with a collection time of 120 s). The operating voltage for the SEM was maintained at 20 kV throughout the analysis.

Results and Discussion

The monomer is oxidized at the surface of the positively polarized working electrode during an electrochemical polymerization of pyrrole. As a result, the black homogeneous and coherent polypyrrole layer with cauliflower-like structure constituted by micro-spherical grains is formed.

Silver nanoparticles were deposited on the pre-formed PPy layer. The size of Ag nanoparticles and surface coverage was lowest for PPy/Ag layers deposited in 10 cycles of Ag (Fig. 1). The increase in diameter of Ag nanoparticles with increasing number of deposition cycles was

observed. The diameter of Ag nanoparticles deposited in 10, 20 and 40 deposition cycles was about 100 nm, 130 nm and 200 nm, respectively.

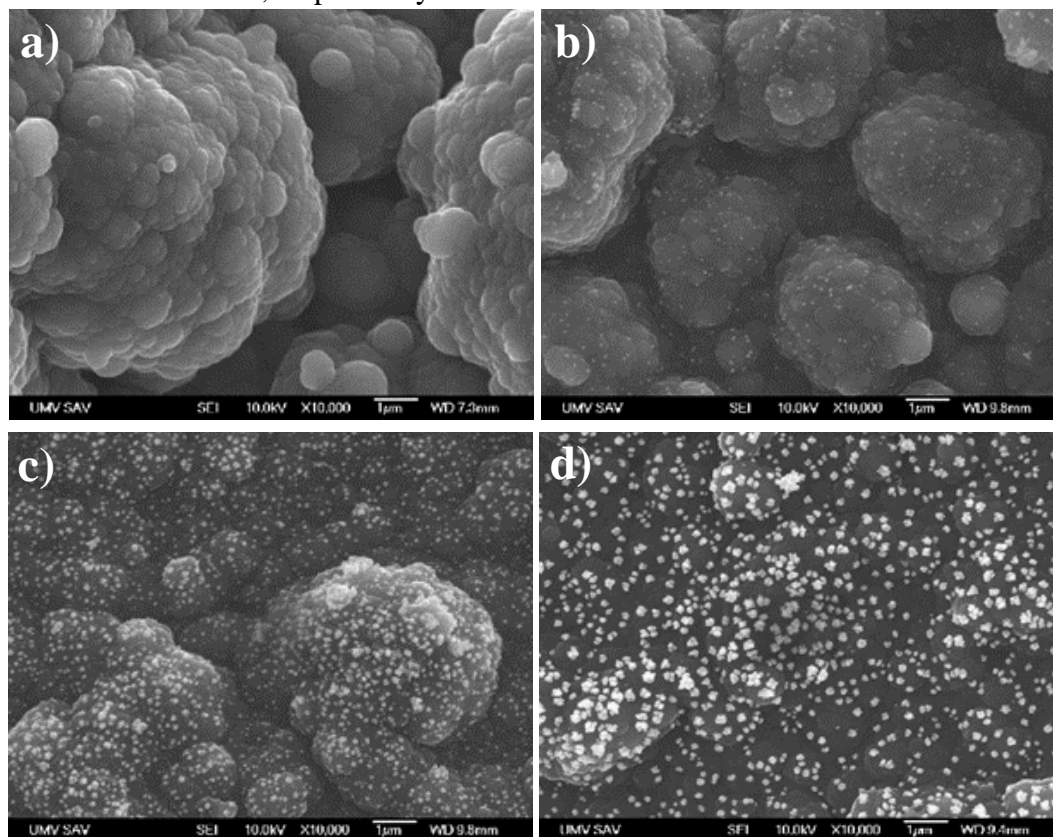


Figure 1. SEM micrographs of PPy (a) and PPy/Ag films produced by electrodeposition of PPy followed by potentiodynamic deposition of Ag in 10 cycles (b), 20 cycles (c) and 40 cycles (d).

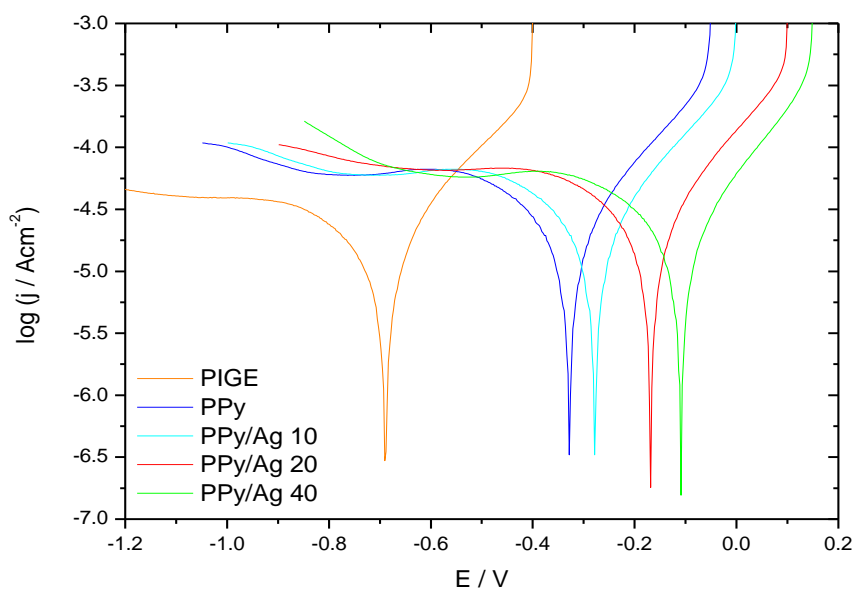


Figure 2. Tafel polarization curves for HER on Pige, PPy, and different PPy/Ag electrodes in 0.1 mol/l H_2SO_4 solution.

The HER activity of resulting PPY/Ag electrode was evaluated depending on Ag loading. Fig. 2 shows the representative Tafel polarization curves for hydrogen evolution on PIGE, PPY, and PPY/Ag electrodes in 0.1 mol/l H₂SO₄ solution applying a slow potentiodynamic sweep of 1mV/s. The equilibrium potential values on modified PPY/Ag electrodes for HER are shifted to less negative potentials compared to the values on bare PIGE and PPY blank. The best catalytic activity was obtained for the catalytic layer produced by electrodeposition of Ag in 40 cycles. It is obvious that the electrodeposition of Ag in 10 cycles as well in 20 cycles resulted in PPY/Ag electrode with smaller surface area available for HER.

Conclusions

Electrocatalysts play key roles in the chemical processes but often limit the performance of the entire systems due to insufficient activity, lifetime, or high cost. It has been a long-standing challenge to develop efficient and durable electrocatalysts at low cost.

A clear relationship exists between electrocatalytic activity towards the HER and the corresponding increase in the extent of surface coverage on the PPY electrode.

Acknowledgments

The authors wish to acknowledge the financial support from the Grant Agency of Ministry of Education of the Slovak Republic (Grant No. 1/0211/12).

References

1. F.Y. Yan, B.Y. Xia, Z. Xu, X. Wang, *ACS Catal.*, 4, 1693 (2014).
2. Y. Zheng, Y. Jiao, Y. Zhu, L.H. Li, Y. Han, Y. Chen, A. Du, M. Jaroniec, S.Z. Qiao, *Nat. Commun.*, 5, Article No. 3783 (2014).
3. R. Aydin, F. Köleli, *Progr. Org. Coat.*, 56, 76 (2006).
4. E. Navarro-Flores, S. Omanovic, *J. Mol. Catal. A: Chem.*, 242, 182 (2005).
5. X. Mo, J. Wang, Z. Wang, S. Wang, *Synth. Met.*, 142, 217 (2004).
6. P.R. Zabinski, R. Kowalik, M. Piwowarczyk, *Arch. Metall. Mater.*, 52, 627 (2007).
7. P. Xiao, M. Alam Sk, L. Thia, X. Ge, R.J. Lim, J.Y. Wang, K.H. Lima, X. Wang, *Energy Environ. Sci.*, DOI: 10.1039/C4EE00957F (2014).
8. V.M. Jovanovic, S. Terzic, A. Dekanski, *J. Serb. Chem. Soc.*, 70, 41 (2005).
9. K. Bouzek, K.M. Mangold, K. Juttner, *Electrochim. Acta*, 46, 661 (2000).
10. Z. Peng, E. Wang, S. Dong, *Electrochem. Commun.*, 4, 210 (2002).

Investigation on the Role of Individual Components of a CNT-RGO Hybrid Support in the ORR Activity of the PEMFC Catalyst

M. Hashempour ^{a,b}, S. Sharma ^b, D. Gonzalez ^b, G. Gupta ^b,
A. Vincenzo ^a, M. Bestetti ^a

^a Dipartimento di Chimica, Materiali e Ingegneria Chimica "Giulio Natta", Politecnico di Milano,
Via L. Mancinelli 7, 20131, Milan, Italy

^b Centre for Hydrogen and Fuel Cell Research, School of Chemical Engineering, University of
Birmingham, Edgbaston, Birmingham, B15 2TT, UK

In this work, multi-walled carbon nanotubes (MWCNTs), reduced graphene oxide (RGO) and MWCNT-RGO hybrid were used as the support materials for platinum as a catalyst for the proton exchange membrane fuel cell (PEMFC). Pt was synthesized by microwave assisted polyol process on the different supports and each support was individually characterized for the oxygen reduction reaction (ORR) activity of PEMFC. Finally, the two carbon materials were mixed to make a hybrid support and its electrochemical behavior was compared to that of the CNT and RGO. CNT-Pt sample showed a remarkably high activity toward ORR compared to RGO-Pt. RGO-Pt on the other hand showed a well-developed diffusion controlled region as a distinct advantage compared to CNT-Pt. Interestingly, hybrid CNT-RGO support showed the positive characteristics of both components borrowing the high current harvest from the CNT and the well-developed plateau from RGO system. This hybrid catalyst-support system also showed the highest mass-specific activity.

Introduction

Carbon nanostructures have been widely investigated as support materials for PEMFCs due to their particular characteristics such as high specific surface area, high electrochemical stability under fuel cell operating conditions and high conductivity (1). Carbon nanotubes have been investigated intensively for this purpose and though showing significant performance, there are a couple of issues that are still to be addressed (2). Due to the inert nature of the CNT walls, the effective attachment of metal catalysts remains a challenge (3). CNT functionalization, as the first solution to this problem, has been reported to have a negative impact on the structure and properties of CNTs.

After the discovery of graphene (4), intensive attention has been paid to this material as a catalyst support for fuel cell applications (5). Methods such as reduction of the graphene oxide prepared by robust oxidation of graphite, has been widely explored due to their competence for scale up production of graphene. Microwave assisted process has shown promising results in simultaneous reduction of graphene oxide and synthesis of catalyst nanoparticles (6,7).

In this work, CNTs prepared by a CVD method and RGO were used as support materials for Pt catalyst. Pt was successfully synthesized on both supports by a microwave assisted polyol process. Moreover, a hybrid support made by the combination of the two materials and decorated with Pt via the same method, was prepared and underwent similar characterizations. The behavior

of the hybrid support was interpreted based on the observations of the individual components of the support.

Experimental

MWCNTs were prepared through a CVD method in a fluidized bed using Fe/Al₂O₃ catalyst at 650 °C (8). Graphene oxide was prepared by the modified Hummer's oxidation method (9). Pt nanoparticle synthesis on carbon supports and also reduction of graphene oxide was carried out by microwave assisted polyol process (6). Microstructure and composition of the materials were characterized by TEM, TGA and XPS and the electrocatalytic activity towards ORR was measured using a three electrode set-up with the support-catalyst slurry being cast on a rotating glassy carbon (GC) as the working electrode. A 0.1 M HClO₄ solution was used as the electrolyte.

Results and Discussion

Fig. 1a, b and c show the TEM images of the Pt nanoparticles on CNT, RGO and CNT-RGO, respectively. Particle sizes were observed to be 3.6, 3 and 4.3 nm for the CNT, RGO and CNT-RGO supports, respectively. Particle size is supposed to have a remarkable effect on the electrochemical surface area of the each sample. TGA results (not shown here) showed Pt contents of 23.38, 46.80 and 30.73 wt% on CNT, RGO and CNT-RGO, respectively. This is due to the availability of various anchoring sites on the different supports' surface. Obviously, the hybrid support exhibits an intermediate behavior with respect to the defective RGO and the inert CNT.

Fig.2 shows the ECSA and ORR results for the three supports. The results are also quantitatively shown in Table 1. It is seen that CNTs, in spite of their larger particle size, show higher ECSA than RGO, a fact that is probably due to higher electrical conductivity of CNT compared to RGO. The hybrid support combines the higher surface area of RGO and good conductivity of CNTs. The CNT sample also shows the highest current harvest in ORR experiment, though the plateau is not very even and well-developed. In contrast, a flat plateau is observed in the case of RGO demonstrating a well-developed diffusion controlled region that might be stemming from the good quality of its thin film and a reasonable hydrophilicity. The hybrid support benefits from both, high ORR current of the CNT and well-developed plateau of RGO, with an area-specific activity (I_s) larger than all samples and a mass-specific activity (I_m) close to that of CNT. Considering also the highest ECSA found for this hybrid support, further research toward optimized performance conditions of such support is advisable.

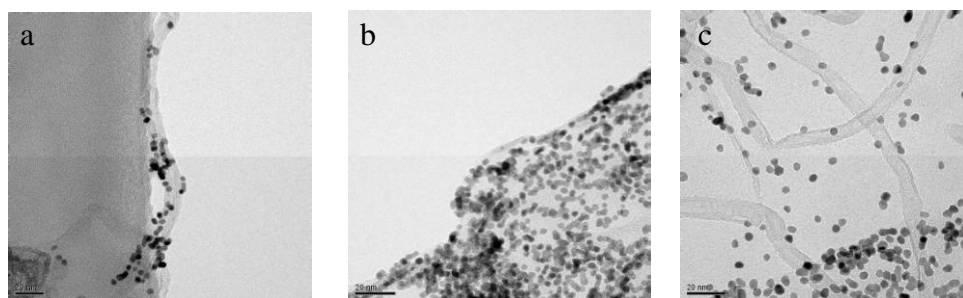


Figure 1. TEM micrographs of Pt catalyst particles synthesized on (a) CNT, (b) RGO and (c) CNT-RGO supports by microwave assisted polyol process.

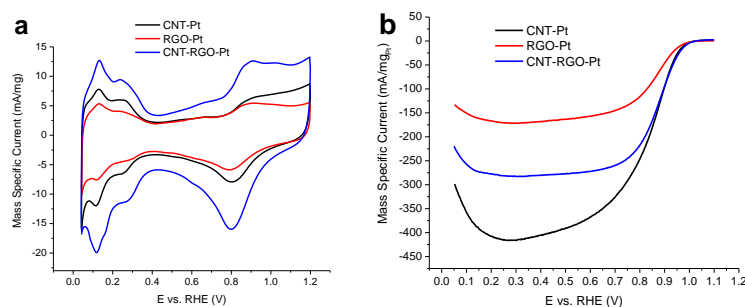


Figure 2. (a) ECSA results of the three supports measured in N_2 purged 0.1 M $HClO_4$ solution at 30 °C and (b) ORR results of the three supports measured in oxygen purged 0.1 M $HClO_4$ solution at 30 °C and 1600 rpm.

TABLE I. Comparison of the electrocatalytic activities of different supports for ORR.

Parameters / Samples	L_{Pt} ($\mu g_{Pt} cm^{-2}$)	ECSA ($m^2 g_{Pt}^{-1}$)	I_m (0.90 V), 20 mV/s (A mg_{Pt}^{-1})	I_c (0.90 V), 20 mV/s ($\mu A cm^{-2}_{Pt}$)
CNT-Pt	13.64	25.62	-0.119	-446.54
RGO-Pt	27.3	14.70	-0.052	-321.10
CNT-RGO-Pt	17.5	41.03	-0.135	-329.05

Conclusion

The structure of the carbon support has a strong effect on the amount of Pt loaded. CNTs with expectedly the lowest defect density, caught showed the lowest loading and RGO with large number of defects showed the highest amount of Pt. Hybrid support was in the middle in this respect. Higher ECSA of CNT based system was attributed to the high conductivity of the CNTs. In case of the hybrid support, due to presence of conductive CNTs between RGO sheets, possibly working as nano interconnects, ECSA improved considerably. RGO based samples show a well-developed diffusion controlled region which is their advantage over CNTs. Good quality of RGO thin film on GC caused by their hydrophilicity could be a reason for this. Hybridizing the 1-d and 2-d support families (CNT-RGO), shares the features of individual components of the hybrid, so as to combine the high current harvest of CNT and well developed plateau of RGO. Accordingly, this sample shows the highest mass-specific activity among the others.

References

1. S. Sharma and B. G. Pollet, *J. Power Sources*, **208**, 96–119 (2012).
2. Z. Jiang and Z.-J. Jiang, in *Carbon Nanotubes - Growth and Applications*, M. Naraghi, Editor, p. 567–604, InTech (2011).
3. K. Balasubramanian and M. Burghard, *Small*, **1**, 180–192 (2005).
4. K. S. Novoselov et al., *Science*, **306**, 666–669 (2004).
5. D. A. C. Brownson, D. K. Kampouris, and C. E. Banks, *J. Power Sources*, **196**, 4873–4885 (2011).
6. S. Sharma et al., *J. Phys. Chem. C*, **114**, 19459–19466 (2010).
7. P. Kundu et al., *Chem. Mater.*, **23**, 2772–2780 (2011).
8. S. Nunga, A. Tito, F. Bianco, M. Bestetti, and V. Mazzocchia, in *12nd SFGP Conference*, p. 617–623, Marseille, France (2009).
9. M. Hirata, T. Gotou, S. Horiuchi, M. Fujiwara, and M. Ohba, *Carbon*, **42**, 2929–2937 (2004).

Internal steam reforming of iso-octane on Co-based anodes in a solid oxide fuel cell

A. Al-Musa^{*1}, V.Kyriakou^{2,3}, N. Kakkidis⁴, M. Al-Saleh¹, A. Al-Zahrani¹, G.E. Marnellos^{2,4}

¹Water and Energy Research Institute, King Abdulaziz City for Science and Technology, KACST
11442, Riyadh, Saudi Arabia

²Chemical Processes and Energy Resources Institute, CERTH, 57001 Thessaloniki, Greece

³Department of Chemical Engineering, Aristotle University of Thessaloniki, 54124, Thessaloniki,
Greece

⁴Department of Mechanical Engineering, University of Western Macedonia, 50100, Kozani, Greece

Tel.: +966 11 4814316

Fax: +966 11 4813880

aalmusa@kacst.edu.sa

Abstract

Global energy demands are continuously growing, with the last estimations speaking of an average growth of 1.8% per year from 2000 to 2030 [1], resulting in an increased interest for electrical vehicles, as the corresponding internal combustion engines are characterized by low efficiencies and high specific pollution levels. This transition requires the development of a new type of energy storage and conversion system, such as fuel cells. However, H₂'s high cost of transporting and storing renders H₂ vehicles prohibitive for commercial use. On the other hand, gasoline and diesel have higher energy density and are easier to handle. Also, in contrast to hydrogen, the necessary production, storage and distribution infrastructure for these liquid fuels already exists. To this end, direct, high efficiency diesel or gasoline fed fuels cells seem to be ideal for use in electric vehicles [1].

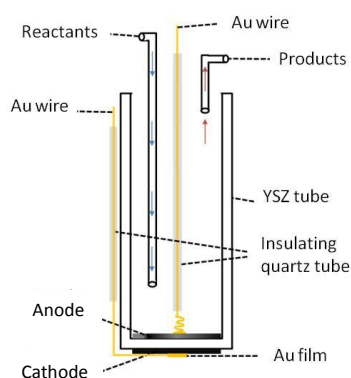


Figure 1. Schematic diagram of the fuel cell reactor

The steam reforming of hydrocarbons for H₂ production has been studied, mainly on Ni-based catalysts [2]. These catalysts showed high catalytic activity and selectivity at elevated temperatures, but they suffer from sintering of the Ni particles and carbon deposition which results in their rapid deactivation. Thus, in this work Co-based supported on rare earth oxides catalysts are used as anodic composites in an iso-octane (surrogate of gasoline) internal reforming SOFC. These

materials have been reported to exhibit high catalytic activity for hydrogen production, good ionic and electronic conductivity and excellent resistance to carbon deposition [3]. The performance of these materials is evaluated with both catalytic and electro-catalytic techniques.

References

1. M. Liu, Y. Choi, L. Yang, K. Blinn, W. Qin, P. Liu, M. Liu, *Nano Energy* 1, 448 (2012).
2. J. Zhang, Y. Wang, R. Ma, D. Wu, *Appl. Catal. A* 243, 251 (2003).
3. N. Kaklidis, P. Michail, S. Pandis, G.E. Marnellos, 8^o Panhellenic Conference of Chemical Engineering, Thessaloniki (2011).

Development of Zinc-Air Fuel Cell

J. Dundálek^a, J. Pociďič^b, P. Mazúr^b, J. Vrána^a and J. Kosek^a

^a Department of Chemical Engineering, Institute of Chemical Technology Prague, Technická 5, 166 28 Praha 6, Czech Republic

^b New Technologies – Research Center, University of West Bohemia, Univerzitní 8, 306 14 Plzeň, Czech Republic

The use of electric vehicles is limited by the lack of suitable mobile power systems. Although hydrogen fuel cell was intensively developed as promising energy storage system, massive production of this technology is limited by the high costs of the system and safety issues linked with the use of pressurized gaseous hydrogen. Therefore, the development of new power systems remains the key for the successful commercialization of the electric car.

Metal-air fuel cells are candidates to compete with the hydrogen technology. The use of metals as the fuel promise several benefits as follows: high energy densities (Wh/l), low environmental impact and simplified storage and transportation. Most studies in this field were done on the zinc-air chemistry as it is very simple and promises low manufacturing costs. Zinc is also abundant, produced in large quantities and cheap. The products of the Zn-air fuel cell are entirely recyclable. When the renewable power source for the fuel regeneration is used, the zinc-air technology may be consider as a clean storage system.

This work presents the development of laboratory zinc-air fuel cells that utilize zinc powder as the fuel and oxygen taken from the surrounding air as the oxidant. Presented design of the fuel cell solves many technical problems linked with use of solid fuel. The clogging of the cell with excess of zinc powder was overcome using the fuel overflow output line. A structured zinc anode bed with low pressure drop was developed to maintain sufficient flow rate of the electrolyte. The assembled fuel cells were characterized by measuring current-voltage curves and subjected to discharge under constant current load. The obtained results are presented and discussed with respect to the further optimization of the zinc-air fuel cell.

Fabrication of Transition Metal Alloy Catalysts for Water Electrolysis using Electrodeposition

Jin Yeong Kim^a, Sung Hoon Hong^a, Sang Hyun Ahn^b, Sung Gyu Pyo^a, Jong Hyun Jang^b,
Soo-Kil Kim^{a*}

^aSchool of Integrative Engineering, Chung-Ang University, Heukseokno 84, Dongjak-gu, Seoul 156-756, Republic of Korea

^bFuel Cell Research Center, Korea Institute of Science and Technology, Hwarangno 14-gil 5, Seongbuk-gu, Seoul 136-791, Republic of Korea

For the production of hydrogen, steam reforming of fossil fuels and coal gasification have been widely used due to the high efficiency and cost effectiveness. However, water electrolysis using electric energy from new/renewable sources must be adopted in near future to prevent the environmental issues such as CO₂ emission. Some key technology issues in the water electrolysis are high activity catalysts for hydrogen and oxygen evolution reactions (HER & OER), bubble managements during the electrolysis, and high conductivity membrane/separator. Particularly for the catalysts, various transition metal catalysts and oxide catalysts have been developed for alkaline and acidic water electrolysis. In this work, we have developed some alloy catalysts and oxide catalysts for both HER and OER. In detail, various Ni-based binary alloys (Ni_xM_y where M = Cu, Co, W) having different composition were fabricated using electrodeposition for HER in alkaline water electrolysis. Various electrochemical and spectroscopic analyses have been adopted to evaluate the activities of those catalysts. The alloy catalysts having specific composition exhibited superior activities to HER than single metal catalysts and the mechanism of the enhanced activities were studied. Besides the alkaline HER catalysts, some recent results on the oxide OER catalysts under acidic medium will be introduced as well.

Electrodeposition-fabricated Alloy Catalysts for High Temperature Proton Exchange Membrane Fuel Cells

Ji-Eun Lim^a, Uk Jae Lee^a, Sung Hoon Hong^a, Jin Yeong Kim^a, Sang Hyun Ahn^b, EunAe Cho^b,
Hyoung-Juhn Kim^b, Jong Hyun Jang^b, Hyungbin Son^a, and Soo-Kil Kim^{a*}

^aSchool of Integrative Engineering, Chung-Ang University, Heukseokno 84, Dongjak-gu, Seoul 156-756, Republic of Korea.

^bFuel Cell Research Center, Korea Institute of Science and Technology, Hwarangno 14-gil 5, Seongbuk-gu, Seoul 136-791, Republic of Korea.

Unlike the low temperature proton exchange membrane fuel cells (PEMFCs), high temperature PEMFCs normally use phosphoric acid (PA)-doped polymer membrane as an electrolyte to maintain the proton conductivity at higher temperature than 100°C. Though the faster electrode kinetics and enhanced CO-tolerance are expected in HT-PEMFC, PA causes a new technical issue of catalyst poisoning and deterioration of its performance. This is due to the nature of phosphate species to strongly adsorb on Pt catalyst surface. Therefore, new catalysts having high activity as well as strong tolerance to PA poisoning is necessary. In this work, we first studied the adsorption behaviour of phosphate on a certain noble metal using in-situ electrochemical surface enhanced Raman spectroscopy and found that the adsorption of phosphate was strongly dependent on the electrode potentials and electrolyte acidity. Based on the observation, we further tried to fabricate PtM alloy catalyst, where M was the studied noble metal, using electrodeposition and tested the catalyst for oxygen reduction reaction (ORR) in the presence of PA. For the tested range of M contents, all the catalysts have exhibited the better activity toward ORR than pure Pt, of which the reason were explained in terms of alloying effect and alteration of phosphate adsorption on M surface. Details will be introduced in the conference.

Pressure mechanism of conductivity in the ternary ZrO₂-systems

V. Barbashov, E. Nesova

Donetsk IPE of the NAS of Ukraine, R. Luxemburg St. 72, 83114 Donetsk, Ukraine

Zirconia (ZrO₂) is one of the better known and sought-after conducting materials. Conductivity in this material is provided by oxygen anions. In earlier studies [1], it was found that dopants can put the "positive" and "negative" pressure on the crystal. It causes by the difference in the ionic size of dopant and matrix ions. This mechanism of action has been considered in [2] for zirconia doped with yttria. Y³⁺ has larger ionic radius compared to Zr⁴⁺ ($r_{\text{Zr}} = 0.98 \text{ \AA}$; $r_{\text{Y}} = 1.16 \text{ \AA}$; $r_{\text{Y}} / r_{\text{Zr}} > 1$). In this case, increasing the dopant concentration leads in the monoclinic-to-tetragonal-to-cubic phase transition. The end result of this transition is forming the high-conductive and stable modification of cubic-ZrO₂. Similar effects are seen in the rising external pressure or temperature.

In the present paper, the experimental simulation of zirconia co-doped with 6-12 mol.% Y₂O₃ and 2 mol.% Fe₂O₃ was performed. In this case we suggest that Fe doping can lead to reducing the hydrostatic pressure and affect the stabilizing action of yttrium. Fe³⁺ has smaller ionic radius compared to Y³⁺ and Zr⁴⁺ ($r_{\text{Fe}} = 0.92 \text{ \AA}$; $r_{\text{Fe}} / r_{\text{Zr}} < 1$). Concentration of Fe dopant was chosen by the condition of Fe₂O₃ full solubility and its separated phase exclusion [3]. Y₂O₃ concentration was chosen by the condition of conductivity maximum at the tetragonal-to-cubic phase transition.

Using the experimental arrhenius plots of ionic conductivity $\lg(\sigma T) - 1/T$ for all studied ceramic specimens, we calculated the thermal activation energies of oxygen ion motion at low- and high-temperature ranges (fig. 1).

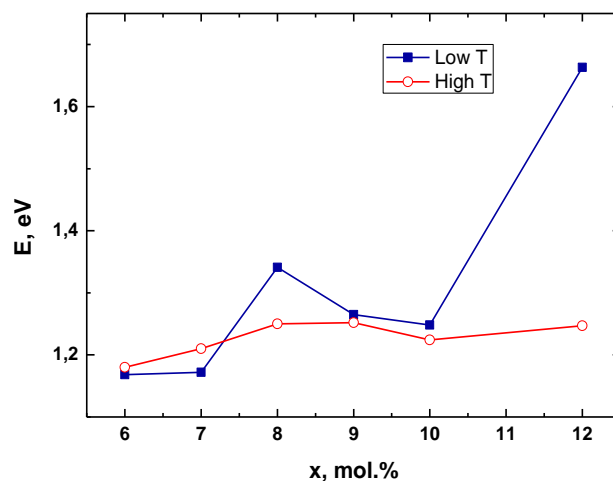


Figure 1. Activation energy in the $((\text{ZrO}_2)_{1-x}(\text{Y}_2\text{O}_3)_x)_{0.98} + (\text{Fe}_2\text{O}_3)_{0.02}$ system via Y₂O₃ concentration at low- and high-temperature ranges.

In terms of our recent study [2] we perform the analysis of plots at fig.1. We can assume that transition in the cubic phase of zirconia appears in the concentration range of 7-10 mol.% Y₂O₃. This transition leads in a reduction of the lattice volume and the internal pressure of Y₂O₃ dopant, Fig. 1. The decrease in the activation energy of oxygen ion mobility is observed despite the densification of material. It is due to reducing the hydrostatic pressure. At a completion of cubic phase transition, addition of the dopant will result in the growth of the internal pressure in a single phase material, increasing the activation energy and diffusion slowdown.

Authors of other studies [4, 5] also show reducing the activation energy for the $\text{ZrO}_2 - \text{Y}_2\text{O}_3$ system at the tetragonal-to-cubic phase transition. It occurs at about 8 mol.% Y_2O_3 .

In the present study for indicated system we perform the numerous calculation of the activation energy and conductivity in the range 3-12 mol.% Y_2O_3 at 1000 °C (fig.2 and 3). These dependences were found to agree qualitatively with experimental data. The extreme points occur at 8 mol.% Y_2O_3 .

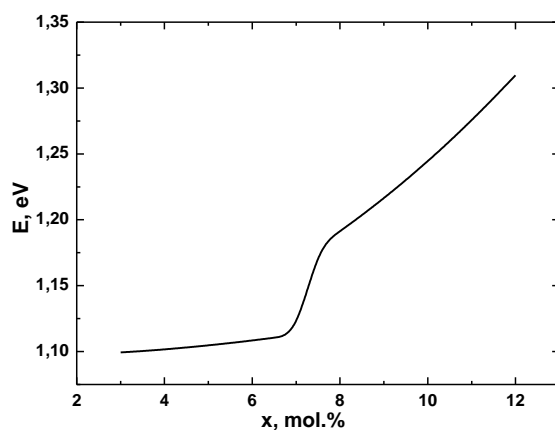


Figure 2. Activation energy for the simulated $\text{ZrO}_2 - \text{Y}_2\text{O}_3$ system

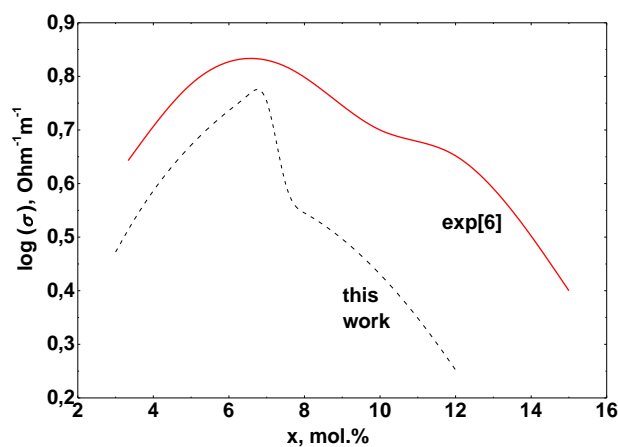


Figure 3. Conductivity for the simulated $\text{ZrO}_2 - \text{Y}_2\text{O}_3$ system

Conclusions

It was experimentally found the decrease in the activation energy of oxygen ion motion in the ternary $\text{ZrO}_2 - \text{Y}_2\text{O}_3 - \text{Fe}_2\text{O}_3$ system at the tetragonal-to-cubic phase transition. Using the dependency of the activation energy, the numerous simulation of the $\text{ZrO}_2 - \text{Y}_2\text{O}_3$ system was performed. The obtained composition dependency of the electric conductivity was found to agree qualitatively with experimental data.

Acknowledgments

We wish to thank Dr N. Belousov from Donetsk IPE of the NAS of Ukraine for his collaboration.

References

1. R. Sobczak, H. Boller, R. Bittner, *Mh. Chem.*, 99, 2227 (1968)
2. V.Barbashov, Yu. Komysa, E. Nesova, *High pressure physics and technics*, 18 (3), 148 (2008).
3. A.G. Belous, K.V. Kravchik, O.I.V'yunov, O.Z. Yanchevskiy, O.Bohnke, V.Gunes, *J. Chem*, 78 (11), 3, 2012
4. A. Ivanov – Schitz, I. Murin, *Solid State Ionics*, p. 122, Publishing House of St.-Petersburg University, St. - Petersburg. (2000).
5. M. Tsuchiya, B. Lai, A. C. Johnson, S. Ramanathan, *Journal of Power Sources*, 195, 994 (2010)
6. Peters Ch., *Grain-size effects in nanoscaled electrolyte and cathode thin films for solid oxide fuel cells (SOFC)*, p.10, Universität Karlsruhe, Karlsruhe. (2009).

Hydrogen Evolution Reaction at Pd-Modified Nickel Foam Material

B. Pierozynski

Department of Chemistry, Faculty of Environmental Management and Agriculture, University of Warmia and Mazury in Olsztyn, Plac Lodzki 4, 10-957 Olsztyn, Poland

E-mail address: bogpierzynski@yahoo.ca or boguslaw.pierzynski@uwm.edu.pl

Phone: +48 89 523-4177; Fax: +48 89 523-4801

Abstract

This work reports on hydrogen evolution reaction (HER), studied at Ni foam and Pd-activated nickel foam materials in 0.1 M NaOH solution over the temperature range 20-60 °C. Catalytic modification of Ni foam is performed via spontaneous and PVD depositions of palladium on MTI-delivered nickel foam material. Pd-modified foam is characterized by significantly facilitated, temperature-dependent HER kinetics, as manifested through radically reduced values of charge-transfer resistance parameter, as well as substantially modified Tafel polarization curves. The presence of a catalytic (Pd) additive is evidenced through Scanning Electron Microscopy (SEM) and X-ray Diffraction (XRD) analyses.

Keywords: Nickel foam; Catalytic Pd modification; HER; Electrochemical impedance spectroscopy

Hydrogen Technologies In The Project SUSEN At Research Center Rez

M. Tkáč, K. Stehlík, M. Zychová

Research Center Rez, 25068 Rez, Czech Republic

The Research Center Rez CVR, close to Prague, is well known in the field of material research for nuclear applications. Within the European infrastructure programme SUSEN a laboratory for testing and manufacturing of high-temperature electrolysis cells will be built up until 2015. The first objective is hydrogen production using coupling to a high-temperature process, e.g. generation IV gas-cooled nuclear reactor.

Introduction

Research and development in the Research Centre Rez (CVR) is focused on the area of nuclear energy, nuclear reactor physics, chemistry and materials. CVR participates in joint European research projects and provides irradiation services to organizations from different countries. Two research reactors and a set of experimental equipment (probes and loops) form the backbone of the research infrastructure. Besides commercial services CVR offers open access to the research reactors for scientific and technical organizations. Thanks to the Sustainable Energy (SUSEN) project, financed from the structural funds of the European Union, the existing infrastructure will be significantly enhanced. State-of-the-art research facilities will be required for existing and new scientific areas.

The project Sustainable Energy (SUSEN)

Overall

The SUSEN project includes the construction of research infrastructure to extend the possibilities of energy research with an emphasis on nuclear technologies. The implementation of this infrastructure will create prerequisites for enabling not only CVR but also (within the compulsory free access to constructed installations) other research institutions. New construction or reconstruction of the existing buildings on the ÚJV Řež, a. s. premises in Řež will set the foundations for a diagnostic centre, technological experimental loops, laboratories for radioactive waste processing and management, hot cells, neutron source, and laboratories for radioactive waste disposal. A new experimental hall is presently under construction in Plzeň. The SUSEN project is divided into four research programs.

Structural and System Diagnostics

Structural and system diagnostics of nuclear power plants, this mainly involves the life extension of current generation II generation nuclear power plants

Nuclear Fuel Cycle

Research infrastructure to support the back end of the nuclear fuel cycle, i.e. specifically aimed at separating and depositing of radioactive waste

Material Research

Investigation in material degradation at demanding conditions, e.g. high temperature, static and cyclic stress, corrosion-aggressive environment

Technological Experimental Loops

Installation of large-scale experimental facilities for research in fusion and generation IV nuclear reactors

Hydrogen Technologies within SUSEN, TEO

Within the research program “Technological Experimental Loops” one task is to build up an experimental facility for hydrogen generation by high-temperature water electrolysis using high-temperature helium and heat recovery. I.e. to study hydrogen production using heat from nuclear reactor.

Realization of hydrogen production in co-generation

Scientific Approach

The testing of high-temperature electrolysis using heat from another technological process should show if this coupling is technically possible, economically reasonable, and should clarify the long-term degradation behavior of the incorporated components and materials. Therefore a loop was planned, where the central component is a heat exchanger for gas and water steam. Figure 1 is a schematic sketch of the planned system. The gas side of the heat exchanger simulates a high-temperature process, in the beginning a high-temperature gas reactor. The water side of the heat exchanger will supply the electrolysis system. The water supply allows for at least 1kW electrolysis stack. The first studies will be conducted with a ceramic dummy, later on it will be replaced by a commercial available stack.

Heat recuperation is implemented as well from the cathode as from the anode side gas stream. The aim is to create a system as energetic efficient as possible. Variations of the system in certain limits regarding temperature, pressure, and different types of gases are possible to simulate other high-temperature processes, e.g. bio mass gasification, new gas turbine processes, etc.

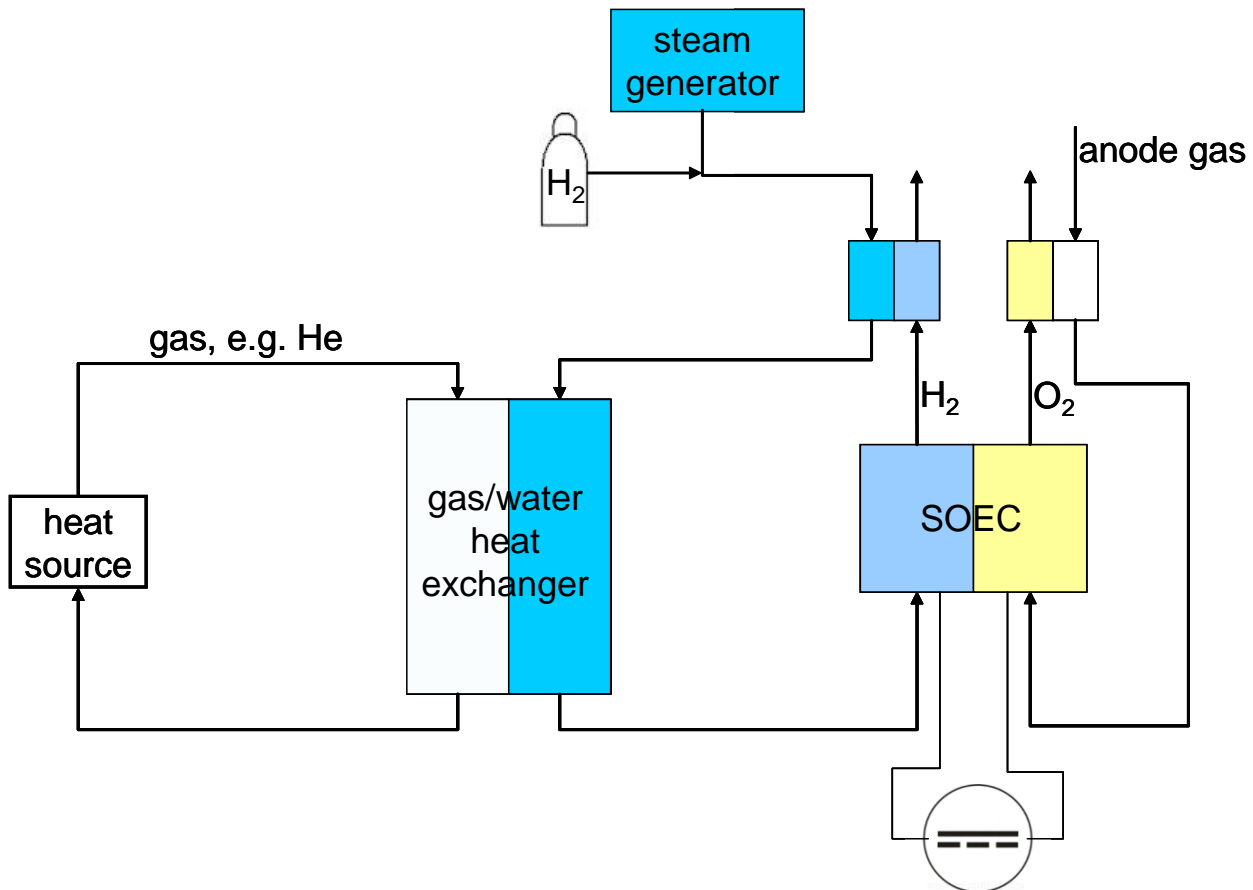


Figure 1. Scheme of hydrogen generation loop.

In a second step of building up test facilities for high-temperature electrolysis, cell manufacturing and characterization will be implemented. This is necessary to get a deep insight in the cell behavior and to realize and test suggestions for improvement at cell and system level. Manufacturing will be concentrated on state-of-the-art oxygen ion-conducting, planar, ceramic cells with an edge-length of maximum 20cm. For the future, proton-conducted cells are not excluded from investigation as they enable a hydrogen production free from residue water.

As an outlook to future research of high-temperature electrolysis there are two more technologies kept in mind. This is co-electrolysis of water and carbon dioxide and the reversible testing of ceramic cells in electrolysis and fuel cell mode.

For an economic application of the high-temperature ceramic cell all the named fields need to be investigated also in co-generation mode to verify the potential of this interesting and highly efficient technology

Planned experiments

Hydrogen production. The testing of the hydrogen production via co-generation, see fig. 1, will initially concentrate on thermodynamics of the system, i.e. stationary and dynamical behavior. The most important parameters are therefore temperature and mass flow of the gas from the co-generation process and water steam for the electrolysis system.

Dynamic Testing. The aim is to know, understand, and then be able to predict the characteristics of the system during heating- up and cooling down. This is necessary to predict the

needed time for starting the system and to avoid technical problems, mainly condensation of water, in the real application of such a system. The duration of tests will be in the range of some hours or days until the system has reached a stable state.

Long-term Testing. For the prediction of operation characteristics, efficiency, and degradation behavior tests with duration of minimum 240h are planned.

Cell characterization.

As mentioned in chapter 1 for the further development of testing facilities it is planned to produce and test ceramic cells. The produced cells will undergo two different types of testing: characterization and long-term testing.

Characterization Tests. The electrochemical characterization of the cells will include all state-of-the-art methods, i.e. determination of gas-tightness of the electrolyte, measuring of U-i-curves, conduction of impedance analysis and gas analysis as well as post mortem studies of the tested cells to identify deposition or reaction of the cell materials.

Long-term Tests. Long-term tests will be in the range of approx. 1000h. It is not enough to conduct long-term tests within the co-generation set-up. After the conduction of long-term tests with single cells it should be possible to separate the influence of the co-generation set-up and of the cell itself on the degradation behavior from each other. This approach enables a better interpretation of the degradation results.

Conclusions

As described in the previous chapters it is the aim of the Research Center Rez ‘CVR’ to establish high-level research in the field of high-temperature electrolysis. The research started with the project SUSEN and the building-up of testing facilities. A first focus lays on hydrogen production applying co-generation with a high-temperature gas-cooled nuclear reactor. Research activities should continuously grow and will include in future testing of ceramic cells in fuel cell as well as in reversible mode, and the manufacturing of planar cell.

Acknowledgments

The presented work was financially supported by the SUSEN Project CZ.1.05/2.1.00/03.0108 realized in the framework of the European Regional Development Fund (ERDF).

Electrochemistry in the electrochemical cells: There is more than just the working electrode

P. Vanýsek^{a, b}, H. Tavassol^c, and K. L. Pilson^b

^a CEITEC - Central European Institute of Technology BUT, Technická 3058/10, CZ-616 00 Brno, Czech Republic

^b Department of Chemistry and Biochemistry, Northern Illinois University, DeKalb, Illinois 60115, USA

^c Department of Chemistry, University of Illinois at Urbana-Champaign, 505 South Mathews Avenue Urbana, IL 61801, USA

The tacit assumption in an electrochemical experiment is that a properly set up electrochemical cell, working electrode, counter electrode, reference electrode and a potentiostat, will perform an experiment by "applying potential on the working electrode" without any need to consider the properties of the reference electrodes, the effect of electrochemistry on the counter electrode and the real properties of the potentiostat. While this is in first approximation valid assumption, in the extremes it is also necessary to consider the other parts of the system. In this work we will visit two interesting cases that may lead to experimental artifacts. The first is the effect of solution changes during impedance measurement. The second is effect of the time constant of a reference electrode on an impedance measurement in an electrochemical cell.

A Potentiostat as a Probe for Aqueous Conductometry

A potentiostat is a main tool in electrochemistry and it plays significant role in a wide range electrochemical experiments (1xxx). The basic function of the three-electrode potentiostatic design can be illustrated by a circuit with a single operational amplifier, which performs the following function: Via a feedback resistor it applies on its output (connected to a counter electrode) such potential, so that the potential on its inverting input (as supplied via the reference electrode via a feedback through solution of the cell), is identical to the potential on the noninverting input. The noninverting input is usually biased by an external source, which dials in the desired experimental potential. The potential sensed in the solution by the reference electrode is generated by the electric field created by the potential between the counter electrode and the grounded working electrode.[†] The reference electrode potential is then chosen by an adjustable voltage applied to the inverting input.

The main purpose of the three-electrode potentiostat, a device with a feedback through the reference electrode, is two-fold (a) to allow passage of current through the system, without need to

[†] Potential on an electrode is always correctly expressed as a potential between two points. The fact that the working electrode is at ground potential means, it has zero volts vs. ground. For an electrochemical experiment what matters is the potential of the working electrode vs. the surrounding solution potential monitored by the reference electrode. Thus, for example experimental potential of + 1 V "on the working electrode" means in the potentiostatic circuit *negative* 1 V on the reference electrode vs. the working electrode (and hence, vs. ground).

pass this current through the reference electrode and (b) to compensate for the voltage drop occurring in the solution. The three electrode system is in most modern potentiostats augmented by a potential feedback to both the working and the counter electrode, thus actually a four-electrode potentiostat, rather than three) is in place, although many times the second sensing probe is simply hard-connected to the working electrode, without being effectively used. However, this four-electrode setup is very useful in impedance measurement, when two probes are used as the current supplying electrodes (the counter and the working electrodes of the voltammetric world), whereas the reference and the sense (as they are often called) inputs are used as the potential sensing electrodes. The properly mathematically treated ratio of the voltage and current and their phase shift is then used to find impedance of the material between the two voltage sensing electrodes.

Experimental Observations During Conductometry

In what was expected to be a routine measurement of solution resistance we discovered an interesting phenomena. While performing calibration of an immersion conductometric cell with four electrodes with solutions of potassium chloride, gas evolution at the counter electrodes was observed, this in spite of the fact that the perturbing voltage applied, ca. 25 mV, was nowhere near the water oxidation/reduction potentials. Second observation was related to the appearance of the probe electrodes. All four electrodes of a brand new cell were uniformly black of the platinized platinum appearance. However, upon prolonged use the electrodes, predominantly the outer electrodes used to supply current, became rather shiny, something we preliminarily assigned to electrochemical polishing (1). To understand the observed phenomena and to understand any implications this behavior may have on impedance measurement, we designed the following study.

A Solartron potentiostat and analyzer were used to measure impedance spectrum measurement. A Topac 4-electrode immersion conductivity cell (CS SK41T) was immersed in a 250-ml beaker containing the studied electrolyte, an aqueous solution of potassium chloride. Enough of electrolyte was used to cover all four electrodes in the cell.

PowerLab 2/26 (AD Instruments) was connected to the circuit. The signal from the impedance analyzer was recorded as the difference between the two (high impedance, vs. ground) inputs of the PowerLab instrumental voltmeter.

Results

Fig. 1 is a typical result obtained during the experiments. It shows the voltage difference between the current-supplying electrodes (counter and working electrodes) of the potentiostatic setup. The switching between the two extremes (ca. 2.7 V) was accompanied by appearance of gas evolution on both current-supplying electrodes and temporary disappearance of the gas evolution while the voltage was switching to the opposite extreme.

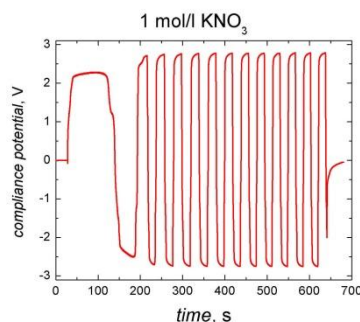


Figure 1. Potential between two counter electrodes during impedance measurement. The ac peak-to-peak voltage used during the impedance work was set to 25 mV.

Cause of the oscillations and effect on impedance data

It is evident that presence of a redox couple is needed for stability. However, it is not outright clear why absence of the redox couple should result in periodic swings, rather than some kind of a drift in the direction of single extreme potential. We propose the following mechanism. Over time the reduction causes more alkalinity in the local environment of the electrode, which either means higher concentration of dihydrogen or lower concentration of dioxygen. In both cases the potential of the electrode, in which vicinity the oxidation occurs, becomes more negative. Similarly, for reduction, the potential becomes more positive (considering reactions 2) as time goes by. Fig. 2 depicts in a cartoon form events on each of the four electrodes over time. In addition to this process, the effect of convection as a result of gas formation cannot be ignored.

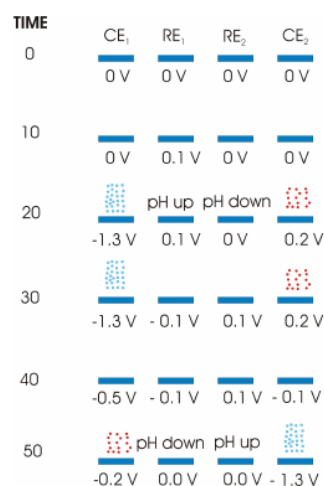


Figure 2. Potentials and events on each of the four electrodes over time. Blue points (longer stream of dots) show the dihydrogen bubble evolution, the red points (shorter stack) show the dioxygen bubbles.

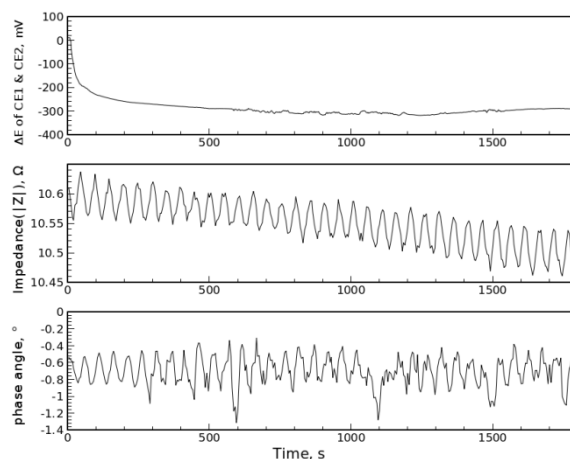


Figure 3. The simultaneous measurement of potential difference between counter electrodes of conductivity cell and impedance measurement at 100 Hz. The potentiostat was in the galvanostatic mode with the perturbing current of 0.1 mA on a 1 mol/l potassium nitrate solution.

Conclusions

It can be seen from the results, in particular as presented in Fig. 10 and Fig. 11, that the potential excursions do not disturb the obtained impedance data substantially, so they might be considered unimportant. However the high potentials can affect the chemistry of the electrodes environment like the local pH changes (or change in other chemical compositions). In addition, the high potentials can also change unfavorably the electrode surfaces and cause some subsequent undesirable issues. Also, in terms of instrumentation effects, although we have not observed this, the electrical demands on the potentiostat could likely distort some data and in some cases could prevent a potentiostat with lesser current/potential capability from proper operation.

Acknowledgments

This project was funded in part by financial support from NSF-CHE0615129.

References

1. V. S. Bagotsky: Fundamentals of Electrochemistry, 2nd Ed. John Wiley & Sons, Inc., Hoboken (2006).

Electrochemical properties of CeVO_4 and FeVO_4 at high temperatures

T. Behofsits^a, M. Malys^b, G. Pani^a, G. Fafilek^a

^aVienna University of Technology, Institute of Chemical Technologies and Analytics
Getreidemarkt 9/164ec, A-1060 Vienna

^bFaculty of Physics, Warsaw University of Technology, Koszykowa 75, PL-00-662 Warszawa,
Poland

Abstract

High temperature corrosion of steel is dramatically accelerated by ashes and scales, containing compounds of iron, vanadium, oxygen and sulphur. High temperature electrochemical impedance spectroscopy (HT-EIS) on ash samples from a heavy crude oil furnace, showed high conductivity of at least one of the several existing phases. High temperature cyclic voltammetry (HT-CV) on such ashes revealed also some redox activity, which could be related to redox processes of vanadium containing compounds. It was shown, that these redox processes increase largely the corrosion rate of steel. On the one hand, it is unfavourable for the corrosion stability of construction materials, on the other hand it might be an effective material for several applications, like high temperature fuel cells electrodes, intercalation materials in ion-batteries or as catalyst.

Since the composition of the ashes is quite complicated, it is not clear which part of these phases is responsible for the conducting and electrochemical properties. FeVO_4 was identified as one of the few potentially highly conductive phases in the scale of steel parts from the furnace. Therefore pure FeVO_4 was synthesized and investigated by HT-EIS and HT-CV on micro-samples. For comparison CeVO_4 was included in this investigation. Results were compared with those from the investigation of the ash.

Vanadium Redox Flow Battery – Electrolytes Preparation

J. Vrána^a, P. Mazúr^b, J. Pocič^b, J. Dundálek^a, M. Bobák^a, and J. Kosek^a

^a Department of Chemical Engineering, Institute of Chemical Technology Prague, Technická 5, 166 28 Praha 6, Czech Republic

^b New Technologies – Research Center, University of West Bohemia, Univerzitní 8, 306 14 Plzeň, Czech Republic

The increasing production of electricity from renewable power sources is strongly supported by all developed countries. Non-stable and hardly predictable power from wind and solar renewable sources demands for an effective management on the power transmission level. Thus, an engineering development of new local energy storages as a part of the modern transmission network tailored to the efficient and smart electricity distribution is vitally needed. Vanadium redox flow battery (VRFB), using vanadium ions in four different oxidation states (II, III, IV and V) in both half-cells, excels as the stationary energy storage in its sufficient capacity (kWh) proportional to the electrolyte volume, long lifetime and high efficiency.

In this work, the lab-scale VRFB single-cell was developed with the stable round-trip energy efficiency of 83 % at the current density of 56 mA/cm². The achieved battery characteristics (i.e., the efficiency and current density) are acceptable for the industrial utilization of the system.

The development of the device for the electrolyte production is an integral part of the successful scale-up of the VRFB technology. The common method for the electrolyte production is based on the reductive dissolution of the vanadium(V) oxide in diluted sulfuric acid.

In this work, we present the design, construction and evaluation of two membrane flow electrolyzers of different arrangements (i.e., plan-parallel and coaxial) for the electrolyte preparation. The constructed devices enabled the production capacity scale-up to more than 5 l/day. Optimal operating conditions of the both systems were determined by the load characteristics of the electrolysis in galvanostatic mode. As the initial cathode electrolyte, we used the mixture of vanadium(V) oxide and diluted sulfuric acid. The electrolyte quality was monitored by conductometry and visible and adjacent ultraviolet and infrared spectroscopy.

Batteries Based on Sodium Intercalation

J. Vondrák*, M. Sedlaříková and P. Špičák

Department of Electrical and Electronic Technology, Faculty of Electrical Engineering and Communications, Brno University of Technology
Correspondence author: vondrakj@feec.vutbr.cz

Introduction

Present situation on the market with lithium battery can be shown on the example of U.S.A. The volume of sold batteries in 2012 corresponded 12 billions of \$ and an expansion to 33 billions of \$ is expected for year 2019. Most of the batteries nowadays are of medium or large size up to the power as large as tens of kWh and their main field would be for battery driven cars (electromobiles). Essentially, modern lithium batteries utilise the principle of electrochemical intercalation twice; it is the essential phenomenon used both for positive electrodes as well for negative ones. This situation will need an essential increase of lithium production. Large quantities of lithium will be available in Southern America and in Eastern Asia. From economic and political reasons it would be convenient to discover any possible replacement for metallic lithium anodes. Due to chemical similarity, the first candidate to replace lithium in intercalation batteries is sodium. The intercalation of alkali metals into graphite and other forms of carbon is the oldest point of interest which attracted the inorganic chemist to the intercalation process. However, the intercalation of alkali metals was done by strong agents such as butyl lithium, potassium malimide, alkali metal amalgams and so forth. The electrochemical intercalation of sodium, which is essential for the battery design has not been thoroughly investigated until present time.

State of art

Intercalation consist in penetration of ions (alkali metal ions mostly) into regularly spaced voids in the structure of a solid body. The position of the voids is governed by the rules of crystallography; the penetrated or inserted particles are called *guest* and the term *host* or *host lattice* should be used for the solid matrix. These host substances can be either lamellar or they form a three-dimensional lattice in which the voids create series of parallel tunnels. Despite of these two possibilities, both systems are called *intercalation ones*. In fact, there is only marginal difference between named two groups. However, it is rather interesting that it has arisen in last two – three years just because of the situation on the market in lithium batteries, which has reached a stable situation now. Moreover, most of the papers have been written by people from East Asia.

Actually, the term “intercalation” was introduced for materials of the second group. Due to deep similarities in the way of electrochemical preparation and other aspects, substances of both groups are considered and “intercalation materials”. It is of course sometimes fairly difficult to distinguish with certainty to which of these named groups any material should be associated.

First of all, the oldest intercalation compounds of graphite with sodium have been studied by methods of quantum chemistry. According to Nobuhara et al there is a substantial difference between intercalation of sodium in comparison to other alkali metals. Also Wang obtained similar results and both studies indicated lower stability of Na – C₆ configuration. Third theoretical paper by Okamoto tried to explain the differences by oxidation potential of sodium in the carbonaceous lattice.

Explicitly pronounced layered structure in was announced by Chagas et al in material of composition $\text{Na}_{0.45}\text{Ni}_{0.22}\text{Co}_{0.11}\text{Mn}_{0.66}\text{O}_2$. From an electrochemical point of view, the usage of ionic liquids as electrolyte for this purpose is interesting. The material based of delithiated olivine LiFePO_4 was according to Vujkovic et al found to be useful in sodium batteries with specific capacity 118 mA.h/g. Based on ammonium vanadate $(\text{NH}_4)_2\text{V}_6\text{O}_{16}$, a cathode material for sodium batteries was announced by Fei et al and similar vanadium phosphate was described by Lim et al. An interesting material based on derivatives of indigo was declared by Yao et al. Also single walled carbon nanotubes were studied from the viewpoint of battery design by Kamal et al and Zhao et al. The potentialities of sodium batteries has been reported several times

Our investigations were oriented towards insertion of sodium into simple binary oxides. In this way, we have confirmed the Crandall – Faughan isotherm for metal insertion together with the explanation of the linear term in the isotherm and the concentration dependence of diffusion coefficient by the changes of lattice energy due to lattice expansion and volumetric expansivity of the lattice. The isotherm of sodium intercalation into γ - MnO_2 was detected by us simply chemical analysis of the electrode saturated at chosen potential value by electrode potential in a solution of sodium salt in propylene carbonate. Moreover, we have tried to design a Na - γ - MnO_2 model cell. Its discharge characteristics are given in Fig. 1.

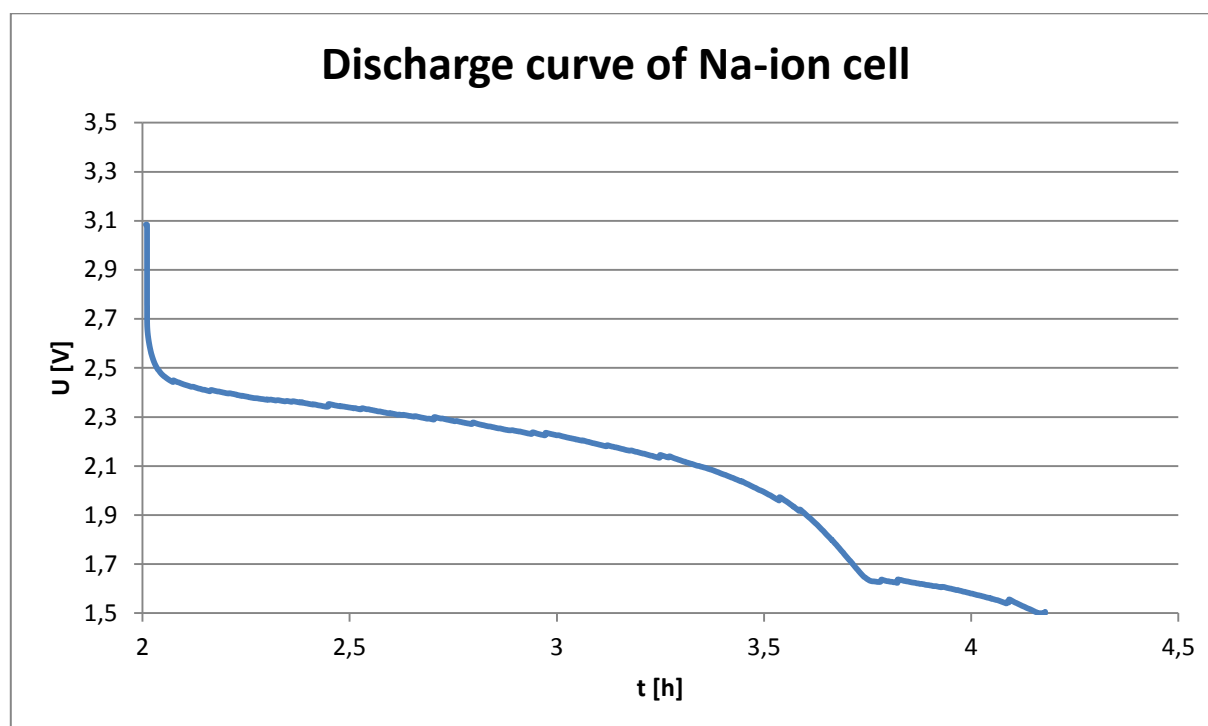


Figure 1. Discharge curve of an experimental cell Na- MnO_2

Both the capacity and the position of discharge plateau were in a good agreement with other available facts.

As another research method, the electrochemical quartz microbalance EQCM was applied by us. We have used thin films of vanadium or tungsten oxide deposited by vacuum evaporation on the sensor for QCM device.

Both named oxides exhibited the possibility to intercalate sodium from sodium perchlorate solution in propylene carbonate. As an example, comparison between mass increment and integrated charge accepted by a WO_3 thin layer prepared by vacuum deposition is shown in Fig. 2.

The voltammogram is depicted there by red colour and the mass increment obtained by its integration and by application of faraday law is plotted in green colour. Finally, the output of the QCB is drawn in blue. As we see, both mass increments from charge and from QCM output are in a reasonably good agreement.

Diffusivity of sodium ions

The mobility of ions in the host substance is controlled by two factors with opposite action. First, smaller ions should move easier. Second, electric field and coordination forces of smaller ions slow their movement down. For example, in the case of β -alumina lattice of alumina is just that of sodium ion. This question is to be solved also for intercalation compounds.

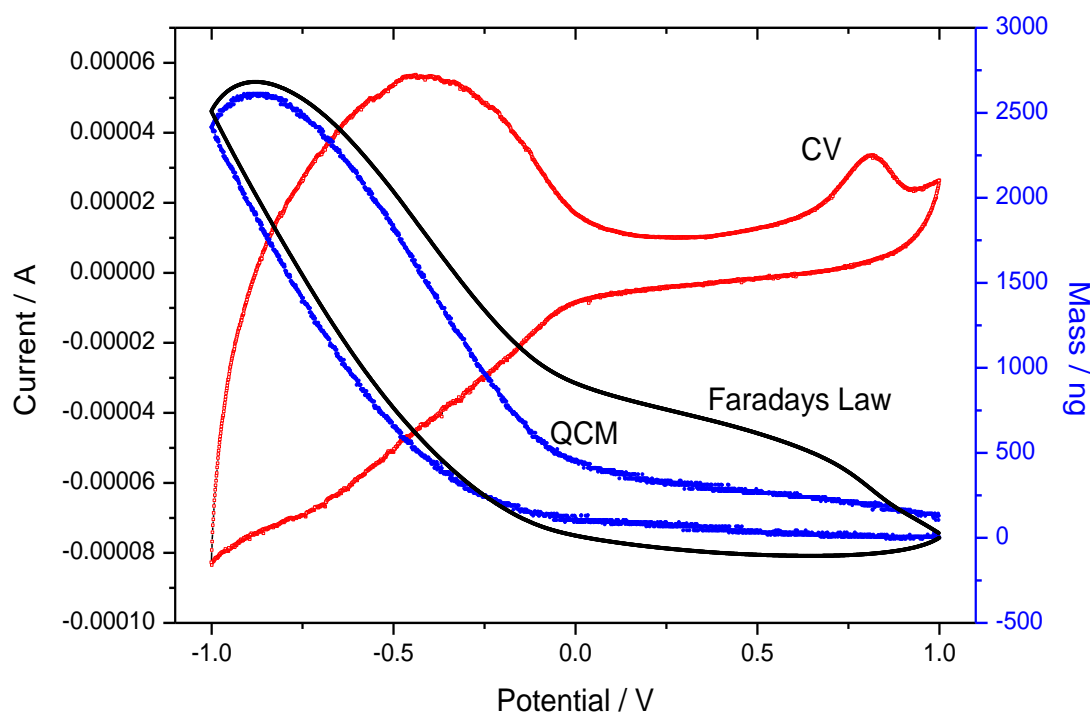


Fig. 2.

Figure 2. Behaviour of a thin layer WO_3 electrode .

Voltammetric curve: red, left axis; mass from integrated current and Faraday law : green, light axis; mass estimated by QCM: blue, right axis

Prospects of sodium batteries

There are no fundamental objections against the usage of sodium in aprotic batteries. Generally speaking, cell voltage lower than the value known in the case of their lithium analogues must be expected.

We have not to forget differences between both alkali metals. From the application point of view one must important is lower melting point of sodium (ca. 93 °C) which would cause difficulties at elevated temperature. The use of sodium metal as anode material does not seem so easy and intercalation anodes must be used in real cells.

Acknowledgement

Authors gratefully acknowledge financial support from the Ministry of Education, Youth and Sports under project No. LO1210 – „Energy for Sustainable Development (EN-PUR)“

References

1. Nobuhara, Kunihiro; Nakayama, Hideki; Nose, Masafumi; et al. JOURNAL OF POWER SOURCES 243 (2013) 585-587
2. Wang, Zhaohui; Selbach, Sverre M.; Grande, Tor: RSC ADVANCES 4(8) (2014) 4069 Published: 2014
3. Chagas, Luciana Gomes; Buchholz, Daniel; Wu, Liming; et al.: JOURNAL OF POWER SOURCES Volume:247 Pages: 377-383 Published: FEB 1 2014
4. Yao, Masaru; Kuratani, Kentaro; Kojima, Toshikatsu; et al.: SCIENTIFIC REPORTS 4, Article No. 3650 (2014)
5. Kamal, C.; Chakrabarti, Aparna; Banerjee, Arup; et al.: PHYSICA E-LOW-DIMENSIONAL SYSTEMS & NANOSTRUCTURES 54 (2013) 273
6. Zhao, Liping; Qi, Li; Wang, Hongyu : JOURNAL OF POWER SOURCES 242 (2013) 597
7. Yoshida, Hiroaki; Yabuuchi, Naoaki; Komaba, Shinichi: ELECTROCHEMISTRY COMMUNICATIONS 34 (2013) 60
8. Chen, Chih-Yao; Matsumoto, Kazuhiko; Nohira, Toshiyuki; et al. JOURNAL OF POWER SOURCES 237 (2013) 52
9. Vondrak, J., Velicka, J; Klapste, B; Sedlarikova, M; Novak, V : JOURNAL OF SOLID STATE ELECTROCHEMISTRY 7 }2003) 361

Non-Isothermal Modeling and Simulation of a Soluble Lead-Acid Redox Flow Battery

H. Al-Fetlawi

Electrochemical Engineering Department, College of Engineering, University of Babylon, Hilla, Iraq.

fetlaw@uobabylon.edu.iq

One of the benefits of modeling is the ability to predict quantities that can be difficult, in some cases impossible to obtain through *in-situ* experimental measurements. This information, however, can be of vital importance to ensuring both good performance and longevity of the battery – knowledge of the likelihood of localized reactant depletion, localized heating and of a steep rise in potential.

A non–isothermal two–dimensional dynamic model of a soluble lead-acid redox flow battery based on mass, charge, energy and momentum transport and conservation, together with a kinetic model for redox reactions has been developed.

Numerical simulations demonstrate the effect of changes in the operating temperature on performance of the soluble lead-acid redox flow battery [1-3]. It is shown that variations in the electrolyte flow rate and the magnitude of the applied current substantially alter the charge/discharge characteristics, the temperature rise and the distribution of temperature. The effects of heat losses on the charge/discharge behavior and temperature distribution are investigated. Conditions for localized heating and membrane degradation are discussed.

The numerical simulations suggest that the most favorable operating conditions are at high flow rate, low current density, low temperature and sufficient heat loss to prevent the fast temperature rise.

References

1. H. Al-Fetlawi, A.A. Shah, F.C. Walsh, *Electrochimica Acta* 55 (2009) 78-89.
2. A.A. Shah, H. Al-Fetlawi, F.C. Walsh, *Electrochimica Acta* 55 (2010) 1125-1139.
3. H. Al-Fetlawi, A.A. Shah, F.C. Walsh, *Electrochimica Acta* 55 (2010) 3192-3205.

Zinc-Air Flow Batteries for Electrical Power Distribution Networks

A. Gavrilović-Wohlmuther^{1,*}, A. Laskos¹, Ch. Zelger^{1,2}, B. Gollas^{1,2}, A. H. Whitehead³

¹Centre of Electrochemical Surface Technology (CEST GmbH)
Viktor-Kaplan Straße 2, 2700 Wr. Neustadt, Austria

²Institute of Chemistry and Technology of Materials, Graz University of Technology
Stremayrgasse 9, 8010 Graz, Austria

³Gildemeister Energy Solutions (Cellstrom GmbH)
Industriezentrum NÖ-Süd, Straße 3, Objekt M36, 2355 Wr. Neudorf, Austria

*aleksandra.gavrilovic@cest.at

Major challenges presented by renewable energies, such as fluctuations in output, unavailability (e.g. sunlight in the night) and unpredictability (e.g. wind power), limit their popularity. As a solution to these problems, energy storage technologies are attracting attention [1]. The alkaline Zn-air flow battery possesses favourable properties such as high specific energy, fast response, low cost materials and environmental compatibility [2-4]. However the battery underperforms because of known difficulties such as OH⁻ ion depletion occurring during discharging and dendrite formation during recharging [5]. In our efforts to achieve dendrite-free Zn electrodeposition, which can be utilised in the Zn-air flow battery, the surface morphology of the electrolytic Zn deposits on a polished polymer carbon composite electrode in alkaline, additive-free solutions was studied. Experiments were carried out with 0.1 M, 0.2 M and 0.5 M zincate concentrations in 8 M KOH. The effects of different operating conditions such as: elevated temperatures, different current densities and different flow velocities, on current efficiency and dendrite formation were investigated. For this purpose, a specially designed test flow-cell with a central transparent window was employed. The highest Coulombic efficiencies of 80-93 % were found for 0.5 M ZnO in 8 M KOH, at increased temperatures (50-70°C), current densities of up to 100 mA cm⁻² and linear electrolyte flow velocities higher than 6.7 cm s⁻¹. Deposits were examined ex-situ by SEM.

References:

1. P. Leung, X. Li, C. P. de Leon, L. Berlouis, C. T. J. Low, F. C. Walsh, RSC Adv. 2 (2012) 10125-10156.
2. F. Cheng, J. Chen, Chem. Soc. Rev. 41 (2012) 2172-2192.
3. X. G. Zhang in: J. Juergen, C. Dyer, P. Moseley, Z. Ogumi, D. Rand and B. Scrosati (Eds.), Encyclopedia of Electrochemical Power Sources, Elsevier, Amsterdam, 2009, pp. 454.
4. X. G. Zhang, Corrosion and Electrochemistry of Zinc, Plenum Press, New York and London, 1st Ed., 1996.
5. R. Y. Wang, D. W. Kirk, G. X. Zhang, J. Electrochem. Soc. 153 (2006) C357-C364.

Rejuvenation of a NiFe accumulator from 1930's

P. Vorel^a, P. Prochazka^a, I. Pazdera^a, D. Cervinka^a

^a Department of Power Electrical and Electronic Engineering, Brno University of Technology, Technicka 12, 616 00 Brno, Czech Republic

Introduction

A rejuvenation process of a very old nickel-iron accumulator (about 75 years old) is described in this article. The supposed nominal parameters of the accumulator are 12V/(8Ah -10Ah). All cells of the accumulator were rejuvenated by a quite long and laborious process including 11 cycles of charging and discharging, several changing of the electrolyte and even using a deep discharging to improve the capacity of the negative iron electrode. The charging and discharging characteristics of all cells were measured during the rejuvenation. Finally the internal resistance of the accumulator was measured too. The wooden case, output terminals and all the accumulator accessories were renovated. The work showed a surprising durability of old NiFe accumulators (see below).

Description and history of the rejuvenated accumulator

The described accumulator consists of 10 serial connected cells type MK86 (trademark FERAK) placed in a wooden case with dimensions 110x355x245mm. The dimensions of one cell container (made from nickelled iron plates) are approx. 25x80x180mm. The weight of one cell is approx. 0.9kg. Most probably it was manufactured shortly before the World War II (end of 1930's) by Prazska akumulatorka a.s. It was used in a telephone exchange or railway station. In 1950's it was used for lighting during electricity blackouts. Approx. 1960-1980 it was not used and it was stored in a dry place at approx. 25°C without any care. In 1980 the electrolyte was changed and it was used for starting a garden tractor. From 1981 to 2014 it was stored in a dry place at 25°C without any care. In 2014 the electrode system of the cells was full of potassic carbonate but no cell was rusted or even rusted through.

The cell type MK86 is unknown today, even not in older archives of the companies Saft Ratiskovice, Akuma Praha or Akuma Mlada Boleslav. The specific energy of NiFe cells is about 30Wh/l – see (4), (6). At the average voltage of ca 1.1V this represents ca 27Ah/l. The volume of our cell is approx. 0.36l. **Therefore we can deduce that the nominal capacity of the accumulator cells could be $27 \times 0.36 = 9.7\text{Ah}$ (10Ah). Maybe it was only about 8 Ah.**

Choice of the electrolyte

Both potassic hydroxide (KOH) and sodium hydroxide (NaOH) were used in NiFe cells. Usually KOH was used because of its higher conductivity. Moreover using NaOH at lower temperatures (below +15°C) the capacity is decreased. However NaOH ensures a longer life of the positive electrode which is more stable than if pure KOH is used (without addition of lithium hydroxide LiOH). If it is necessary to ensure the capacity at lower temperatures, the highest electrolyte conductivity (low internal resistance) and good life time at normal temperatures (+15°C to +35°C) then KOH with an addition of 10-15g/l of LiOH is used.

Our accumulator will be not used at lower temperatures and there is no demand on the lowest internal resistance. **This is why we used NaOH to protect the positive electrode without the necessity of using the problematic LiOH.** The density of NaOH aqueous solution should be 1.17 to 1.19 to ensure its maximum conductivity (1 weight part of NaOH and 5 weight parts of distilled water).

Rejuvenation process

There was a lot of carbonate inside the cells. The electrodes of some cells were almost dry (only rests of liquid electrolyte). This is why the cells were firstly refilled with a distilled water and left to stand through the night. After proper shaking they were spilled. 2 cycles of filling distilled water, shaking and spilling followed. Immediately a new electrolyte was filled. The normal charging current of NiFe cell equals to $\frac{1}{4}$ of the nominal capacity. Decreasing the charging current under $\frac{1}{8}$ the negative (iron) electrode is charged worse. With respect to the expected nominal capacity approx. 10Ah we used a charging current 2.5A. The charging time was 6hours (15Ah) i.e. 150% of the nominal capacity (standard normal charging of NiFe cells). The final voltage on all cells in the 1st charging cycle was equalized to $1.72V \pm 30mV$ (before switching-off the current). A discharging with a normal discharging current 1.25A (around $\frac{1}{8}$ of the nominal capacity) followed. The cells were connected to series. Discharging current 1.25A was kept constant and each cell was removed from the circuit separately – just when the bend on its characteristics appeared.

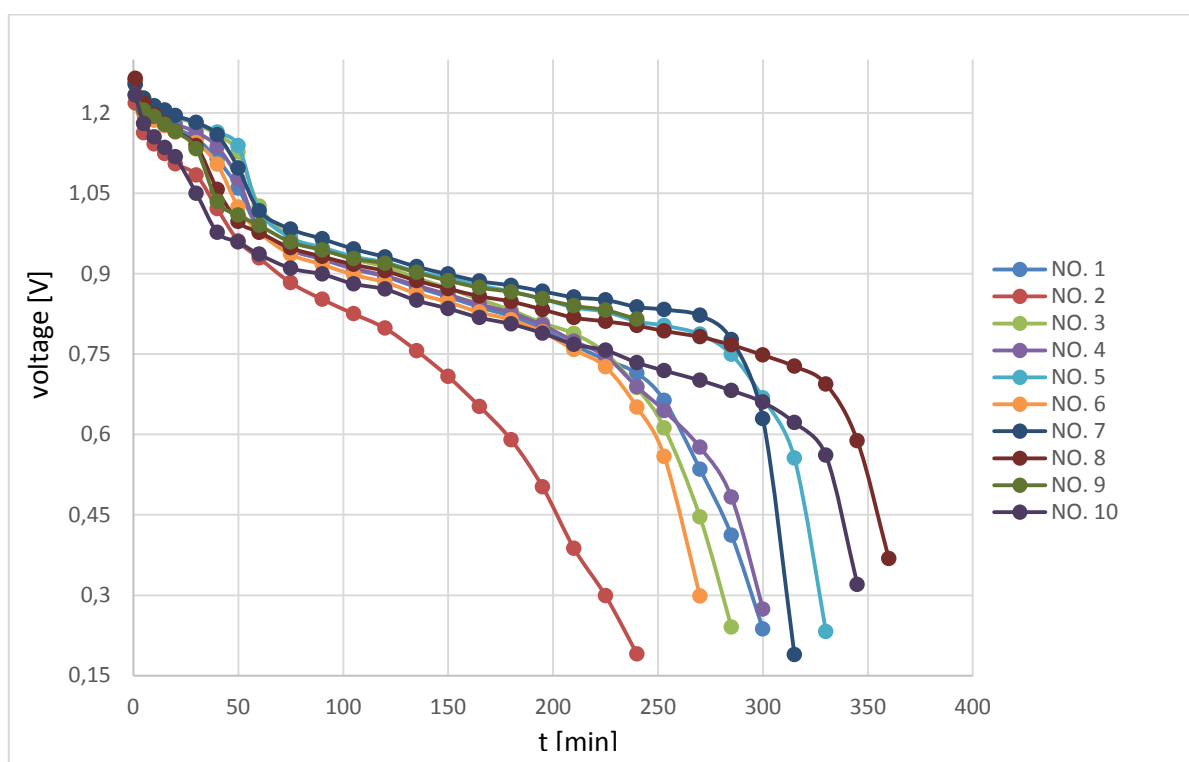
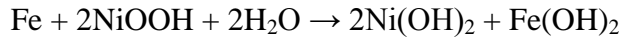
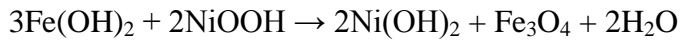


Figure 1. Discharging 1.25A – 1st cycle

From Fig. 1 we can see the normal 1st plateau (ca 1.2V) was very short and the undesired 2nd plateau (ca 1V) was keeping for the absolute most time of discharging (firstly we thought the discharging voltage is so low because of higher internal resistance of the old cells). The discharging reaction for 1st plateau is (5):



This proper reaction was replaced too soon with the reaction for the 2nd plateau (5):



Probably the reason was a **degradation of the negative iron electrodes**. Maybe there was not much pure active iron (deep layers of the negative electrode not active). After the first discharging cycle the cells were spilled and immediately filled with a fresh electrolyte. The same cycles of charging 2.5A and discharging 1.25A were repeated twice (2nd and 3rd cycle). During the 2nd and 3rd cycle the internal resistance of the cells was decreased (higher voltage values of both plateaus). In the cell no. 2 also the duration of the first plateau was prolonged (see Fig. 2). Also the capacity of all cells (including the dominant 2nd plateau) was prolonged in comparison with the first cycle. Now it reached approx. 6.3Ah (worst cell) to 7.5Ah (best cells).

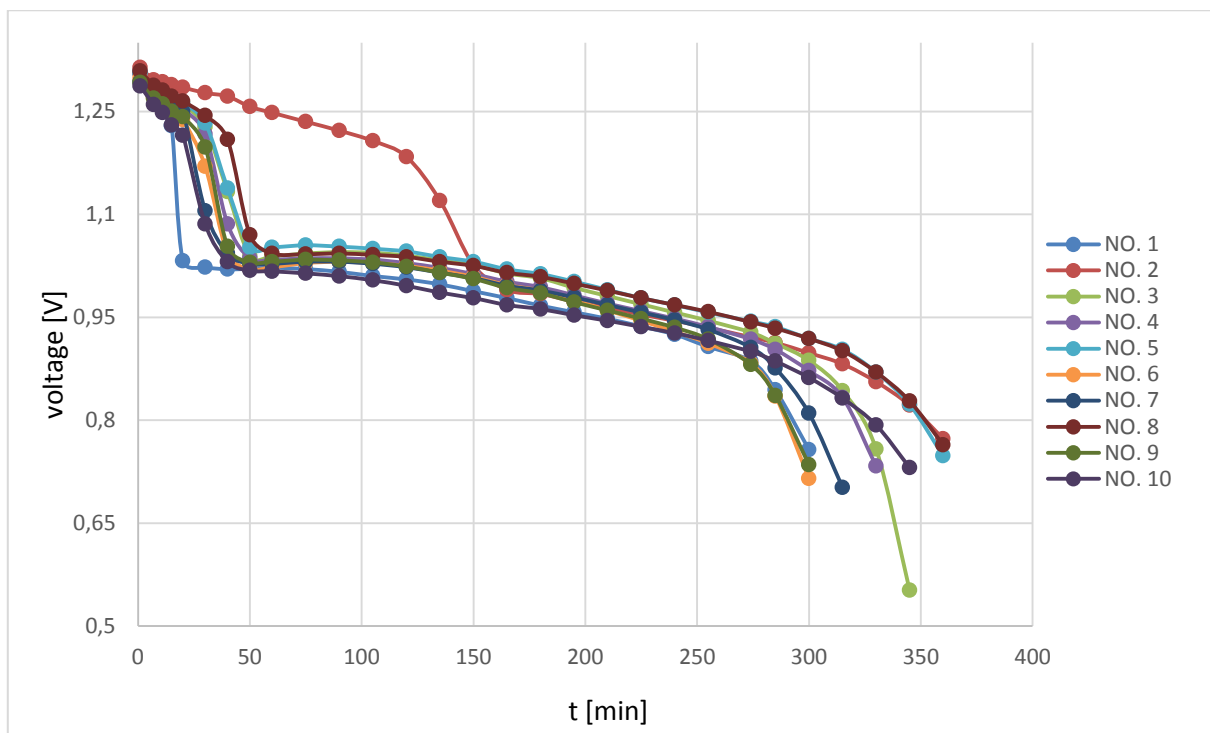


Figure 2. Discharging 1.25A – 3rd cycle

Fresh electrolyte was filled again and the 4th charging 2.5A/ discharging 1.25A followed. In the 5th cycle the charging current was decreased to 2A and the discharging current was decreased to 1A. From Fig. 3 we can see the useful 1st plateau was prolonged in all cells (especially in no. 2 and also in no. 1). However the remaining 2nd plateau was shortened significantly – in the result the capacity including both plateaus decreased in comparison with the earlier cycles - first bend after the second plateau in Fig. 3 (time ca 135min). Fortunately next experiments showed that in fact the capacity did not decrease so much and forever: At the characteristics bend (approx. at the time 135min) we interrupted the discharging and after ca 4hours we tried to continue - the 2nd plateau surprisingly continued keeping for a long time (see Fig. 3). Maybe the deep layers of the negative electrode were not “available” immediately for the discharging reaction and they needed some time

(discharging interruption) for “getting contact” with the reactants. **Measuring the potential of the negative electrode (using a zinc measuring electrode) the problem with the capacity of the negative electrode was confirmed:** If the bend of the characteristic (behind the 2nd plateau) started to appear then the potential of the negative electrode grew up to 0.75V while the potential of the positive electrode did not fall and kept ca 1.6V.

In the 6th cycle the currents were returned to 2.5A (charging)/1.25A (discharging). The situation was similar like in the 5th cycle only the 1st plateau of all cells was prolonged a bit. **Knowing the problem is in the negative electrode we decided further to use the regeneration method of “deep discharging”:** All the cells except of no. 2 were discharged with 1.25A to zero voltage a then they were “charged” for 5 hours and 40 minutes with 1.25A to the opposite polarity (ca -0.75V per cell). After this procedure the electrolyte was changed.

A prolonged charging (7th charging cycle) followed: ca 4hours 2.5A and ca 8hours 1A. The 7th discharging cycle (1.25A) showed a significant prolongation of the 1st plateau. The short duration of the following 2nd plateau remained. The 8th and 9th cycles (charging 2.5A, discharging 1.25A) brought again next small improvement (prolongation of the 1st plateau).

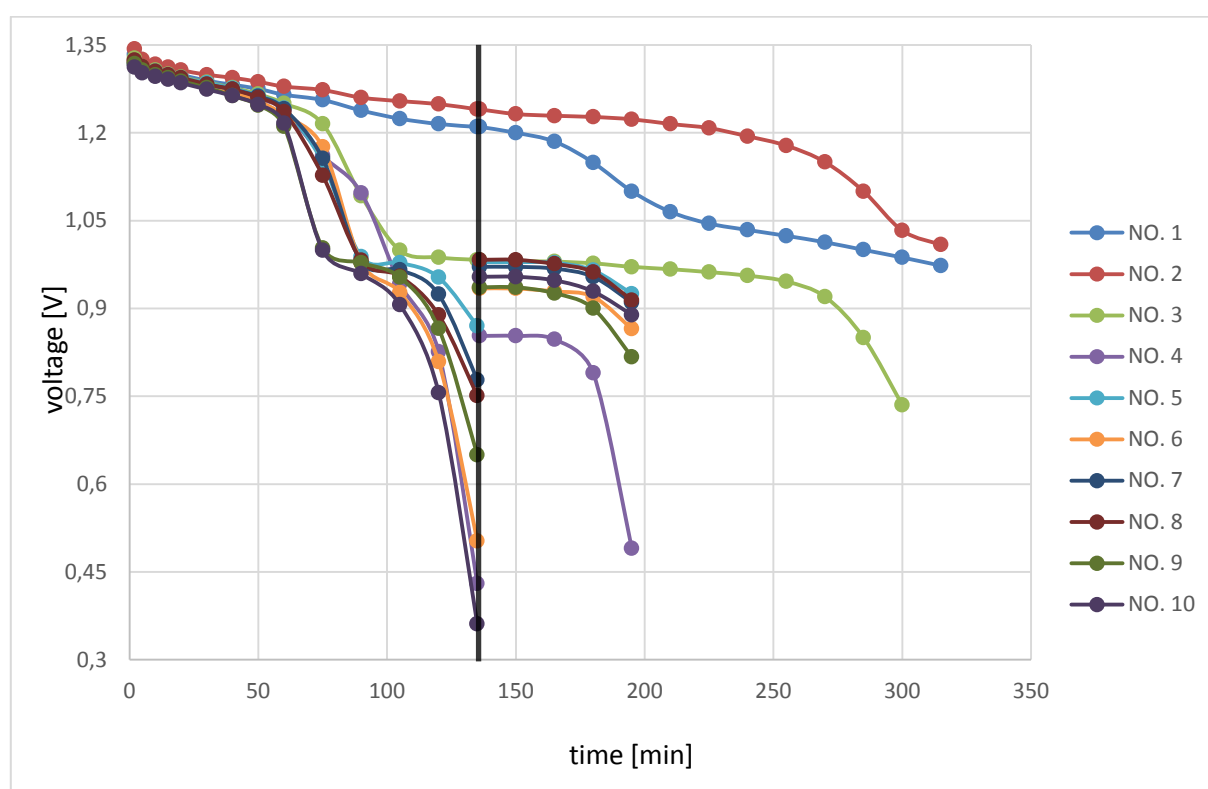


Figure 3. Discharging 1A – 5th cycle

In the 10th cycle a charging with only 1A and discharging with only 0.5A was used – to get hopefully higher capacity when the discharging chemical process goes slowly and there is more time for the reaction of deeper layers of the negative electrode.

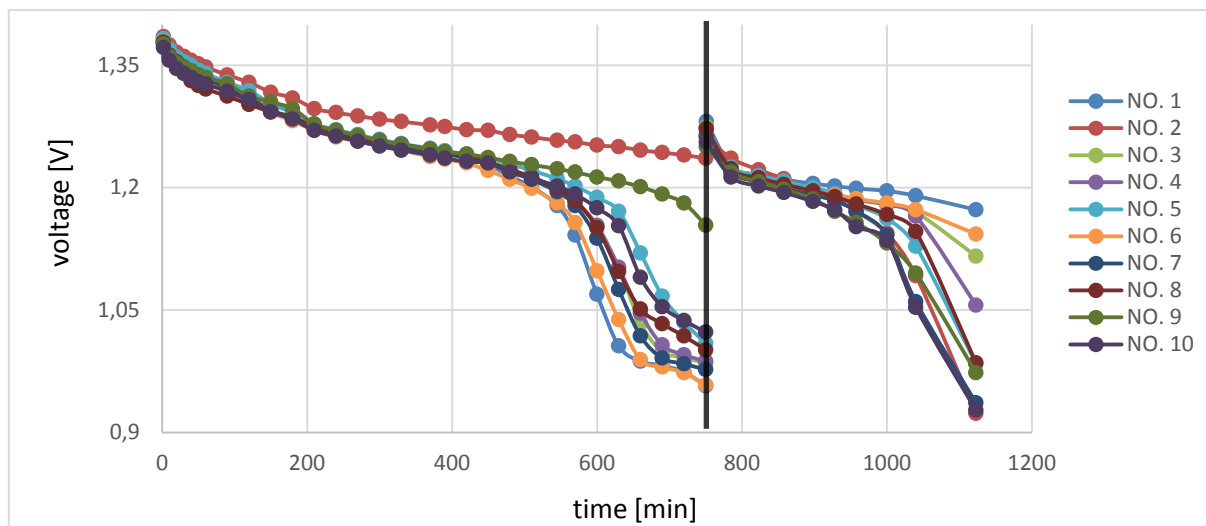


Figure 4. Discharging 0.5A – 10th cycle

Although again a regeneration “time-out” during the discharging was necessary (see Fig. 4) the total capacity of all cells reached a value about 8.6Ah (for final voltage 1V).



Figure 5. View of the renovated accumulator

In the last 11th cycle again a charging with 2.5A and discharging with 1.25A was done to get comparable conditions with earlier cycles. In this regime the capacity almost 8Ah was achieved what was a pleasant result. Finally the internal resistance of all cells was measured in a half-discharged state. Values between 45mΩ and 64mΩ per cell were obtained what is a satisfactory result.

Conclusion

The described rejuvenation experiment confirmed an extraordinary durability of these old NiFe accumulators - see also e.g. (1) or (2). The capacity of the 75 years old battery is now almost 8Ah instead of the original 8-10Ah (exact nominal values unknown). The charged battery showed a standard (not increased) self-discharging. The internal resistance corresponds to the capacity size. The main problem of the rejuvenation was the capacity of the negative iron electrode. A bit “violent” method of deep discharging helped to solve it well. Several electrolyte changes during the rejuvenation were done, especially in the beginning and after a deep-discharging cycle this is desirable. Eleven rejuvenating charging/discharging cycles were performed. No hydrogen peroxide was used.

Acknowledgement

Authors gratefully acknowledge financial support from the Ministry of Education, Youth and Sports under project No. LO1210 – „Energy for Sustainable Development (EN-PUR)“

References

1. P. J. DeMar, “Thomas Edison had it Right When He Said that his Nickel-Iron Batteries Would Last 100 Years”, The Battcon 2011 Conference Proceedings, Orlando, FL, pp. 21-1/7 (2012)
2. P. J. DeMar, „Nickel-Iron“, Telecommunications Energy Conference (INTELEC), 2011 IEEE 33rd International, Amsterdam, Netherlands, pp. 1 – 5, ISBN 978-1-4577-1249-4, (2011)
3. <http://www.nickel-iron-battery.com/Edison%20Cell%20Rejuvenation%2085%20yr-old%2013.%20DeMar.pdf>
4. <http://www.nickel-iron-battery.com/>
5. http://opensourceecology.org/wiki/Nickel-Iron_Battery/Chemistry
6. http://en.wikipedia.org/wiki/Nickel%E2%80%93iron_battery
7. Edison NiFe battery manual 1914
https://ironedison.com/images/products/Iron%20Edison/Edison%20Manual%20of%20Storage%20Battery%20Practice%20%28c%29%201914_.pdf

Hydrogen explosion risk in mining locomotive unit

B. Polnik, B. Miedziński

Abstract.

Application of battery powered mining locomotives with lead-acid cells is associated with secretion of hydrogen under charging. Modern systems of powering and control of these machines allow electrical braking with simultaneous energy recuperation. This however, increases the efficiency of operation while, increasing the risk of dangerous hydrogen concentration. Manufacturers do not take this fact into account basing on the relevant standards which, do not changed for more than 20 years. In the Institute of Mining Technology KOMAG was developed modern battery-type locomotive Lda-12K-EMA therefore, in order to obtain the ATEX certificate a number of relevant studies have been conducted. A part of them concerned the ventilation system of the battery explosive-proof housing therefore, the measurement of the hydrogen concentration during both charging and recharging processes. In addition, measurements of the quality of electricity provided via the control system to the battery under braking were performed.

The paper presents and discusses the results of both tests for real objects in mine and the results of relevant simulation analysis. The results were confronted with the formal applicable requirements. In this work also attempt to determine the correlation between the quality of electrical energy provided to the battery and the intensity of electrolytic gas emission.

Simulation analysis

An analysis of the literature shows that has not yet been carried out considerable research to determine the amount of electrolytic gas emission inside the battery during braking process with electrical energy recuperation. In addition, any assumptions made at the design stage of explosion-proof housing that assume uniform distribution of hydrogen inside and at the air vents (in housing enclosures) are made based on the experience of the manufacturer with participation of the user, of course. Hence, the appropriate simulation tests of the problem were conducted by authors for the object as shown in Fig.1.1.

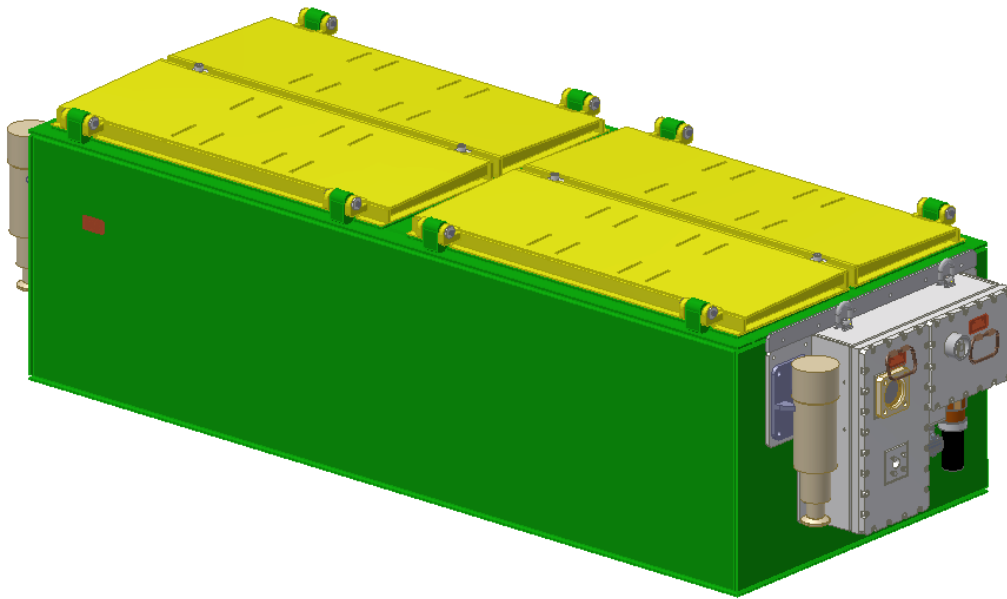


Figure 1.1 Geometric model of the battery explosion-proof housing

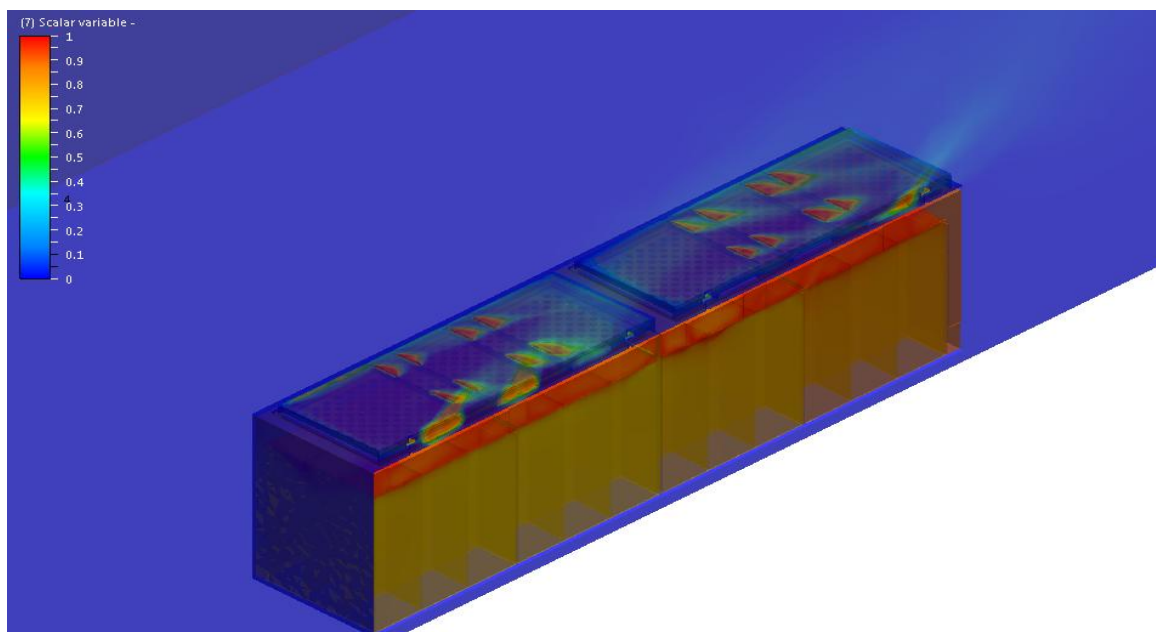


Figure 1.2 Selected simulation results

Experimental results

In order to confirm the results of the simulation the respective investigations of ventilation efficiency of the battery module were carried out in three steps. The first determined the size of the flow rate of hydrogen inside the battery module according standard PN-EN 60079-7:2010. The second included preparation of the batteries for testing by: charging the cells, the electrolyte supplementing (according to manufacturer indications) and closing plugs for filling cells. A control measurement of the overload current value and ambient temperature of the module and cells was carried out also. Under the third stage the hydrogen concentration at selected points (that in

accordance with standard PN-EN 60079-7:2010 should be located midway between the upper surface of the cell and the cover as well as close to plugs for filling and ventilation) was measured.

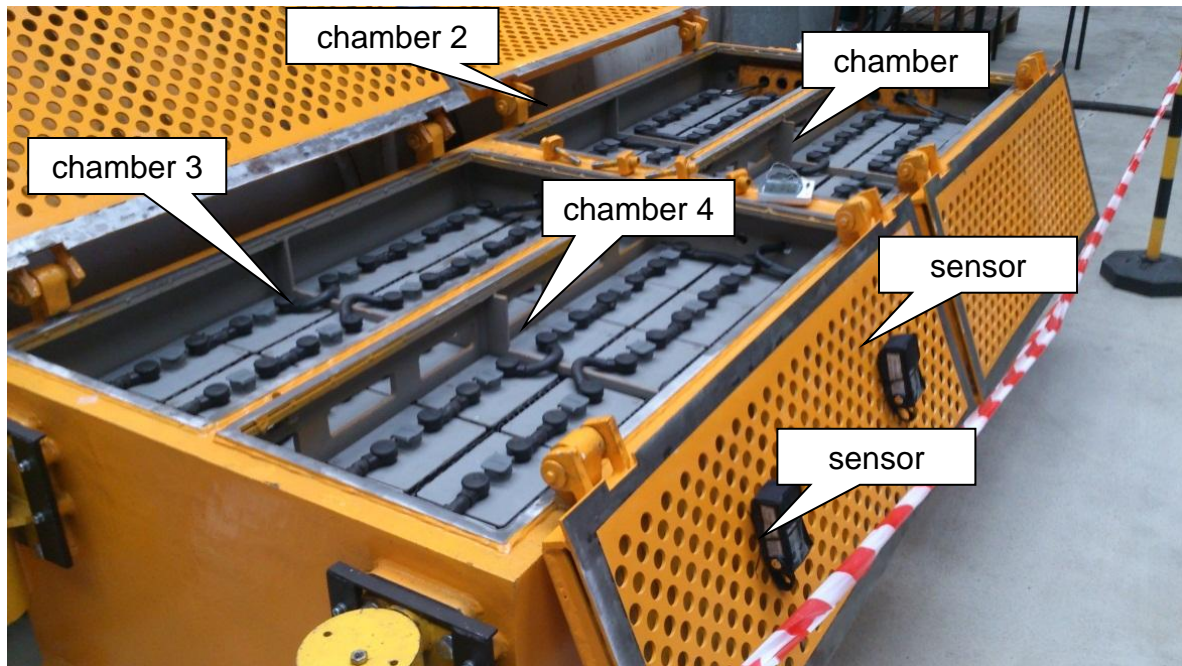


Figure 2.1 View of the object under test

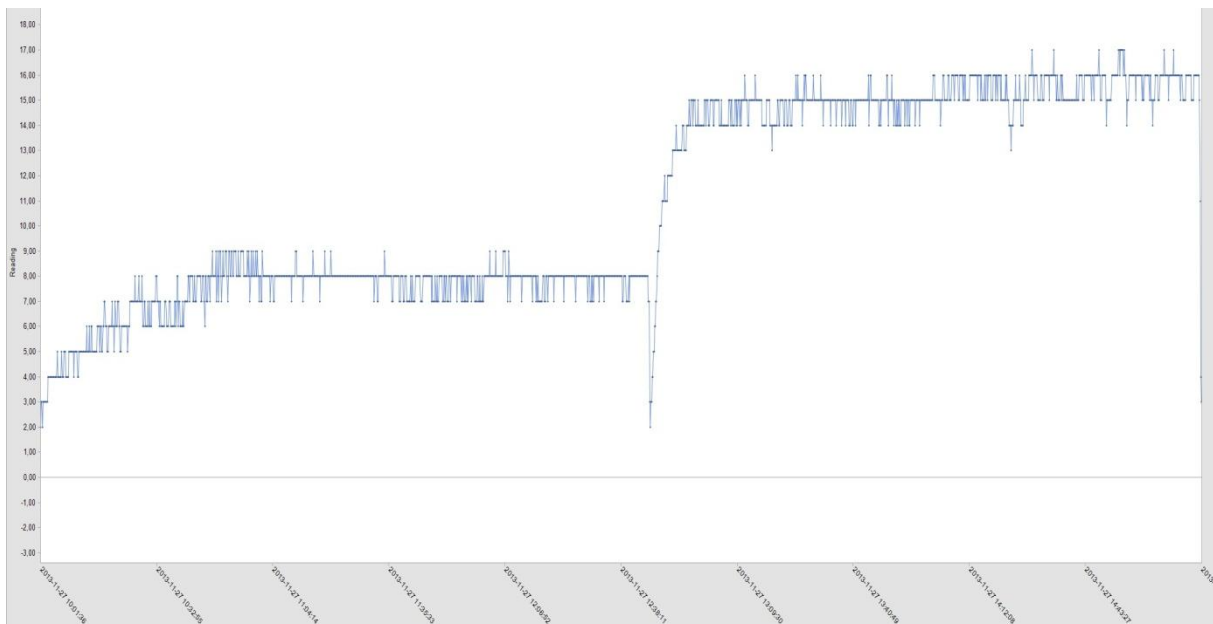


Figure 2.2 An example of emission intensity of hydrogen measured under test

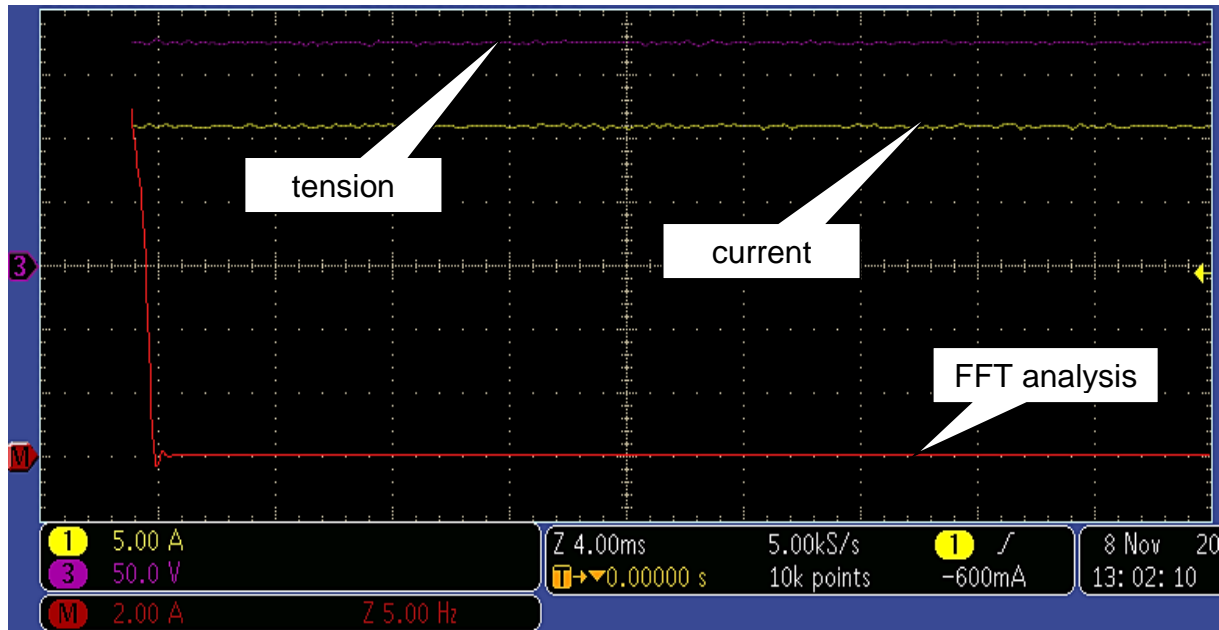


Figure 2.3 Variation of selected electric quantities with time under test.

Summary

In the paper will be presented detailed information on the research as well as on development trends in this area. The applied research methodology will be discussed and problems that authors faced during the study will be characterized. Conclusions will be formulated and indicated directions for further work.

Thermal Analysis of Thermophotovoltaic Emitter

J. Maxa¹, P. Vyroubal¹, L. Šimonová¹

¹Department of Electrical and Electronic Technology, Faculty of Electrical Engineering and Communication, BUT, Technická 10, 616 00 Brno, ČR

Corresponding author: Petr Vyroubal (xvyrou02@stud.feec.vutbr.cz)
Phone: +420 541 146 154

ABSTRACT

Thermophotovoltaic (TPV) belongs to the third generation of photovoltaics. This technique works on the principle of an effect of use as much of the radiation spectrum for optimal system operation. Traditional photovoltaic solar cells have an inherent limit on the efficiency at which they can convert sunlight into energy. Conventional solar cells are able to operate in the visible to near-infrared region of the spectrum. This limit, based on the band gap of the material, used and known as the Shockley-Queisser limit is about 33.7 percent for standard solar cells [1].

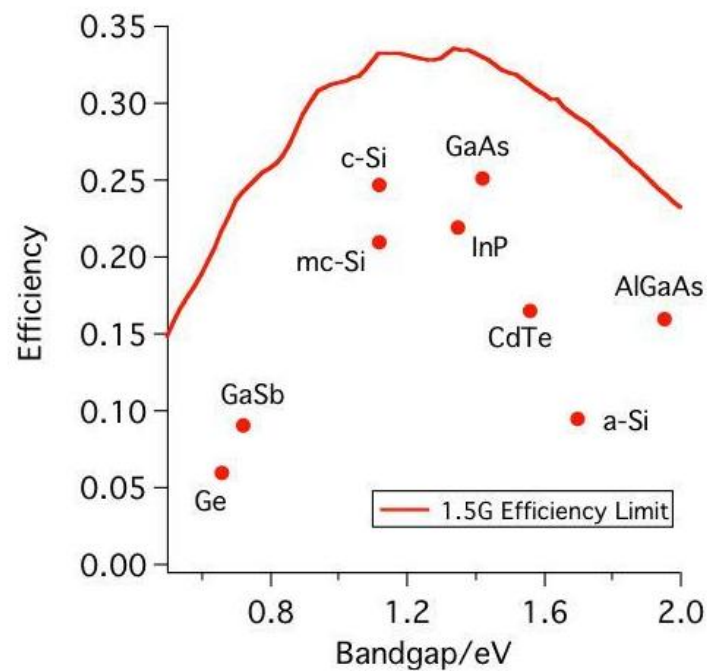


Figure 1. Band gap and efficiency [1].

Thermophotovoltaic systems have great potential application in commerce, military and aerospace industry. At present, the research on TPV primarily focuses on the spectral control technology and system construction.

To achieve the maximum efficiency, all photons should be converted. A process often termed photon recycling can be used to approach this. Here reflectors are placed behind the converter and

anywhere else in the system that photons might not be efficiently directed to the collector. These photons are directed back to the concentrator where they can be converted, or back to the emitter, where they can be reabsorbed to generate heat and additional photons. An idealized TPV system would use photon recycling and selective emission to convert all photons into electricity.

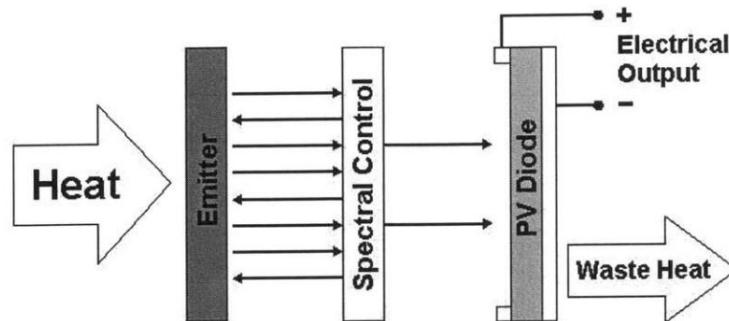


Figure 2. The efficient TPV system [2].

For the emitter, deviations from perfect absorbing and perfect blackbody behavior lead to light losses. For the case of selective emitters, any light emitted at wavelengths not matched to the band gap energy of the PV may not be efficiently converted (for reasons discussed above) and leads to reduced efficiency. In particular, emissions associated with phonon resonances are difficult to avoid for wavelengths in the deep IR, which cannot be practically converted. Ideally, an emitter will not emit in this range, and energy will only be converted at wavelengths that are easily converted. Examples of material with varying indices that results in selective emission for TPV applications are rare-earth oxides, such as holmium (Ho) or erbium (Er) oxide, and transition metals, such as hafnium (Hf) or tungsten (W) [2].

For blackbody emitters or imperfect selective emitters, filters are needed to reflect non-ideal wavelengths back to the emitter. In practice, these filters are rarely perfect. Any light that is absorbed or scattered and not redirected to the emitter or the converter is lost. Additionally, practical filters often reflect a small percentage of light in desired wavelength ranges or transmit light of non-ideal wavelengths. Both can lead to inefficiencies.

Even for systems where only light of optimal wavelengths is passed to the converter, inefficiencies associated with non-radiative recombination and ohmic losses exist. Since these losses can depend on the intensity of light incident on the cell, real systems must consider the intensity produced by a given set of conditions (emitter material, filter, operating temperature) [3].

The mathematical model includes the laws of conservation of momentum (represented by the full Navier-Stokes equation), mass and energy. The energy equation is in the form:

$$\frac{\partial(\rho E)}{\partial t} + \frac{\partial}{\partial x_k} u_k \rho E + p = \frac{\partial}{\partial x_k} k \frac{\partial T}{\partial x_k} - \sum_{j'} h_{j'} J_{j'} + u_j \tau_{ij} + S_h$$

where S_h is absorbed/emitted radiative energy defined as:

$$\frac{dI(r, s)}{ds} + a + \sigma_s I(r, s) = an^2 \frac{\sigma T^4}{\pi} + \frac{\sigma_s}{4\pi} \int_0^{4\pi} I(r, s) \Phi(s \cdot s') d\Omega'$$

Where I is radiation intensity, which depends on position and direction, r position vector, s direction vector, a absorption coefficient, σ_s scattering coefficient, n refractive index, T local temperature, σ Stefan-Boltzmann constant ($5.672 \cdot 10^{-8} \text{ Wm}^{-2}\text{K}^{-4}$), Φ phase function, s' scattering direction vector, Ω' solid angle.

CONCLUSION

The potential efficiency of such a system is much larger than expected performance of conventional photovoltaic system. Real experiments are much worse. In the TPV are mainly very expensive materials [4]. Production of such a system is a lengthy, time-consuming and costly, and the resulting efficiency is around 0% to 2% in laboratory conditions. Therefore, it is more efficient to perform a first simulation that can at least partially approximate the properties of the system.

ACKNOWLEDGMENT

Authors gratefully acknowledges financial support from the Centre for Research and Utilization of Renewable Energy under project No. LO1210 – „Energy for Sustainable Development (EN-PUR)“, by the specific graduate research of the Brno University of Technology No. FEKT-S-14-2293.

REFERENCES

1. BORELAND, M., Ch., DEY, N., EKINS-DAUKES and Y., YIN. *The Solar Energy Group: Photovoltaics Research*. [online]. The University of Sydney [cit. 2014-07-31]. Available from: <http://www.physics.usyd.edu.au/app/solar/research/pv.html>
2. LIN, S. Y., J. MORENO and J. G. FLEMING. *Three-dimensional photonic-crystal emitter for thermal photovoltaic power generation* [online]. [cit. 2014-07-31]. ISBN <http://dx.doi.org/10.1063/1.1592614>.
3. COUTTS, T., J. *An overview of thermophotovoltaic generation of electricity*. Solar Energy Materials and Solar Cells. 2001, roč. 66, 1-4, s. 443-452. ISSN 09270248.
4. GREEN, M., A. *Third generation photovoltaics: advanced solar energy conversion*. New York: Springer, 2006, xi, 160 p. Springer series in photonics, v 12. ISBN 35-404-0137-7.

Heat transfer fluids for optimal year-round operation of solar thermal systems in Central Europe

L. Šimonová¹⁾; J. Hylský; M. Frk²⁾; J. Šubarda³⁾

¹⁾ FEKT, Brno University of Technology, Technická 10, 616 00 Brno, xsimon09@stud.feec.vutbr.cz

²⁾ FEKT, Brno University of Technology, Technická 10, 616 00 Brno, frkmar@feec.vutbr.cz

³⁾ FEKT, Brno University of Technology, Technická 10, 616 00 Brno, subarda@feec.vutbr.cz

Abstract

Heat transfer fluids are used for many years in many sectors. These include engineering and the automotive industry, but also in the field of renewable resources, these fluids are very used. Such fluids can be used in two ways. Either it can be fluids, which transmit heat away for later use, or it can take heat from a source such as a cooling function.

In the area of solar thermal systems it is possible to meet with similar liquids as at present relatively normal solar systems for their activities using photovoltaic cells. It is a device that many people own the roofs of their houses. This system is mainly used for domestic hot water, pool heating, while it produces electricity. These are mostly small systems, used for personal use.

The second option is a solar thermal system that does not use photovoltaic cells, but this system uses for its activities so called mirror. These systems concentrate all the heat in the focus point or line. They also work with much higher temperatures than commonly known solar heat systems, which use photovoltaic cells. These two systems also have a different application. Solar thermal systems with mirrors are not small systems. These systems do not serve as an additional source of heat or energy. These are large systems that make efficient solar thermal power plants.

Despite the fact that these two systems are not very similar, they have one thing in common. For its proper function used heat transfer media. It is very interesting that has not been produced such a heat transfer medium, which was designed only for these systems. Of course, in areas where year-round temperatures keeps positive, these systems are much more efficient and also the heat transfer medium are placed different demands than in areas where year-round operation is limited by significant temperature changes in winter and summer.

For heat transfer in solar systems, from the point source collector to the point of consumption (usually storage tank) the use of different heat transfer media. Most often it is air or a fluid different. For year-round use fluid solar systems then it is the most common use antifreeze, with regard to the protection system in winter against frost damage. Fluids that are suitable for winter, on the contrary do not work so well in the summer. This also results undesirable heat losses and thus to losses of production of the system.

Any such heat carrier must meet certain requirements in order to be trouble-free operation of the system, reliable, and longest. Significant factors are the low pour point, good thermal-physical properties such as heat capacity or viscosity. Other important parameters are fireproof, corrosion protection system, compatibility with other materials in system, the long-term stability properties - especially heat resistance and no less important is the ecological and economic aspects. Very hard to find a liquid that would meet all of these opinions while the system could be used as long as possible without changing the properties.

In our work, we focused on the problems of heat transfer fluids, these systems are used commercially, and also to alternative heat transfer fluids, which could have the potential to succeed in solar thermal systems for optimal year-round operation. We focused on both the thermal and physical properties of these substances, and the environmental and economic aspects and all other important properties, such that the liquid should ideally have. All measurements and evaluation was conducted with a focus on Central Europe.

Acknowledgements

This work was supported by grant FEKT-S-14-2293, by project CZ.1.07/2.3.00/20.0103 and by project no. LO1210.

References

1. Dow Chemical Company. OPTIM Synthetic Glycerine – Physical properties, (2011), WWW: <http://www.dow.com/optim/optim-advantage/physical-properties.htm>
2. Elektřina ze slunce: Fotovoltaika a solárně termické elektrárny, EkoBonus, WWW: <http://www.ekobonus.cz/elektrina-ze-slunce-fotovoltaika-a-solarnetermicke-elektrarny>
3. M. Conde Engineering: Thermophysical Properti of Brines, (2002), WWW: <http://www.mrc-eng.com/Downloads/Brine%20Properties.pdf>
4. F. Mikšík, Nemrznoucí teplonosné kapaliny pro solární systémy, Brno, 66 p (2010)
5. F. Mikšík, Teplonosné kapaliny pro celoroční termické solární systémy, Brno, 29, (2008)
6. V. Quaschnig, Solar thermal water rating, Renewable Energy World (2004)

Analysis of the effect of heat on photovoltaic cells in thermophotovoltaic system

L. Šimonová¹⁾; J. Kolář; P. Vyroubal²⁾

¹⁾ FEKT, Brno University of Technology, Technická 10, 616 00 Brno,
xsimon09@stud.feec.vutbr.cz

²⁾ FEKT, Brno University of Technology, Technická 10, 616 00 Brno,
xvyrou02@stud.feec.vutbr.cz

Abstract

Thermophotovoltaic falls into the third generation of photovoltaic. Thermophotovoltaic system consists of several parts, each of which has in this system its function. The base is commercially available photovoltaic cell, which is able to work with the energy of particles mainly in the visible spectrum. Some cells can work as energy radiation in the visible spectrum, so the energy in the near infrared region. Everything depends on the materials from which the cell is made. Conventional photovoltaic cells thus cover only a small part of the spectrum and the remaining energy is converted to heat and it is a heat loss of system. This also reduces the overall performance and efficiency of the photovoltaic cell and the entire panel.

Thermophotovoltaic is trying to take advantage of the heat losses in your favor. Conventional PV cell is not able to convert excess heat into electricity, but this heat contributes thermofotovoltaice to make this system work optimally. Another part of the system is a radiator that with high temperatures can operate and subsequently emits radiation at only a part to a photovoltaic cell that it can already be processed. If the spectrum of the radiation emitted still too broad, between the radiator and the solar cell can be equipment filter that an unwanted spectrum of light reflected back to the radiator.

The basic principle of thermophotovoltaic systems parts is the ability to work with high temperatures and different spectral radiation than conventional photovoltaic systems. Therefore, it is also assumed that the materials used thermophotovoltaic individual parts of the system are sufficiently resistant to heat. With the highest temperatures and the lowest work radiator should work photovoltaic cell. Unfortunately photovoltaic cells are to change their temperature very dependent. Generally the efficiency and thus the performance of the photovoltaic cell decreases with the increasing temperature (Fig. 1). With every increase in temperature of cell about 1 °C it reduces the efficiency of this article about 0.4% (5). Such a drop in efficiency in thermophotovoltaic system may exhibit very much. Similarly materials from which the solar cell or panel is made (the most common materials are glass, EVA film, solar cells, Tedlar, aluminum), these can very quickly damage. This could lead to further reduction in efficiency, and also reduce the overall operation of the photovoltaic cell.

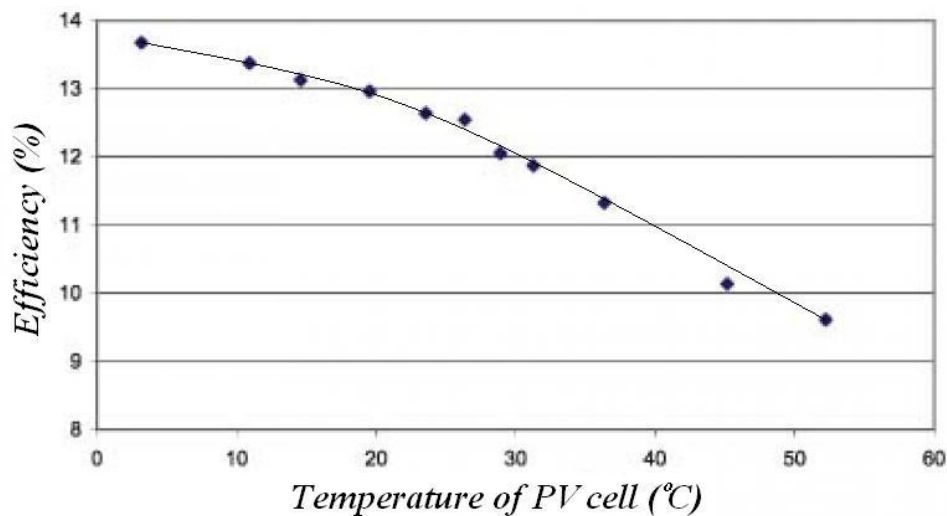


Figure 1. Example of the effect of temperature on PV cell efficiency. (4)

In the following study, we therefore focused on how much the effect of temperature on thermophotovoltaic system for photovoltaic cells. Because the materials used in the manufacture of individual parts thermophotovoltaic system, they are usually very expensive, we performed a preliminary analysis of the effect of heat on the photovoltaic cells in thermophotovoltaic system.

Acknowledgements

This work was supported by grant FEKT-S-14-2293, by project CZ.1.07/2.3.00/20.0103 and by project no. LO1210.

References

1. T. J. Countts, *An overview of thermophotovoltaic generation of electricity*. Solar Energy Materials and Solar Cells (2001), ISSN 09270248.
2. K. J. Cheetham, P. J. Carrington, N. B. Cook, A. Krier, *Low bandgap GaInAsSbP pentanary thermophotovoltaic diodes*. Solar Energy Materials and Solar Cells (2011), ISSN 09270248.
3. M. A. Green, *Third generation photovoltaics: advanced solar energy conversion*. New York: Springer (2006), 160 p, Springer series in photonics, ISBN 35-404-0137-7.
4. Z. Macháček, V. Benda, *Zkušenosti z provozu fotovoltaického systému FVS 2003A na Fakultě elektrotechnické ČVUT v Praze* (2008),
WWW: <http://imaterialy.dumabyt.cz/TZB/Zkusenosti-z-provozu-fotovoltaickeho-systemu-FVS-2003A-na-Fakulte-elektrotechnicke-CVUT-v-Praze.html>
5. C. Hu, R. M. White, *Solar Cells*. University of California, Berkeley (1979)

Thermal Analysis Of The Photovoltaic Concentrator Cell

S. Vaculík^a, P. Vyroubal^a, J. Maxa^a, J. Vaněk^a

^a Brno University of Technology, Antonínská 548/1, 601 90 Brno, Czech Republic

Introduction

Photovoltaic cells are using for conversion energy from renewable energy source (sun) to electrical energy.

The main advantages of this cells are [1]:

- Using of inexhaustible source of energy (sun).
- No emission during use
- No noise during use
- Simple installation of solar cells
- High operational reliability

The main disadvantages are [1]:

- The average annual intensity of solar radiation is relatively low.
- Large fluctuations in the solar radiation during the year
- High investment costs
- Need a backup power source
- Small energy conversion efficiency

Concentrators systems of photovoltaic cells use mirrors or lens for concentrating the sun's rays and its subsequent routing onto solar cell.

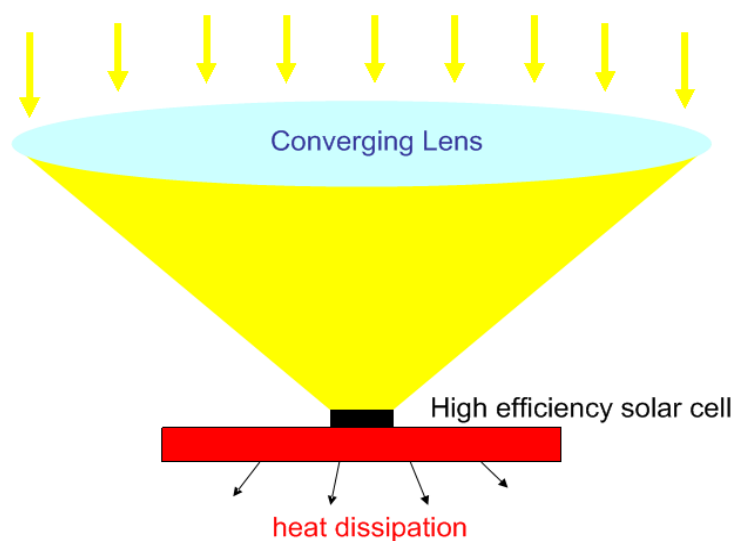


Figure 1. Example of concentrator photovoltaic system [4]

Thereby higher efficiency is achieving. But temperature has an increased impact on the position of the operating point. At high temperatures, electrical properties of the cell change. Due to this change the terminal voltage decreases, thus causing a decrease in the load output [2], [3].

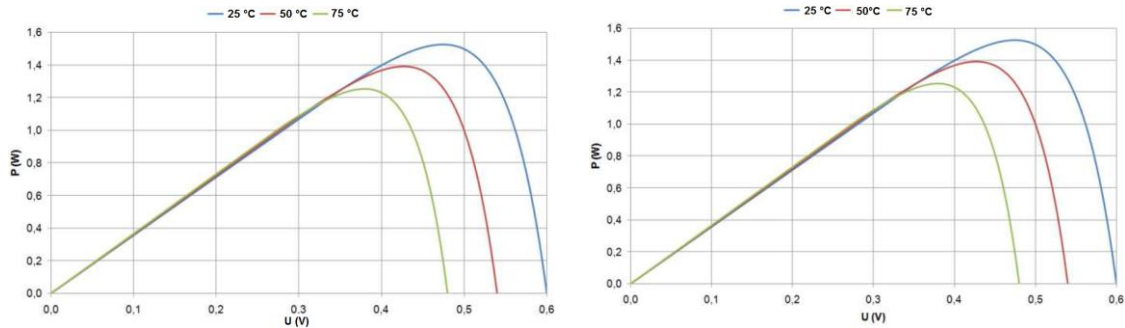


Figure 2. The influence of temperature on the VA characteristic, and the P characteristics

Analysed models

Design of the analysed model is based on sample, which was implemented and investigated at the Department of Electrical and Electronic. Five variants with different geometry have been tested:

- Basic (Figure 3)
- Basic with extended inlet pipe (Figure 4)
- Optimized basic model with extended inlet pipe – This model have rounded corner and bevelled edges of photovoltaic cell.
- Bath's model (Figure 5)
- Bath's model with optimized attachment of photovoltaic cell (Figure 6)

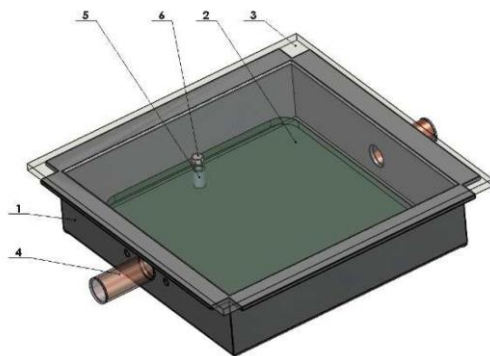


Figure 4. Basic model (1 – tub, 2 – photovoltaic cell, 3 – glass, 4 – inlet pipe, 5 – spacer)



Figure 3. Shape of extended inlet pipe in the tube

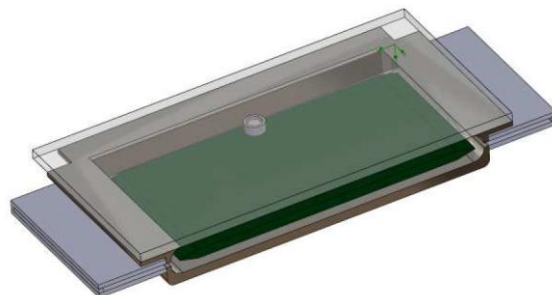


Figure 5. Bath's model

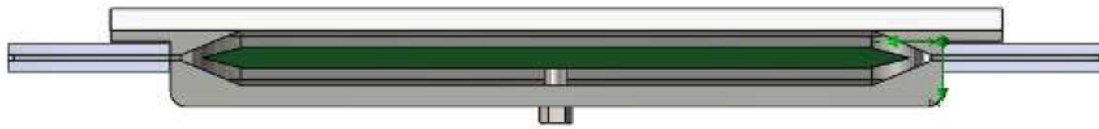


Figure 6. Bath's model with optimized attachment of photovoltaic cell

Boundary conditions

Cooling medium inflow: Volume flow: $3 \text{ l} \cdot \text{min}^{-1} = 0.00005 \text{ m}^3 \cdot \text{s}^{-1}$,

Temperature 20.05.

Cooling medium: Outflow into atmosphere – statistic pressure 101325 Pa.

Onto the upper surface of glass plate: Heat brought to the surface: 15000 W/m^2 .

Conclusion

This article deals with optimize cooling system of concentrator photovoltaic cell. For above mentioned simulation was used simulation program SolidWorks. For the basic simulation was used basic model. In this model was testing the position of inlet pipe. Best results achieved the model with the smallest distance between the centre of inlet pipe and glass. The inlet pipe was subsequently extended. This model was called “Basic with extended inlet pipe”. Further improvement was achieved by rounded corner and bevelled edges of photovoltaic cell. The best results have the “Bath's model with optimized attachment of photovoltaic cell”.

Acknowledgements

This work was supported by the LO1210 and by the specific graduate research of the Brno University of Technology No. FEKT-S-14-2293.

References

1. KUSALA J. Solární energie [online]. 2006 [cit. 29. 7. 2014].
Available on: <http://www.cez.cz/edee/content/microsites/solarni/k32.htm>
2. SOLČANSKÝ, M.; VANĚK, J. Influence of quinhydrone concentration on chemical passivation in solar cell technology. In *Elektrotechnika a informatika 2010 - elektrotechnika*. Nečtiny: 2010. s. 1-4. ISBN: 978-80-7043-913- 5.
3. Vaněk, J., Stojan, R. Concentrator Photovoltaic Systems. In *Proceeding of the ABAF-12 Meeting*. Brno, CZ: ABAF, 2011. s. 159-164. ISBN: 978-80-214-4357- 0.
4. LIANG D. Concentrated Photovoltaics [online]. 2010 [cit. 29/ 7. 2014].
Available on: <http://large.stanford.edu/courses/2010/ph240/liang2/>

Photovoltaic Modules Destruction Analysis

J. Vanek, J. Zimakova, M. Sturm

Department of Electrotechnology, Brno University of Technology, Faculty of Electrical Engineering and Communication, Technicka 10, 616 00 Brno, Czech Republic

In this paper we present the analysis of the causes that caused the destruction of photovoltaic modules cover glass in the group of modules randomly located in the photovoltaic field. Operator of photovoltaic system excluded the possibility of damage of these modules by impact of foreign objects because of their location in the photovoltaic field and because of no records of hail or similar events in this area. Damage of the cover glass in analyzed module appears to be adequate of safety glass cracking - uneven web of cracks in the glass with six central location with a different structure cracking. In the three of these areas is possible to find the area with the browning of the surface on the photovoltaic cells main contacts. This article also includes summarization of method which is possible to use for analyses of photovoltaic modules state.

Analysis of the module condition

At the first examination of damage module there can be found only damage on the front side of the module – the rear side of the module appears to be without of signs of damage and without observable damage to the junction box and to module frame and wires. Cover glass module damage seems to be appropriate to safety glass cracking – an uneven web of cracks in the glass with six central location with a different structure cracking. Upon closer inspection of these areas there had been suggested that these areas may be the cause of the total destruction of the module.

There are no noticeable signs of impacts of foreign objects in these areas or warping of the glass of the module inwards. The plant operator also excludes the possibility of damage of these module by impact of foreign objects on the surface because of their location in the photovoltaic field, which does not allow the intervention of a firearm or a casting object by an extraneous person.

The browning occurs on the surface of the electrode system in the three positions related to the six possible sources areas of cover glass cracking. After the next detailed comparison of the visible areas of browning from the front side and from the back side there can be found on the back side bulge corresponding to the location of the browning electrode systems. After exclusion of foreign culpability of glass damage it can be concluded that as one of possibilities these areas could be the source of destructive forces that caused the cracking of broken glass from inside the module.

After analyzing of electroluminescence radiation it was confirmed the correlation of destruction of photovoltaic cells with the areas of heavy damage of the cover glass and there were detected several other places with a strong destruction of the cells, which were further analyzed.

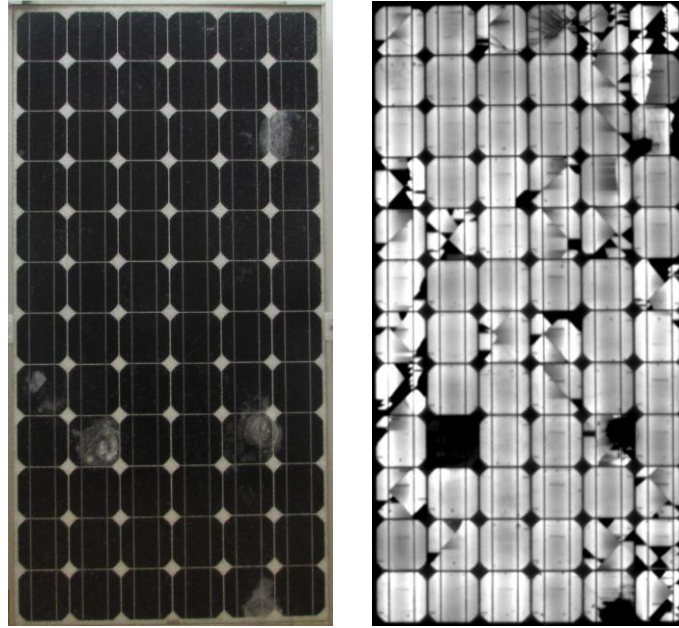


Figure 1. Optical and electroluminescent display of the front side damaged module Antaris AS_M_180

There was also made an analysis of electrical current-voltage characteristics of the analyzed module.

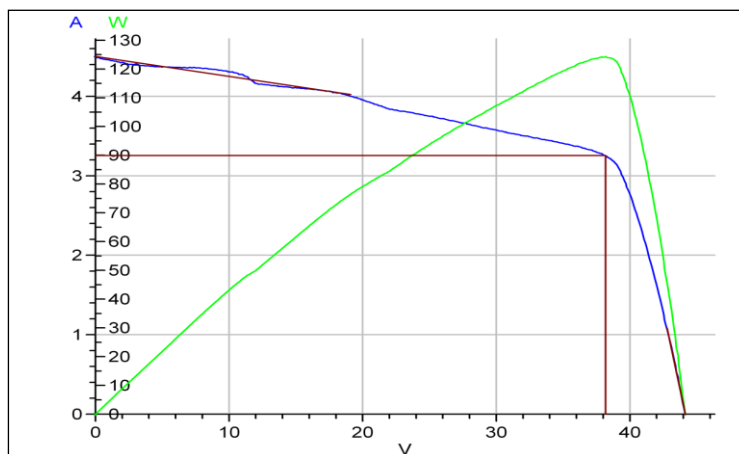


Figure 2. VA characteristic of module ANTARIS SOLAR M-180 AI at standard measurement conditions

T_p	25.0 °C
$G_{(i)}$	1.0 kW/m ²
I_{sc}	4.503 A
V_{oc}	44.145 V
Eff.	9.74 %
FF	62.53 %
P_{mpp}	124.284 W
V_{mpp}	38.183 V
I_{mpp}	3.255 A
R_{ser}	1.3 Ohm
R_{sh}	39.9 Ohm

In comparison of measured results with the manufacturer's information (see Attachment Datasheet - Antaris AS M 180) can be stated the decrease of peak power of about 56 W, the loss is caused by a significant decrease of current (from 5A to 3.25 A) versus of a slight increase of the

open circuit voltage (from 36.0 V to 38.2 V). This shows again that the damaged cells are no longer able to supply the required current. Ripple in VA characteristics near the short current (I_{SC}) is due to the cooperation of bypass diodes, just as would be in case of shaded cells.

Detailed analysis of damaged areas

To determine the causes of the electrode system surface browning and further analysis it was performed a microscopic analysis and an elemental analysis of these damaged areas. The four areas were chosen for this analysis and there were cut three samples. (Sample No. 1 was not cut for technical reasons)

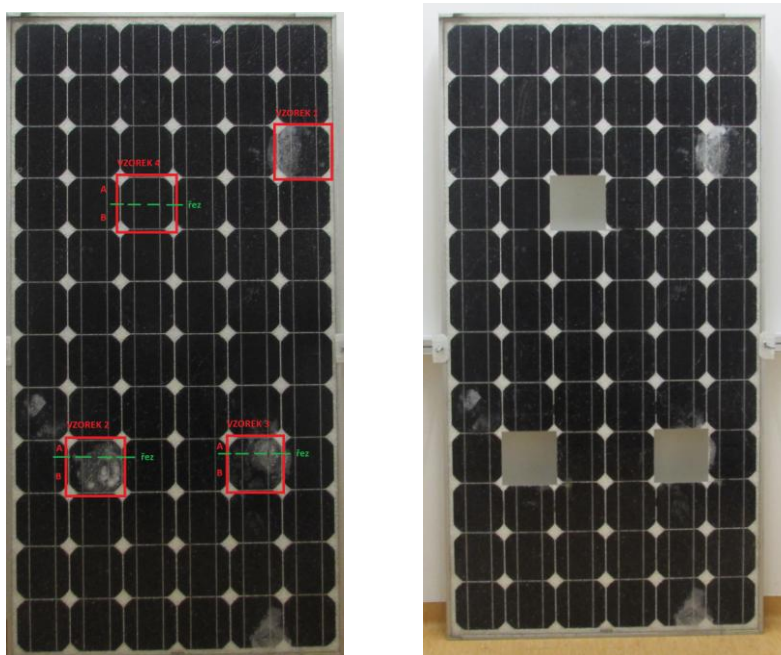


Figure 3. Sample areas from a module Antaris AS M 180 and outlined the analyzed cuts

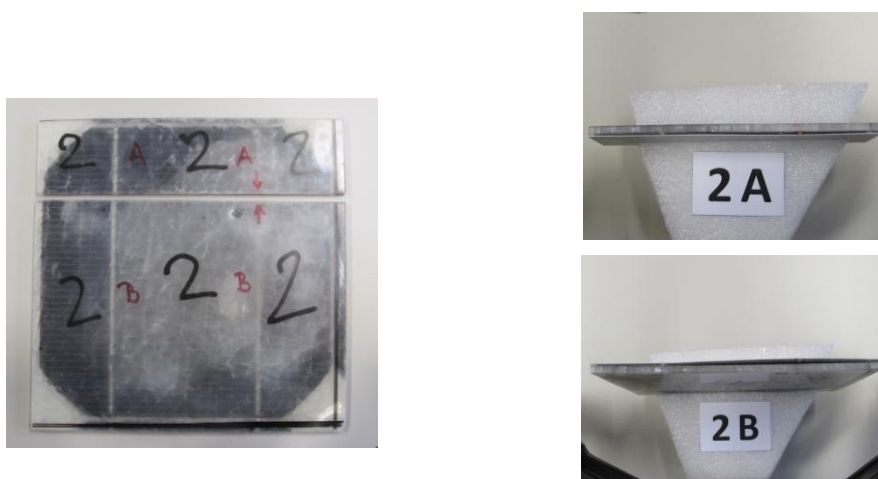


Figure 4. Sample No. 2 of damaged photovoltaic cell cut from module ANTARIS M 180 AI. The cut is made during electrode system surface browning.

Module surface was modified by using embedding materials to allow cutting the samples. In samples No. 2 and 3 with the detected browning of electrode system a cut was made through the

browning area as shown in Fig. 6. Both of these samples was evidently delamination between the glass and the laminating material EVA. Though the sample No. 4, which was chosen as a reference sample without detected areas, was made the cut to make the comparison analysis. In this sample no delamination was detected. The resulting cuts of samples can be seen in Fig. 4.

Scanning electron microscopy analysis was performed in places of electrodes browning and for comparison also in the undamaged second electrode area and in the comparative reference Sample No. 4

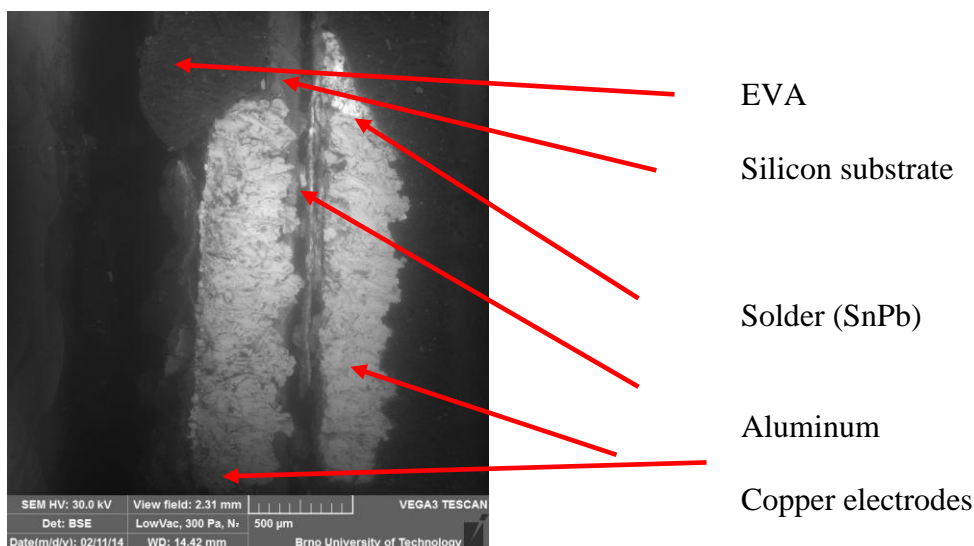


Figure 5. Detail of browned area on the sample 2A. There are observable copper electrodes and thin contacts of solar cells. The silicon substrate between the electrodes is missing and the space between the electrodes is collapsed.

Conclusions

As the cause of the cover glass cracking was excluded outside intervention (hail or small objects falling on the surface of the solar module). One of the causes of the protective glass cracking could be a tension induced by crooking of the supporting frame either by mount design or poor technological procedure for module assembling. This tension and cracking of the glass would subsequently cause cracks in photovoltaic cells. In the case that the current passing through the substrate can flow only between metal electrodes, it had increased the current density, and before the bypass diodes were fully opened, it could cause a short-term local heating to the temperatures of silicon melting and evaporation. This process could be the cause of the local delamination and bulges on the rear side. Because an increased temperature had worked for a short time, there would be no extensive damage as in case of a normal long-term heating of local hot spots in solar modules.

Acknowledgement

Author(s) gratefully acknowledge financial support from the Centre for Research and Utilization of Renewable Energy under project No. LO 1210 Energy for Sustainable Development and FEKT-S-14-2293 “Materiál a technologie pro elektrotechniku II”.

Preparation of Lead Electrodes For Measurement By Using AFM

D. Fryda^a, J. Zimáková^a, P. Bača^a

^a Brno University of Technology, Antonínská 548/1, 601 90 Brno, Czech Republic

Introduction

AFM (atomic force microscopy) is microscopic technique that is used for displaying the three-dimensional surfaces, invented in 1986 by Binnig, Quate and Gerber. The image surfaces are gradually compiled, point by point. The method achieves very high resolution. AFM can be used not only to display but also to the formation of structures or processing surfaces in nanometer region. It can display non-conductive samples. Sometimes it is called SFM (scanning force microscopy). The basic part of AFM is a very sharp tip that is mounted on a flexible cantilever.

AFM can only display surface of samples, not their volume structure. But in comparison with optical microscopy it achieves considerably greater resolution, which is comparable with resolution of electron microscopy. The disadvantage of AFM is very limited image size and speed of rastering. Maximum image size is in order of hundreds of micrometers and building one image takes several minutes. Problems are also caused by distance between the tip and the sample (strong interaction, the possibility of tip catching, pollution of the tip, damaging sample) and by non-zero width of the tip which leads to deformation of the image. [1,2]

Furthermore, AFM is limited by vertical range (maximum height of the sample), which is typically tens of micrometers. Part of our work is to monitor morphological changes at the electrode surface during the cyclic voltammetry by using AFM. Because of grown of large crystals on the surface, it is important to prepare samples with the smoothest surface as possible.

The aim of this work is to determine the most appropriate method for the preparation of samples for measurement by using AFM.

Preparation of samples

At first, the lead plates (samples) were cutted at the desired sizes (20 x 20 mm) and then aligned by molding machine Trystom H-62 with pressure 50 kN.

The surface of the samples was modified with 3 different methods:

- polished by separator
- polished by grinding wheels
- plasma technology

a) polished by separator

Figure 1 shows surface morphology of sample polished by separator. It was used separator with glass fibers size 0,8 μm . Polishing was conducted for 5 minutes. Maximum size of particles on the surface reached 80 nm.

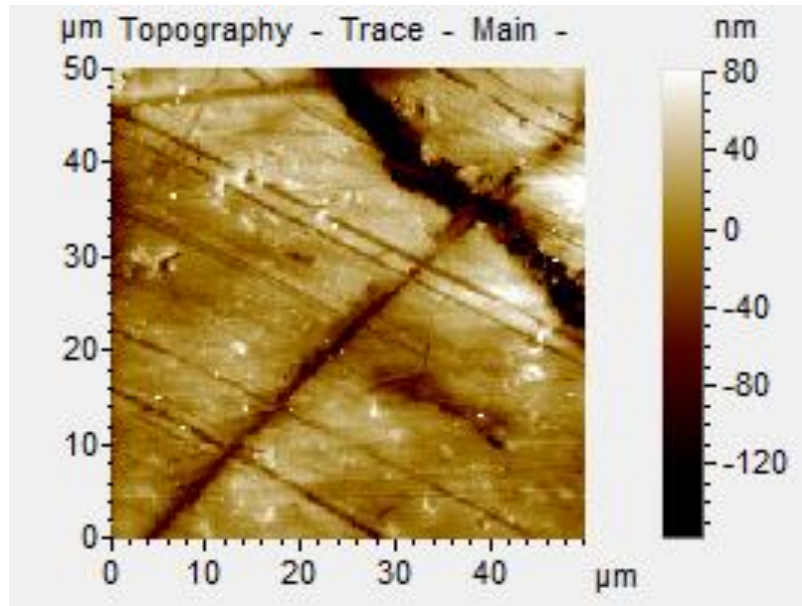


Figure 1. surface morphology of electrode polished by separator

b) polished by grinding wheels

Figure 1 shows surface morphology of sample polished by grinding wheels. It was used abrasive paper with a grain size 600 and then 1200. Maximum size of particles on the surface reached 30 nm.

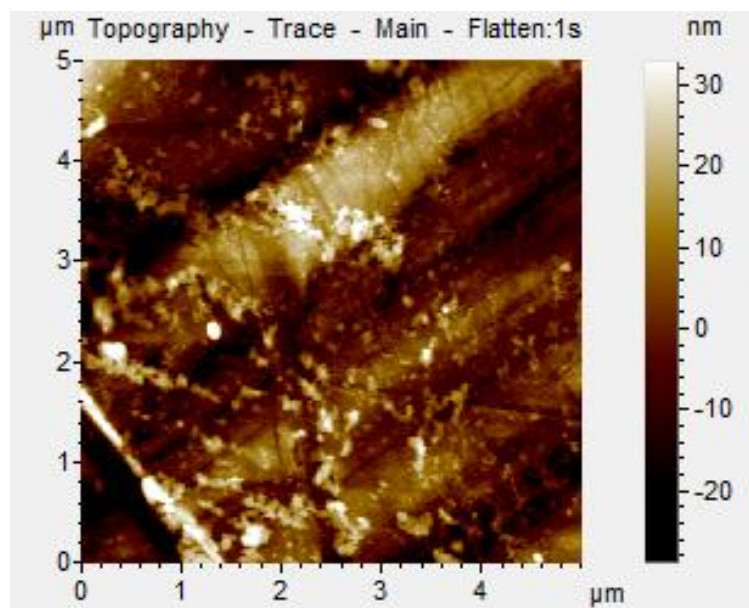


Figure 2. surface morphology of electrode polished by grinding wheels

c) using plasma technology

The best results were achieved by using plasma (surface is shown at figure 3). The surface seemed to be the smoothest. Maximum size of particles on the surface reached 17 nm.

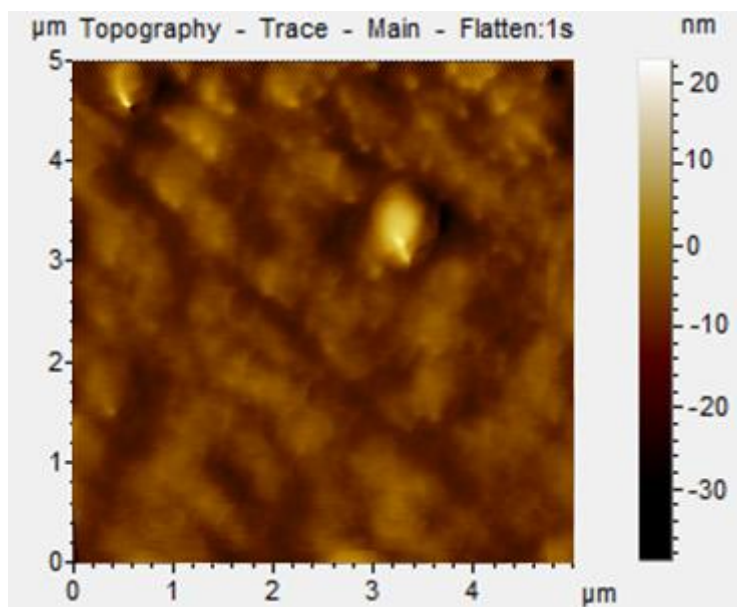


Figure 3. surface morphology of electrode modified by plasma technology

Acknowledgements

This work was supported by the specific graduate research of the Brno University of Technology No. FEKT-S-14-2293 and Centre for Research and Utilization of Renewable Energy under project No. LO1210 - Energy for Sustainable Development (EN-PUR).

References

1. BŘEŇ D.; KULHÁNEK P., Pikoškály aneb jak uvidět atom, ALDEBARAN BULLETIN, 27/2004, ISSN 1214-1674, http://aldebaran.cz/bulletin/2004_27_pic.html
2. P. E. West, *Introduction to Atomic Force Microscopy, theory, practice, applications*, [S.I.] P. West, 2006, www.AFMUniversity.org

Climatic Chamber Designed For Curing Positive Electrodes

M. Kadlec^a, J. Zimáková^a, D. Fryda^a

^a Brno University of Technology, Antonínská 548/1, 601 90 Brno, Czech Republic

Introduction

Lead-acid batteries are the oldest type of rechargeable battery, invented in 1858 by French physicist Gaston Plante. Batteries have changed little since 19th century although improvements in materials and manufacturing methods continue to bring improvements in energy density, life and reliability. Major change was in 80's when the flooded design was replaced by VRLA with immobilized electrolyte. All lead-acid batteries consist of flat lead plates immersed in a pool of electrolyte (solution of sulfuric acid). The main advantages are well mastered technology, relatively low cost of manufacture and high power. The lead-acid battery has become one of the main portable sources of electric power with wide applications in man's everyday life (telecommunications, information technologies, ect.). Relative good specific power has enabled its widespread use for starting, lighting and ignition of engine purpose for vehicular applications.

Resulting properties of lead-acid batteries are affected by the parameters set in manufacturing of electrodes: [1,2,4]

- composition of the active mass
- temperature and humidity during the process of curing
- formation

Curing

During the process of curing, paste particles are interconnected to form an uninterrupted strong porous mass (skeleton) which is tightly bound to the grid.

Depending on the values of ambient temperature and the humidity are on the surface of the electrodes produced two kinds of sulfate particles: tribasic lead sulphate (3BS) and tetrabasic lead sulphate (4BS).

Tribasic lead sulphate particles are obtained when the paste preparation is performed at temperature from 30 °C to 60 °C and plate curing is conducted within same temperature. These particles are 1 – 2 µm long and tightly interconnected.

Tetrabasic lead sulphate particles are performed at the temperature from 80 °C to 95 °C. Length of these particles is 15 – 20 µm and 4 – 5 µm in diameter. [3]

Climatic chamber

One of the most important factor that influence the formation of sulphate crystals is humidity in the chamber. Sulphate crystal starts to form only when the humidity in the chamber is 100%. This value has to be set up during the entire process of curing.

Curing was conducted in laboratory incucell incubator (Fig. 1A) with possibility to set up the temperature from 20 °C to 150 °C. The electrodes were placed into separated chamber with 100%

humidity. This chamber was hermetically sealed. Humidity was ensured by mist maker. Conditions during the process of curing were monitored by sensors of humidity and temperature placed in the chamber. There were also one special recording sensor which periodically recorded the measured values and allowed us to monitor conditions online. Placement of the devices and electrodes in the chamber is shown in figure 1B.

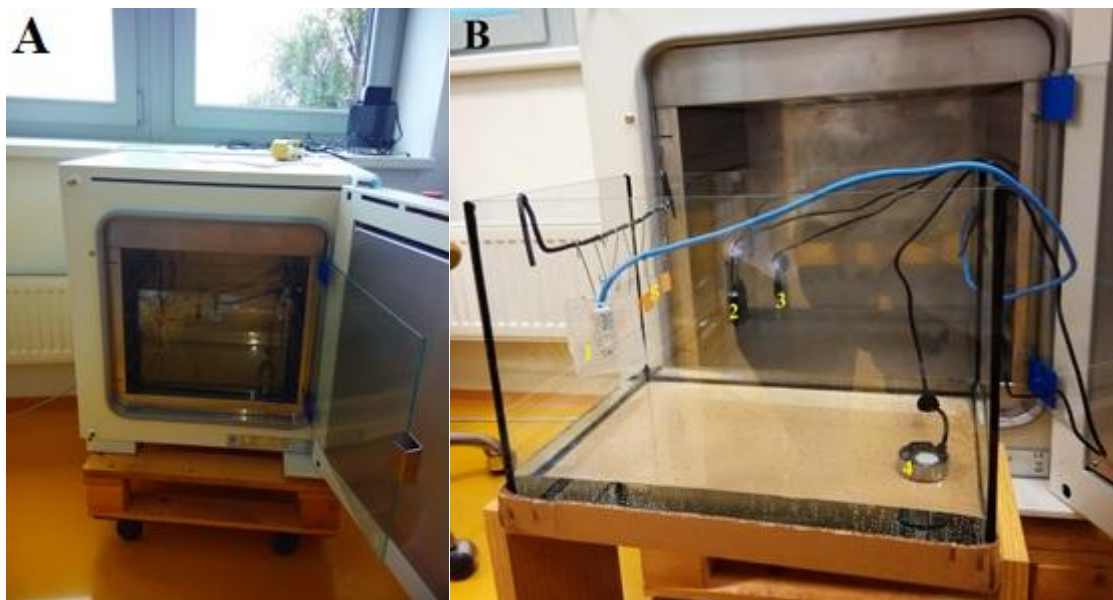


Figure 1.: A) chamber located in incubator; B) placement of measurement device: 1 - recording sensor, 2 - sensor of humidity, 3 - sensor of temperature, 4 - mist maker, 5 - Pb electrodes

Figure 2 shows electrodes after process of curing. There are two types of electrodes: at figure 2A is electrode cured at separated climatic chamber with 100% humidity, figure 2B shows electrode cured at incubator without separated chamber. Electrodes were cured at temperature 75 °C for 48 hours.

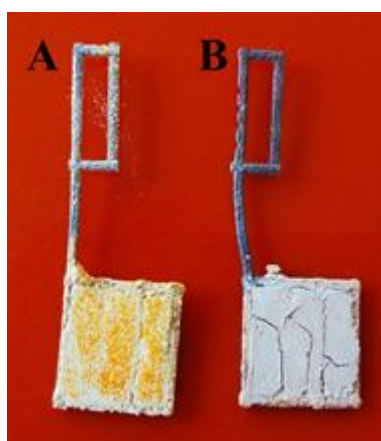


Figure 2. comparing of surfaces Pb electrodes after curing process; A) electrode cured at new climatic chamber; B) electrodes cured at incubator

The aim of our work is upgrade the conditions during the process of curing, especially humidity in the chamber at higher temperatures. The experiment is still ongoing and therefore the results are not complete. To determine the exact modification needs to be done XRD analysis and ESEM observation as well as electrochemical parameters of the electrodes after the formation. The results will be published in following works.

Acknowledgements

This work was supported by the specific graduate research of the Brno University of Technology No. FEKT-S-14-2293 and Centre for Research and Utilization of Renewable Energy under project No. LO1210 - Energy for Sustainable Development (EN-PUR).

References

1. H. Karami, M. Shamsipur, S. Ghasemi, Journal of power sources, 164, 2007
2. R. Kiesling, Lead acid battery formation techniques, Digatron firing circuits
3. D. Pavlov, Lead-acid batteries: Science and technology, A handbook of lead-acid battery technology and its influence on the product, Elsevier, 2011
4. S. Vaculík, J. Zimáková, P. Bača, The influence of temperature in curing process in the manufacturing of electrodes of lead-acid batteries, ABAF 2014

Hybrid membranes for vanadium redox flow battery

Jong Deok Park¹, Young Min Park², Haekyoung Kim^{1,*}

¹ School of Materials Science and Engineering,
Yeungnam University, Gyeongsan, Gyeongbuk

² Fuel Cell Project, Research Institute of Industrial Science and Technology, Pohang, Gyeongbuk
South Korea

*hkkim@ynu.ac.kr

With the expanding need for large electrical energy storage systems in connection with renewable energy sources, flow batteries, have been enormously considered due to their high flexibility in upgrade and low cost associated with scale-up. Of all the flow batteries, vanadium redox flow battery (VRFB) use of same element in both half-cell solutions that overcomes the inherent issue of cross contamination by diffusion of different ions across the membrane. Together with the absence of any toxic emissions, the vanadium redox flow battery has demonstrated its uniqueness in terms of safety and long life cycle. Typical charge–discharge reactions of a VRFB involve two vanadium redox couples, V(II)/V(III) and V(IV)/V(V), in the negative and positive half-cells, respectively. In a fashion similar to most batteries, electrons are transferred between the two electrodes through the external circuit during the charge and discharge processes. In a VRFB, the ion exchange membrane is a key component as an ionic conductor and separator: it not only provides an ionic conduction pathway between the two electrolytes but also prevents mixing of the negative and positive electrolytes. The crossover of ions through the membrane, with the diffusion of vanadium ions from one half-cell to the other due to the concentration gradients between the two electrolytes, will result in self-discharge and thus the loss of the chemical energy.

In this study, the hybrid membrane of inorganic materials with perfluorinated organic membrane were fabricated and characterized in terms of ionic conductivity and permeability. The ionic conductivity was measured with four point probe method and the permeability was measured with UV spectroscopy. The hybrid membrane exhibited similar ionic conductivity with perfluorinated organic membrane and 30% lower permeability than perfluorinated organic membrane.

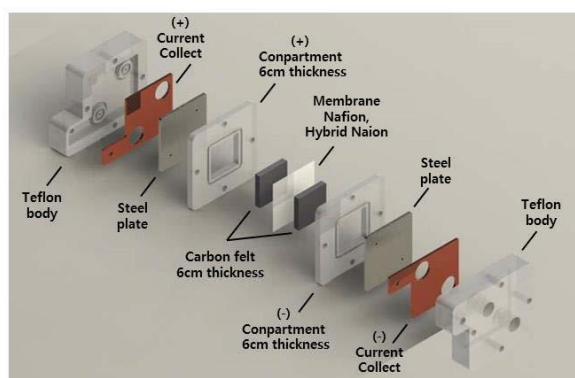


Figure. 1. Schematic diagram of RFB cell measurement.

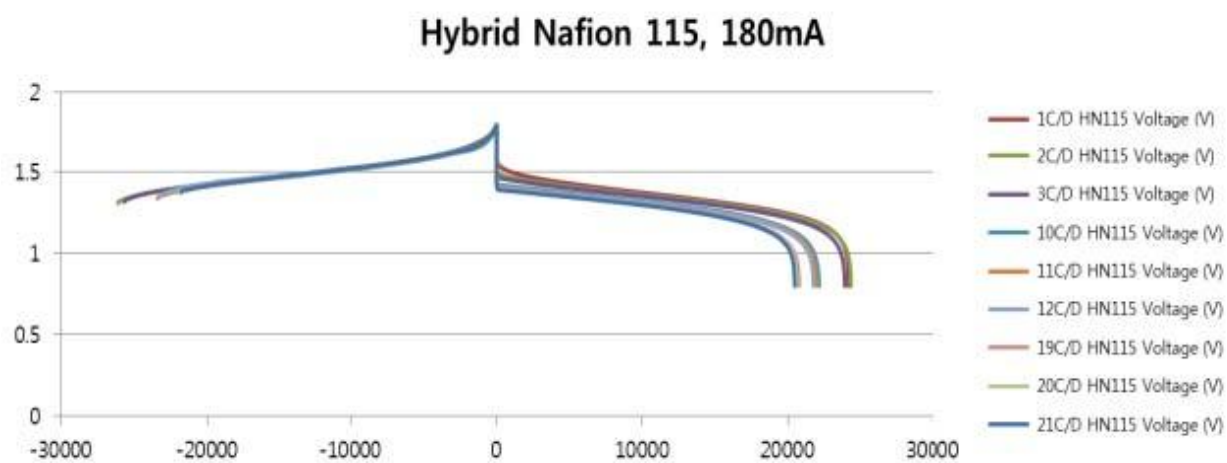


Figure. 2. Charge-discharge characteristics of membranes at 20mA/cm² of current density.

In Situ Observation of Morphology Changes on Lead Electrodes During Cyclic Voltammetry by Using AFM

J. Zimáková^a, D. Fryda^a, P. Bača^a

^a Brno University of Technology, Antonínská 548/1, 601 90 Brno, Czech Republic

Introduction

Cyclic voltammetry is the most widely used technique for acquiring qualitative information about electrochemical reactions. It belongs to potentiodynamic experimental methods. They have evolved of rapid development in the last decades and great expansion in laboratory practice. The reason for this is rapid development of computer-controlled experimental facilities with automated data collection and also the development of a mathematical description of the potentiodynamic curves. This makes it possible to use these techniques to obtain relatively quickly basic characteristics of studied system, with regard to the mechanism of electrode action.

Cyclic voltammetry is characterized by continuous growth potential of the working electrode from one limit to the other and back to the starting point. It follows that the fundamental adjustable parameters of the experiment are limits and feed rate potential. It can be also affected the properties of the electrolyte especially the concentration of electroactive material and temperature. System response is called electrochemical system spectrum. [1]

Atomic force microscopy (AFM) is a form of scanning probe microscopy. It is powerful tool to observe surface characteristics on electrodes at nanometer resolution. An AFM is a mechanical imaging instrument that measures the three dimensional topography as well as physical properties of a surface with a sharpened probe. The sharpened probe is positioned close enough to the surface such that it can interact with the force fields associated with the surface. Then the probe is scanned across the surface such that the forces between the probe remain constant. An image of the surface is then reconstructed by monitoring the precise motion of the probe as it is scanned over the surface. Typically the probe is scanned in a raster-like pattern. [2]

Up this time, some observation of chemical reaction and materials in lead-acid battery system have been reported. The aim of our work is in situ observation of morphology changes on electrodes in different stages of cyclic voltammetry by using AFM.

Electrochemical cell

Figure 1 shows used electrochemical cell and configuration of electrodes. A polished lead electrode was used as a working electrode (size 20 x 20 mm). A pure lead wire was used as counter electrode and as a referent electrode was used cadmium wire. Sulfuric acid solution (density 1,28 g/ml) was injected from side ports of electrochemical cell.

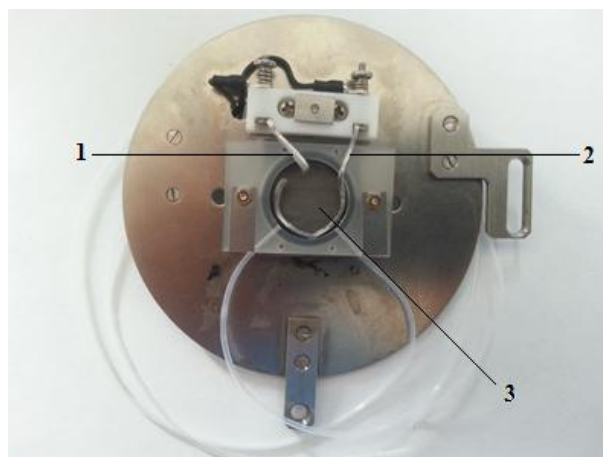


Figure 1. Electrochemical cell: 1 – referent Cd electrode, 2 – counter electrode, 3 – working electrode

Conditions of electrochemical measurement was as follows:

- limit of potential: from -0,2 V to +0,2 V
- feed rate potential: 100 mV/s

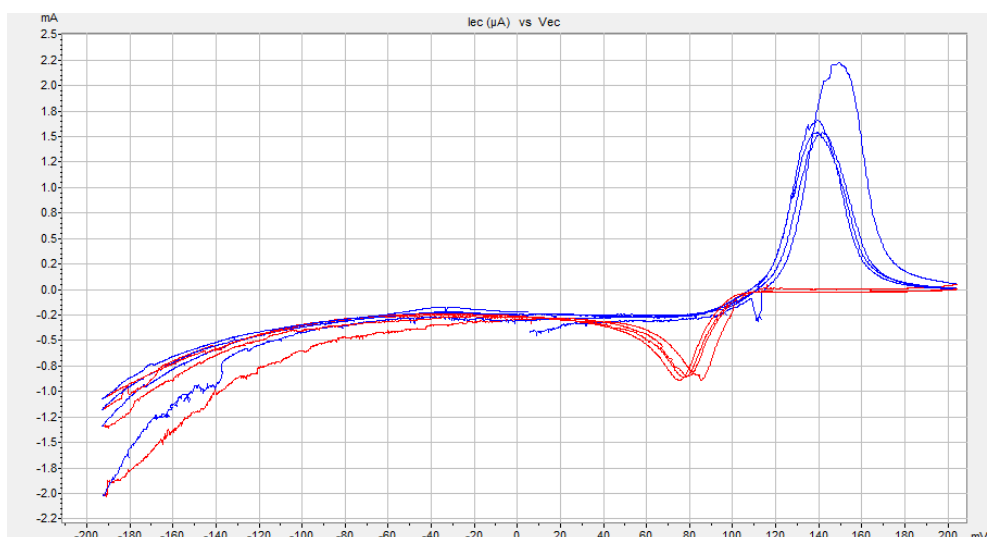


Figure 1. the course of cyclic voltammetry

Figure 2 shows process of cyclic voltammetry. Cyclic voltammetry was held four times and during process was observed morphology of working electrode by using AFM. Results from first 2 cycles are shown at figure 3. These results shown changes in particle size on the electrode surface. During two cycles was changed the maximum size of these particles from 80 nm to 1 μ m.

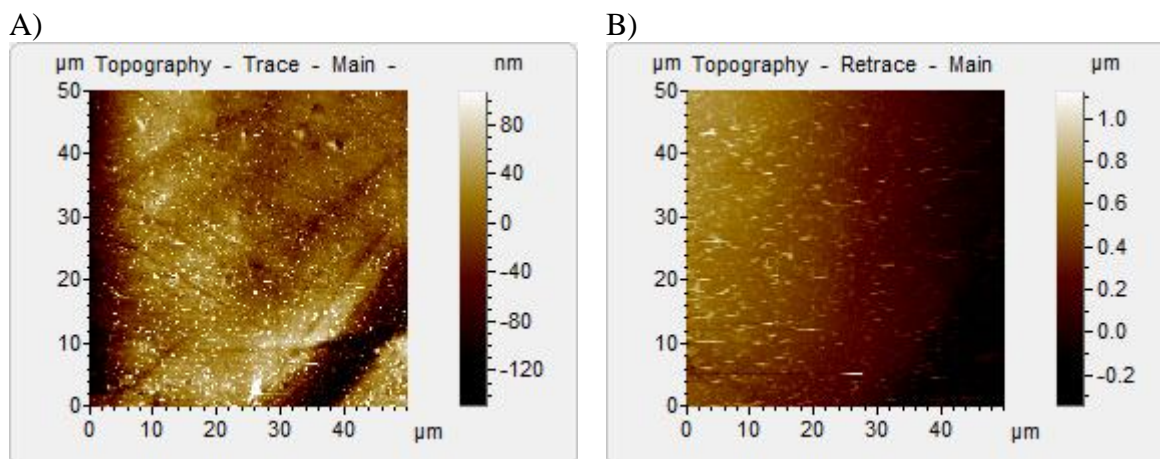


Figure 2. results of observation by using AFM: A – first cycle, B – second cycle

The experiment is still ongoing and therefore the results are not complete. To determine the exact changes during cyclic voltammetry it needs to be done more AFM observation. The results will be published in following works.

Acknowledgements

This work was supported by the specific graduate research of the Brno University of Technology No. FEKT-S-14-2293 and Centre for Research and Utilization of Renewable Energy under project No. LO1210 - Energy for Sustainable Development (EN-PUR).

References

1. D. Adrienko, *Cyclic voltammetry*, 2008
2. P. E. West, *Introduction to Atomic Force Microscopy, theory, practice, applications*, [S.I.] P. West, 2006, www.AFMUniversity.org
3. M. Shiota, *In situ EC-AFM observation of antimony effect for lead dioxide electrode*, *Journal of Power sources*, volume 113, 2003, pages 277 - 280

Temperature changes in lead acid battery during pulse charging

P. Krivík

Department of Electrotechnology, Faculty of Electrical Engineering and Communication, Brno University of Technology, Technická 10, 616 00 Brno, Czech Republic

Abstract

This paper explores temperature changes of lead acid battery cell during discharging and pulse charging. It is studied the effect of different settings of pulse charging regime on the cycle life and on increase of cell temperature during pulse charging. Appropriate adjustment of charging current and both charging and standing intervals during pulse charging has a significant impact not only on the cycle life but also on the size of the temperature changes of lead-acid battery [1] [2]. At the same time sufficient standing time of pulse charging is necessary not only to allow balancing the concentration of ions in the electrolyte by relatively slow diffusion processes and thus reduce the polarization resistance of the cell, but also allows greater equalization of the temperature of the cell and the temperature of surroundings with all cooling processes - radiation, convection and conduction, that prevails in the cooling process.

Experiment

For the experiment investigating the temperature changes in the lead acid battery during the pulse charging were manufactured the test cells with a capacity of about 0.8 Ah. Cells were composed of one positive and one negative electrode separated by a separator made of glass fibers of 1 mm thick, cast by the electrolyte containing water solution of sulphuric acid with a concentration of 1.24 g/cm³, inserted into a container made of PVC. It was placed in the water bath due to thermal stabilization. Temperature sensor PT100 was inserted from the inner side of the positive electrode and the mercury sulphate reference electrode was placed to the electrolyte. Another temperature sensor was placed in a water bath for detecting the ambient temperature. After assembly, the cells were initially subjected to 10 formation cycles. One formation cycle included a first charging with constant current of 0.15 A for 4 hours and then 2 hours of standing. After the formation the cells were subjected to conditional cycles, ie charging with constant current of 0.3 A with voltage limitation of 2.45 V, discharge with current of 0.3 A to voltage of 1.6 V. Then, cells were subjected to pulse charging.

Discharge was carried out by constant current of 0.3 A to a final voltage of 1.6 V. Pulse charging of the first cell was composed of two parts - the charging with current of 0.3 A for 8 s and standing of 10 s. It was recorded both voltage and potentials of positive and negative electrodes at the end of the charging period (U_{ch} , E_{ch+} , E_{ch-}) and at the end of the standing interval (U_{st} , E_{st+} , E_{st-}) and voltage during discharge (U_{st}) and differentiation of the cell temperature and ambient temperature (t_{dif}). Charging was finished after delivery of 110 % of the capacity obtained from the previous discharge.

As it is apparent from the dependencies of discharge voltage and electrode potentials in Fig. 1, the limiting electrode is the positive one. On the beginning of the discharge temperature in the cell drops sharply. This relates to the fact that in the first stage of charging the Joule heat is very small because of the low internal resistance and polarization. The cell is cooling from its maximum temperature at the end of charge, where the Joule heat is greatest due to the large polarization resistance. During discharge the internal resistance of the cell starts to increase, especially due to the internal resistance of the limiting positive electrode, which is reflected in an increase in the Joule heat and thus the temperature of the cell from about 50 % of discharge. In the first stage of charging the temperature of the cell falls due to sharp fall of the internal resistance of the positive electrode. The polarization resistance at the beginning of the pulse charging is small. From about 70 % of the delivered charge the temperature in the cell starts to grow to its maximum value at the end of the charge, which is related to the increase of the polarization resistance of the cell. From the potential dependencies it is evident that the increase in polarization resistance is mainly due to the negative electrode, where there is a much sharper change in potential than at the positive one. The resulting difference in cell temperature and ambient temperature is relatively low - around 0.8 °C, which is related to the fact that the cell was surrounded by a water bath with high thermal conductivity and high thermal capacity and therefore there was rather fast levelling of the temperatures of the cell and its surroundings.

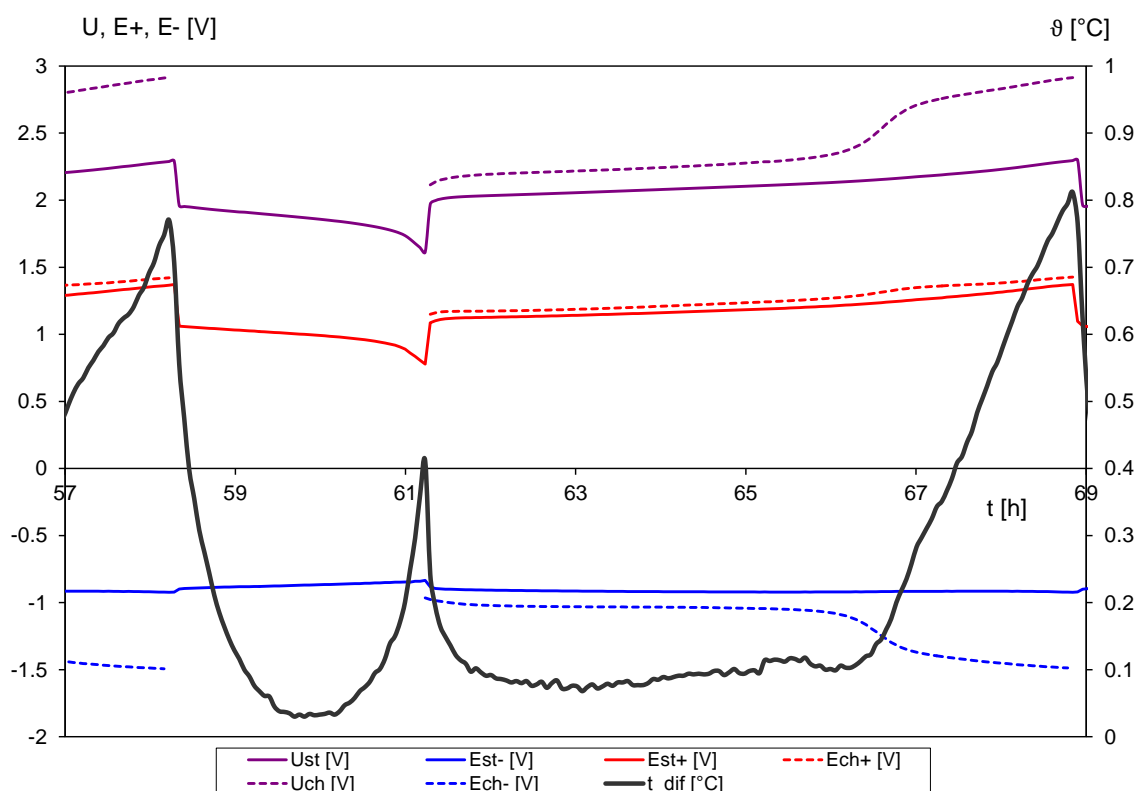


Figure 1. The dependence of temperature, voltage, and potentials for discharging and pulse charging of the first cell.

The second cell was again discharged with a constant current of 0.3 A to a final voltage of 1.6 V. The pulse charging was composed of two parts - a charging with current of 0.2 A for 8 s and standing for 10 s. Resulting temperature, voltage and the potentials dependencies are presented in Fig. 2. It is clear that the limiting electrode is the positive one again. The dependencies of voltage,

potentials and temperature are similar to the first cell. Only the temperature rise at the end of charging is lower - 0.45 °C. This is probably due to the lower charging current and hence the Joule heat during charging. Temperature rise at the end of the charging was by 0.1 °C higher than at the end of discharge, even though the discharge current was higher than charging current and discharging was not interrupted by intervals of standing, as during charging. It is clear that the increase of polarization resistance at the end of charging is much higher than the increase of internal resistance at the end of discharging.

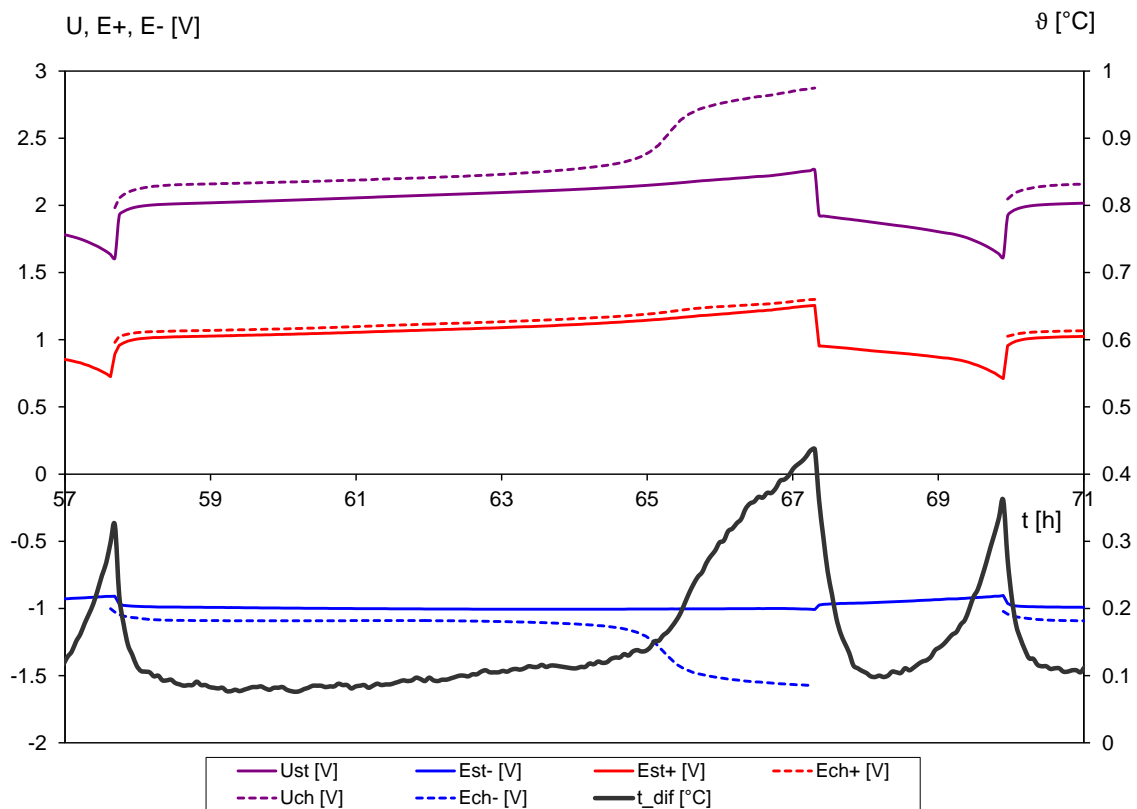


Figure 2. The dependence of temperature, voltage, and potentials for discharging and pulse charging of the second cell.

After finishing of pulse cycling cells were subjected to several conditioning cycles, ie discharging with current of 0.3 A to voltage of 1.6 V and constant current charging with current of 0.3A with voltage limitation of 2.45 V. One such cycle lasted 24 hours. During charging the cell obtained about 110 % of capacity. During this mode were again recorded temperature, voltage, electrode potentials and electric current. The resulting dependencies of the first cell are shown in Fig. 3.

As it is apparent from the dependencies of the discharge voltage and potentials, the limiting electrode is the positive one again. The temperature dependence of the cell differs from the dependence in pulse mode. On the beginning of the discharge the temperature of the cell grows. This is related to the increase in Joule heat during discharge when compared with previous charging, where because of a very small charging current at the end of charging the Joule heat was negligible. In further course of discharging it was a slight decrease in cell temperature from yet unknown causes. From about 50 % of discharging the temperature of the cell starts to increase especially due to the growth of internal resistance of the cell, especially of the limiting positive electrode, which is

reflected in an increase in the Joule heat like at the pulse mode. In the first phase of charging it is again a slight decrease in temperature of the cell due to a sharp decrease of the internal resistance of the positive electrode. This decrease is followed again by increasing of the cell temperature due to the increase of polarization resistance. After reaching the voltage limit, then cell temperature starts to fall again slowly to the ambient temperature in order to reduction of the charging current to the several mA at the end of charging. The resulting temperature difference of the cell and the ambient temperature is relatively low - around 0.8 °C, similar to the first pulse charging of the 1st cell.

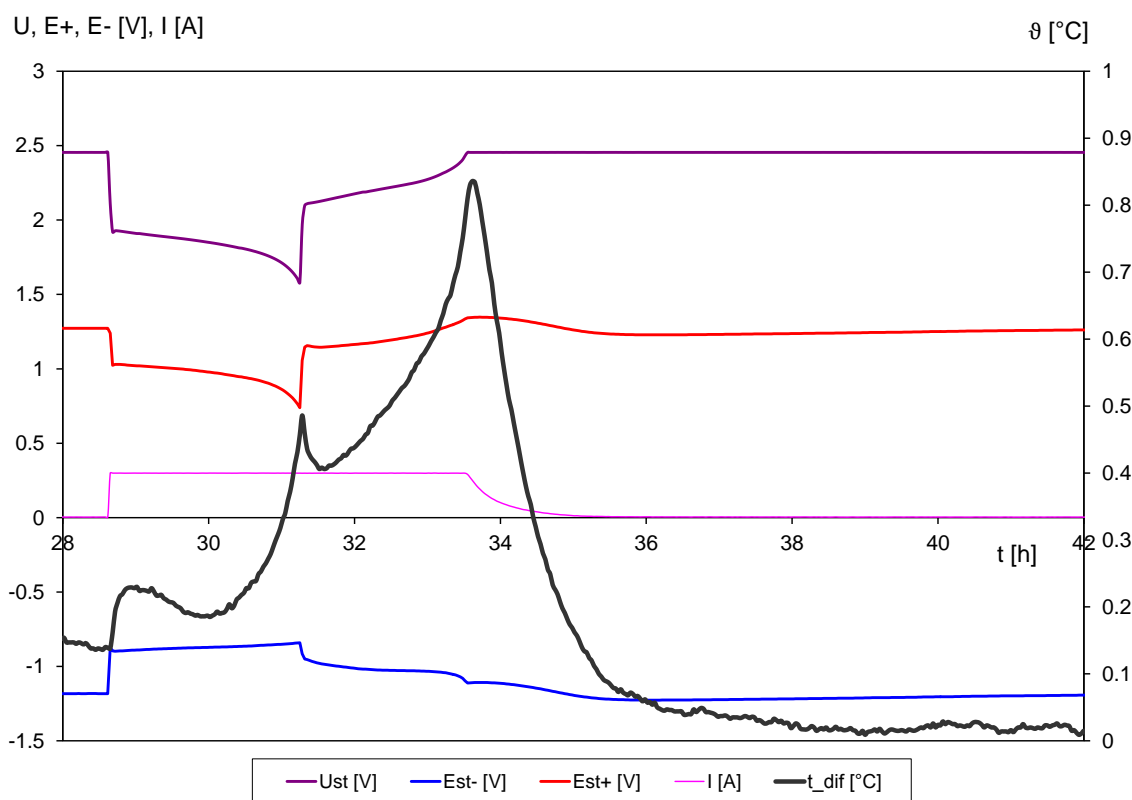


Figure 3. Dependence of temperature, voltage and potentials of the first cell for discharge with current 0.3 A to voltage 1.6 V and constant current charging 0.3A with voltage limitation 2.45 V.

Conclusions

Pulse charging method can, when properly set intervals charging current and a standing lead both to reduce charging times, both to extend the life of lead-acid battery. Moreover, it is also possible to restrict a dangerous rise in temperature inside the cell during charging.

Acknowledgements

This work was supported by the project LO1210 Energy for Sustainable Development Centre for Research and Utilization of Renewable Energy (CVVOZE), by the ‘Support for human resources and transfer of knowledge in conditions of international cooperation of research teams no. CZ.1.07/2.3.00/20.0103’ and by the specific research of the Brno University of Technology No. FEKT-S-14-2293.

References

1. P. Křivík, Heat changes in the lead acid battery cell, proceeding from international conference Advanced Batteries Accumulators and Fuel Cells – 13th ABAF, ISBN 978-80-214-4610-6, 2012, p. 258 – 262
2. P. Křivík, Pulse charging of lead acid batteries, book of abstract from international conference Advanced Batteries Accumulators and Fuel Cells – 14th ABAF, ISBN 978-80-214-4767-7, 2013, p. 121 – 124

Simulation of Current Distribution in Lead Acid Battery Grid Using FEM

P. Vyroubal^a, P.Tošer^a, J.Maxa^a, P.Bača^a, S.Vaculík^a

^aDepartment of Electrotechnology, FEEC, Brno University of Technology, Technická 3058/10, Královo Pole, 61600, Brno, Czech Republic

This article is focused on understanding of the current distribution on lead acid battery grid. To develop this understanding two primary designs of the grid were modeled and then tested. The first design uses the standard lead grid casting part. The second modified design derives benefit from the current collector position which is located in the middle. FEM calculation gave us the comparison between the current densities of both solutions. After the results were evaluated the real experiments started. It can be seen that the FEM could influence an effect of the real tests.

The numerical model description

The numerical model was prepared by using finite element method and it joins electric, magnetic and current fields. The results were solved by means ANSYS APDL system.

The mathematical model is derived from reduced form of Maxwell equations:

$$\begin{aligned} \operatorname{rot} \mathbf{H} &= 0 \\ \operatorname{div} \mathbf{B} &= 0 \\ \operatorname{rot} \mathbf{E} &= 0 \\ \operatorname{div} \mathbf{J} &= 0 \end{aligned} \quad [1]$$

where \mathbf{H} is the vector of magnetic field intensity, \mathbf{B} is the vector of magnetic field induction, \mathbf{E} is the vector of electric field intensity and finally \mathbf{J} is the vector of current density [2], [4], [5].

Current density is expressed by the equation:

$$\mathbf{J} = \gamma(\mathbf{E} + \mathbf{v} \times \mathbf{B}) \quad [2]$$

where γ is conductivity and \mathbf{v} is the velocity of moving ion and \mathbf{B} is outer magnetic field. Between electrodes E_1 and E_2 is the different potential, then the current density \mathbf{J} is created in the area Ω (the area according to the computational domain) and the electric current I_L flows in the ion solution (the equation below) [2], [4], [5].

$$I_L = \int_{S_E} \mathbf{J} \cdot d\mathbf{S} = \int_{S_E} \gamma(\mathbf{E} + \mathbf{v} \times \mathbf{B}) \cdot d\mathbf{S} \quad [3]$$

where S_E is the area of the electrode. The electric field intensity \mathbf{E} is much smaller than the product of $\mathbf{v} \times \mathbf{B}$, than we can neglect it. The force affects the moving charge q and the force \mathbf{F} in the whole area Ω is expressed by:

$$\mathbf{F} = \int_{\Omega} \mathbf{J} \times \mathbf{B} \, dV \quad [4]$$

Types of lead grid design

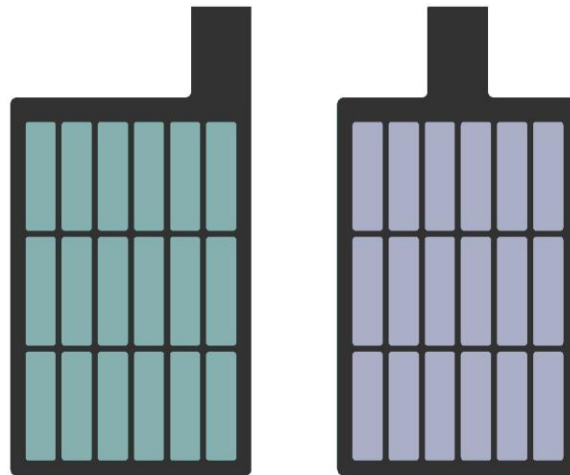


Figure 1. Lead grid design a) typical current collector b) current collector in the middle

The 3D model was created on the basis of real lead acid battery electrodes which were used in 12V / 12 Ah sample. The original dimensions are 60 x 42 x 1 mm according to the casting part. All corners and edges have to be included in 3D because of meshing. The mesh process has a big influence on the final results and it is time dependent on the other hand. The material used as an alloy was define by the datasheets and compared with [1], [3].

The boundary conditions are the most critical point of the analysis. We have to define load, potentials etc. based on the real situation. We can see that the highest current density is located at the area which connects lead grid and current collector. The Joule heat will have the same location as the highest current density. We need to have current density distribution on the entire surface the same but it hold generally in the ideal state.

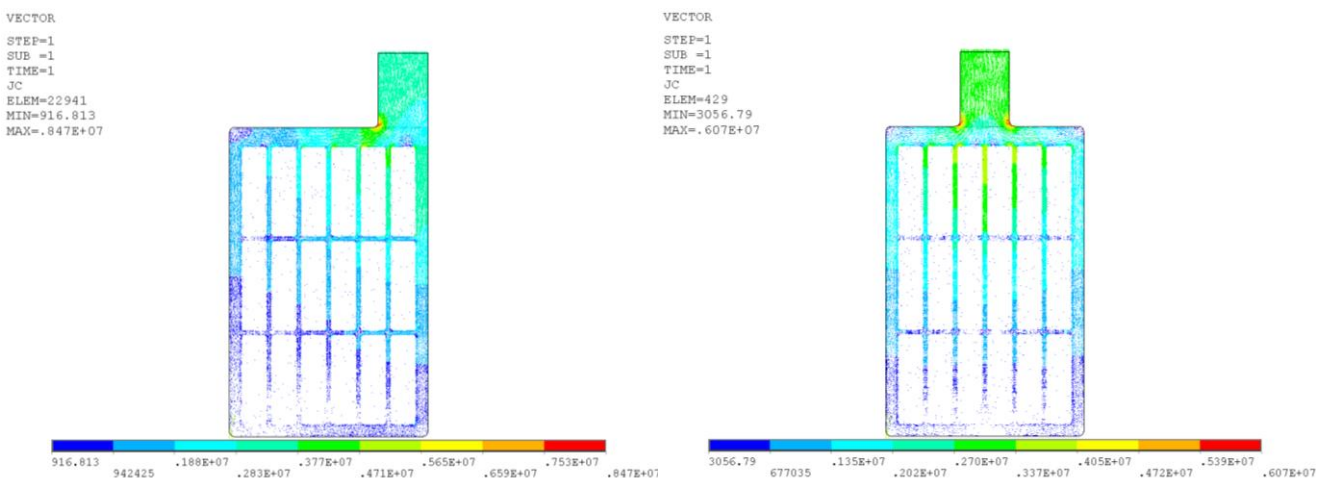


Figure 2. Current density – vector format a) typical current collector b) current collector in the middle

Real samples testing

For the real testing the design with a current collector in the middle was chosen. We have tried to check the capacities of the cells in comparison with a standard grid. We have obtained pretty nice results. The tests are still at the beginning, but now we can see that the modified design works fine. We had to secure the link between the lead grid and current collector because the casting parts were adjusted due to laboratory conditions.

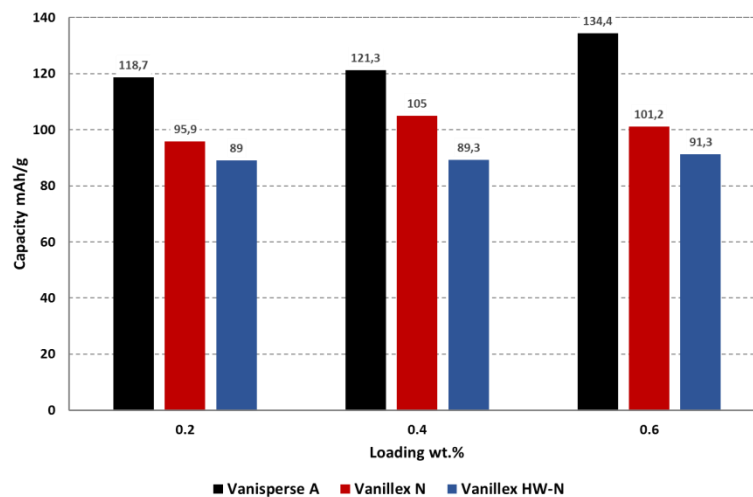


Figure 3. Real samples testing - capacities comparison after 10 DOD cycles

Conclusion

Due to a complex geometry of the lead grids, the finite element method is the best solution. We saw that a higher current density can lead to a raised local temperature from resistance heating. Several models suggest that the cycle life of the positive plates depends on the variations in current density on the lead grid surface and then the destructive processes can influence the active mass during operation. The preliminary real tests shown the stable experimental cells under several testing methods.

Acknowledgments

This work was supported by the specific graduate research of the Brno University of Technology FEKT-S-14-2293 and Centre for Research and Utilization of Renewable Energy under project No. LO1210 – ‘Energy for Sustainable Development (EN-PUR)’.

References

1. P. Bača, K. Micka, P. Křivík, K. Tonar, P. Tošer, J. Power Sources **196** (2011) 3988.
2. E. Kadlecova, I. Behunek, P. Fiala, PIERS ONLINE, vol. 2, No.6, (2006)
3. R. J. Ball, R. Evans, R. Stevens, J. Power Sources **103** (2002) 213-222.
4. Ansys User's Manual, Svanson Analysys System, Inc., Huston, USA, 2003.
5. Electromagnetic Theory, Julius Adams Stratton, ISBN: 978-0-470-13153-4, 640 pages, February 2007, Wiley-IEEE Press

Pulse Deposition of Zinc in Alkaline Electrolytes for Ni-Zn Secondary Batteries

L. Chladil^{1,2}, P. Čudek^{1,2}, V. Novák¹

¹ Institute of Electrotechnology, Brno University of Technology, Faculty of Electrical Engineering and Communication, BUT, Technická 10, 616 00 Brno, Czech Republic

² Centre for Research and Utilization of Renewable Energy, Faculty of Electrical Engineering and Communication, BUT, Technická 10, 616 00 Brno, Czech Republic

Abstract

Electrochemical deposition of Zn under DC and various frequency of pulse deposition modes was studied in pure 6 M KOH electrolyte saturated by zinc oxide. Current density was set up to the level of mossy deposit creation under DC condition. Morphology of deposit was visualized by scanning electron microscopy and the corrosion properties of the deposited layers examined by discharging/dissolution of the deposit after different open circuit voltage waiting times. The results show that the pulse deposition essentially influences the morphology of deposit along wide range of pulse frequencies 0.5-500 Hz.

Introduction

Ni-Zn alkaline accumulators have the big advantages in comparison with Ni-Cd or Ni-MH thanks to their high energy density, higher output voltage and thanks to beneficial ecological aspect. One of the biggest and still actual problems, which limit the battery life, is the dendritic or mossy porous layer growth (1-3), which proceeds during electro-deposition of dissolved zinc ions on the negative electrode (4). For this reason this article examines the influence of charging/deposition mode on the resulting morphology of zinc dendrites over the wide range of deposition frequencies. Depositions were performed in the mostly used 6 M KOH saturated by zinc oxide. Deposited layers were evaluated from their morphology point of view and also the corrosion parameters were measured.

Experimental

The working electrode was made from tin sheet. The active area 5 x 20 mm was defined by silicone sealant and shrink tube. Before start of measuring the whole electrode was submerged into 0.1 M HCl with 0.1 M H₂O₂ which ensured the reproducible rough surface (Fig. 1). As a reference electrode was used Hg/HgO electrode and a platinum black sheet (1 cm²) was used as the counter electrode. As the deposition electrolyte was used 6 M KOH with 37.2 g/l ZnO, which corresponds to the saturation state.

Deposition of Zn layers was carried out by galvanostatic pulses with various frequencies 500 Hz, 50 Hz, 5 Hz, 0.5 Hz and DC deposition mode was also performed. The time parameter of deposition was 1 h for all electrodes. Galvanostatic deposition current density at DC mode and also the mean value of current density at pulse deposition mode in 6 M KOH was set to 10 mA/cm²,

which is still in the region when the mossy porous deposit layer without any spiked dendrites is growing. The duty cycle of pulses was 0.5 for all electrodes.

Results and discussion

Morphology of all electrode surfaces deposited at selected deposition modes with different pulse frequencies are shown in Figure 1. Highly porous mossy clumps with uneven distribution grew at DC deposition regime. At transition to the pulse mode, the layer like structure was observed already at 0.5 Hz deposition. This is caused by increased deposition potential which is need for the two-dimensional nucleation and which has the origin in increased deposition current at pulse deposition mode. Layer like structure is characterized by the epitaxial growth which tends to copy the surface crystal orientation [5]. Further increase in deposition frequency leads to large-sized anisotropically oriented crystals. This layer is called a Boulder type and its presence is typical for moderate current density at DC deposition mode. The third type of layer is observed under transition to 500 Hz deposition frequency. This compact deposit is similar to the layer like, but no edges of the layer are observed. The orientation of the crystals is not influenced by the underlying materials as was observed in the case of layer like deposit. This suggests, that this layer consists of small boulders with a tight arrangements.

The corrosion measurements were performed and the results can be seen in Table 1. The measurements were performed by discharging of deposited layer after different times at (OCV) rest (15 min and 300 min). Discharging consists of two steps, galvanostatic discharging was followed by chronoamperometric measurement at -1.2 V. Average corrosion rate during the first 4.75 hour, was calculated from the standing time and charge change and is related to theoretical capacity 20 mAh. The corrosion current was calculated from the same values. The values $Q_{15\text{min}}$ are proportional to efficiency of deposition at these low corrosion rates. In each case the deposition efficiency is greater than 98% and in case of 1 Hz deposition it is more than 99.1%. At higher deposition frequencies above 50 Hz the efficiency is decreased with $\log f$.

TABLE I. Corrosion parameters of electrodes deposited in 6 M KOH saturated by ZnO. $Q_{15\text{min}}$ = discharge capacity after 15 minutes OCV rest, $Q_{300\text{min}}$ = discharge capacity after 300 minutes OCV rest.

Deposition frequency	0 Hz	0.5 Hz	5 Hz	50 Hz	500 Hz
$Q_{15\text{min}}$ [mA·h]	19.62	19.82	19.81	19.75	19.66
$Q_{300\text{min}}$ [mA·h]	17.60	19.30	19.37	19.45	19.45
Average corrosion rate [%/h]	2.16	0.54	0.48	0.32	0.23
Average corrosion current i_o [μ A]	424	107	94.3	64.0	45.7

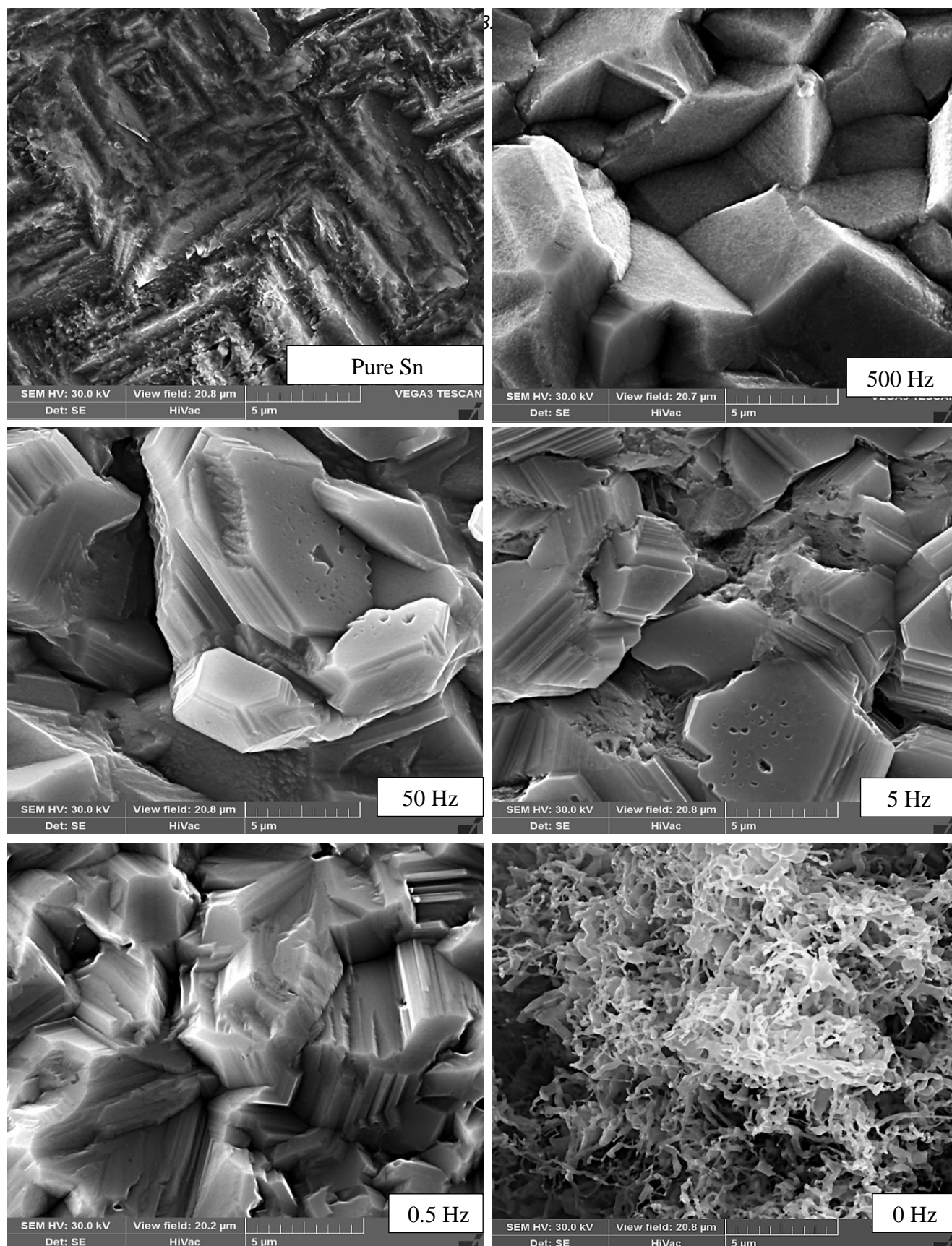


Figure 1. Morphology of the zinc layer in relation to different frequencies of deposition pulses in the 6 M KOH solution saturated by zinc oxide

Conclusions

Influence of different pulse deposition frequencies on the morphology of Zn deposit was investigated. In case of the pure 6 M KOH saturated by zinc oxide, transition from the mossy deposit to layer like and boulder was observed at transition from DC to 0.5 Hz and 5 Hz. Further deposition frequency increase resulted in the smaller particles with tight arrangements. Usage of the pulse deposition mode brings the increase of current efficiency of deposition. In case of the pulse mode deposition, current efficiency slowly decreases with increase of deposition frequency. Also significant reduction of corrosion parameters was observed after transition to the pulse mode deposition and also with deposition frequency increase. This decrease of corrosion has an origin in the changing morphology of deposit, which tends to create more compact structures with reduced surface area.

Acknowledgement

This work was supported by the grant FEKT-S-14-2293 "Materiály a technologie pro elektrotechniku II", and project CZ.1.07/2.3.00/20.0103 „Support for human resources and transfer of knowledge in conditions of international cooperation of research teams“.

References

1. J. Jindra, *J. Power Sources.*, **37**, (1992)
2. J. Jindra, *J. Power Sources*, **66**, . 15-25, (1997).
3. J. Jindra, *J. Power Sources*, **88**, 202-205 (2000)..
4. R. D. Armstrong, M. F. Bell, in *Electrochemistry*, **4** 1-17 (1974).
5. R. Y. Wang, D. W. Kirk, G. X. Yhang, *J. Electrochem. Soc.*, **153**, (5) (2006).

Improvement of Cyclability of Ni(OH)₂ in the Presence of Zincate Ions

L. Chladil^{1,2}, V. Novák¹

¹ Institute of Electrotechnology, Brno University of Technology, Faculty of Electrical Engineering and Communication, BUT, Technická 10, 616 00 Brno, Czech Republic

² Centre for Research and Utilization of Renewable Energy, Faculty of Electrical Engineering and Communication, BUT, Technická 10, 616 00 Brno, Czech Republic

Abstract

The influence of addition of cobalt into the nickel oxide electrodes (NOE) on their stability and electrochemical performance was investigated. The article deals with the evaluation of the two options of NOE stabilization by cobalt addition. An electrode containing the cobalt in the whole volume of active material as well as an electrode which has active material covered by Co(OH)₂ were prepared and measured. The different process of cobalt addition leads to the different electrode behavior. Whereas the first cobalt addition leads to the stable discharging capacities accompanied with negligible mass changes during cycling, the second one leads to the gradual increase of discharge electrode capacity. This capacity increase is accompanied with significant increase of electrode weight.

Introduction

During the last two decades many research groups were focused on the influence of the zincate on the electrochemical properties and cyclability of nickel oxide electrodes (NOE) (1,2). It was also shown that zincate incorporates into the NOE during cycling and suppresses the volume expansion of active material by reducing the overcharging and associated transformation of inner structure from $\beta \rightarrow \gamma$ phase (3). On the other hand, it was also shown, that the discharging capacity of NOE is not fully stable in the pure form of Ni(OH)₂ and some additives as Co into the active material or LiOH into the electrolyte is desirable (4). Some electrolytes with reduced zinc solubility (5) can not to be used in combination with LiOH because this addition may lead to creation of insoluble compounds such as LiF or Li₃PO₄. This implies that the complete stabilization of NOE by cobalt addition must be achieved in these types of electrolytes. For this reason this article is focused on the study of Ni(OH)₂ stability in the presence of zincate and also on the stabilization addition of the cobalt. The positive electrode material was prepared by electro-deposition precipitation reaction from nickel and cobalt nitrate. We consider the two option of cobalt addition. In the case of the first electrode, the cobalt was incorporate into to the whole volume of Ni(OH)₂ by its addition into the deposition electrolyte. In the case of the second electrode, the thin covered layer of Co(OH)₂ was deposited on the surface of Ni(OH)₂. The stability of all electrodes was investigated by cyclic voltammetry measurements.

Experimental

All the measurements were performed on the EQCM (electrochemical quartz crystal microbalance) in the three-electrode set up. As electrolyte, 3 M KOH saturated by zinc oxide was used. The three types of positive material were electrochemically deposited from the nickel and cobalt nitrate solution. The first electrode was deposited from the pure 0.1 M Ni(NO₃)₂ solution under galvanostatic condition. Thus prepared active material contain only the Ni(OH)₂ active material. The second electrode was prepared from mixture 0.095 M Ni(NO₃)₂ and 0.005 M Co(NO₃)₂. Resultant active material contains 10 % of Co and active material can be written as Ni_{0.9}Co_{0.1}(OH)₂. The third electrode was prepared by two-stage electrodeposition. The first deposition was performed in 0.1 M Ni(NO₃)₂ and second one from 0.1 M Co(NO₃)₂. The first stage of deposition was stopped after precipitation of 24 μg of material and second stage after 2.4 μg. Thus prepared electrodes contain 10 % of Co(OH)₂ coating and are marked as Ni(OH)₂ + SK. All the depositions were performed under galvanostatic condition $I_{\text{dep}} = 0.5$ mA. Before the start of the measurement or between each deposition step the electrode was rinsed by distilled water for at least 2 minutes. All measurements were performed under N₂ protective atmosphere to exclude the possibility of electrolyte carbonation.

Results and discussion

Fig. 1 presents the discharging capacities, mass changes and exchange molecular weight of the pure Ni(OH)₂ and Ni_{0.9}Co_{0.1}(OH)₂, which was doped by 10 % of cobalt at preparation and Ni(OH)₂ coated by 10 % of Co(OH)₂. The discharge capacities of the pure Ni(OH)₂ contains the two directions of decline. The first drop can be seen from 5 to 25 cycle and is accompanied by high decrease of exchange molecular weight to a maximum value -52. Second one is observed with simultaneous decrease of electrode mass. The maximum value of exchange molecular weight M_w suggest that exchange of some heavy ions with M_w higher than 52 has occurred between electrode and electrolyte during oxidation and reduction reactions. In regard to the facts that this behavior is not observed in electrolyte without zincate, and that the molecular weight of zinc (65.4) is close to the measured value, we can ascribe this behavior to the intercalation/adsorption of zincate ions in the active material. The negative value of the exchange molecular weight indicates that zincate is detained in discharge state, whereas release/deintercalation is observed during oxidation reaction. This behavior is in opposite direction to the intercalation of hydrated positive ions of the base electrolyte (K⁺, Na⁺ and Li⁺) which occurs at cycling of α-phase Ni(OH)₂. After reaching the minimum value of M_w , mass of the whole electrode Δm decreased to the -28 μg during following 30 cycles. This indicates complete loss of the active materials, which gradually fell down from the working electrode.

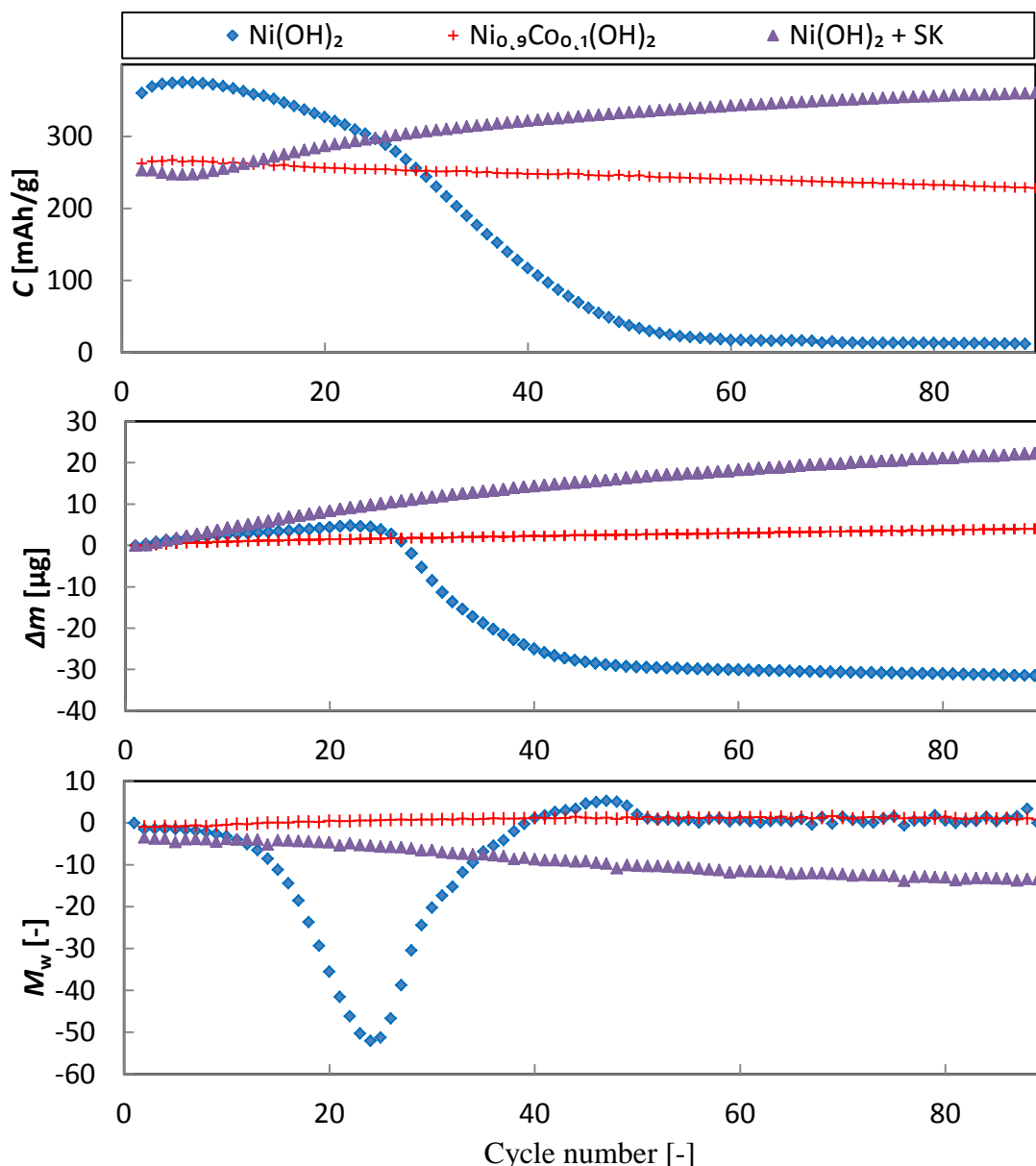


Figure 1. Discharge capacities – A, mass changes of measured electrodes - B and exchange molecular weight – C for the pure Ni(OH)_2 , $\text{Ni}_{0.9}\text{Co}_{0.1}(\text{OH})_2$ and Ni(OH)_2 coated by 10 % of Co(OH)_2 . Measured in 3 M KOH saturated by zinc oxide.

Behavior of $\text{Ni}_{0.9}\text{Co}_{0.1}(\text{OH})_2$ which contain the 10 % of cobalt in the structure shows the complete stabilization of the active material. Discharge capacities linearly decrease from initial 267 mAh/g to final 228 mAh/g. The exchange molecular weight slowly increased from -1 to 1, which indicated partial transformation the phase from $\alpha \rightarrow \beta$ system. The stable values of parameter M_w pointed to the good long-term material stability.

Nickel hydroxide coated with 10 % of cobalt hydroxide behaves differently from $\text{Ni}_{0.9}\text{Co}_{0.1}(\text{OH})_2$. Whereas the discharge capacity of $\text{Ni}_{0.9}\text{Co}_{0.1}(\text{OH})_2$ has the downward trend, the active material with cobalt hydroxide coating shows a gradual increase of discharge capacity to 359 mAh/g. This value can be typically achieved thanks to partial transition of β -phase to α -phase but no increase of weight during oxidation is observed in the massogram. Moreover the discharge capacity increase is accompanied with significant increase of active material weight. This increase of mass cannot be caused only by incorporation of zincate ions into the interlayer sites of active

material, because the value of weight increase is too high. Any other mechanism as the precipitation of ZnO or Zn(OH)₂ on the electrode surface can be expected. The exchange molecular weight is not stable as in the case of Ni_{0.9}Co_{0.1}(OH)₂ and shows the similar behavior as the electrode without cobalt addition but the decrease of M_w is less pronounced.

Conclusions

The electrochemical behavior of pure nickel hydroxide electrode and two nickel hydroxide electrodes stabilized by cobalt was investigated. From the stability point of view, It can be concluded that the replacement of nickel atom by cobalt in whole volume of electrode lead to stable cycling with gradual decrease of exchange capacity while the coating of Ni(OH)₂ by Co(OH)₂ lead to increase of discharge capacity during cycling but without any evidence of presence of α or γ -phase. The increase of discharging capacity proceeded with significant increase of electrode weight. This can be partially in relation of incorporation of zincate into the active material but also the other mechanism like the precipitation of ZnO or Zn(OH)₂ on the electrode surface can be expected. An XRD analysis must be performed for determining the nature of capacity increase.

Acknowledgement

This work was supported by the grant FEKT-S-14-2293 "Materiály a technologie pro elektrotechniku II", and project CZ.1.07/2.3.00/20.0103 "Support for human resources and transfer of knowledge in conditions of international cooperation of research teams".

References

1. J. Jindra, J. Power Sources, 66, 15-25 (1997).
2. J. Jindra, J. Power Sources, 88, (2000).
3. C. Tessier, C. Faure, L. Guerlou-Demourgues, C. Denage, G. Nabias and C. Delmas, J. electrochem. Soc., 149, (9) (2002).
4. J. Cheng, Y.-H. Wen, G.-P. Cao and Y.-S. Yang, J. Power Sources., 196, 1589-1592, (2011).
5. R. F. Thornton, E.J. Carlson, J. Electrochem. Soc., 127, (1980).

Optimization of electrospraying for preparation of supercapacitive MnO₂-based electrode

R. Fojtíková^a, P. Mazúr^b, J. Pociďič^b, J. Maršálek^a and J. Kosek^a

^a Department of Chemical Engineering, Institute of Chemical Technology Prague, Technická 5, 166 28 Praha 6, Czech Republic

^b New Technologies – Research Center, University of West Bohemia, Univerzitní 8, 306 14 Plzeň, Czech Republic

The electric double-layer capacitors, also referred to as supercapacitors, pose the attractive combination of fast energy storage/release (specific power > 10³ W/kg) and extended capacitance (up to hundreds of F/g of electrode material). Due to this supercapacitors are widely applied in various systems, e.g., for the recuperation of braking energy and delivery of starting energy for electric vehicles.

In our contribution porous manganese oxide electrodes for supercapacitors were prepared by electrospraying of aqueous Mn-based precursor solution. For that purpose we developed the electrospraying device. The choice of Mn was motivated by low costs, low environmental impact and pseudo-capacitive behavior. The latter property enables the further extension of the specific capacitance by the contribution of faradaic processes taking place on the electrode-electrolyte interface or in the surface layer of the electrode¹.

The electrospraying provided us with the direct and homogeneous deposition manganese oxide particles of uniform size in the range of 10-100 nm. Within the study, the electrospraying procedure was optimized with respect to the composition of precursor solution and its flow-rate, operating voltage of electrospray, inter-electrode distance and amount of deposited matter. The modification of the deposited layer by cyclic voltammetry resulted in the substantial capacitance growth due to enlarged electrode-electrolyte interface. Subsequently, the optimized electrode was characterized in lab-scale supercapacitor.

Reference

1. Conway, B.E., V. Birss, and J. Wojtowicz, The role and utilization of pseudocapacitance for energy storage by supercapacitors. *Journal of Power Sources* 1997, 66 (1–2), p. 1-14.

The changes of surface texture parameters of the duplex systems: nitrided layer – coating at CoCrMo alloy

D. Dobrocký^a, O. Klanica^a, F. Onderka^a, J. Kadlec

^a Department of Mechanical Engineering, University of Defence in Brno, Kounicova 65, 602 00 Brno, Czech Republic

CoCrMo alloys have been used for biomedical implants for a number of years. One of the important parameters which influences durability of the coating and thus whole implant are parameters of surface texture, namely Ra and Rt, which are determined by standards ISO 7206-2:2011 and ISO 7207-2:2011. Three duplex surface systems were applied to improve mechanical properties. The combination of plasma nitriding and subsequent deposited thin films of the nACo³®, DLC and ZrN were used as a duplex treatment. Plasma nitriding was implemented under these conditions: duration time 10 hours, the ratio of gases H₂:N₂=3:1, process temperature 450 °C, 500 °C and 550 °C. The surface texture parameters were measured on the polished surface of the CoCrMo alloy at first, then on the polished surface after plasma nitridation process and finally on the polished surface of deposited coating. It has been demonstrated that deposition of the selected coatings on the nitride surface influences the surface texture parameters Ra and Rt.

Introduction

CoCrMo alloys are frequently used for the metal-on-metal hip resurfacing due to their high corrosion and wear performance. Thermal treatments are used on these alloys in attempt to alter the microstructure to improve the mechanical properties. However, the effect that this then has on the mechanical properties is in many cases insufficient especially in terms of wear resistance and low hardness. For this reason, the biocompatible coatings on CoCrMo alloys are used (1, 2). The duplex surface system was applied to improve surface and subsurface properties. The combination of plasma nitriding and subsequent depositing thin films of the nACo³®, DLC and ZrN were used as a duplex treatment. Plasma nitriding is universal chemical-heat treatment process which was used for creation of hard layer on CoCrMo alloy which serves as an underlayer for coatings. These duplex systems have very high hardness and good corrosion resistance. High hardness, chemical inertness and excellent tribological properties of nanocomposite coating of titanium aluminium nitride matrix of silicon nitride (nACo³®), amorphous carbon coatings often called like diamond-like carbon (DLC) coating and zirconium nitride (ZrN) coating are of great interest for technological applications (2, 3, 4). The surface texture has a decisive effect on the properties and behaviour of spare biomedical implants during their using (e. g. wearing, fatigue properties, connection strength and dynamic binding of surfaces, etc.). In case of coatings creation on implants, they may improve their properties using a duplex system nitriding – coating. Selected surface texture parameters Ra – arithmetical mean deviation of the assessed profile (µm), Rt – total height of the assessed profile (µm), according to (5), quantify the state of the surface before nitriding, after nitriding and after the deposition of coatings. Surface texture parameters Ra, Rt must be lower than Ra = 0.05 µm, Rt = 1 µm for the femoral component of the hip joint with using a wavelength 0.08 mm (6). Surface texture parameters Ra, Rt must be lower than Ra = 0.1 µm for the femoral component of the knee joint (7). The finishing treatment of inarticulating areas of metal components

of knee joints that may come into contact with soft tissues must be smooth and non-abrasive. The value of surface roughness $R_a = 1.5 \mu\text{m}$ is considered sufficient (8).

Experimental material and methods

For the preparation of the specimens were chosen cast CoCrMo alloy rollers of labeled B1, B1.2, B1.3 and M1, M1.2, M1.3. A series of specimens B and M differ by method of casting. Analysis of the chemical composition of the surface of the substrate of alloy CoCrMo (ISO 5832-4) was performed on a Noran EDS System SIX/300 and it is listed in Table I.

TABLE I. Chemical composition of CoCrMo alloy

Element	Chemical composition wt (%)						
	Cr	Mo	Fe	Si	P	Ti	Co
Specimen B1	31.46	5.81	-	2.5	-	-	60.23
Specimen M1	30.22	4.81	-	1.47	-	-	63.50

The preparation of specimens consists of several consecutive steps. Each specimen was manually wet fine grained using by six grained papers from company HERMES with decreasing grain size of abrasives 120, 240, 500, 1000, 2500 and 4000. After grinding, the specimens were polished with diamond polishing paste (type POM L) with granularity $1 \mu\text{m}$. Subsequently, the experimental specimens were plasma nitride according to the parameters listed in Table II.

TABLE II. Parameters of plasma nitriding process

Specimen	B1.3, M1.3	B1.2, M1.2	B1, M1
Parameter	Plasma nitriding		
Temperature (°C)	450	500	550
Time/Duration (h)	10	10	10
Flow H ₂ (l/min)	24	24	24
Flow N ₂ (l/min)	8	8	8

Then plasma nitriding specimens were polished, cleaned and degreased. PVD coatings according to Table III, were deposited on surfaces thus prepared specimens. Selected surface texture parameters R_a , R_t were measured on the surface of the polished substrate CoCrMo alloy, polished nitride surface and subsequently on the deposited coatings. It was measured on five selected places for qualitative evaluation of the surface. The measurement was carried out by Talysurf CLI profilometer with diamond stylus and inductive gauge. Subsequently surfaces were evaluated by software TalyMap.

TABLE III. The overview of the used coatings

Specimen	Deposited coating
B1	M1 nACo ³ ®
B1.2	M1.2 DLC
B1.3	M1.3 ZrN

Results and discussion

The results of the measured Ra parameter. The default values of the parameter Ra substrates of experimental specimens B1 – B1.3 did not differ significantly from each other. After application of plasma nitriding and subsequent polishing, the parameter Ra increased for all three cases of plasma nitriding. This phenomenon represents the increase of surface caused by the absorption (condensation) of nitrides during the process of plasma nitriding and simultaneously at its formation has the proportion even increase in the volume of material due to diffusion of nitrogen during nitriding process, as it is mentioned by other authors (9, 10). Subsequently, in two cases B1 and B1.3 occurred after the deposition of the coating (B1 – nACo³®, B1.3 – ZrN) to increase the values of the parameter Ra.

In case of the experimental specimen B1.2 was detected the lowest surface roughness. The final value of Ra for sample B1.2, after deposition of DLC coating, was $0.039 \pm 0.004 \mu\text{m}$. The highest value of Ra parameter reached a sample B1.3 namely $0.054 \pm 0.006 \mu\text{m}$.

In case of experimental specimens M1, M1.2 and M1.3, the lowest final value of the parameter Ra reached specimen M1, after the deposition of the coating (coating nACo³®). In this case, the parameter Ra reached $0.042 \pm 0.014 \mu\text{m}$. Conversely, the highest value was measured on a specimen of M1.3 (ZrN coating) whose surface roughness reached $0.052 \pm 0.004 \mu\text{m}$.

The results of the measured Rt parameter. Another evaluation parameter, which is binding by standard (5), is the parameter Rt. As well as at the parameter Ra, also in case of parameter Rt occurred to increase of its values after plasma nitriding and subsequent polishing. The lowest value of parameter Rt was measured for a specimen B1.2 (DLC coating). Parameter Rt reached value of $0.039 \pm 0.004 \mu\text{m}$. The highest values of the parameter Rt was achieved for specimen B1.3 (ZrN coating).

In the case of sets of specimens M1 – M1.3 occurred in two cases to a decrease parameter Rt after plasma nitriding and subsequent polishing. The final value of the parameter Rt was the lowest for the specimen M1 (coating nACo³®) and it reached a value of $0.841 \pm 0.105 \mu\text{m}$. The parameter Rt had the highest value for a specimen M1.3.

Conclusion

The measured results point out that duplex system nitriding layer - coating which effect final values of the parameters surface textures. Analysis of changing parameters Ra, Rt of the surface texture was carried out depending on the different temperatures of the nitriding process and different type of the coating (DLC, ZrN, nACo³®). Maximum standardized values of the parameters Ra and Rt for the production of the femoral component of the hip and knee joint are shown in ISO 7206-2, ISO 7207-2. After the experiments it can be stated that the maximum values given by standards are not exceeding. However, in some cases, some values move closer to the maximum permissible value. From the analysis it can be stated that the duplex surface nitrided layer (500 ° C) - DLC coating (sample B1.2) showed the lowest values of parameters $Ra=0,039\pm0,004 \mu\text{m}$ and $Rt=0,719\pm0,101 \mu\text{m}$. The best results showed duplex system nitrided layer (550°C) - nACo³ coating in terms of the different way of the casting specimens M1 - M1.3. The lower values of the parameters surface textures are associated with less wear and, together with the properties of the surface layer are critical factors for their durability and service life.

Acknowledgments

The work presented in this paper has been supported by the specific research project 2014 at the Department of Mechanical Engineering, University of Defence in Brno.

References

1. G. Bellefontaine, *The corrosion of CoCrMo alloys for biomedical applications*, p. 3, University of Birmingham (2010).
2. Z. Joska at al., *Testing of DLC Coating on Plasma Nitrided Austenitic Stainless Steel*, in 14th ABAF: Advanced Batteries, Accumulators and Fuel Cells. Brno, 2013, s. 99-100, ISBN 978-80-214-4767-7.
3. M, Jelinek at al., *Laser Physics*. **13**, 10 (2003).
4. M, Jelinek at al., *Laser Physics*. **15**, 2 (2005).
5. ČSN EN ISO 4287. Geometrické požadavky na výrobky (GPS) – Struktura povrchu: Profilová metoda – Termíny, definice a parametry struktury povrchu (1999).
6. ISO 7206-2. Implants for surgery – Partial and total hip joint prostheses – Part 2: Articulating surfaces made of metallic, ceramic and plastics materials (2011).
7. ISO 7207-2. Implants for surgery – Components for partial and total knee joint prostheses – Part 2: Articulating surfaces made of metallic, ceramic and plastics materials (2011).
8. M. Novotný, ČSN EN ISO 21536, Neaktivní chirurgické implantáty – Implantáty pro náhradu kloubů – Specifické požadavky na implantáty pro náhradu kolenních kloubů, (2009).
9. V. Hrubý and A. Holemář, *Iontová nitridace v praxi*, SNTL Praha, ISBN 80-0300001-7 (1989)
10. D. Pye, *Practical nitriding and ferritic nitrocarburizing*, USA, ISBN 0-87170-791-8 (2003)

The Effect of Electrodeposited PANI on Corrosion Behavior of 316 Stainless Steel Coated by CVD Grown MWCNTs under PEMFC Bipolar Plate Working Condition

M. Hashempour ^{a,b}, A. Vicenzo ^a, M. Bestetti ^a, S. Sharma ^b, D. Gonzalez ^b

^a Dipartimento di Chimica, Materiali e Ingegneria Chimica "Giulio Natta", Politecnico di Milano, Via L. Mancinelli 7, 20131, Milan, Italy

^b Centre for Hydrogen and Fuel Cell Research, School of Chemical Engineering, University of Birmingham, Edgbaston, Birmingham, B15 2TT, UK

Polyaniline (PANI) electrodeposition on bare and carbon nanotube (CNT) coated 316 SS was carried out using a cyclic voltammetry electropolymerization method in diluted H₂SO₄ media containing aniline monomer. CNTs were grown in a thermal CVD on 316 SS either by direct growth using ethylene precursor or by continuous feeding of an external catalyst, ferrocene, dissolved in toluene as the carbon precursor. Corrosion behavior of the coated materials was assessed by potentiodynamic and potentiostatic methods in an attempt to simulate the working condition of proton exchange membrane fuel cell (PEMFCs) bipolar plates. While a thick PANI coating could not provide a protective barrier to either bare or CNT coated 316 SS samples, a thin PANI layer showed interesting potential to improve the corrosion resistance. However, the deterioration caused by the initial carbon treatment of CNT coated 316 SS, was beyond the protective capacity of PANI to fulfill the anti-corrosive requirements of bipolar plates of PEMFCs.

Introduction

Metallic bipolar plates of fuel cells offer several advantages compared to their traditional graphitic counterparts, including lower size and weight, higher mechanical stability, increased thermal and electrical conductivity and easier and cheaper manufacturing (1,2). However, their corrosion in the fuel cell environment, with release of metal ions to the cell, formation of a passive oxide film and increased contact resistance, are the critical issues that need to be addressed for this type of bipolar plate materials (3). Stainless steel (SS) as a cheap, easy to manufacture and intrinsically corrosion resistant metal has been paid the utmost attention for this application. A variety of surface engineering solutions have been proposed to address the issues of corrosion and passive film formation, which include protective coatings using PVD and sputtering, CVD, plating, cladding and heat treatment. Another category of solutions is relying on organic coatings. It has been developing simultaneously with emphasis on conducting polymers (4). These polymers can be coated on SS and other metals both chemically and electrochemically. However, the major focus has been on electrochemical methods as they are quick and the parameters such as coating thickness and rate of deposition can be controlled easily (5). This work, reports an attempt to combine both strategies by first growing CNTs on SS via a CVD method and then electrochemically coat them with PANI. Previously, it has been shown that the corrosion behavior of SS is negatively affected by the high temperature and carbonaceous atmosphere of the CVD process during CNTs growth (6). Therefore, in this work, the main focus is on the competence of electrodeposited PANI for

recovering the corrosion resistance of CNT coated SS. Moreover, the PANI electropolymerization mechanism is assessed and compared for deposition on bare and CNT coated SS.

Experimental

CNTs were grown on SS by two different methods as described in details in previous works; 1- direct growth by CVD method using ethylene as the carbon source (CNT-ETH) (7) and 2- continuous feeding of ferrocene catalyst dissolved in toluene as the carbon source (CNT-TOL) (8).

PANI electrodeposition was conducted using cyclic voltammetry at room temperature, in the potential window of -50 to $+1400$ mV_{SHE}. A 0.5 M H₂SO₄ + 0.1 M aniline monomer electrolyte was used for PANI electrodeposition on bare SS and a 0.1M H₂SO₄ + 0.1M aniline electrolyte for deposition on CNT coated SS. Corrosion behavior of all samples was studied by potentiodynamic and potentiostatic tests in 0.001 M H₂SO₄ at 80 °C. Potentiodynamic polarization was carried out in the potential window of -400 to $+1400$ mV_{SHE} (-1050 to $+750$ mV_{MSE}) with a scan rate of 1 mVs⁻¹ after 1 h of sample stabilization in the nitrogen purged electrolyte. Potentiostatic test was carried out at 1 V_{SHE} after sample stabilization for 1 h in the air purged electrolyte. Microstructural characterizations of the coatings were carried out by a Jeol 6060 scanning electron microscope (SEM).

Results and Discussion

Fig. 1a shows the voltammogram of PANI electrodeposition on 316 SS during the fourth cycle at 50mV/s. Four peaks are seen as indicated in the figure referring to (assigned by numbers): 1- The start of the aniline monomer oxidation (formation of emeraldine (EM) oligomers), start of coating nucleation, start of SS transpassive region, and water dissociation at 1275 ± 25 mV_{SHE}, 2- Oxidation of leucoemeraldine (LE) to EM at 390 ± 30 mV_{SHE}, 3- Oxidation of EM to pernigraniline (PE) at 990 ± 20 mV_{SHE} and 4- Redox behavior of the reaction intermediates at 685 ± 20 mV_{SHE}. One of the key points of a successful PANI electrodeposition is the right choice of potential window as it is important to include the nucleation potential of the coating (peak 1, 1275 ± 25 mV_{SHE}). Since this happens at a high potential, an extra current related to the transpassive region of SS and also water dissociation is also observed. However, ending up at even 50 mV less, could barely result in reproducible electrodeposition. Continuation of this process up to higher number of cycles results not only in the enlargement of the peaks (9,10), but also in deformation and displacement of the peaks which finally leads to peaks coalescence and formation of wide and non-distinguishable peaks as shown in Fig. 1b. This increased current at higher cycles is a direct indication of the increase in coating thickness. Basically, the thickness of the coating depends mainly on the time in which the sample is kept at appropriate potentials for oxidation of the Aniline. Therefore, lower scan rates can provide quite thick and homogeneous coating in just 2-3 cycles, while at higher scan rates, this can happen at extended number of cycles. Furthermore, by passing a certain thickness, also the morphology of the coating changes from a flat and smooth mode to a fibrous and porous mode (11), as shown in Fig.1 c and d. Both CNT coated samples showed similar features in PANI electrodeposition according to voltammograms

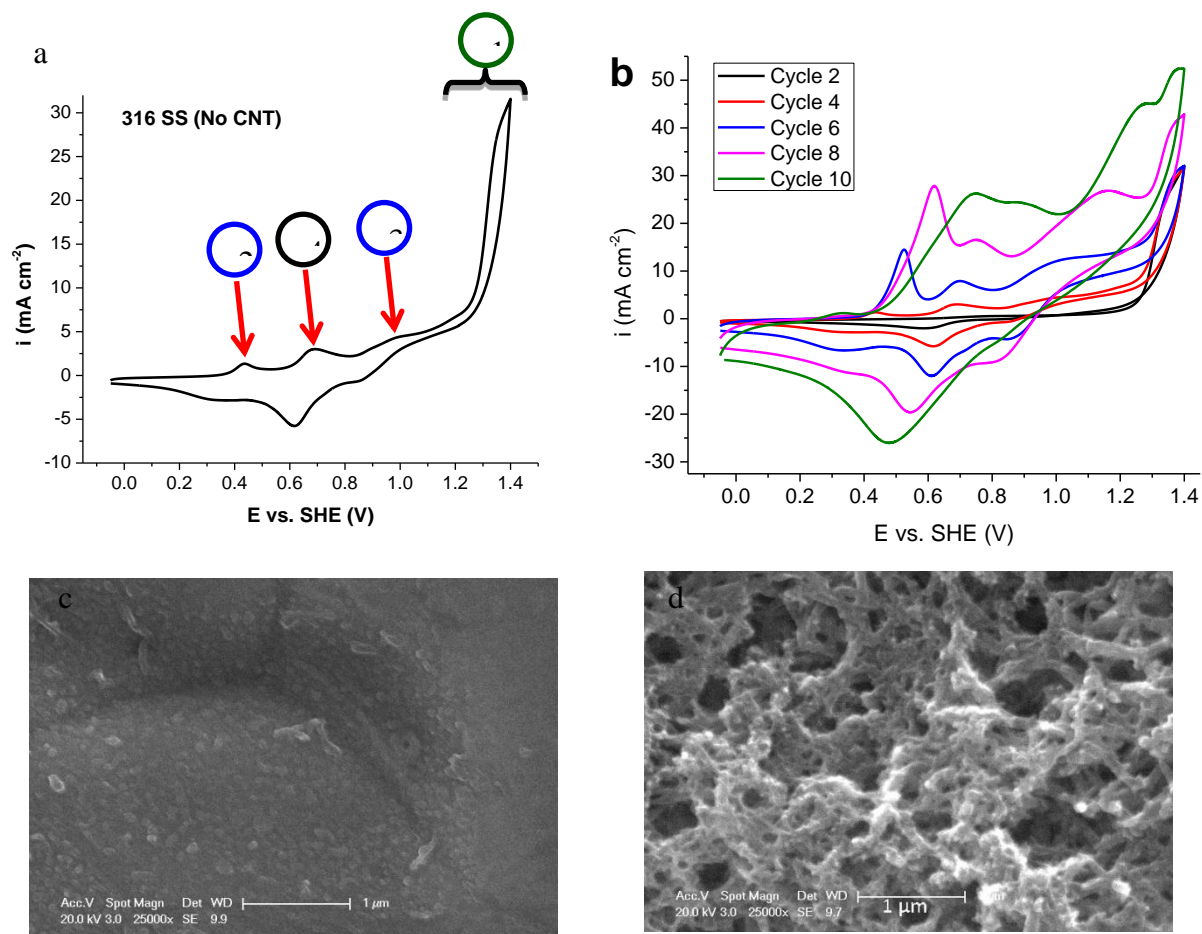


Figure 1. (a) Voltammogram of PANI electrodeposition on 316 SS at 50mV/s in fourth cycle, (b) voltammograms of PANI electrodeposition on 316 SS at 50mV/s up to 10 cycles, (c and d) SEM micrographs of a thin and thick PANI coatings obtained in 3 and 8 cycles at 50mV/s, respectively.

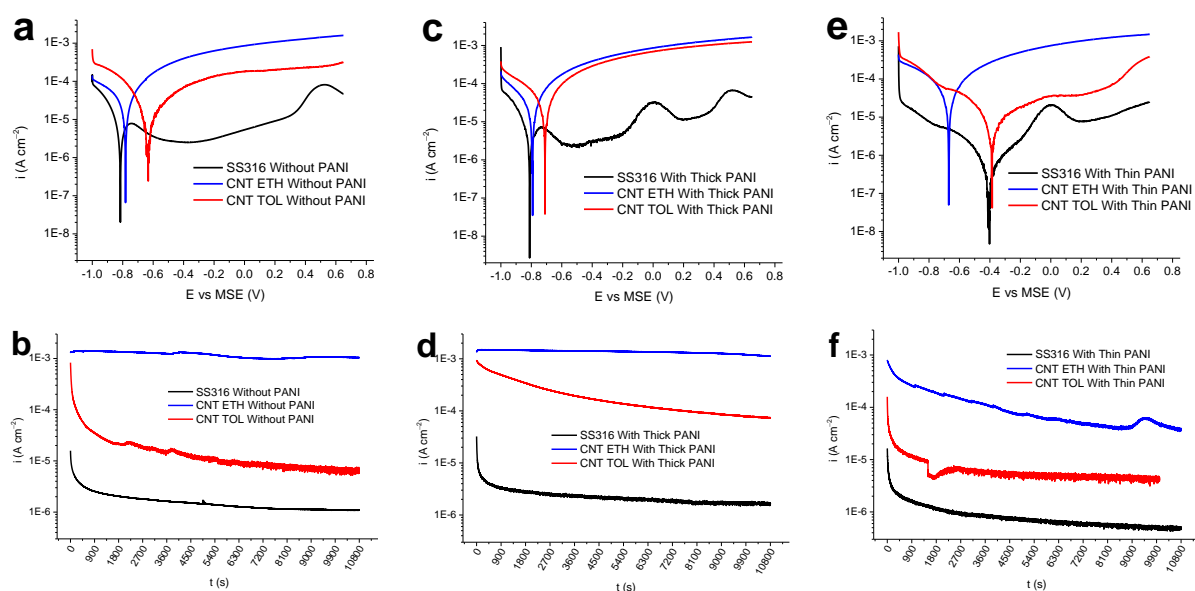


Figure 2. Potentiodynamic and potentiostatic measurements of different samples (a, b) without PANI coating, (b, c) with thick PANI coating and (e, f) with thin PANI coating, respectively.

(not shown here) suggesting a similar electropolymerization mechanism in both cases. They also confirmed similar electrochemical and morphological characteristics at higher number of cycles, i.e., increased thickness and lower adhesion.

Fig.2 shows overlaid potentiodynamic and potentiostatic plots of all the three samples without (Fig.2 a and b) and with (Fig.2 c and d for thick and d and e for thin) PANI coating. It is seen that CNT-TOL sample is showing a nobler free corrosion potential (potentiodynamic) and a lower corrosion current density (potentiostatic) compared to CNT-ETH in all conditions, revealing its more corrosion resistant nature. However, it is still corroded quite faster than uncoated SS. Thick PANI coating on all CNT samples decreased the corrosion resistance. Thin PANI coating however, improved the corrosion resistance considerably on both CNT coated and uncoated samples.

Conclusion

Growth of CNT/CNFs on 316 SS is accompanied by modifications in the substrate microstructure and surface chemistry, namely, sensitization, that decreases the corrosion resistance of the material. These modifications are stronger when ethylene gas is used as carbon precursor compared to liquid toluene. PANI electrodeposition on carbon coated 316 SS is possible by cyclic voltammetry with convincing control over the coating thickness. The key points of PANI electrodeposition on bare 316 SS apply to carbon coated 316 SS as well. While thick PANI coating does not add any value to corrosion resistance of the sample, thin PANI coating provides considerable protective effect resulting in reduced corrosion current densities. CNT-TOL sample as the superior carbon coated corrosion resistant candidate, can reach a potentiostatic corrosion current density ($3.5\mu\text{A}$) close to that of uncoated 316 SS ($1.5\mu\text{A}$). However, thin PANI coated 316 SS is still corroded almost one order of magnitude slower ($0.45\mu\text{A}$). Notwithstanding the potential of thin PANI coatings for corrosion protection, CVD deposited filamentous carbon coating on SS 316 does not seem to be a promising candidate for bipolar plates of fuel cells.

References

1. H. Tawfik, Y. Hung, and D. Mahajan, *J. Power Sources*, 163, 755–767 (2007).
2. S. Karimi, N. Fraser, B. Roberts, and F. R. Foulkes, *Adv. Mater. Sci. Eng.*, 2012, 1–22 (2012).
3. D. Bloomfield and V. Bloomfield, in *Modern Aspects of Electrochemistry No. 40, Modern Aspects of Electrochemistry*. R. E. White, C. G. Vayenas, and M. E. Gamboa-Aldeco, Editors, vol. 40, p. 1–35, Springer, New York, US (2007).
4. D. E. Tallman, G. Spinks, A. Dominis, and G. G. Wallace, *J. Solid State Electrochem.*, 6, 73–84 (2002).
5. G. Ćirić-Marjanović, *Synth. Met.*, 177, 1–47 (2013).
6. M. Hashempour, A. Vincenzo, F. Zhao, and M. Bestetti, *Mater. Charact.*, 92, 64–76 (2014).
7. M. Hashempour, A. Vincenzo, F. Zhao, and M. Bestetti, *Carbon*, 63, 330–347 (2013).
8. M. Hashempour, A. Vincenzo, and M. Bestetti, *ECS Trans.*, 58, 21–31 (2014).
9. C. Dalmolin, S. C. Canobre, S. R. Biaggio, R. C. Rocha-Filho, and N. Bocchi, *J. Electroanal. Chem.*, 578, 9–15 (2005).
10. Y. Zou, L. Sun, and F. Xu, *Talanta*, 72, 437–442 (2007).
11. G. Ćirić-Marjanović, *Synth. Met.*, 177, 1–47 (2013).

Electrochemical deposition of hydroxyapatite coatings on CoCrMo alloy

F. Onderka^{a*}, O. Klanica^a, D. Dobrocký^a

^a Department of Mechanical Engineering, University of Defence in Brno, Kounicova 65, 602 00 Brno, Czech Republic

(*) Corresponding author. Tel: +420 776769869. Email: filip.onderka@gmail.com

The aim of this work is to present hydroxyapatite (HA) coatings which were prepared on CoCrMo as-cast alloy by electrochemical deposition technology in the mixed solution $\text{Ca}(\text{NO}_3)_2 \cdot 4\text{H}_2\text{O}$ and $\text{NH}_4\text{H}_2\text{PO}_4$. CoCrMo alloy complies with the ISO 5832-4 standard and is widely used in the manufacturing of orthopedic implants because of its high strength, good corrosion resistance and excellent biocompatibility properties. HA coating is used to ensure sufficient bioactivity, but application of hydroxyapatite in orthopedic implants suffers from its low fracture toughness and poor wear resistance. Carbon nanotube (CNT), with its high stiffness and mechanical strength, is an attractive reinforcement for HA to surmount these issues.

Keywords: hydroxyapatite, carbon nanotubes, electrochemical deposition, orthopedic implants

Introduction

Nowadays in the surgical implant manufacture Co base alloys, Ti base alloys and stainless steels are used due to their good mechanical stability and biocompatibility (1). The Co base alloys – specifically CoCrMo alloys are typical non-magnetic metallic biomaterials because they have excellent abrasive and corrosion resistances in chloride environments, so they have a proven track record as materials for artificial hip and knee joints (2, 3). The corrosion resistance is related to surface oxide formation which is strongly enriched with Cr_2O_3 (2). The most used as-cast alloys are CoCrMo (ISO 5832-4, ASTM F75).

Hydroxyapatite (HA) is a bioceramic material with poor mechanical properties, especially for load-bearing applications (4). It is characterized by low toughness and poor flexural strength (< 140 MPa) (5). Nevertheless, HA has a structure similar to human bone and it is capable of supporting the growth of living tissue because it contains almost equal proportions of calcium and phosphorus as a human bone (6, 7). The low mechanical strength of HA restricts use mainly for bearing applications, therefore, accesses the various forms of reinforcement, mainly at the level of nanometers (4).

In 1991 Sumio Iijama discovered carbon nanotubes (CNT) with outer diameter 4-30 nm and length up to 1 mm (5, 8). CNT have specific structural characteristics, such as very small dimensions, low density, high tensile strength (~ 60 GPa), high Young's modulus (up to 1 TPa) and high resilience, superb flexibility, excellent electric and thermal properties (5, 9).

Material and methods

CoCrMo alloy

Two different samples of CoCrMo alloys were poured in a vacuum furnace, all of them complying with the ISO 5832-4 chemical composition standard. The precision casting technique was performed to obtain two samples, this technology utilizes injection wax (REMET RF 1/478) into the cavity of the metal mold under pressure. Models are bonded to a common inlet, then they are immersed in a zirconia ceramic slurry to form a ceramic shell. The sample M was immersed firstly in ceramic slurry with the addition of inoculant ($\text{Co}(\text{AlO}_2)_2$), the sample B is without inoculant. This process form approximately 8 mm thin film that dries for 24 hours. The wax is melted out from the shell and before pouring the shell is annealed at temperature 1030 ± 10 °C, at least 4 hours. The mold is preheated at 1380 ± 10 °C and the pouring temperature was 1360 ± 10 °C, pouring time is 2 s. After cooling, the castings samples (cylinders) are cut off and cleaned. Chemical composition of substrate was measured by GDOES.

Hydroxyapatite

Electrochemical deposition of hydroxyapatite in a mixed aqueous solution of $\text{Ca}(\text{NO}_3)_2 \cdot 4\text{H}_2\text{O}$ and $\text{NH}_4\text{H}_2\text{PO}_4$ is one of the most effective methods of creating bioactive hydroxyapatite coatings on metal implants more than ten years (10). During the process, DC electric current is applied to the electrolyte by means of two electrodes that are immersed in the electrolyte. The electrolyte comprises calcium and phosphate and chemical changes can be observed there. During the process, hydroxyapatite is electrochemically deposited on the surface of the cathode (11). Deposition can be performed at room temperature or in a heated bath.

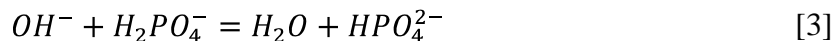
The formation of hydroxyapatite coating consists of the following combination of reactions. Firstly, the electrolyte undergoes an equilibrium reaction as:



The amount of HPO_4^{2-} ions in the solution is small since the ionization constant in equation [1] is only $6,3 \cdot 10^{-8}$. With the aid of the electric field, the water at the cathode (substrate) surface is decomposed into hydrogen gas and hydroxide ions:



The formation of OH^- can enhance the reaction in equation [1] to produce HPO_4^{2-} . Also OH^- can react with HPO_4^{2-} according to the equilibrium below:



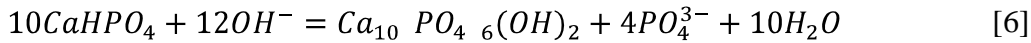
HPO_4^{2-} combines with Ca^{2+} to produce a $\text{CaHPO}_4 \cdot 2\text{H}_2\text{O}$ precipitations and deposits on the surface of CoCrMo substrate and forms the coating.



The electrochemical deposition process comprises the ionization reaction, the electrochemical half reaction, the acid base reaction, and the precipitation reaction. During hydrothermal treatment, the water in the steam is reduced according to the following equation:



This allows the following reaction to take place, when formed coating is influenced by OH⁻.



By combining equations [5] and [6] hydroxyapatite is formed. The reaction may take following form:



During the hydrothermal process, the pH of water decreases. If the pH is reduced too much, the reaction will be interrupted. By adding ammonia may increase the rate of formation of hydroxyapatite (12).

The experiment was performed by the Kavalier facilities with heated water bath. The container has its own heating and there is also secure own circulation. The temperature can be set and control by the thermostat. The characterization of HA was achieved by using scanning electron microscopy (SEM) and by using optical microscopy.

Results and discussion

Table I. presents chemical composition of the alloy CoCrMo measured by GDOES. Firstly, a comparison is made for ISO 5832-4 and secondly is made for ASTM F-75.

TABLE I. Chemical composition of as-cast CoCrMo alloy

<i>Element</i>	<i>Sample M</i> <i>wt [%]</i>	<i>Sample B</i> <i>wt [%]</i>	<i>ISO 5832-4</i> <i>wt [%]</i>	<i>ASTM F75</i> <i>wt [%]</i>
Co	62.5	62.1	balance	balance
Cr	29.0	28.7	26.5-30.0	27.0-30.0 ± 0.30
Mo	6.07	6.05	4.5-7.0	5.0-7.0 ± 0.15
Mn	0.45	0.41	max. 1.0	max. 1.0 ± 0.03
C	0.217	0.218	max. 0.35	max. 0.35 ± 0.02
Ni	0.50	1.15	max. 1.0	max. 0.5 ± 0.05
Si	0.82	0.81	max. 1.0	max. 1.0 ± 0.05
W	0.079	0.084	-	max. 0.2 ± 0.04
Ti	0.051	0.059	-	max. 0.10 ± 0.02
Others	0.313	0.419	-	-

The comparison shows that only the B sample exceeds the limit value of 0.15% for nickel. Other elements are in accordance with limits given by ISO standard. The amounts of tungsten and titanium are not specified in standard ISO, it is only defined by ASTM standard. For all samples the amounts of tungsten and titanium are in the limits by ASTM standard.

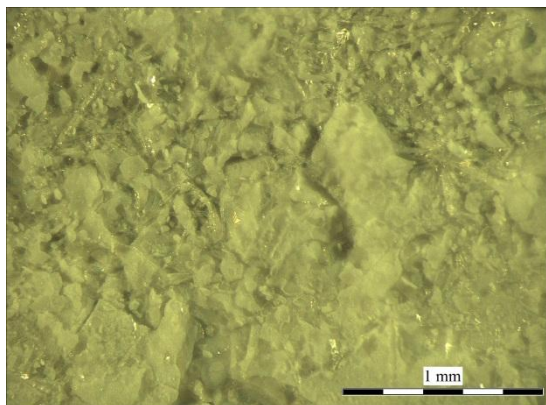


Figure 1. Hydroxyapatite coating on sample B, optical microscopy

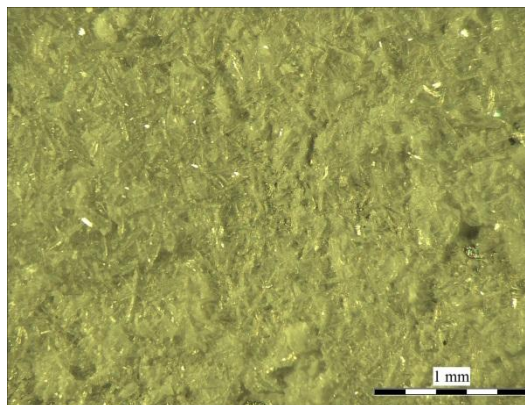


Figure 2. Hydroxyapatite + carbon nanotubes coating on sample M, optical microscopy

The results obtained by optical microscopy (Fig. I and Fig. II) indicate that the electrochemical deposited coatings, prepared at 65 °C in 800 ml distilled water 7.936 g $\text{Ca}(\text{NO}_3)_2 \cdot 4\text{H}_2\text{O}$ and 2.304 g $\text{NH}_4\text{H}_2\text{PO}_4$, contain pure calcium hydrogen phosphate dehydrates ($\text{CaHPO}_4 \cdot 2\text{H}_2\text{O}$). Hydroxyapatite coating on sample M (Fig. II) has structure rather fine, on the other hand, the structure on sample B (Fig. I) has bigger crystals and its structure is coarser.

Fig. III shows the structure of the HA-CNT coating obtained by SEM. There are many plate-like particles. All of the coatings examined by OM and by SEM contain a number of pores on the surface. This is no doubt beneficial to the growth of bone tissue.

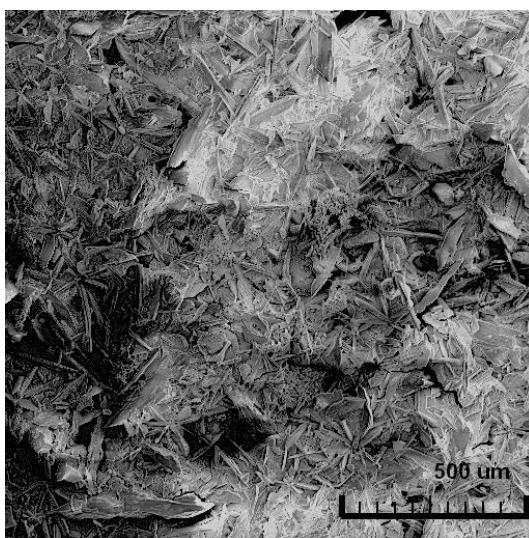


Figure 3. Hydroxyapatite + carbon nanotubes coating on sample M, scanning electron microscopy

Conclusions

Two Co-based alloys with a composition conforming to the ISO 5832-4 standard poured in a vacuum furnace. Both samples correspond to limits given by ISO standards. The amounts of tungsten and titanium are not specified in standard ISO, but the limits are in ASTM standard and the samples are in accordance with them.

Pure $\text{CaHPO}_4 \cdot 2\text{H}_2\text{O}$ coatings on two CoCrMo substrates can be prepared at relatively low temperatures from aqueous electrolytes containing Ca^+ and P^- bearing ions using an electrochemical deposition process. After hydrothermal treatment, $\text{CaHPO}_4 \cdot 2\text{H}_2\text{O}$ is converted into hydroxyapatite coating. The structure is porous and it allows ingrowth of bone cells.

References

1. L. E. Ramírez-Vidaurre, M. Castro-Román, M. Herrera-Trejo, C. V. García-López, E. Almanza-Casas, *J. Mater. Process. Technol.*, **209**, (2009).
2. S. Bauer, P. Schmuki, Klaus von der Mark, J. Park, *Prog. Mater. Sci.*, **58**, (2013).
3. M. Mori, K. Yamanaka, H. Matsumoto, A. Chiba, *Mater. Sci. and Eng.*, **528**, (2010).
4. H. Zhou and J. Lee, *Acta Biomaterialia*, **7**, (2011).
5. S. Mukherjee, B. Kundu, S. Sen, A. Chanda, *Ceram. Int.*, **40**, (2014).
6. A. Arifin, A. B. Sulong, N. Muhamad, J. Syarif, M. I. Ramli, *Mater. Des.*, **55**,n(2014).
7. J. Faig-Martía, F. J. Gil-Murb, *Rev. esp. cir. Ortop. Traumatol*, **52**, (2008).
8. S. Iijima, *Physica B*, **323**, 1-5 (2002).
9. D. Lahiri, S. Ghost, A. Agarwal, *Mater. Sci. Eng. C*, **32**, (2012).
10. S. K. Yen and C. M. Lin, *Mater. Chem. Phys.*, **77**, (2002).
11. L. Wang and J. Luo, *Mater. Charact.*, **62**, (2011).
12. L. Huang, K. Xu, J. Lu, *J. Mater. Sci. - Mater. Med.*, **11**, (2000).

Protective coatings against thermal degradation of the metal thin film

L. Šimonová¹⁾; J. Šubarda²⁾; J. Danovič

¹⁾ FEKT, Brno University of Technology, Technická 10, 616 00 Brno,
xsimon09@stud.feec.vutbr.cz

²⁾ FEKT, Brno University of Technology, Technická 10, 616 00 Brno, subarda@feec.vutbr.cz

Abstract

Thin films have been used for many years in different sectors, where they can have different exercise options. Very often thin films of different materials are used in engineering, which improve the resistance, hardness and lifetime of the substrate in general. In recent years, thin films are widely used in medicine as well. In the adjustments of joint replacements, it reduces friction and thus the lifetime those joints, for artificial organs and valves, dental implants and more. No less important are the thin films in electrical engineering and microelectronics and optics. Thin films are also used to make lights for cars and many other places.

In many cases, these thin films are subjected to adverse effects, due to which, over time, begin to degrade and thus lose their visual but also functional properties. The biggest problem with thin metal films are degradation processes, which are caused by extreme temperatures, temperature fluctuations, acidic environment, too damp environment, chemical reactions with its surroundings and many others. Against some of these processes, it is possible to use different ways of protecting the base material thin metal film.

In this case, we focus on permanent and extreme thermal effects, which can provide a thin metal films disrupt and even destroy. The work was divided into several parts selection of suitable substrates and thin metal layers, cleaning substrates, creating the desired thin metal films using magnetron sputtering, selection of appropriate protective coatings, their application and subsequent testing in two ways.

Substrates for the testing were selected so that the surface structure and properties of the substrate are different. Glass and corund ceramic were used. In the same way, we chose a metal thin films. These are thin films of titanium and aluminum, because their heat resistances are differends.

Our idea was to find out how much the individual materials are resistant separately for long term aging and in extreme short aging. In addition, we also focused on a variety of protective coatings that we tested under the same conditions, we investigated whether these coatings are able to protect the thin film at elevated temperatures and extreme temperatures.

The formed thin films are very sensitive to environmental effects and their exposed surface. These layers are subsequently subject to degradation processes - such as corrosion, cracks or mechanical damage. These symptoms are very undesirable. One of the main causes of degradation of the different thin metal films in normal operation it is a temperature and thermal stress. Therefore, we focused on this issue. Protective films were chosen to cover a wide range of commercially available materials. Conform to standards EN 60068-2-2, we have created the conditions for accelerated examination by dry heat at a given temperature and a given time for all samples. Next, we tested the short-term effects of extreme temperatures on all samples. Again, apply the same conditions for all samples.

After the thermal test, all samples were subjected to examination of the differences in the individual protective surfaces before aging and after using various methods. The results of each sample were compared to each other and evaluated in terms of the best protection of different thin metal films and the thermal resistance of the coatings. Procedures for cleaning substrates before the creation of thin layers of metal it has also been taken into account.

Acknowledgements

This work was supported by grant FEKT-S-14-2293, by project CZ.1.07/2.3.00/20.0103 and by project no. LO1210.

References

1. J. Hamerník, *Koroze a ochrana před korozi*, (2006)
2. WWW: <http://jhamernik.sweb.cz/Koroze.htm>
3. P. Novák; M. Kouřil, J. Bystrianský, *Koroze a degradace kovových materiálů*, (2009)
WWW:
4. http://www.vscht.cz/met/stranky/vyuka/predmety/koroze_materialu_pro_restauratory/kadm/pdf/
5. H. Polsterová, VUT FEKT BRNO. *Spolehlivost v elektronice*, 106 p, Brno (2003).
6. K. Dvořáčková, *Studium vlastností vybraných prostředků používaných pro ochranu kovu proti korozi*, Brno: Masarykova univerzita, Přírodovědecká fakulta (2007), 53 p

Title: Advanced Batteries Accumulators and Fuel Cells – 15th ABAF
Edited: Jiří Vondrák
Marie Sedlaříková
Vítězslav Novák
Petr Bača
Publishing Office: Jiří Vondrák
Marie Sedlaříková
Vítězslav Novák
Petr Bača
Deadline: August 7th 2014
Publisher: Brno University of Technology
Faculty of Electrical Engineering and Communication
Department of Electrical and Electronic Technology
Year: 2014

The authors are fully responsible for the content and language of their contribution

ISBN 978-80-214-5008-0